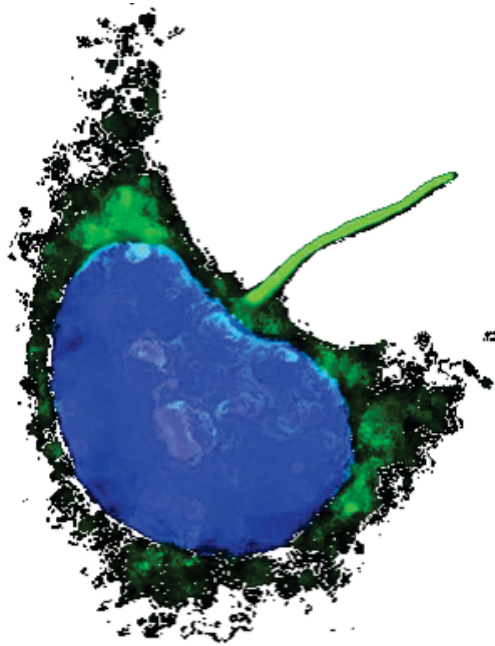


Cell-based studies of ciliary transport



Stefanie Kristine Kösling



Cell-based studies of ciliary transport

Inaugural-Dissertation

zur Erlangung des Doktorgrades
der Mathematisch-Naturwissenschaftlichen Fakultät
der Heinrich-Heine-Universität Düsseldorf

vorgelegt von

Stefanie Kristine Kösling

aus Essen

Düsseldorf, Februar 2018

aus dem Institut für Biochemie und Molekularbiologie II
der Heinrich-Heine-Universität Düsseldorf

Gedruckt mit der Genehmigung der
Mathematisch-Naturwissenschaftlichen Fakultät der
Heinrich-Heine-Universität Düsseldorf

Berichterstatter:

1. Prof. Dr. Reza Ahmadian
2. Prof. Dr. Lutz Schmitt
3. Prof. em. Dr. Alfred Wittinghofer

Tag der mündlichen Prüfung: 14.05.2018

Die vorliegende Arbeit wurde von Dezember 2013 bis Februar 2018 in der Emeritusgruppe Strukturelle Biologie am Max-Planck-Institut für Molekulare Physiologie in Dortmund unter der Betreuung von Prof. em. Dr. Alfred Wittinghofer angefertigt.



Ich versichere an Eides Statt, dass die Dissertation von mir selbstständig und ohne unzulässige fremde Hilfe unter Beachtung der „Grundsätze zur Sicherung guter wissenschaftlicher Praxis an der Heinrich-Heine-Universität Düsseldorf“ erstellt worden ist. Die Dissertation wurde in der vorgelegten oder in ähnlicher Form noch bei keiner anderen Fakultät eingereicht. Ich habe bisher keine erfolglosen oder erfolgreichen Promotionsversuche unternommen.

Düsseldorf, den 23.02.2018

S. Köstling

Stefanie Kristine Köstling

„Hope is not the conviction that something will turn out well
but the certainty that something makes sense,
regardless of how it turns out.“

Václav Havel

Content

Abstract	1
1 Introduction	3
1.1 Structure, occurrence and history of the cilium.....	3
1.2 Functions of the cilium.....	5
1.3 Cilia defects lead to ciliopathies.....	7
1.4 The intraflagellar transport system.....	8
1.5 Ciliary assembly and disassembly.....	11
1.6 Regulation of ciliary entry.....	13
1.7 Guanine nucleotide-binding proteins	16
1.8 Post-translational modifications of small G proteins	21
1.9 ADP-ribosylation factor like (Arl) proteins and the interswitch toggle	23
1.10 Arl2 and Arl3 and the ciliary Arl3•GTP compartment.....	25
1.11 Effectors of Arl2 and Arl3	26
1.12 Guanine nucleotide dissociation inhibitors (GDIs) and the GDI-like protein PDE6δ.....	27
1.13 PDE6δ and RabGDIs are regulated by GDI displacement factors (GDFs).....	31
1.14 The ciliary inositol polyphosphate 5'-phosphatase INPP5E	32
1.15 Unc119a/b shuttle myristoylated cargo proteins	36
1.16 The Arl2/Arl3 system sorts lipidated cargo proteins	38
2 Publication I.....	40
The interaction of CCDC104/BARTL1 with Arl3 and implications for ciliary function....	40
3 Publication II.....	72
PDE6δ-mediated sorting of INPP5E into the cilium is determined by cargo-carrier affinity	72
4 Publication III	92
Novel biochemical and structural insights into the interaction of myristoylated cargo with Unc119 protein and their release by Arl2/3	92
5 Publication IV	108
Mechanism and dynamics of INPP5E transport into and inside the ciliary compartment	108
6 Discussion	132
6.1 The interaction of CCDC104/BARTL1 with Arl3 and implications for ciliary function.....	132
6.2 PDE6δ-mediated sorting of INPP5E into the cilium is determined by cargo- carrier affinity	135

6.3	Novel biochemical and structural insights into the interaction of myristoylated cargo with Unc119 protein and their release by Arl2/3	137
6.4	Mechanism and dynamics of INPP5E transport into and inside the ciliary compartment	140
6.5	Summary.....	145
6.6	Zusammenfassung	148
	References	149
	Acknowledgements	167

Abstract

Primary cilia are microtubule-based cellular protrusions essential for several developmental signaling pathways. Defects in ciliary structure and protein trafficking lead to genetic human diseases, called ciliopathies. The intraflagellar transport (IFT) system regulates the transport within the cilium. Protein entry to and exit from the ciliary compartment are strictly regulated by the ciliary gate, which separates the ciliary lumen from the cytoplasm and thereby allows control over cilia-associated signaling pathways. Currently, the precise ciliary sorting and retention mechanisms of many ciliary proteins remain unclear.

The ADP-ribosylation factor (Arf-) like proteins Arl2 and Arl3 are homologous guanine nucleotide-binding (G) proteins and belong to the Ras superfamily. Despite their similarity, only Arl3 localizes to primary cilia. Shared effectors of Arl2 and Arl3 are BART (Binder of Arl2), the homologous proteins delta subunit of phosphodiesterase 6 (PDE6 δ), human retina gene 4 (HRG4)/Unc119a (uncoordinated) and Unc119b. PDE6 δ is a general prenyl-binding protein and solubilizes prenylated proteins to facilitate intermembrane transport of prenylated cargo proteins, such as the inositol polyphosphate 5'-phosphatase E (INPP5E), or the small G proteins Ras (rat sarcoma virus) and Rheb (Ras homolog enriched in brain). Unc119a/b binds and shuttles myristoylated cargo proteins such as the ciliary proteins NPHP3 (Nephrocystin-3), Cystin1 or non-ciliary Src kinase family members. Arl2/3 act as GTP-specific release factors for lipidated cargo proteins from the effectors PDE6 δ and Unc119a/b. The high interest in investigating the molecular transport mechanisms and interactions of proteins in this network is given by their implication in different ciliopathies, such as the renal-retinal disorder Joubert syndrome in case of PDE6 δ and INPP5E, or rod-cone diseases for Arl3 and Unc119 proteins.

In this thesis, the Arl2/Arl3-related protein network with their interaction partners, the effector proteins PDE6 δ and Unc119a/b with lipidated cargo proteins, especially INPP5E, were studied with a focus on ciliary transport processes using cell-based experiments. CCDC104 (coiled coil domain containing)/BARTL1 (BART-like 1) is a newly identified binding partner of Arl3, that interacts with a conserved LLxILxxL motif located in the Arl3 N-terminus, as shown by x-ray structure determination of a CCDC104-Arl3 complex (Mandy Lokaj). CCDC104 was found as ciliary and transition zone enriched protein. The N-terminal amphipathic helix of Arl3 was shown to be crucial for Arl3 ciliary localization (with Mandy Lokaj).

Both farnesylated INPP5E and Rheb interact with PDE6 δ . However, INPP5E with a high affinity towards PDE6 δ is sorted to cilia, where it is exclusively released by ciliary Arl3•GTP, whereas Rheb with low affinity is released at endomembranes by Arl2•GTP. This affinity

difference is mediated by the -1 and -3 positions relative to the farnesylated cysteine, and was found to determine the cellular sorting, also highlighted by an INPP5E low affinity mutant losing exclusive ciliary localization (with Eyad Fansa). A similar sorting principle was shown to be relevant for Unc119a/b and myristoylated proteins. Myristoylated peptides of NPHP3, Cystin1 and GNAT-1, that bind with high affinity to Unc119 proteins, localize to cilia and are specifically released by Arl3•GTP, whereas Src with a low affinity is not found in cilia. The +2 and +3 positions relative to the myristoylated glycine seem to be important for the distinction of low or high affinity, underlined by a partial mislocalization of an NPHP3 low affinity mutant (with Mamta Jaiswal and Eyad Fansa). These findings suggest a general sorting principle of lipidated cargo proteins, being dependent on the affinity towards PDE6 δ /Unc119a/b, on the specificity of release by Arl2/3 and the localization of Arl3•GTP inside the cilium.

Using the live cell fluorescence recovery after photobleaching (FRAP) microscopy technique, the cellular dynamics of INPP5E and Arl3 were analyzed. Within cilia, INPP5E was shown to be transported via IFT, but independent of PDE6 δ or INPP5E farnesylation. However, ciliary targeting and/or entry of INPP5E require PDE6 δ activity, farnesylation, and the dynein transport system. In contrast, Arl3 seems to freely diffuse into and within cilia. The farnesylation-defective INPP5E CaaX box mutant is enriched at the centrioles before ciliary entry, suggesting an affinity trap at the ciliary base, that is overcome by PDE6 δ interaction for the wild type protein. A three-step mechanism for the regulation of INPP5E localization to cilia was postulated to be composed of PDE6 δ - and farnesylation-mediated targeting, diffusion of the INPP5E-PDE6 δ complex into the ciliary compartment and transfer to the IFT system, and final retention inside the cilium (with Stefano Maffini).

This thesis leads to a better understanding of the Arl2/3-related protein network with a focus on the sorting and transport processes of lipidated cargo proteins of PDE6 δ and Unc119a/b. The studies show that the primary cilium is an Arl3•GTP compartment. Considering the implication of these proteins in different ciliopathies, by the new findings an essential step to gain an insight to the molecular basics of these diseases and ultimately their treatment was taken, and will require further research.

1 Introduction

1.1 Structure, occurrence and history of the cilium

Cilia are hair-like cellular organelles that project from the apical surface of most eukaryotic cells (Wheatley, 1995; Pazour and Witman, 2003). Their scaffold, which forms the entire length of the cilium and is called axoneme, is built by nine doublets of microtubules that are anchored to the mother centriole derived basal body. The basal body connects the cilium to the cell body and is linked to the daughter centriole by an interconnecting fiber (De Robertis, 1956; Sorokin, 1968; Berbari et al., 2009; May-Simera and Kelley, 2012). The ciliary lumen is surrounded by the ciliary membrane and both differ from the cellular cytosol and the plasma membrane in its protein and lipid composition (Bloodgood, 1984; Rohatgi and Snell, 2010; Garcia-Gonzalo et al., 2015). At the base of the cilium, the plasma membrane forms an endocytic depression at the transition to the ciliary membrane, the ciliary pocket (Molla-Herman et al., 2010). In terms of the physical properties, cilia can be divided into motile and non-motile, also referred to as primary cilia with a $9 + 0$ structure, whereupon motile cilia or flagella exhibit an additional central microtubule pair, encircled by the nine microtubule doublets, and thus have a $9 + 2$ arrangement (Porter, 1957; Satir, 2005; Satir and Christensen, 2007).

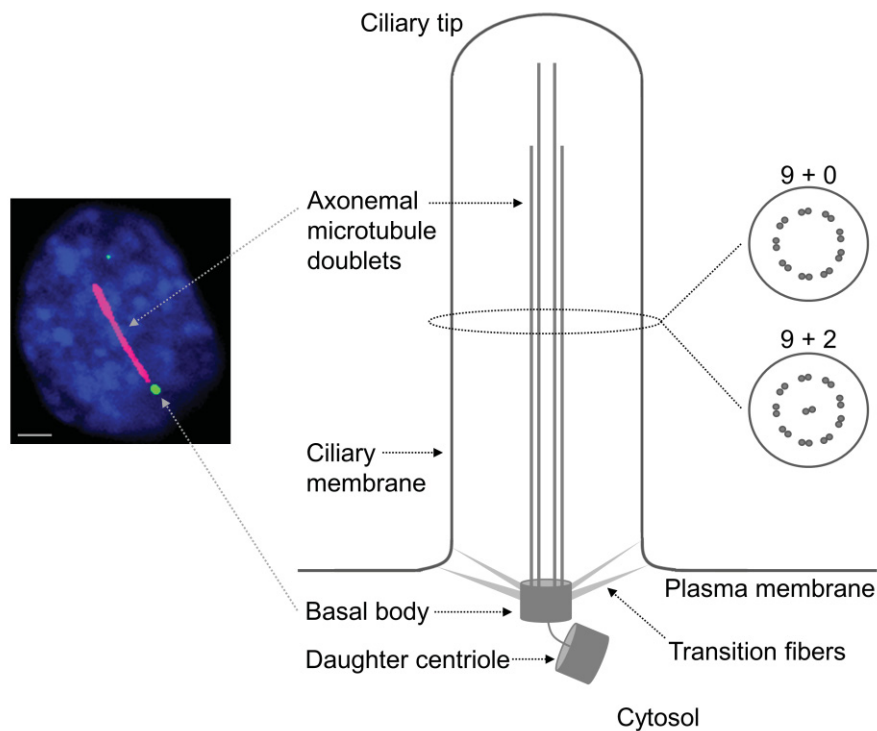


Figure 1: The axoneme is the scaffold of the cilium and is established from nine doublets of microtubules, which are surrounded by the ciliary membrane. Primary cilia have a $9 + 0$ structure, whereas motile cilia have an

additional central microtubule pair ($9 + 2$). The microtubules derive from the basal body (mother centriole) and the ciliary lumen is separated from the cytoplasm by transition fibers and transition zone proteins. The immunofluorescent image of a renal epithelial IMCD3 cell shows the nucleus, stained with DAPI (blue), the axoneme, immunostained for acetylated α -tubulin (red) and the basal body, immunostained for CEP135, a centriolar protein (green). Scale bar indicates 2 μm .

The first investigations of mammalian cilia were carried out by Purkinje and Valentin in 1835 (Satir and Christensen, 2008). Later in 1954, Fawcett and Porter first described the ultrastructure of motile cilia by electron microscopy of epithelial cells of mollusks, amphibians, mice and humans in more detail and discovered the described $9 + 2$ pattern (Fawcett and Porter, 1954). The structure of immotile cilia was first characterized in studies of mammalian photoreceptors (De Robertis, 1956; Porter, 1957; Satir, 2005). In the early 1960s, the $9 + 0$ structured cilia were termed primary cilia by Barnes in a study of the mouse hypophysis (Barnes, 1961). Further electron microscopic studies revealed the presence of primary cilia on a variety of different cell types of vertebrate and mammalian tissues. For instance, they were discovered on Langerhans islets of the pancreas (Munger, 1958), on renal epithelial cells (Latta et al., 1961), neurons (Rosenbluth and Palay, 1961; Taxi, 1961; Grillo and Palay, 1963), smooth muscle cells and fibroblasts (Sorokin, 1962).

During the last decade, the historical classification, that $9 + 2$ structured cilia reveal only functions in motility, whereas $9 + 0$ cilia are exclusively sensory, was questioned as too simplistic and should be rethought (Berbari et al., 2009; May-Simera and Kelley, 2012). There are olfactory sensory cilia, which are not motile and nevertheless possess a $9 + 2$ symmetry (Lidow and Menco, 1984). The primary cilia at the embryonic node with a $9 + 0$ structure are able to move. They create a left-directed flow, which is necessary to create an asymmetric development of the embryo (Nonaka et al., 1998; McGrath and Brueckner, 2003; McGrath et al., 2003). Even cilia revealing a $9 + 3$ symmetry, where the nine microtubule doublets enclose a central microtubule triplet, were discovered in a number of species of *Coniopterygidae* (Zizzari et al., 2008), and motile cilia with a $9 + 4$ axoneme were identified on the notochordal plate in the rabbit embryo (Feistel and Blum, 2006). However, it remains unclear which specific function these additional inner microtubules have. Cells with motile cilia generally appear to be multiciliated, whereas a primary cilium occurs as singlet (Wheatley, 1995; Wheatley et al., 1996; Satir and Christensen, 2007; Mahjoub, 2013).

Commonly used ciliated model organisms in the cilia research field are the green alga *Chlamydomonas reinhardtii* (Pazour et al., 2005) and *Tetrahymena thermophila* (Smith et al., 2005), another protozoan, both of which possess motile cilia or flagella, which however have

similarities to primary cilia. The nematode *Caenorhabditis elegans* has a special type of primary cilia, and widely used in studies of primary cilia are established cell lines, such as human RPE1 (human retinal pigment epithelium) (Matsunaga et al., 1999), murine renal epithelial IMCD3 (inner medullary collecting duct) (Rauchman et al., 1993) and embryonic fibroblast NIH/3T3 cells (Todaro and Green, 1963).

1.2 Functions of the cilium

Cilia have various essential functions in different organisms and eukaryotic cell types and the functions of motile cilia differ from that of primary cilia. In general, motile cilia play essential roles in the motility of entire cells or of the cilia themselves. These 9 + 2 cilia possess the additional central microtubule and dynein arms that facilitate the movement. For instance, sperm cells or many protozoans move by their flagella, whereas in the respiratory tract, motile cilia are responsible for mucous clearance (Afzelius, 1959, 1976; Camner et al., 1975; Sanderson et al., 1985; Satir and Christensen, 2007).

Primary cilia are established in various differentiated and growth-arrested cell types in vertebrates (Wheatley, 1995; Wheatley et al., 1996; Eggenschwiler and Anderson, 2007). Research on primary cilia was neglected for a long time. However, during the last decades, their importance and functions in eukaryotic organisms were discovered. Primary cilia exhibit various sensory functions which were first analyzed in studies of mammalian photoreceptors (Porter, 1957; Pazour and Witman, 2003; Satir, 2005). They sense different signals, such as chemicals or light, explaining their role in olfaction and vision. For example, a specialized primary cilium is the connecting cilium of rod photoreceptors. It is required for fundamental steps in the transduction cascade of visual signals (Besharse et al., 1977; Nachury et al., 2010). Moreover, primary cilia of epithelial cells in kidney tubules sense physical signals such as extracellular fluid flow, leading to increased intracellular calcium levels (Praetorius and Spring, 2001; Nauli et al., 2003; Watnick and Germino, 2003; Shiba et al., 2005; Fry et al., 2014). Poole et al. were the first to hypothesize about the functions of primary cilia in connective tissues. They suggested the function of primary cilia as regulatory antennae of the cell exhibiting various features, such as obtaining, converting and transferring external signals to organelles inside of the cell. Thus, primary cilia were thought to cause adequate homeostatic intracellular replies to alterations of the extracellular environment (Poole et al., 1985).

The tiny organelles are involved in signal transduction pathways during both embryo development and in tissue homeostasis in adults, offering a further compartment with the

required environment for these pathways (Goetz and Anderson, 2010). In detail, primary cilia are essential for a number of developmental signaling pathways (Eggenchwiler and Anderson, 2007; Goetz and Anderson, 2010), such as Hedgehog (Hh) (Huangfu et al., 2003; Corbit et al., 2005; Haycraft et al., 2005; Liu et al., 2005), platelet-derived growth factor receptor α (PDGFR α) (Schneider et al., 2005) and Wnt (Wingless and Int-1) signaling (Cano et al., 2004; Simons et al., 2005; May-Simera and Kelley, 2012).

During limb bud development in vertebrate embryogenesis, the Hedgehog pathway is important for a proper differentiation of cells. It was first studied in the fruit fly *Drosophila melanogaster*. The Hh protein is a ligand of the receptor Patched, which is inactivated through ligand binding. This in turn leads to the activation of the G protein-coupled receptor (GPCR) Smoothened (Smo), a regulator of the Hh pathway (see also chapter 1.7 for G proteins). There are three known Hh proteins in mammals: Sonic hedgehog (Shh), Indian hedgehog (Ihh) and Desert hedgehog (Dhh) and three glioma-associated oncogene (Gli) proteins, which are transcription factors and the final target of Hh signaling (Liu et al., 2005). Corbit et al. provided evidence, that Smo has to localize to the primary cilium to execute its correct functions (Corbit et al., 2005). Furthermore, the ciliary IFT (intraflagellar transport) proteins play a crucial role in the transduction of the Hh signal, specific for vertebrates (Huangfu et al., 2003; Liu et al., 2005) (see chapter 1.5 for IFT). The primary cilium was also hypothesized to play a direct role in the processing of Gli transcription factors. It was shown that Gli2 and Gli3 localize to the cilium (Haycraft et al., 2005). Moreover, distinct cilia-related IFT proteins might be necessary to process Gli3 proteolytically and a proper function of IFT is essential to control the negative and positive activities of Gli proteins during transcription (Liu et al., 2005).

The receptor tyrosine kinase PDGFR α is involved in cellular growth control. It was shown that a proper function of the receptor requires localization to the cilium (Schneider et al., 2005). Wnt signaling is involved in the coordination of developmental processes, such as the renal and colon development, and it was hypothesized that primary cilia are involved in these processes (Cano et al., 2004). The Inversin (Inv) protein was shown to localize to primary cilia of tubular epithelial cells. Extracellular fluid flow, which is recognized by these cilia, leads to increased intracellular Inv levels and thereby Inv switches between canonical and noncanonical Wnt pathways (Simons et al., 2005; May-Simera and Kelley, 2012).

1.3 Cilia defects lead to ciliopathies

Defects in the structure and function of cilia cause a large number of human genetic diseases, collectively called ciliopathies (Badano et al., 2006; Novarino et al., 2011; Waters and Beales, 2011). These disorders appear with characteristic phenotypes and overlapping pathologies. Several ciliopathies derive from defects in genes encoding the ciliary ADP-ribosylation factor (Arf) like (Arl) proteins (see chapter 1.9). In more detail, mutations of the genes encoding the ciliary Arl proteins Arl3, Arl6 (BBS3) and Arl13B themselves or their effectors lead to ciliopathies, such as Retinitis pigmentosa, Bardet-Biedl syndrome and Joubert syndrome, respectively (Schwahn et al., 1998; Chiang et al., 2004; Schrick et al., 2006; Cantagrel et al., 2008). X-linked retinitis pigmentosa is a congenital eye disease with a slow progressing degeneration of the retina and finally leads to blindness. The retinal disorder affects 0.03 % of all humans (Haim, 2002) and is caused by mutations in different genes, such as the gene encoding for rhodopsin (Dryja et al., 1990) or for RP2 (retinitis pigmentosa 2) (Schwahn et al., 1998; Schrick et al., 2006). The Bardet-Biedl syndrome (BBS) is an autosomal recessive hereditary disease and is caused by mutations of the BBS proteins. It is characterized by varying phenotypes, such as mental retardation, disablements in learning, obesity, renal defects, polydactyly, hypogonadism and rod-cone dystrophy (Beales et al., 1999; Zaghloul and Katsanis, 2009; Waters and Beales, 2011).

The MKS and JBTS modules are protein complexes that localizes to the ciliary base and the transition zone and build a network with the NPHP (nephronophthisis) protein module. A number of proteins of that network are responsible to anchor the basal body and to establish the so-called ciliary gate (see chapter 1.6). Almost all of them are mutated in Joubert syndrome (JBTS), Meckel-Gruber syndrome (MKS) and Nephronophthisis (NPHP) (Sang et al., 2011; Williams et al., 2011; Garcia-Gonzalo and Reiter, 2012; Blacque and Sanders, 2014). If the protein interaction networks, especially those of the proteins localized in the transition zone, are disrupted, ciliogenesis and signal transduction of cilia-associated pathways may be disturbed (Lancaster et al., 2011; Sang et al., 2011). Characteristic for the Joubert syndrome are defects in the peripheral and central nervous system and a distinct phenotype is the “molar tooth sign”, a malformation of the midbrain-hindbrain. Patients suffer from mental retardation, psychomotor delay, ataxia, hypotonia, irregularities in breathing, and oculomotor apraxia (Waters and Beales, 2011). Joubert syndrome is caused by mutations in a number of genes, e. g. Arl13B (Cantagrel et al., 2008), INPP5E (encoding inositol polyphosphate 5'-phosphatase E) (Bielas et al., 2009), RPGRIP1L (encoding RPGR-interacting protein 1-like) (Delous et al.,

2007), NPHP1 (Nephrocystin) (Parisi et al., 2004), CEP290 (Centrosomal protein of 290 kDa) (Nephrocystin-6) (Sayer et al., 2006), MKS3/TMEM67 (transmembrane protein 67) (Baala et al., 2007), TMEM216 (Valente et al., 2006). The Meckel-Gruber syndrome (MKS) overlaps with the Joubert syndrome with regard to the phenotype and some of the mutated genes leading to the disease, such as RPGRIP1L. MKS is characterized by bone abnormalities, including polydactyly, neural tube defects, liver defects and cystic kidneys as a cause of an abnormal development (Waters and Beales, 2011).

Mutations of proteins that localize to primary cilia of tubular epithelial cells can provoke cystic diseases of the kidney. The ciliopathy nephronophthisis is an autosomal recessive renal disease, which is caused by mutations in the genes NPHP1-11, such as Nephroretinin (NPHP4) and Nephrocystin-3 (NPHP3) (Watnick and Germino, 2003; Wolf and Hildebrandt, 2011). It is distinguished by interstitial fibrosis and insufficiency of the kidney and tubular cysts. Type II nephronophthisis is caused by mutations in the gene encoding the ciliary protein Inversin (NPHP2) (Simons et al., 2005). Besides the serious renal cysts, this ciliopathy which is characterized by organ laterality defects such as *situs inversus*, can finally lead to a complete kidney failure (Otto et al., 2003). Associated with nephronophthisis is the Senior-Løken syndrome, a retinal-renal disorder, which is caused by mutations in NPHP1-5, NPHP6/CEP290 and NPHP10. The phenotype resembles to that of nephronophthisis, linked to retinal degeneration (Ellis et al., 1984; Tobin and Beales, 2009; Hildebrandt et al., 2011; Wolf and Hildebrandt, 2011; Ronquillo et al., 2012; Szymanska and Johnson, 2012). Furthermore, mutations in polycystin 1 and polycystin 2 lead to autosomal dominant polycystic kidney disease (ADPKD), and Cystin1 was found to be mutated in autosomal recessive polycystic kidney disease (ARPKD) in a mouse study (Watnick and Germino, 2003). Primary ciliary dyskinesia is another ciliopathy and patients show respiratory dysfunctions (Waters and Beales, 2011).

1.4 The intraflagellar transport system

Within the ciliary compartment, proteins are transported by the intraflagellar transport (IFT) system. This bidirectional movement was first observed in *Chlamydomonas reinhardtii* flagella by Kozminski, Beech and Rosenbaum (Kozminski et al., 1993). IFT is driven by the motor proteins heterotrimeric and homodimeric kinesin-2, which by direct binding move along the axonemal microtubules in anterograde or plus-end direction from the base to the tip (Cole et al., 1993, 1998, Kozminski et al., 1993, 1995; Orozco et al., 1999; Ou et al., 2005; Girotra et

al., 2017), and IFT dynein, which mediates the reverse movement in retrograde or minus-end direction. IFT dynein is also called cytoplasmic dynein 1b/2 due to its close relation to cytoplasmic dynein (Gibbons and Rowe, 1965; Rosenbaum and Witman, 2002; Scholey, 2003, 2008).

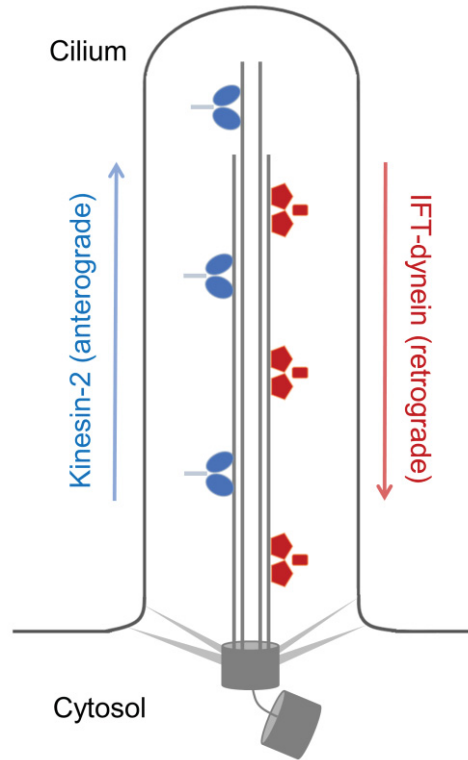


Figure 2: The intraflagellar transport (IFT) system regulates active transport within cilia. Kinesin-2 moves along the axonemal microtubules in anterograde direction from the ciliary base to the tip, whereas the retrograde transport is mediated by IFT-dynein.

Both IFT dynein and kinesin-2 are ATPases which couple adenosine triphosphate (ATP) hydrolysis to active transport of their cargo proteins (see also chapter 1.7). The motor proteins bind ATP and as a result of ATP hydrolysis to ADP and phosphate, the energy used for the movement is released. However, IFT dynein and kinesin-2 ATPases are members of distinct classes of enzymes. IFT dynein belongs to the AAA+ (ATPases associated with diverse cellular activities) ATPases, but kinesin-2 is supposed to have a guanine nucleotide-binding (G) protein (GNBP) common ancestor (Erdmann et al., 1991; Kull et al., 1996; Iyer et al., 2004; Mizuno et al., 2004) (see chapter 1.7 for G proteins). In cilia, speeds of retrograde directed IFT dynein driven movement range from 0.14 $\mu\text{m/s}$ to 5.60 $\mu\text{m/s}$ and velocities of heterotrimeric kinesin-2 driven movement vary between 0.20 $\mu\text{m/s}$ and 2.40 $\mu\text{m/s}$, depending on the analyzed organism and cilium type (Lechtreck, 2015). In cilia of IMCD3 cells, the main cell line used for this thesis, anterograde and retrograde IFT speeds in the range of 0.30 $\mu\text{m/s}$ to 0.63 $\mu\text{m/s}$

were observed (Besschetnova et al., 2009; Ye et al., 2013).

IFT dynein is a homodimer of heavy chains and interacting subunits (Mikami et al., 2002; Perrone et al., 2003; Roberts et al., 2013). In cilia, kinesin-2 occurs as heterotrimer, consisting of the subunits kinesin-2 α , kinesin-2 β and the kinesin associated protein (KAP) (Cole et al., 1993; Wedaman et al., 1996), and as homodimer, which was found in *Caenorhabditis elegans* as OSM-3 (osmotic avoidance defective 3)/Kif17 (kinesin-like protein 17) (Snow et al., 2004; Ou et al., 2005).

Two large IFT protein complexes interact with the motor proteins and in turn are linked to IFT cargo proteins. The IFT-A complex mediates the retrograde transport of ciliary proteins as it is associated to IFT dynein, whereas the IFT-B complex is associated to kinesin-2 and is involved in anterograde transport (Sung and Leroux, 2013). The IFT-A complex is composed of the six IFT particle proteins IFT 144, IFT 140, IFT 139, IFT 122, IFT 121 and IFT 43, whereas IFT-B is a much larger complex of sixteen proteins: IFT 172, IFT 88, IFT 81, IFT 80, IFT 74, IFT 70, IFT 57, IFT 56, IFT 54, IFT 52, IFT 46, IFT 38, IFT 27, IFT 25, IFT 22 and IFT 20 (Lechtreck, 2015; Taschner and Lorentzen, 2016). The IFT-A and IFT-B complexes also interact with each other and thereby build the so-called IFT particles, and several of these particles that are connected to kinesin-2 or IFT dynein build the IFT-trains, which can reach lengths of 100 nm to 700 nm in the *Chlamydomonas reinhardtii* flagellum (Pigino et al., 2009).

The cargo proteins that are transported via IFT are mostly membrane proteins, which are simultaneously attached to IFT complexes and the ciliary membrane (Qin et al., 2005; Nachury et al., 2010). Besides its function for the innerciliary protein transport, the IFT machinery is involved in the loading of IFT cargo into the cilium at the ciliary base (Jensen and Leroux, 2017). IFT particles were found to accumulate at transition fibers and in the transition zone (Yang et al., 2015) and IFT trains to queue at the base before entering the cilium (Wingfield et al., 2017). Furthermore, the IFT system participates in the assembly of cilia during ciliogenesis (see also chapter 1.5), where kinesin-2 transports subunits of axonemal tubulin, IFT dynein and IFT particles from the base to the tip, as shown in *Caenorhabditis elegans* (Rosenbaum and Witman, 2002; Qin et al., 2004; Hou et al., 2007; Pedersen et al., 2008; Silverman and Leroux, 2009; Scholey, 2012), and is important for the maintenance of cilia (Cole et al., 1998).

The BBSome, a large complex of at least eight BBS proteins found in the ciliary membrane and on centriolar satellites, is involved in the cilium-directed trafficking of membrane proteins (Nachury et al., 2007). It was shown that it assists in the assembly of IFT complexes in the basal body region, followed by BBSome binding to IFT particles that move in anterograde fashion inside cilia. The BBS protein complex moves with a speed similar to that of IFT. At the ciliary

tip, the BBSome controls the recycling of the IFT particles. Collectively, the BBSome is crucial for the regulation of IFT particle assembly and turnaround (Wei et al., 2012).

1.5 Ciliary assembly and disassembly

During the eukaryotic cell cycle, the cell undergoes four different stages, which are mitosis (M), gap 1 (G1), DNA synthesis (S) and gap 2 (G2) phases. G1, S and G2 phases are collectively termed interphase. In mitosis and subsequent cytokinesis, the nuclear DNA and the cytoplasm and thus the entire cell are divided. The cell grows during G1 phase, which acts as branching point, where the cell either passes to S phase or arrests in G1 phase and thereby leaves the cell cycle, which is then termed as G0 phase. Cells that are differentiated for a distinct function in the organism and thus do not undergo cell division anymore, arrest in this resting phase. During S phase, the DNA is replicated. When a cell enters the G2 phase, it is prepared for the subsequent cell division (Alberts et al., 2008).

Ciliogenesis of primary cilia is tightly coupled to the eukaryotic cell cycle. Therefore, ciliary assembly and disassembly are dynamically regulated (Doxsey et al., 2005; Nigg, 2006; Plotnikova et al., 2009). The mother centriole at the ciliary base is bifunctional. If an arrested cell is ciliated, the centriole builds the basal body, whereas it acts as microtubule-organizing center (MTOC) during cell division (Sánchez and Dynlacht, 2016). During the cell cycle, the primary cilium may appear with the entry to the G1/G0 phase and during this phase it will reach its maximal length. At first, the cilium starts to assemble by docking of the centrosome to the plasma membrane. In this process, the proteins ODF2 (outer dense fiber of sperm tails 2) and CEP164 (Centrosomal protein of 164 kDa) are associated to the distal tubulin appendages, that support the anchorage of the mother centriole to the plasma membrane, whereas the interaction between CEP290 and the vesicular transport regulatory GTPase Rab8a was shown to promote ciliogenesis. Also, the interaction of Rab8 with the BBSome promotes the biogenesis of the ciliary membrane (Nachury et al., 2007; Tsang et al., 2008; Plotnikova et al., 2009). During the growth process of the cilium, structural proteins for the axoneme were found to be localized on vesicles in the cytoplasm. Additionally, the IFT system is involved, as kinesin-2 transports vesicles from the trans-Golgi network along microtubules in the cytosol to the ciliary base, where these vesicles fuse with the cell membrane and the BBSome and IFT trains take over the axonemal proteins and transport them along the axoneme. Thereby, kinesin-2 supports the establishment of the axoneme and the extension of the microtubules that are connected to the mother centriole (Sorokin, 1968; Wei et al., 2012; Wood and Rosenbaum, 2014). The cilium

starts to disassemble in the end of G1/G0, shrinks and is mostly degraded during S/G2 phase. Thereby, the frequency of anterograde IFT movements is reduced, whereas the retrograde transport is enhanced. In the end of G2 phase, the remaining shrunk axoneme is internalized with the mother centriole, and at the onset of mitosis, the ciliary membrane which is attached to the mother centriole is endocytosed. During mitosis, this membrane persists at one of the spindle poles and remains asymmetrically at one daughter cell. The mother centriole again functions as MTOC in mitotic spindle formation for the next cycle. After completion of cell division, both daughter cells may rebuild cilia, and the daughter cell with the remaining ciliary membrane can do this earlier. Taken together, the centriole's oscillation between the function as MTOC or as basal body is usually coupled to cilium growth in cells before mitosis in G1 or G0, and later to a shrinking of the cilium before the cell enters mitosis (Sorokin, 1968; Archer and Wheatley, 1971; Fonte et al., 1971; Tucker and Pardee, 1979; Pan and Snell, 2007; Plotnikova et al., 2009; Paridaen et al., 2013; Sánchez and Dynlacht, 2016).

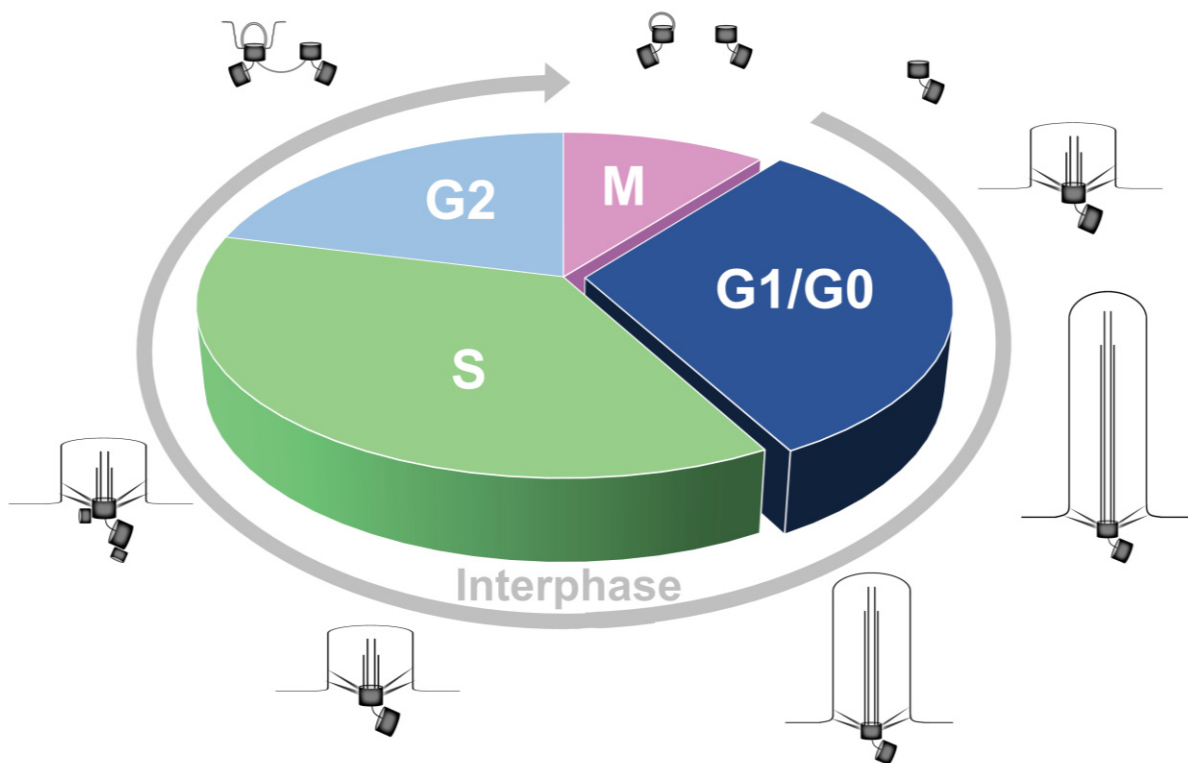


Figure 3: Ciliogenesis and ciliary disassembly are tightly coupled to the eukaryotic cell cycle. The cilium is built in the G1/G0 phase, where the axoneme nucleates from the mother centriole that builds the basal body, and the cilium reaches its entire length. In the end of G1/G0 phase, ciliary disassembly starts. During S phase, the cilium is mostly disassembled. In G2 phase, the remaining shortened axoneme is internalized with the basal body. At the beginning of mitosis (M), the ciliary membrane is endocytosed and remains at one spindle pole, and the centrioles are duplicated. The cell with the duplicated centrioles is divided in mitosis and the daughter cells may rebuild cilia. Modified from Paridaen et al., 2013, and Sánchez and Dynlacht, 2016.

1.6 Regulation of ciliary entry

Although the cilium is topologically a cellular membrane protrusion, the lipid composition of the ciliary membrane differs significantly from that of the plasma membrane (Rohatgi and Snell, 2010; Garcia-Gonzalo et al., 2015). Also, the ciliary lumen is densely packed with proteins, partly post-translationally modified, and a few proteins are enriched several thousand-fold in the cilium, in levels different from the protein composition in the cytosol. There is no ribosomal protein synthesis inside the cilium and the proteins carry their post-translational modification before entry (Bloodgood, 1984; Ostrowski et al., 2002; Pazour et al., 2005). Obviously, the cilium is an independent cellular compartment and enables cellular processes on a highly regulated level due to this compartmentalization (Nachury, 2014).

Protein entry to and exit from the ciliary compartment are strictly regulated by the ciliary gate that separates the ciliary lumen from the cytosol. It was first discovered at the flagellum of *Chlamydomonas reinhardtii*, where it was also called flagellar pore complex. The flagellar pore complex was described to exclude vesicles from the cilium, prevent the diffusion of membrane proteins from the plasma membrane to the ciliary membrane, selectively regulate protein entry and facilitate intraciliary protein retention (Rosenbaum and Witman, 2002). The ciliary gate does not completely separate the cilium from the cell body by a membrane, but restricts access to the ciliary lumen by basal body and transition zone associated proteins and transition fibers, and thus regulates the transport of mainly membrane but also soluble proteins between the compartments, allowing control over cilia-associated signaling pathways (Nachury et al., 2010; Hu and Nelson, 2011; Williams et al., 2011; Jensen et al., 2015; Jensen and Leroux, 2017). In the transition zone, the NPHP-JBTS-MKS protein network and the proteins RPGRIP1L and TCTN2 (Tectonic-2) are localized. CEP290 is located between the MKS and NPHP protein modules and the basal body, whereas CEP164 is found at the transition fibers (Yang et al., 2015). Moreover, the transition zone was also described as ciliary zone of exclusion (CIZE), which, besides its function as gate for ciliary proteins, might act as a lipid gate by restricting the amount of the phosphoinositide PI(4,5)P₂ inside the ciliary compartment (Jensen et al., 2015) (see chapter 1.14 for phosphoinositides). Thus, the CIZE might be involved in the regulation of the ciliary membrane composition, that differs from the plasma membrane.

Different studies of diverse organisms describe that the ciliary gate functions as a diffusion or sieve-like barrier which excludes proteins above certain size limits, depending on the analyzed model organism (Lin et al., 2013). Small-sized proteins are described to move freely by diffusion between cell body and cilium across the ciliary transition zone. A general size limit

cannot be defined, as it shows distinct variations between different kinds of cilia. Calvert et al. and Najafi et al. reported free diffusion of triple GFP with a size of 81 kDa through the connecting cilium of rod photoreceptors (Calvert et al., 2010; Najafi et al., 2012). Another study showed free entry into the cilium of RPE1 cells for proteins smaller than 10 kDa and restriction above 40 kDa (Kee et al., 2012). However, it was shown in a study using IMCD3 cells that proteins larger than approximately 100 kDa are restricted from entering cilia, determined in live cell experiments. In this study it was revealed that passive diffusion of proteins decreases sharply with increasing size, indicating the sieve-like behavior of the ciliary transition zone (Breslow et al., 2013). Therefore, ciliary proteins larger than the limit for free diffusion require active transport processes to enter cilia. Nevertheless, not every small protein just diffuses through the ciliary gate but needs additional features for ciliary entry. Also, ciliary proteins have special characteristics to be recognized as such. Import and also retention of proteins to and within the cilium are highly regulated and determined by various apparently unrelated ciliary targeting sequences (CTS) suggesting a number of different molecular mechanisms for entry into the compartment (Nachury et al., 2010). A number of studies about ciliary proteins were conducted to uncover these sequences and the protein-protein interactions by which they are recognized. However, no unique consensus was found for CTS and their amino acid sequences show high variations. For example, a VxP (V = valine, x = any amino acid, P = proline) motif was found as C-terminal SSSQVSPA (S = serine, Q = glutamine, A = alanine) motif in rhodopsin (Tam et al., 2000), as C-terminal KVHPST (K = lysine, H = histidine, T = threonine) motif in polycystin-1 (Ward et al., 2011) and as N-terminal RVxP (R = arginine) motif in polycystin-2 (Geng et al., 2006), whereas Cystin1 contains an N-terminal AxEGG (E = glutamate, G = glycine) motif as CTS (Tao et al., 2009). For some ciliary GPCRs, an AxS/AxQ motif was determined to regulate the ciliary targeting of Sstr3 (Somatostatin receptor 3), Htr6 (serotonin receptor 6) and Mchr1 (melanin-concentrating hormone receptor 1), whereat Sstr3 and Htr6 additionally require the cytoplasmic loop 3 to localize to cilia (Berbari et al., 2008; Jin et al., 2010). For other proteins, larger sequences were shown to be responsible for ciliary localization, such as the 193 last C-terminal amino acid residues of fibrocystin (Follit et al., 2010) or the 201 N-terminal residues of NPHP3 (Nakata et al., 2012).

Moreover, post-translational modifications (see also chapter 1.8) such as different lipidations were shown to be involved in the sorting or retention of ciliary proteins. For instance, the myristoylation of the ciliary proteins NPHP3 and Cystin1 (Tao et al., 2009; Wright et al., 2011; Jaiswal et al., 2016), the dipalmitoylation of rhodopsin and fibrocystin (Tam et al., 2000; Follit et al., 2010) and Arl13B (Cevik et al., 2010; Li et al., 2010), and the farnesylation of INPP5E

were shown to be essential for a correct ciliary localization (Jacoby et al., 2009; Thomas et al., 2014; Fansa et al., 2016; Kösling et al., 2018) (More details about INPP5E and NPHP3 ciliary localization will be discussed in the chapters 1.14 and 1.15). Collectively, the precise targeting and retention mechanisms of ciliary proteins are diverse and despite the described insights, their trafficking into the ciliary compartment is a complex process and is as yet not fully understood.

1.7 Guanine nucleotide-binding proteins

Guanosine-5'-triphosphate (GTP) and adenosine-5'-triphosphate (ATP) play highly important roles in biological processes. The nucleoside triphosphates have very different functions. ATP is responsible for the storage and delivery of energy in the cell. This energy is released in the hydrolysis reactions of one of its phosphoanhydride bonds and is used in enzymatic reactions for cell metabolism. ATP hydrolysis provides the energy which is needed for intracellular movement processes driven by various motor proteins, such as kinesin, myosin or dynein. Moreover, ATP is used in intracellular regulation processes for phosphorylation reactions. However, the hydrolysis of GTP is mainly, with some exceptions, used in regulatory processes in the cell that are driven by guanine nucleotide-binding (G) proteins (GNBPs) and is not related to energy consuming procedures (Westheimer, 1987; Kjeldgaard et al., 1996; Sprang, 1997; Vetter and Wittinghofer, 2001; Wittinghofer, 2016). Some proteins that hydrolyze ATP are structurally related to G proteins, and both protein classes share structural similarities during their mode of action (Leipe et al., 2002; Mueller and Goody, 2016).

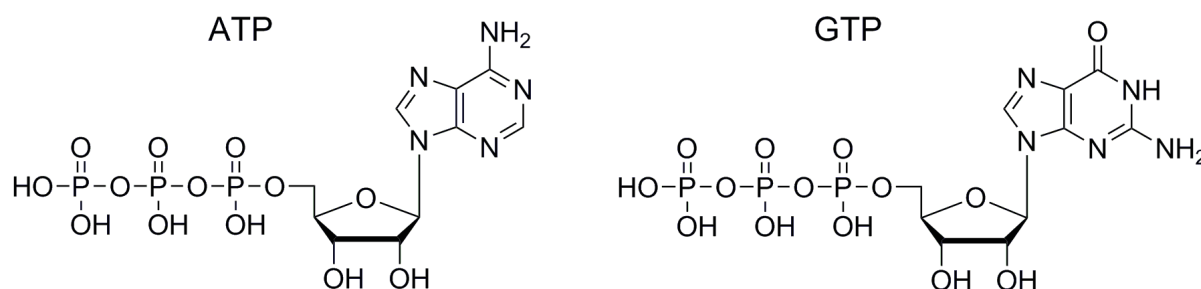


Figure 4: The nucleotides adenosine triphosphate (left) and guanosine triphosphate (right) share a similar structure, consisting of a ribose carbohydrate, three connected phosphate groups and the nucleobase, either adenosine or guanosine. All chemical structures in this thesis were drawn with ChemDraw Professional 17.0.

In 1994, Alfred Gilman and Martin Rodbell received the Nobel prize in medicine for the discovery of G proteins and their mode of action. G proteins play essential roles in trafficking and signal transduction pathways in eukaryotic cells, where they function in the control of the humoral immune response, the neural system and developmental processes, such as transduction of growth signals (Bourne et al., 1990, 1991; Simon et al., 1991). G proteins are subdivided in different classes, which are the dynamin (Obar et al., 1990) and septin family (Field et al., 1996), the translation factors (Qin et al., 2006), the signal recognition particle (SRP) and SRP receptor (SR) family (Walter, 1994; Freymann et al., 1999; Montoya et al., 2000), the heterotrimeric G proteins (Simon et al., 1991) and the Ras (rat sarcoma) superfamily

(Pai et al., 1989; Reuther and Der, 2000; Leipe et al., 2002; Wittinghofer and Vetter, 2011).

The Ras superfamily of small GTPases was named after the Ras protein that was discovered in 1979 and found to be a phosphoprotein and to be encoded by retroviral oncogenes from the Harvey and Kirsten murine sarcoma viruses (Ha/Ki-MuSV) (Shih et al., 1979). Two years later, the origin of these oncogenes was shown in vertebrate genes which were called H-Ras and K-Ras (Ellis et al., 1981). Members of the Ras superfamily in most cases have a molecular weight between 21 kDa and 30 kDa and are classified into the subfamilies Ras, Rab (Ras-related in brain), Rho (Ras homolog), Arf (ADP-ribosylation factor), Rad (Ras associated with diabetes), Ran (Ras-related nuclear protein) and Rag (Ras-related GTPase) (Bourne et al., 1990; Cox and Der, 2010).

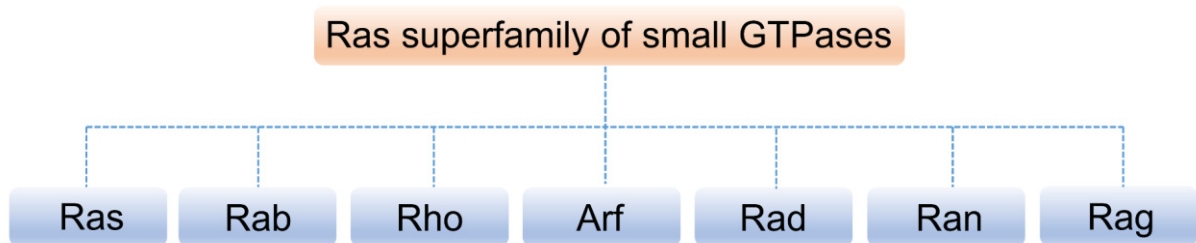


Figure 5: The Ras superfamily of small GTPases is subdivided into the subfamilies Ras, Rab, Rho, Arf, Rad, Ran and Rag, each of which comprises various members.

Being crucial during processes of development and proliferation, the Ras protein isoforms K-Ras, H-Ras and N-Ras play an important role in the formation of cancer. Oncogenic Ras mutants were discovered in approximately 30 % of various tumors in humans (Bos, 1989; Gremer et al., 2008). Characteristic of G proteins is their function as molecular switches in signal transduction pathways (Milburn et al., 1990). Their functional cycle is highly regulated on the cellular level. In response to cellular signals, such as extracellular growth factors binding to cell surface receptors, G proteins switch between an inactive guanosine-5'-diphosphate (GDP)-bound to an active guanosine-5'-triphosphate (GTP)-bound state (Boguski and McCormick, 1993; Vetter and Wittinghofer, 2001). During this activation of the G protein, the bound GDP is exchanged against GTP. The molecular switch mechanism allows the cell to react specifically to the cellular signals as the G protein in its active GTP-bound state interacts with various downstream effectors in diverse signal transduction cascades, thereby transferring the signal, initiating and regulating effects in the cell such as differentiation, cell proliferation, nuclear and vesicular transport (Wittinghofer and Herrmann, 1995; McCormick and Wittinghofer, 1996; Vetter and Wittinghofer, 2001).

The G protein is switched off by hydrolysis of the bound GTP to GDP and inorganic phosphate, thus this reaction is termed a GTPase. If the deactivation of the G protein is defective, this may lead to cancer formation. Numerous G proteins are intrinsically active, but the GTPase reaction is a relatively slow reaction. For instance, the GTP hydrolysis rate of Ras is $4 \times 10^{-4} \text{ s}^{-1}$ (Neal et al., 1990; Wittinghofer, 2016). Nevertheless, a regulated GTPase reaction is mediated through catalysis by GTPase-activating proteins (GAPs), which increase the GTPase reaction by several orders of magnitude. GAPs bind specifically to the GTP-bound form of the G protein and enable a controlled switch off reaction to retransfer the G protein to the inactive state and interrupt the signal transduction cascade. In detail, GAPs increase the hydrolysis rate by stabilization of the G protein's catalytic center in the transition state, where a nucleophilic water molecule is exactly positioned to attack the γ -phosphate of the bound GTP, enabling GTP hydrolysis. Two main residues, glutamine and arginine, take part in GTP hydrolysis (Mishra and Lambright, 2016). In Ras, a conserved glutamine is responsible to locate the water molecule (Bourne et al., 1990, 1991; Wittinghofer et al., 1997; Vetter and Wittinghofer, 2001; Bos et al., 2007). RasGAPs position the so-called arginine-finger in trans into the active center of the G protein. Thereby, the catalytic glutamine is stabilized and the temporary negative charge of the transition state is neutralized by the positive charge of the arginine (Ahmadian et al., 1997; Rittinger et al., 1997; Scheffzek et al., 1997; Wittinghofer et al., 1997; Nassar et al., 1998; Vetter and Wittinghofer, 2001; Bos et al., 2007). The slow intrinsic GTPase reaction of Ras is around 100-fold reduced in oncogenic mutants. These mutants are constitutively activated and cannot be down-regulated by RasGAPs (Ahmadian et al., 1999). The GAP mechanism is variable for different members of the Ras subfamily. For instance, GAPs of the Ras subfamily members Rap (Ras-related protein) and Rheb (Ras homolog enriched in brain) use a catalytic asparagine, the so-called asparagine-thumb, instead of an arginine and do not possess the catalytic glutamine residue (Daumke et al., 2004; Scrima et al., 2008). Also, RanGAP catalyzes the hydrolysis of Ran-bound GTP without participation of the arginine-finger, only the catalytic glutamine is involved in the hydrolysis mechanism (Seewald et al., 2002).

Complementary to GTP hydrolysis, the exchange of GDP to GTP to reactivate the G protein is intrinsically slow and is thereby catalyzed by guanine-nucleotide exchange factors (GEFs). GEFs stimulate the dissociation of the GDP that is bound to the G protein and increase the nucleotide dissociation. The GEF mechanism consists of several steps, which are fast and reversible. First, the G protein is in a binary complex with the nucleotide. Secondly, when the GEF reaches the GDP-bound G protein, GEF, G protein and GDP form a trimeric complex and ultimately, GDP leaves the complex and a binary complex of G protein and GEF is formed.

This binary complex, in which the G protein is nucleotide-free, is more stable when the nucleotide is absent. The GTP concentration in the human cell is approximately tenfold higher with respect to the GDP concentration, with values of 305 μM GTP and 36 μM GDP. Due to the higher cellular GTP concentration, the nucleotide-free G protein binds preferentially to GTP and the GEF dissociates. Generally, the GEF as a catalyst accelerates the dissociation of GDP and thus supports the establishment of an equilibrium between the GDP- and the GTP-bound form of the G protein (Traut, 1994; Klebe et al., 1995; Lenzen et al., 1998; Vetter and Wittinghofer, 2001; Bos et al., 2007).

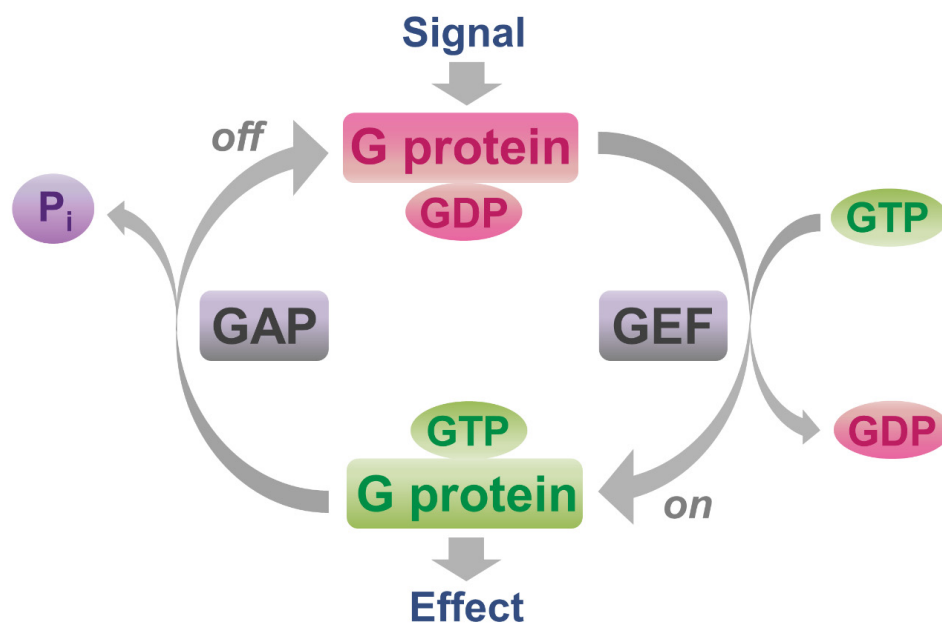


Figure 6: G proteins act as molecular switches and cycle between an inactive GDP- and an active GTP-bound state. During the switch on reaction due to extracellular signals, guanine-nucleotide exchange factors (GEFs) catalyze the exchange of the bound GDP against GTP and the activated G protein transmits the cellular signal to effector proteins. The GTPase and switch off reaction is catalyzed by GTPase-activating proteins (GAPs).

The G domain is the core of most G proteins, in the molecular switch reaction it binds and hydrolyzes the guanine nucleotide. Its structure is highly conserved, and it has a molecular weight of approximately 20 kDa. The G domain is composed of three layers, it has a mostly parallel β sheet with six strands that is surrounded by five α -helices (Schweins and Wittinghofer, 1994; Vetter and Wittinghofer, 2001; Wittinghofer and Vetter, 2011). A magnesium ion (Mg^{2+}) interacts with the phosphate residues of the guanine nucleotide. Ras superfamily proteins exhibit five canonical G motifs in the G domain, G1 to G5 (Vetter and Wittinghofer, 2001; Wittinghofer and Vetter, 2011). The G motifs have a highly conserved structure and function in nucleotide and magnesium ion binding. The G1 motif, which is called

the phosphate-binding (P) loop (Saraste et al., 1990) or Walker A motif, was described by John Walker in 1982 (Walker et al., 1982). The P loop links an α -helix and a β -strand and surrounds the negatively charged phosphate groups of the guanine nucleotide. It contains the GxxxxGKS/T motif. The conserved lysine (K) binds via its positively charged residue the negatively charged β - and γ -phosphates of the nucleotide and thereby neutralizes the negative charge (Saraste et al., 1990).

The G2 and G3 motifs are built by the two switch regions, switch I and switch II. Switch I (G2) contains a conserved threonine, whereas the switch II (G3) motif includes the DxxGq/h (D = aspartate, q = glutamine, h = histidine) sequence motif. The switch domains participate in effector binding. The conserved threonine of switch I and the glycine (G) of the DxxGq/h sequence of switch II interact with the γ -phosphate of the bound GTP via the amino groups of the main chain by building hydrogen bonds. During GTP hydrolysis, the γ -phosphate is then separated from the nucleotide (Milburn et al., 1990). Consequently, the switch regions change their positions to the more relaxed GDP conformation and this nucleotide state dependent mechanism is called loaded spring mechanism (Vetter and Wittinghofer, 2001).

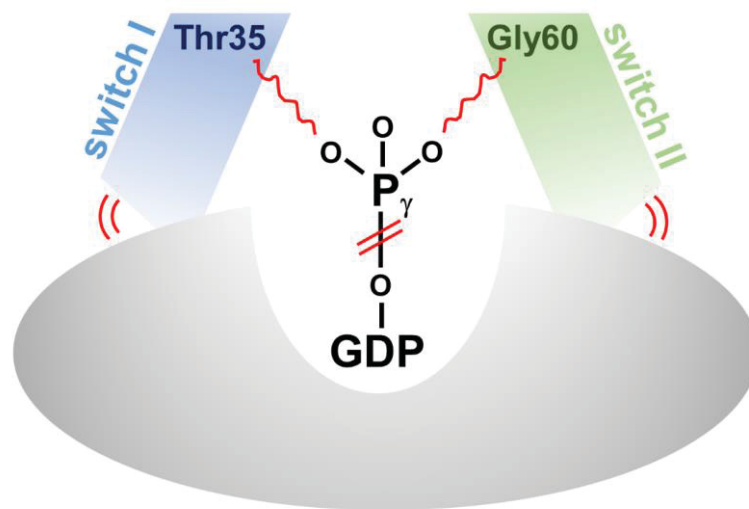


Figure 7: The canonical switch mechanism can be described with a loaded spring model. The main chain amino groups of the invariant residues threonine (Thr35 in Ras) of switch I and glycine (Gly60 in Ras) of switch II mediate the binding of the γ -phosphate of GTP that is bound to the G protein. This state is called loaded spring. After GTP hydrolysis, the γ -phosphate is released, and this leads the switch regions to engage a more relaxed conformation. Modified from Vetter and Wittinghofer, 2001.

The G4 motif is characterized by an N/TKxD (N = asparagine) sequence, the G5 motif with the sAk (s = serine, k = lysine) sequence contains a conserved alanine (A). The G4 and G5 motifs are involved in the guanine base binding, where the high specificity for guanine is ensured by

the aspartate (D) residue of the N/TKxD motif by building a fork-like hydrogen bond to guanine (Vetter and Wittinghofer, 2001; Wittinghofer and Vetter, 2011).

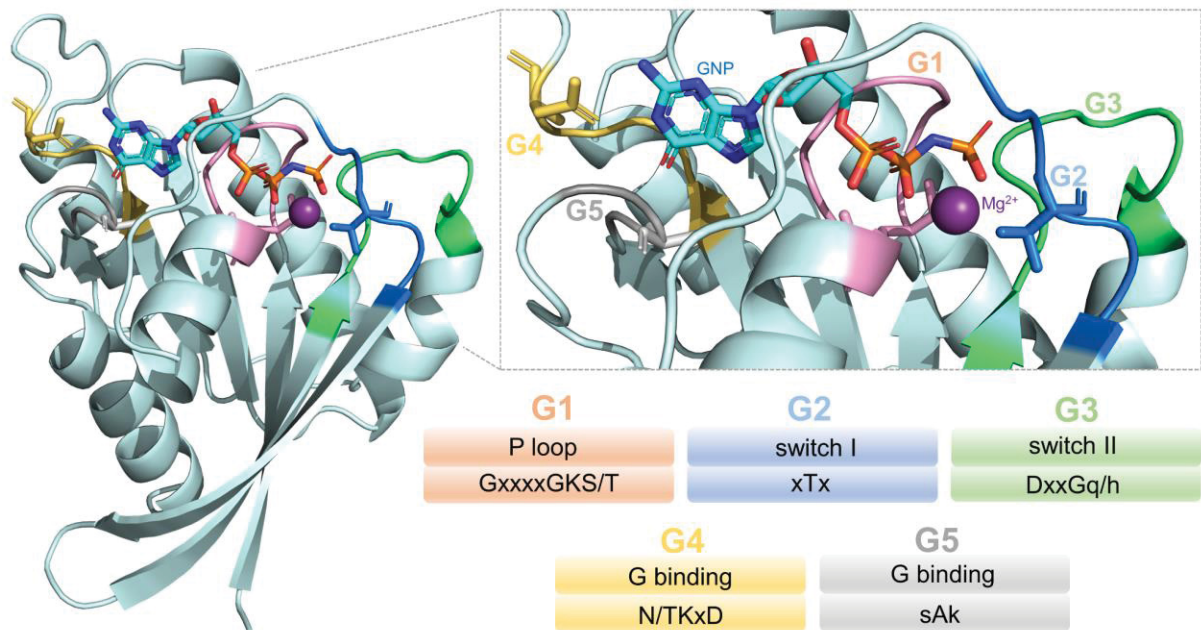


Figure 8: H-Ras with bound GppNHp (GNP), a non-hydrolysable GTP analog, and a magnesium ion (Mg^{2+}) (violet), 1.35 Å resolution crystal structure, PDB: 5P21 (Pai et al., 1990). The G domain of Ras superfamily members contains five canonical G motifs, G1-G5. The P loop has a conserved GxxxxGKS/T sequence motif (G1) (pink), switch I a conserved threonine (G2) (blue), switch II the DxxGq/h motif (G3) (green), and G4 (yellow) and G5 (grey) have an N/TKxD or sAk motif, respectively. H-Ras structure illustration was modified from Wittinghofer and Vetter, 2011. All protein structures shown in this thesis were illustrated using PyMOL.

1.8 Post-translational modifications of small G proteins

Several small Ras-like GTPases are post-translationally modified. This is essential for their full functionality, which is coupled to their cellular localization. After ribosomal synthesis, the soluble proteins receive their post-translational modifications (PTMs) either at their C- or N-termini. Due to lipid modifications, they interact with membranes in the cell that are their final or intermediate destinations (Seabra, 1998). The regulation of Ras localization at membranes is a critical step in the biological function of the G protein (Chandra et al., 2012; Schmick et al., 2014, 2015). For example, members of the Ras, Rab and Rho subfamilies possess C-terminal prenylations, such as farnesyl (C_{15} carbohydrate chain) or geranylgeranyl (C_{20}) isoprenoids (Casey et al., 1989; Hancock et al., 1989; Farnsworth et al., 1991; An et al., 2003; Cherfils and Zeghouf, 2013; Resh, 2013). Besides prenylation, G proteins can be modified by an acyl chain (Carr et al., 1982; Aitken and Cohen, 1984; Wilson and Bourne, 1995; Resh, 1996). There are

two major types of acylation, which are the N-terminal myristoylation (C_{14}), that is characteristic for proteins of the Arf family and occurs on a glycine residue at position 2 (Gallego et al., 1992), or the palmitoylation (C_{16}) on cysteines of Ras and Rho proteins (Hancock et al., 1989; Resh, 1996).

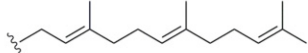
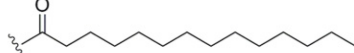
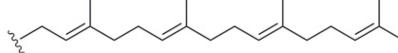
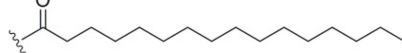
Prenylation	Acylation
Farnesyl (C_{15}) 	Myristoyl (C_{14}) 
Geranylgeranyl (C_{20}) 	Palmitoyl (C_{16}) 

Figure 9: G proteins can be post-translationally modified, for example by a C-terminal prenylation, which can be a farnesylation or geranylgeranylation on cysteines, or by an N-terminal acylation, comprising myristoylation on glycines or palmitoylation on cysteines.

Proteins which become prenylated have a CaaX (C = cysteine, a = aliphatic amino acid, X = any amino acid) sequence at their C-terminus, the CaaX box, where the cysteine is prenylated. The residue X determines if the protein is farnesylated or geranylgeranylated. Processing of the CaaX box comprises three steps, carried out by different enzymes. Farnesyltransferase couples the farnesyl moiety from farnesylpyrophosphate, an intermediate from the cholesterol biosynthesis, to the sulfhydryl group of the cysteine by building a stable thioether bond (Casey et al., 1989; Seabra et al., 1991), or geranylgeranyltransferase I attaches the geranylgeranyl modification (Finegold et al., 1991). An endoprotease removes the -aaX sequence (Boyartchuk et al., 1997) and a carboxyl methyltransferase adds a methyl group to the before prenylated cysteine (Dai et al., 1998; Ahearn et al., 2012).

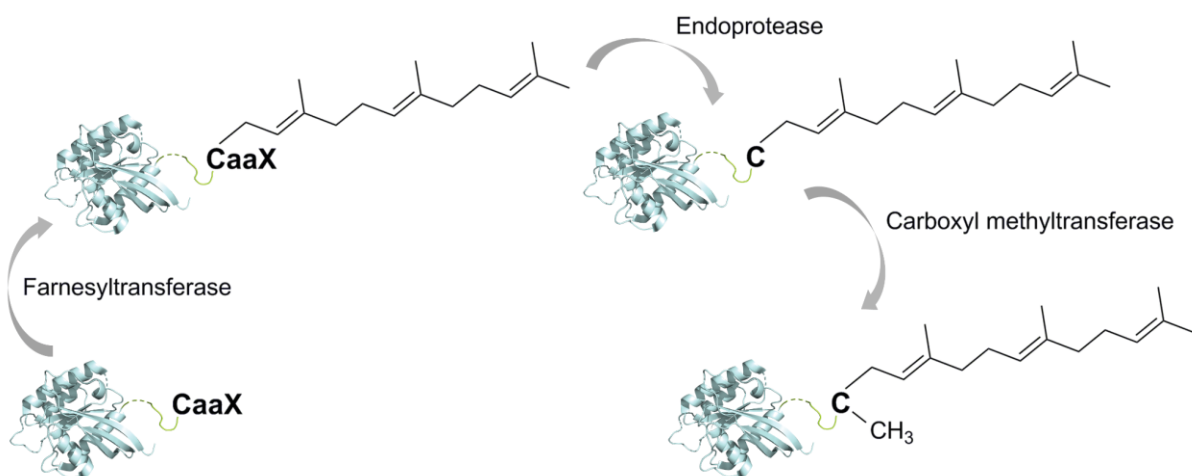


Figure 10: CaaX box processing takes place in three steps, in which either a farnesyl or a geranylgeranyl anchor is added to the C-terminus of the G protein. First, either farnesyltransferase couples a farnesyl moiety to the

cysteine of the CaaX box, or geranylgeranyltransferase I, attaches the geranylgeranyl modification. Secondly, an endoprotease removes the -aaX sequence and then a carboxyl methyltransferase adds a methyl group to the prenylated cysteine residue. Protein structure shows Rheb as example, PDB: 3T5G (Ismail et al., 2011).

1.9 ADP-ribosylation factor like (Arl) proteins and the interswitch toggle

ADP-ribosylation factor (Arf) like (Arl) proteins belong to the Arf subfamily of the Ras superfamily. The cellular functions of Arf/Arl proteins are diverse and unclear in many cases, some are implicated in cytoskeleton organization or intermembrane traffic. As G proteins, Arls act as molecular switches by cycling between the active GTP-bound and the inactive GDP-bound state (Vetter and Wittinghofer, 2001; Gillingham and Munro, 2007; Cox and Der, 2010). As members of the Ras superfamily, Arls share the key characteristics of the conserved conformational switch motif. However, in detail Arf and Arl proteins differ remarkably from other Ras superfamily members in the structure of the interswitch region, which is mobile instead of static. In the off state, the interswitch region, which is built by two β -strands between switch I and switch II, is arranged in a retracted position. Thereby, the conserved aspartate of the DxxGQ motif of switch II is located in such a way, that it mimics the negative charges of the γ -phosphate of GTP, so that GTP binding is hindered. Additionally, the N-terminal helix is located adjacently to the protein surface in the GDP-bound state (Pasqualato et al., 2002). However, in the active conformation, where GTP can be bound, the interswitch β -sheets protrude from the protein surface and drift towards the N-terminal helix via a distance of two residues and the helix consequently kinks out. Thereby, the interswitch drags the switch I and switch II regions towards the helix, GTP enters the binding pocket and the pocket is closed (Goldberg, 1998; Pasqualato et al., 2001). This movement is called interswitch toggle and facilitates a transmission between the membrane-directed N-terminus and the nucleotide binding site, that are positioned at opposite sides of the protein, and thereby mediates a front-back communication (Pasqualato et al., 2002). In the cell, the nucleotide loading state and thus the position of the N-terminal helix may determine if the protein is cytosolic or membrane-bound. For instance, myristoylated Arf1 in its GDP-bound form is predominantly soluble, whereas Arf1•GTP is recruited to membranes, where the membrane interaction is thought to be mediated by the hydrophobic side of the amphipathic helix (Antonny et al., 1997; Goldberg, 1998).

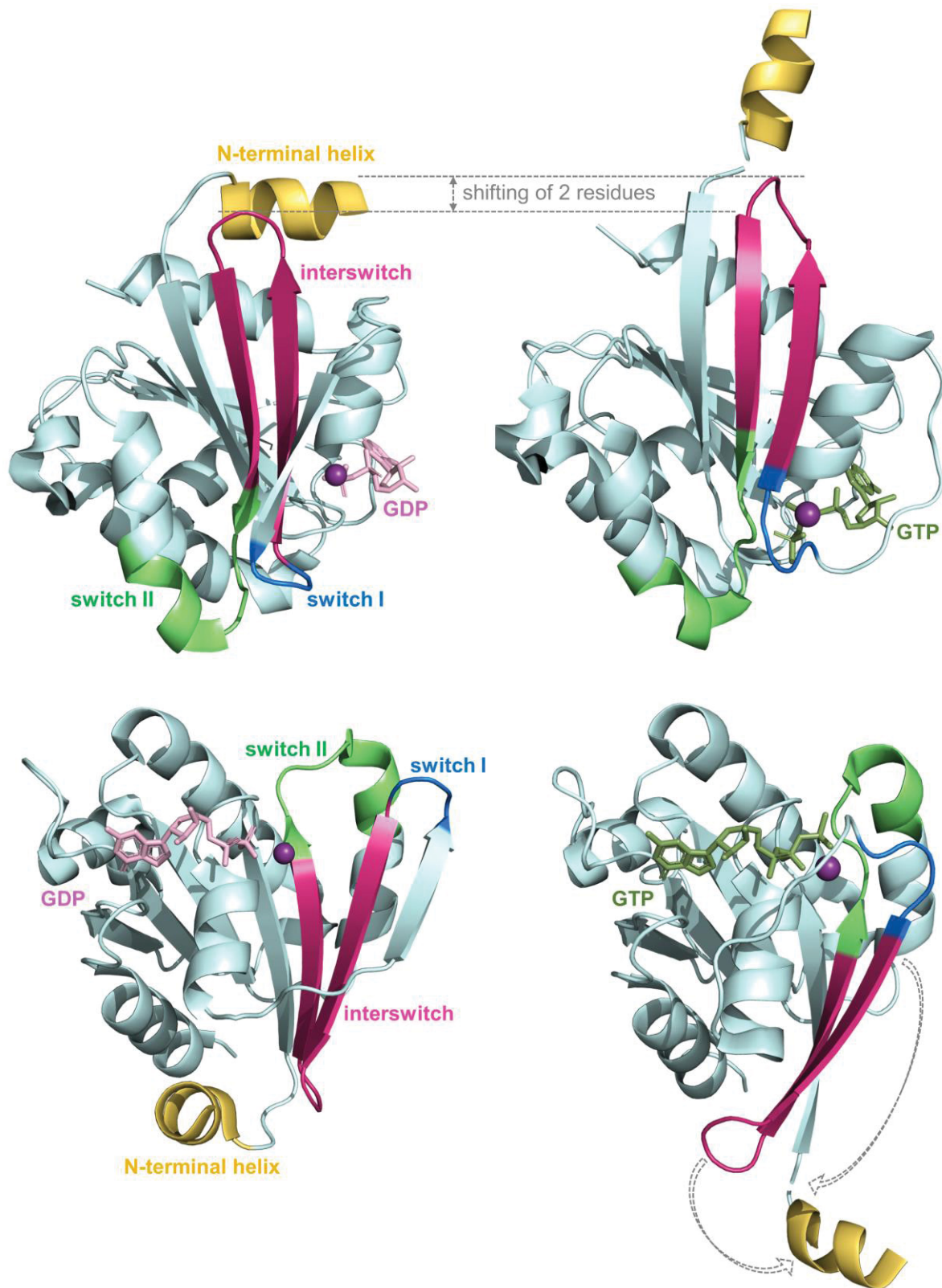


Figure 11: Interswitch toggle of Arf and Arl proteins, shown in two different orientations (lower/upper panel) exemplary for Arf6•GDP (left), PDB: 1E0S (Menetrey et al., 2000) and Arf6•GTP (right), PDB: 2J5X (Pasqualato et al., 2001). The N-terminal helix (yellow) was complemented manually in the structure of Arf6•GTP. In the GDP-bound form, the N-terminal helix stays close to the protein surface, whereas the helix kinks out in the GTP-bound state due to a two residue shifting of the interswitch β-sheets (pink) towards the helix. The interswitch pulls switch I and switch II towards the N-terminal helix and the binding pocket with GTP is closed. Modified from Pasqualato et al., 2002 (upper panel) and Gillingham and Munro, 2007 (lower panel).

1.10 Arl2 and Arl3 and the ciliary Arl3•GTP compartment

The homologous Arf-like proteins Arl2 and Arl3 share a similar structure, exhibiting a sequence identity of approximately 52 % and a sequence similarity of 68 %. Despite their similarity, Arl2 and Arl3 show significant differences in their cellular localization and thus their effects in the cell. Arl3 localizes to cilia and cytosol, whereas Arl2 is excluded from cilia (Avidor-Reiss et al., 2004; Lokaj et al., 2015). By immunofluorescence microscopy it was shown that Arl3 localizes to the connecting cilium of rod and cone photoreceptor cells (Grayson et al., 2002) and to primary cilia of NIH/3T3 cells (Zhou et al., 2006), as well as to cilia of IMCD3 cells, shown by GFP and immunofluorescence (Lokaj et al., 2015). The exact structural details, which determine the localization of Arl3 to the cilium but prohibit ciliary entry of Arl2, remain unclear. However, it was found that the N-terminal amphipathic helix of Arl3 is essential for its ciliary localization (Lokaj et al., 2015).

Common characteristics of Arf proteins are their ability of phospholipase D activation and an N-terminal myristoylation. However, Arl2 and Arl3 features differ from those of most other Arf family members due to a lack of myristoylation, although they possess the required N-terminal glycine 2, and their incapacity for activation of phospholipase D (Hong et al., 1998; Sharer et al., 2002). Arl3 plays important roles in cilia function during photoreceptor and renal development and it was shown that Arl3 knockout mice are embryonic lethal or the embryos die during early postnatal development (Schrack et al., 2006; Hanke-Gogokhia et al., 2016). Furthermore, a specific deletion of Arl3 in rod photoreceptors leads to rod degeneration and subsequent cone defects in the retina with a phenotype similar to that of retinitis pigmentosa, while retina-specific Arl3 knockout causes simultaneous rod and cone degeneration, similar to cone-rod dystrophy (Hanke-Gogokhia et al., 2016). Arl3 was implicated to be involved in ciliogenesis, as shown for the *Leishmania donovani* Arl3 ortholog ARL-3A (Cuvillier et al., 2000). Moreover, Arl3 can be associated to microtubules, was found at centrosomes in non-ciliated cells and was implicated to be involved in a correct progression of the cell cycle (Zhou et al., 2006). Arl2 apparently has different functions from Arl3. It binds to the tubulin folding chaperone cofactor D and thereby participates in the regulation of cofactor D. Cofactor D is involved in the formation of α,β -tubulin dimers before polymerization (Bhamidipati et al., 2000; Shern et al., 2003).

Arl3, Arl6 and Arl13B are the only known ciliary G proteins (Cuvillier et al., 2000; Avidor-Reiss et al., 2004; Caspary et al., 2007). Because Arl3, in contrast to Arl2, is a ciliary G protein, it is more in the focus of this work. The function of Arl3 as molecular switch is regulated by a

the only known Arl3-GAP RP2 (Veltel et al., 2008a) and the recently identified GEF Arl13B (Gotthardt et al., 2015). RP2 is also involved in the ciliopathy retinitis pigmentosa (Schwahn et al., 1998), whereas Arl13B (encoded by the JBTS8 gene) mutations lead to Joubert syndrome (Cantagrel et al., 2008; Su et al., 2012). Arl13B was reported to regulate cilia formation in *Caenorhabditis elegans* (Li et al., 2010) and is an atypical member of the Arf family because of its unique architecture, consisting of an N-terminal short helix which can be palmitoylated at two cysteine residues, followed by the G domain, an α -helical coiled-coil domain and a C-terminal proline-rich domain (Hori et al., 2008). The unusual and special feature of Arl13B being a GEF for Arl3 is that Arl13B is a G protein itself. The G domain and a C-terminal helix of Arl13B are responsible for the GEF activity, whereby the switch I and switch II regions mediate the interaction with Arl3. It was shown that mutations of Arl13B that were identified in Joubert syndrome patients compromise its activity as GEF and as a consequence, the activation of Arl3 is also reduced (Gotthardt et al., 2015). Arl13B exclusively localizes to cilia (Casparly et al., 2007; Cantagrel et al., 2008; Hori et al., 2008). Thus, the ciliary compartment can be characterized as an Arl3•GTP domain (Gotthardt et al., 2015; Fansa and Wittinghofer, 2016). This model is in agreement with the observation that RP2 is excluded from cilia and was shown to localize to the cytosol and to accumulate in the cytosolic basal body close region (Grayson et al., 2002; Blacque et al., 2005; Evans et al., 2010; Lokaj et al., 2015).

1.11 Effectors of Arl2 and Arl3

Shared Effectors of Arl2 and Arl3, which specifically interact with their active GTP-bound form, are BART (Binder of Arl2)/Arl2BP (Arl2 binding protein) (Sharer and Kahn, 1999; Veltel et al., 2008b; Zhang et al., 2009), and the homologous proteins PDE6 δ (delta subunit of phosphodiesterase 6)/PrBP (prenyl binding protein) (Linari et al., 1999; Hanzal-Bayer et al., 2002), HRG4 (human retina gene 4)/Unc119a (uncoordinated), and Unc119b (Van Valkenburgh et al., 2001; Kobayashi et al., 2003; Wright et al., 2011; Jaiswal et al., 2016). BART binds to Arl2•GTP, but also to Arl3•GTP, and was found in mitochondria, where it binds the adenine nucleotide transporter (Sharer and Kahn, 1999; Sharer et al., 2002), and at the basal body of the connecting cilium in photoreceptor cells (Davidson et al., 2013). Binding between Arl2 and BART is mediated by a conserved N-terminal LLxIL motif in the Arl2 sequence, that is enclosed by a hydrophobic cleft of BART, and by the interaction of the Arl2 switch I and switch II regions with an α -helix of BART (Zhang et al., 2009). Another recently identified Arl3 binding partner is the coiled-coil domain containing protein 104 (CCDC104), also called CFAP36 or binder of

Arl2-like 1 (BARTL1). Structural analyses revealed that it contains an N-terminal BART-like domain (amino acid residues 1-133). Furthermore, structural and biochemical analyses showed that CCDC104 interacts with Arl3. CCDC104 localizes to the primary cilium of IMCD3 cells where it concentrates at the transition zone, distal to the basal body and colocalizing with Arl3. The BART-like domain of CCDC104 alone is not adequate to localize to the cilium. The crystal structure with a 2.2 Å resolution of a complex between the BART-like domain and Arl3 bound to the non-hydrolyzable GTP analog GppNHp (5'-guanylyl imidodiphosphate) revealed that CCDC104 interacts with a conserved LLxILxxL motif located in the N-terminus of Arl3 (Lokaj et al., 2015), highlighting the similarity of CCDC104 to BART and the earlier identified LLxIL motif of Arl2 (Zhang et al., 2009). CCDC104 was shown to interact only with the active form of Arl3. Lokaj et al. hypothesized that CCDC104 might mediate the ciliary activity or localization of Arl3 (Lokaj et al., 2015).

The Arl2/3 effectors can be classified into type I and type II effectors, depending on their mode of interaction with the Arl protein. BART and CCDC104 are type I effectors and the interaction is mediated by the N-terminal helix and the switch I and switch II regions of Arl2/3. The type II effectors Unc119a/b and PDE6δ only interact with switch I and switch II and are described in the chapters 1.12 and 1.15 (Fansa and Wittinghofer, 2016).

1.12 Guanine nucleotide dissociation inhibitors (GDIs) and the GDI-like protein PDE6δ

Post-translationally lipid-modified proteins such as Ras, Rho and Rab subfamily members couple their GDP/GTP cycle to a change of their intracellular localization, which means that they are either bound to different membranes or solubilized in the cytosol. At membranes, they can be either in the GDP- or GTP-bound state. The change between the localization of Ras, Rho and Rab proteins at membranes or in the cytosol is regulated by interacting proteins, the guanine nucleotide dissociation inhibitors (GDIs). The main function of GDIs is to maintain the bound G protein in a soluble and inactive complex in the cytosol by covering the hydrophobic lipid moiety of the G protein (Nancy et al., 2002; Cherfils and Zeghouf, 2013).

A difference between the N-terminal myristoylated Arf proteins and Ras, Rab or Rho subfamily members is that no GDIs were identified for Arfs. The nucleotide state regulates the position of the amphipathic helix that mediates membrane binding of the Arf protein. In the GDP-bound form, Arfs can be loosely membrane-attached, as shown for Arf4, Arf5 and Arf6, or cytosolic, whereas they are tightly bound to membranes in the GTP-bound state. Hydrolysis of the Arf-bound GTP can be sufficient for solubilization of the protein, as shown for Arf1 and Arf3 (Chun

et al., 2008; Duijsings et al., 2009; Cherfils and Zeghouf, 2013).

In 1990, the first GDIs were discovered as novel class of regulators of geranylgeranylated Rho and Rab proteins. Originally, RhoGDIs were thought to inhibit only GDP dissociation (Fukumoto et al., 1990). However, now it is known that Rab- and RhoGDIs keep the bound G protein in a soluble and inactive form. Three different types of these regulatory proteins were described (Wittinghofer and Vetter, 2011; Cherfils and Zeghouf, 2013). The structure and mechanisms of GDIs and GDI-like proteins determine their type of regulation. Regulatory proteins of the first type, RhoGDIs, are organized in two diverse domains, an N-terminal α -helical and C-terminal β -sandwich lipid-binding domain. The detachment of Rho from the membrane happens in two steps. First, the helical domain of RhoGDI binds to the switch regions of the Rho G domain. Secondly, the C-terminus that carries the prenylation is encompassed by the lipid-binding domain (Nomanbhoy et al., 1999). After it was originally shown that RhoGDIs interact with Rho•GDP, they later were reported to also interact with Rho•GTP, presumably to sustain a cytosolic Rho•GTP pool (Leonard et al., 1992; Hancock and Hall, 1993; Nomanbhoy and Cerione, 1996). Cytosolic Rho proteins in complex with RhoGDI were shown by structural studies to be unable to exchange their bound nucleotide mediated by RhoGEFs or RhoGAPs. Thus, the interaction of Rho with RhoGDIs and GEFs or GAPs is not possible at the same time (Cherfils and Zeghouf, 2013).

In the same year when RhoGDIs were found, the first RabGDI was purified from bovine brain cytosol (Sasaki et al., 1990). Similarly to RhoGDIs, RabGDIs reveal the two domain structure responsible for the interaction with the G domain and accordingly with the geranylgeranylated C-terminus of Rab proteins. However, the structures of the Rab- and RhoGDI domains are not related (An et al., 2003; Pylypenko et al., 2006). Equivalently to the mechanism of Rho proteins, the Rab-RabGDI mechanism apparently takes place in two steps, because the Rab G domain is distant from the prenyl-binding domain (Ignatev et al., 2008). Currently, three isoforms each of RhoGDI and RabGDI are known.

Besides classical GDIs, a distinct kind of related regulatory proteins was identified as GDI-like factors or GDI-like solubilizing factors (GSF). PDE6 δ is a GSF and was originally discovered in rod photoreceptor cells (Gillespie et al., 1989). Its depletion causes malfunction of kidney and retina in zebrafish (Thomas et al., 2014). Initially, PDE6 δ was shown to be a solubilizing factor for the α and β subunits of retinal rod cGMP PDE6 (Florio et al., 1996). PDE6 δ has an immunoglobulin-like β -sandwich structure with similarities to the lipid-binding domain of RhoGDIs (Hanzal-Bayer et al., 2002; Nancy et al., 2002; Ismail et al., 2011). Subsequently,

PDE6 δ was shown to extract the prenylated Rab subfamily members Rab13 (Marzesco et al., 1998) and Rab6 from membranes, as well as to bind to prenylated members of the Ras subfamily, such as H-Ras, N-Ras and K-Ras 4B, Rheb, Rap1 and Rap2, RalA and RalB, and the Rho subfamily members RhoA, RhoB, Rho6 and Rnd1 and to the G α_{i1} subunit of heterotrimeric G proteins. It was demonstrated for H-Ras that its C-terminus is essential for the interaction with PDE6 δ (Hanzal-Bayer et al., 2002; Nancy et al., 2002). By crystal structure determination of PDE6 δ in complex with farnesylated Rheb it was confirmed that the farnesyl moiety is surrounded by two β -sheets of PDE6 δ , similarly to the structure of RhoGDIs that bind the geranylgeranyl moiety of Rho subfamily members (Ismail et al., 2011).

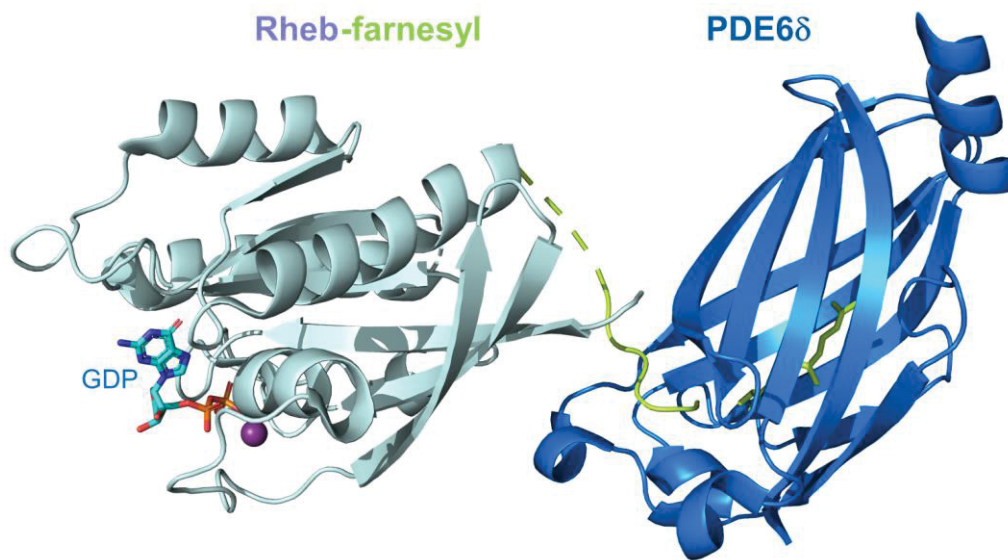


Figure 12: PDE6 δ (right), which has an immunoglobulin-like β -sandwich structure, in complex with farnesylated GDP-bound Rheb (left), 1.7 Å resolution crystal structure, PDB: 3T5G (Ismail et al., 2011). The farnesyl moiety (in green with hypervariable region) of Rheb inserts into the hydrophobic pocket of PDE6 δ .

The interaction of PDE6 δ or RhoGDI with the bound Ras or Rho protein is independent of the nucleotide state of Ras or Rho, whereas an interaction of RabGDIs with Rab•GTP was not reported (Nancy et al., 2002; Cherfils and Zeghouf, 2013). Despite these similarities, PDE6 δ reveals differences to RhoGDIs. In contrast to RhoGDIs, PDE6 δ does not possess a domain which is responsible for the binding of the GTPase core domain of the cargo protein and does not have the two domain structure. The small 17 kDa protein PDE6 δ only binds to the farnesylated C-terminus of the cargo protein. Crystal structures of PDE6 δ in complex with Ras, Rheb or farnesylated peptides have shown that only the farnesylated cysteine methyl ester and three or four extra residues insert into the hydrophobic binding pocket of PDE6 δ (Ismail et al.,

2011; Dharmaiah et al., 2016). All identified PDE6 δ interacting proteins share the CaaX motif and thus are prenylated. Mediated by its hydrophobic GDI-like binding pocket, PDE6 δ binds to prenylated cargoes and thereby was defined as general prenyl-binding and solubilizing or shuttling factor for numerous small GTP-binding proteins and rod PDE (Florio et al., 1996; Hanzal-Bayer et al., 2002; Nancy et al., 2002; Zhang et al., 2004; Ismail et al., 2011; Chandra et al., 2012; Cherfils and Zeghouf, 2013).

Prenylated Ras proteins or peptides are bound by PDE6 δ with affinities in the micromolar range (Chen et al., 2010; Ismail et al., 2011). Zhang and Baehr et al. determined K_d values of PDE6 δ with farnesyl and geranylgeranyl lipid moieties of 0.70 μ M and 19.06 μ M, respectively. Although PDE6 δ binds specifically to prenylated proteins, it reveals a flexibility in its interactions. Because it only recognizes the prenylated C-terminus of its cargo protein, PDE6 δ binds to a broad range of prenylated G proteins and other prenylated proteins (Zhang et al., 2004). PDE6 δ localizes to rod and cone photoreceptor cells, detected by immunocytochemistry (Zhang et al., 2004), and to the ciliary transition zone and proximal cilium in RPE1 cells, as shown by GFP fluorescence (Thomas et al., 2014). Due to these findings, PDE6 δ became part of the cilia research field and was indeed shown to bind to different prenylated proteins that localize to cilia, such as INPP5E, GRK1 (G protein-coupled receptor kinase 1/rhodopsin kinase) and RPGR (retinitis pigmentosa GTPase regulator) (Zhang et al., 2004, 2007; Thomas et al., 2014; Fansa et al., 2015, 2016; Lee and Seo, 2015; Dutta and Seo, 2016). In PDE6 $\delta^{-/-}$ knockout mice, that have a lowered body mass and reveal signs of a cone-rod dystrophy, GRK1 and the catalytic subunits of PDE6 partially mislocalize (Zhang et al., 2007).

According to its function as GSF, PDE6 δ regulates the membrane localization of prenylated cargo proteins and their cellular distribution in a dynamic way. This is critical for the cargo's function in the cell (Chandra et al., 2012; Zhang et al., 2012; Schmick et al., 2014, 2015; Fansa et al., 2016; Kösling et al., 2018). For instance, signaling mediated by H-Ras and K-Ras is enhanced by the activity of PDE6 δ , because PDE6 δ shuttles Ras which is thereby accumulated at the plasma membrane. However, a down-regulation of PDE6 δ leads to a randomized localization of Ras proteins to intracellular membranes and normal and oncogenic Ras signaling are defective (Chandra et al., 2012). The localization of Ras at membranes is thought to be a potential target for oncogenic Ras by inhibiting the interaction between PDE6 δ and Ras. Such small molecule PDE6 δ inhibitors are the pyrazolopyridazinones Deltarasin and Deltazinone 1 (Zimmermann et al., 2013, 2014; Papke et al., 2016).

1.13 PDE6 δ and RabGDIs are regulated by GDI displacement factors (GDFs)

The function of GDIs and GDI-like proteins and their interaction with cargo is modulated by different factors. RabGDIs and PDE6 δ are regulated by GDI displacement factors (GDFs), whereas no GDFs for RhoGDIs were identified so far. RhoGDIs are controlled by a phosphorylation code. GDFs regulate GDIs and the GDI-like PDE6 δ by binding and thereby cause the release of prenylated cargo protein from the GDI. Arl2 and Arl3 were described to act GTP-dependently as GDFs while binding to PDE6 δ , allosterically releasing farnesylated cargo proteins. Shown by structural and in vitro studies, Arl2/3•GTP release farnesylated Rheb from PDE6 δ (Ismail et al., 2011). In an earlier study, Hanzal-Bayer et al. solved the crystal structure of Arl2•GTP in complex with PDE6 δ (Hanzal-Bayer et al., 2002). A comparison of this structure with the structure of a prenylated RheB•GDP-PDE6 δ complex made it conceivable that both Arl2/3 and Rheb might interact synchronously with PDE6 δ (Ismail et al., 2011). The hydrophobic pocket of PDE6 δ is in a closed conformation when the farnesyl moiety of Rheb is bound. Arl2•GTP is thought to prefer to bind to PDE6 δ in this closed conformation in complex with Rheb, generating a ternary complex with a low affinity, which dissociates fast and thereby, Rheb is released from PDE6 δ (Ismail et al., 2011). In view of this study and the variety of prenylated PDE6 δ cargo proteins, Arl2 and Arl3 were suggested to act as general release or displacement factors for farnesylated cargo proteins from PDE6 δ . Coupled to the release, the farnesylated protein is then transferred to inner cellular membranes (Ismail et al., 2011; Cherfils and Zeghouf, 2013). Emphasizing the role of Arl3 as cargo displacement factor, it was shown *in vivo* in mice that a deletion of Arl3 affected the trafficking of peripheral, but not of transmembrane proteins (Hanke-Gogokhia et al., 2016).

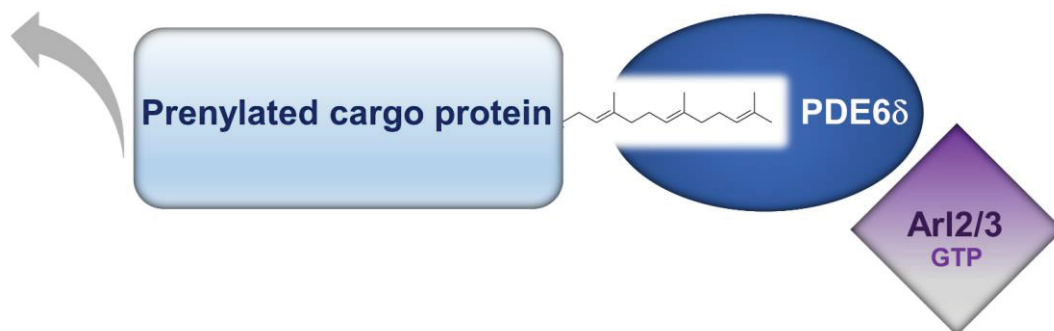


Figure 13: The GDI-like protein PDE6 δ interacts with prenylated cargo proteins through its hydrophobic pocket. Arl2/3 act as GDI displacement factors by GTP-dependent interaction with PDE6 δ and release of the prenylated protein from PDE6 δ .

1.14 The ciliary inositol polyphosphate 5'-phosphatase INPP5E

A number of cell regulatory processes are modulated by phosphoinositides. The hydrophobic moieties of these phospholipids are components of membranes, whereas their inositol headgroups face the cytosol (Balla, 2013). Every distinct cellular membrane occurs with a characteristic membrane lipid composition. This distribution can be described as a membrane code that facilitates the regulation of biological processes (Di Paolo and De Camilli, 2006). Within the eukaryotic cell, phosphatidylinositol kinases and phosphatases strictly and dynamically control phosphatidylinositol composition in space and time. Thereby, the kinases and phosphatases affect downstream signaling processes and are essential in regulating the lipid composition of cellular membranes (Bielas et al., 2009).

Members of the inositol polyphosphate 5'-phosphatase family selectively hydrolyze the 5'-phosphate of the inositol ring of inositol phosphates and phosphoinositides (Astle et al., 2007). The inositol polyphosphate 5'-phosphatase INPP5E, which is a member of this family and shows high expression levels in human and mouse brain, mouse testes and heart, was found to exclusively hydrolyze hydrophobic phosphoinositide substrates. This is in contrast to other known members of this protein family that dephosphorylate hydrophilic substrates. In detail, INPP5E converts phosphatidylinositol (4,5)-bisphosphate (PI(4,5)P₂) to phosphatidylinositol (4)-phosphate (PI4P), thus generating PI(3,4)P₂ from PI(3,4,5)P₃ (Kisseleva et al., 2000; Conduit et al., 2012).

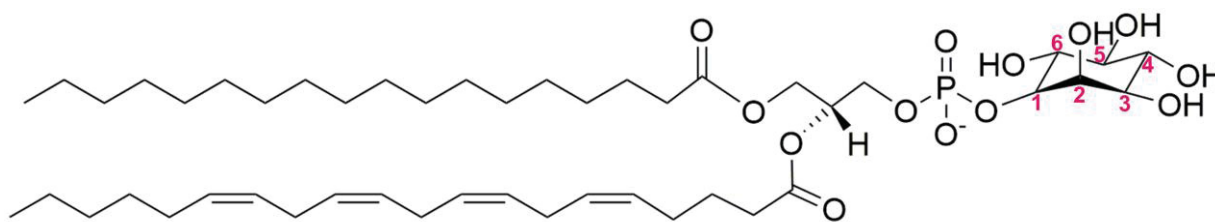


Figure 14: Structure of phosphatidylinositol. At position 1 (magenta), the inositol ring is phosphodiesterified to diacylglycerol, which carries two fatty acid side chains: stearoyl (upper residue) and arachidonoyl (lower residue). Phosphatidylinositol can be phosphorylated and is then called phosphoinositide or phosphatidylinositolphosphate. PI(4,5)P₂, which is phosphorylated at the positions 4 and 5 of inositol, and PI(3,4,5)P₃ are substrates of the inositol polyphosphate 5'-phosphatase INPP5E and are hydrolyzed at position 5 to PI4P and PI(3,4)P₂, respectively.

The 72 kDa protein INPP5E possesses two large domains, which are an N-terminal proline-rich domain and a C-terminal phosphatase domain, and has a C-terminal CaaX motif where the cysteine is farnesylated and further processed (see chapter 1.8 for farnesylation). The CaaX motif is conserved in all mammalian and avian forms of INPP5E and the cysteine residue is

farnesylated (De Smedt et al., 1996; Jacoby et al., 2009).



Figure 15: Predicted domain structure of INPP5E with an N-terminal proline-rich domain (Pro) and the catalytic inositol polyphosphate phosphatase domain (IPPc). The C-terminal cysteine residue is farnesylated. Modified from Bielas et al., 2009.

INPP5E almost exclusively localizes to primary cilia, shown by immunofluorescence microscopy of different cell types. It was found along the axoneme of primary cilia of mouse embryonic fibroblasts (Jacoby et al., 2009), RPE1 cells and the cerebellar internal granule layer (Bielas et al., 2009). GFP fluorescence also revealed the ciliary localization of stably expressed GFP-tagged INPP5E in fixed and living IMCD3 cells (Fansa et al., 2016; Kösling et al., 2018). The almost exclusive localization of INPP5E in primary cilia obviously leads to the conclusion of a cilia-specific function. INPP5E was shown to mediate the modulation of a specific phosphatidylinositolphosphate (PIP) composition of the ciliary membrane. Recent studies by Chávez et al. (2015) and Garcia-Gonzalo et al. (2015) revealed a linkage between the phosphoinositide metabolism and the physiology of primary cilia. The ciliary membrane possesses special domains which comprise distinct characteristic PIPs. In a study of neuronal stem cell primary cilia, phosphatidylinositol (4)-phosphate (PI4P) was identified as the major PIP within the ciliary membrane along the axoneme, generated by INPP5E, whereas PI(4,5)P₂ was found in membranes around the transition zone and the periciliary region. After INPP5E inactivation, PI(4,5)P₂ accumulated in the ciliary membrane, whereas the PI4P concentration drastically decreased. It was shown, that a normal PIP distribution is essential for the trafficking of the ciliary PI(4,5)P₂-binding protein Tulp3 (tubby-related protein 3) and the G protein-coupled receptor Gpr161, which is a cargo protein of Tulp3. Both Gpr161 and Tulp3 are ciliary proteins and regulators of Sonic Hedgehog signaling. Conclusively, a correct INPP5E function seems to be critical for a normal Hedgehog signaling by ensuring these specialized phosphoinositide levels of the ciliary membrane. Moreover, these studies demonstrate that PIP lipids are essential elements to ensure a suitable environment for cilia-associated signaling pathways (Chávez et al., 2015; Garcia-Gonzalo et al., 2015; Nakatsu, 2015). INPP5E was also reported to be involved in ciliary stability and in the regulation of phosphoinositide 3-kinase (PI3K) and ciliary platelet-derived growth factor receptor α (PDGFR α) signaling (Jacoby et al., 2009) and together with the type I γ PI4P 5-kinase (PIPKI γ), INPP5E was implicated in the

coordination of ciliogenesis initiation (Xu et al., 2016). Recently it was shown that INPP5E acts in the restriction of actin polymerization in cilia. The removal of the ciliary tip, called decapitation, was shown to be induced by F-actin and the ciliary INPP5E substrate PI(4,5)P₂, and leads to disassembly of the cilium and thereby to cell cycle progression (Phua et al., 2017). INPP5E^{-/-} embryos showed a reduced Hedgehog signaling and an enrichment of the INPP5E substrates PI(4,5)P₂ and PI(3,4,5)P₃ in the ciliary transition zone, leading to an impaired accumulation of transition zone associated scaffold proteins and of the Smo protein inside cilia. Therefore, INPP5E is thought to be involved in the molecular organization of the transition zone and ciliary enrichment of Smo, and might act as branching point between phosphoinositide and Hedgehog signaling during embryogenesis in cilia (Dyson et al., 2017). INPP5E^{-/-} knockout mice die in a late stage of embryogenesis or contemporary to birth due to brain development defects, skeletal abnormalities, such as hexadactyly, multiple cysts in the kidney and developmental defects of the eye, such as anophthalmia (Jacoby et al., 2009; Chávez et al., 2015). Conclusively, INPP5E possesses a crucial role in the primary cilium and deletion or mutations result in ciliary signaling deficiency and cilium instability and thereby can cause ciliopathies.

INPP5E is encoded by the JBTS1 gene and mutations lead to the cerebrorenal ciliopathy Joubert syndrome (Bielas et al., 2009; Travaglini et al., 2013). Another member of the inositol polyphosphate 5'-phosphatase family is OCRL (oculocerebrorenal), which is homologous to INPP5E. In mutated form, OCRL causes Lowe's oculocerebrorenal syndrome (Attree et al., 1992). The phosphoinositide substrate specificity of both phosphatases overlaps, also their localization to cilia (Luo et al., 2012), where OCRL is involved in ciliary assembly (Coon et al., 2012). Besides Joubert syndrome mutations, a mutation of human INPP5E was identified in patients of a family with MORM syndrome, an autosomal-recessive ciliopathy, that reveals similarities to Bardet-Biedl syndrome. Patients show mental retardation, obesity, retinal dystrophy and micropenis (Hampshire et al., 2006; Jacoby et al., 2009). The identified Q627Stop mutation leads to a truncated protein missing 18 C-terminal amino acid residues, thus also the CaaX motif.

Partially conflicting studies describe the determinants of INPP5E localization in cilia and the role played by PDE6δ in this context. The importance of the farnesylated INPP5E C-terminus was shown by Jacoby et al. and Thomas et al., because the MORM mutation alters the protein localization. MORM-mutated INPP5E does not exclusively localize to the entire axoneme anymore, but accumulates in the transition zone and is also found in the cytosol (Jacoby et al., 2009; Thomas et al., 2014). A single mutation of the CaaX box cysteine to alanine also leads to

localization defects similar to that of the MORM mutant. The CaaX mutant also loses exclusive ciliary localization and is enriched in the transition zone. The mutant was shown to not bind to PDE6 δ . This confirms that the C-terminal farnesylation of INPP5E mediates the interaction with PDE6 δ . Furthermore, a homozygous truncation mutation of PDE6 δ , that is associated to Joubert syndrome and impairs the formation of the hydrophobic binding pocket, inhibits INPP5E localization to cilia. This PDE6 δ mutant does not bind to the releasing factor Arl3•GTP (Thomas et al., 2014). Moreover, knockdown of PDE6 δ by RNAi also impairs INPP5E ciliary localization (Humbert et al., 2012; Thomas et al., 2014).

In contrast, in a study by Humbert et al. the MORM mutant INPP5E was characterized, claiming that the C-terminal truncation and thus missing farnesylation would not impair ciliary localization. They propose that INPP5E ciliary targeting is regulated by a network of PDE6 δ , Arl13B and CEP164, because RNAi-mediated knockdown of these proteins results in INPP5E mislocalization. By immunofluorescence microscopy, an FDRELYL motif between phosphatase domain and CaaX motif of INPP5E was proposed as ciliary targeting sequence. Immunoprecipitation assays show an interaction between INPP5E and Arl13B (Humbert et al., 2012). In another study, the link between both proteins and the role of Arl13B in INPP5E ciliary localization was strengthened, because INPP5E did not localize to cilia after Arl13B knockout. Furthermore, the phenotype of Arl13B knockout cells resembles the phenotype of INPP5E^{-/-} knockout mice, with IFT-A and IFT-B complex enrichment at the tips of cilia. Arl13B was shown to interact with the IFT-B complex proteins IFT46 and IFT56. However, this interaction was shown to not be responsible for INPP5E ciliary localization (Nozaki et al., 2017).

The function as shuttling factor and significance of PDE6 δ for ciliary localization of INPP5E was increased in a study by Fansa et al. (2016). Determining a complex crystal structure of PDE6 δ and farnesylated INPP5E peptide deepened the understanding of the binding mode (1.85 Å resolution, PDB: 5F2U) (Fansa et al., 2016). A superimposition with a complex of PDE6 δ and farnesylated Rheb (PDB: 3T5G) (Ismail et al., 2011) revealed high similarities of the prenyl-binding pocket in both complexes. However, the -1 and -3 positions relative to the farnesylated cysteine of the cargo proteins showed clear dissimilarities between Rheb and INPP5E binding to PDE6 δ . Biochemical studies demonstrated that these structural differences are accompanied by a divergence in the binding affinities between farnesylated cargo protein and PDE6 δ . INPP5E is a high affinity cargo of PDE6 δ with a K_d of $3.7 \text{ nM} \pm 0.2 \text{ nM}$ in the low nanomolar range. In contrast, Rheb has a low affinity to PDE6 δ in the submicromolar range with a K_d of $445 \text{ nM} \pm 83 \text{ nM}$. This difference in affinities is related to different cellular

localization patterns of the ciliary INPP5E and Rheb, which localizes to endomembranes. Cell biological experiments showed that swapping of the -1 and -3 positions from high to low affinity in INPP5E results a loss of the exclusive ciliary localization. Conclusively, this study strengthens the importance of PDE6 δ for the ciliary localization of INPP5E and shows that the high affinity to PDE6 δ determines its sorting to the cilium. It was postulated that the -1 and -3 positions, which are conserved in different farnesylated high or low affinity cargo proteins, could act, beside others, as ciliary sorting signals, that are required for a correct ciliary localization. Moreover, the role of Arl3 in the ciliary sorting mechanism of INPP5E as releasing factor from PDE6 δ was highlighted in this study by RNAi experiments, revealing a partial mislocalization of INPP5E after Arl3 knockdown (Fansa et al., 2016). This contrasts with the study by Humbert et al., who claim that Arl3 downregulation would not impact INPP5E localization (Humbert et al., 2012).

Collectively, based on the combination of structural, biochemical and cell biological experiments, Fansa and colleagues developed the model that PDE6 δ -mediated sorting of farnesylated cargo is determined by the affinity between carrier and cargo protein. High affinity cargo proteins, such as INPP5E, are sorted to cilia and released inside this compartment specifically by Arl3•GTP. An unknown retention signal of INPP5E is supposed to lead to its retention inside cilia. In contrast, low affinity cargo proteins, such as Rheb, are released by Arl2•GTP at internal membranes (Fansa et al., 2016).

1.15 Unc119a/b shuttle myristoylated cargo proteins

Unc119a and Unc119b share a high degree of similarity (58 % sequence identity) and contain a hydrophobic binding pocket that is similarly structured to that of PDE6 δ and the immunoglobulin-like β -sandwich structure which was described for RhoGDIs. However, Unc119a/b bind to N-terminal myristoylated proteins, such as GNAT-1/transducin- α , G α subunits ODR-3 and GPA-13, Cystin1, NPHP3, RP2 and Src-type tyrosine kinases (Cen et al., 2003; Wright et al., 2011; Zhang et al., 2011; Ismail et al., 2012; Jaiswal et al., 2016). Sequence comparison revealed that the hydrophobic pocket contains conserved residues, suggesting a similar interaction mode of Unc119a/b with myristoylated proteins (Jaiswal et al., 2016).

Despite their high similarity, Unc119a/b show a different cellular localization pattern. Besides a cytosolic localization, Unc119a was found at the basal body but not in cilia, whereas Unc119b was enriched at the basal body, transition zone and proximal cilium. The causes of this different

localization are unclear. It is proposed that Unc119b might have an unknown ciliary targeting sequence within its N-terminus, that shows the highest degree of dissimilarity to Unc119a. Furthermore, it was hypothesized that binding of ciliary cargo may trigger the entry of Unc119b into cilia (Wright et al., 2011).

Exclusively Unc119b, but not Unc119a, is thought to be required for the ciliary localization of myristoylated NPHP3, as shown by RNAi-mediated knockdown studies, where only Unc119b knockdown led to NPHP3 mislocalization (Wright et al., 2011; Constantine et al., 2012). Activated Arl2 and Arl3 were shown to specifically release myristoylated cargo from Unc119a/b. The sorting mechanism of the ciliary protein Cystin1 is expected to be comparable to that of NPHP3, because knockdown of Arl3 or Unc119b led to an impaired localization of Cystin1 (Wright et al., 2011).

Structural and biochemical studies revealed that the release of myristoylated ciliary cargo proteins from Unc119 proteins is Arl3-specific, where the Arl3 N-terminal helix is crucial (Wright et al., 2011; Ismail et al., 2012). In a study apart from the cilia research field, it was shown that activated Arl2/3 release myristoylated cargo from Unc119 proteins on perinuclear membranes (Konitsiotis et al., 2017). Recently, the interaction of myristoylated cargo proteins with Unc119a/b was studied in more detail. This study revealed high similarities to the PDE6 δ -mediated sorting of farnesylated proteins, where high affinity proteins were sorted and released into cilia by Arl3•GTP, whereas low affinity cargo proteins were released by Arl2•GTP at endomembranes (Fansa et al., 2016). Jaiswal et al. characterized different myristoylated Unc119a/b interacting proteins with regard to their binding affinity and set this in relation to the cellular localization of the myristoylated proteins. Interestingly, myristoylated peptides of the ciliary proteins GNAT-1, NPHP3 and Cystin1 have a high affinity towards Unc119 proteins, whereas RP2, with an intermediate affinity localizes around the basal body but does not enter cilia, and Src, a low affinity binder, does not localize to or close to the ciliary compartment. It was shown that the peptides that have a low affinity can be released from Unc119 proteins by Arl2 and Arl3 bound to the non-hydrolyzable GTP analog GppNHp. However, only Arl3•GppNHp is able to release peptides with high affinity. In this study, the high affinity interaction was analyzed by x-ray structure determination of a complex between myristoylated NPHP3 peptide and Unc119a. It showed that the +2 and +3 positions relative to the myristoylated glycine residue of NPHP3 are essential to define high or low affinity. In line with this, biochemical measurements revealed that swapping the amino acid residues at the +2 and +3 positions from high to low affinity and vice versa leads to reversed affinities to Unc119a. Moreover, a cell biological localization study of mutant NPHP3, where the +2 and +3 positions

were mutated to that of low affinity cargo protein, revealed a partial mislocalization, highlighting that the sorting of high affinity myristoylated cargo to cilia is regulated by Unc119a/b (Jaiswal et al., 2016).

1.16 The Arl2/Arl3 system sorts lipidated cargo proteins

Collectively, lipidated cargo proteins which interact with the homologous carrier proteins PDE6 δ or Unc119a/b are sorted to their cellular membrane destination by the Arl2/Arl3 system. PDE6 δ shuttles farnesylated cargo proteins, whereas Unc119a/b shuttle myristoylated proteins. Arl2 and Arl3 interact with the carrier proteins in a nucleotide-dependent manner, exclusively in the GTP-bound form, and act as cargo release factors. Thereby, Arl2/3 control the shuttling and sorting of lipidated proteins (Linari et al., 1999; Van Valkenburgh et al., 2001; Ismail et al., 2011, 2012; Wright et al., 2011; Fansa and Wittinghofer, 2016; Fansa et al., 2016; Jaiswal et al., 2016; Ismail, 2017).

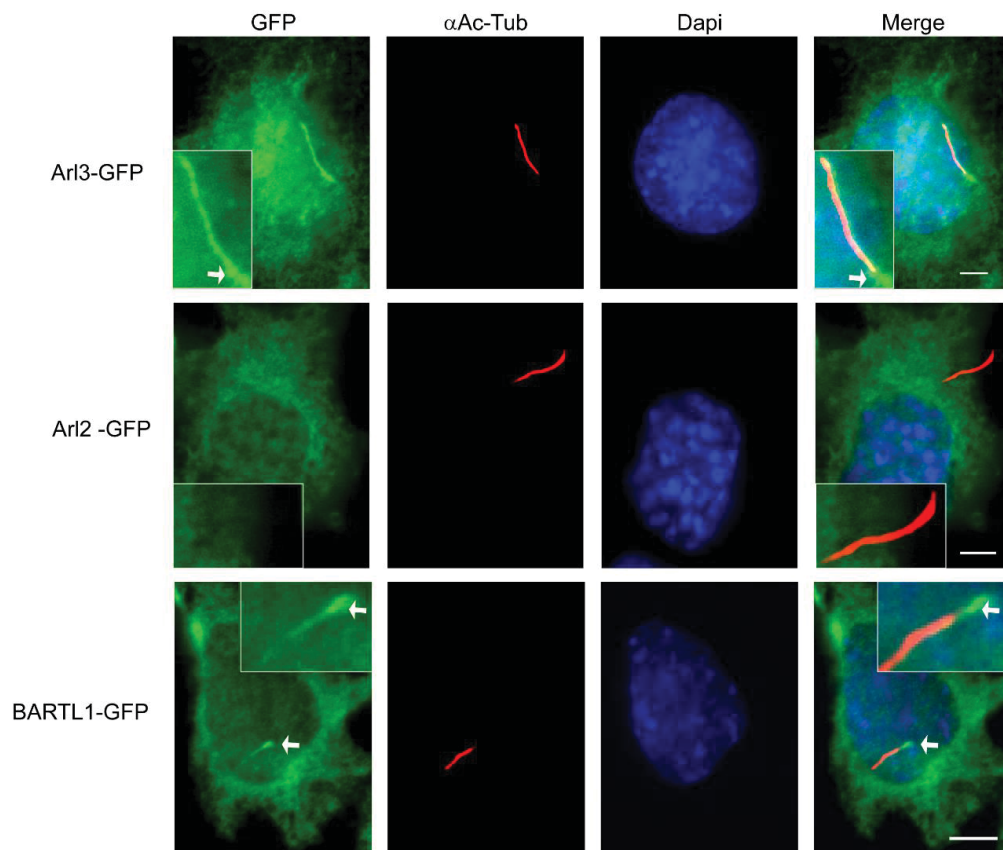
The results of the above described studies by Fansa et al. (2016) and Jaiswal et al. (2016) about the sorting of lipidated PDE6 δ or Unc119a/b cargo proteins to different inner membranes reveal clear analogies. Conclusively, they give high evidence for a general sorting principle for farnesylated or myristoylated cargo proteins of PDE6 δ or Unc119a/b, targeting high affinity binders to the ciliary compartment, where the ciliary proteins are specifically released by Arl3•GTP, whereas low affinity cargo is released at inner cellular membranes by Arl2•GTP (Fansa and Wittinghofer, 2016; Fansa et al., 2016; Jaiswal et al., 2016). Arl3•GTP releases a high affinity farnesylated INPP5E peptide 600 times faster from PDE6 δ than Arl2•GTP, shown by kinetic measurements (Fansa et al., 2016). This diverse specificity raised the question about the difference between Arl3 and Arl2 in this context. Combining the results of different biochemical and structural studies of PDE6 δ /Unc119a/b-Arl2/3 complexes, the N-terminal amphipathic helix of Arl3 was shown to be crucial for the specific release of high affinity cargo proteins. This helix determines the major difference with regard to dynamics and structure. In contrast to Arl2, the Arl3 helix occupies a hydrophobic pocket on the Arl3 protein surface, even in the GTP-bound structure, acting as an opener of the cargo binding pocket in the carrier protein and thereby inducing cargo release (Ismail et al., 2012; Kapoor et al., 2015; Fansa et al., 2016). Although both Arl2 and Arl3 can interact with membranes via their N-terminal amphipathic helix, in case of Arl3, this interaction depends on the GTP loaded state of Arl3 (Kapoor et al., 2015). The ciliary compartment was described as Arl3•GTP compartment and it

was hypothesized that this Arl3•GTP compartment acts as a driving for the release of lipidated proteins from PDE6 δ and Unc119a/b into cilia. This emphasizes the crucial role of Arl3 in the regulation of the trafficking of lipidated proteins to the cilium (Gotthardt et al., 2015; Fansa and Wittinghofer, 2016). For the here described delivery of lipidated proteins to cilia, also the name lipidated protein intraflagellar targeting (LIFT) was supposed. Besides IFT, the LIFT system is a further trafficking system, that in the interplay with the ciliary gate acts in the establishment of a dynamic ciliary signaling compartment (Fansa and Wittinghofer, 2016; Jensen and Leroux, 2017).

2 Publication I

The interaction of CCDC104/BARTL1 with Arl3 and implications for ciliary function

Mandy Lokaj, **Stefanie K. Kösling**, Carolin Koerner, Sven M. Lange, Sylvia E. C. van Beersum, Jeroen van Reeuwijk, Ronald Roepman, Nicola Horn, Marius Ueffing, Karsten Boldt, and Alfred Wittinghofer (2015). *Structure* 23(11), 2122-2132.



These were the questions to be answered by this publication

- Why does Arl3 localize to cilia, whereas the homologous Arl2 does not?
- Is the N-terminal amphipathic helix of Arl3 important for its ciliary localization?
- Where does the newly identified Arl3-interacting protein CCDC104 localize in eukaryotic cells, is it a ciliary protein?
- What is the function of CCDC104?
- Does the interaction of CCDC104 with Arl3 determine the ciliary localization of Arl3 and/or vice versa?

Contribution of 40 %

- Plasmid generation and mutagenesis for transfection of IMCD3 cells.
- Cell cultivation, generation of stable GFP cell lines (Arl2, Arl3 Δ N, Arl2-3Nterm, Arl3 L4D, Arl3 F51A, CCDC104, CCDC104(1-133)), validation by western blotting.
- Cell fixation, immunofluorescence (IF) staining, fluorescence microscopy of GFP fluorescence of the cell lines above and Arl3-GFP and RP2-GFP IF localization studies, Arl3 antibody staining in CCDC104 cell line, image processing.
- Quantification of cilia lengths of IMCD3, Arl3, Arl3 L4D, Arl3 F51A cell lines.
- RNAi knockdown studies of Arl3 in the CCDC104 cell line and of CCDC104 in the Arl3 cell line, validation by western blotting.
- Writing of the methods section in the manuscript regarding IMCD3 cell experiments.

Declaration: Reprinted (adapted) with permission from Structure

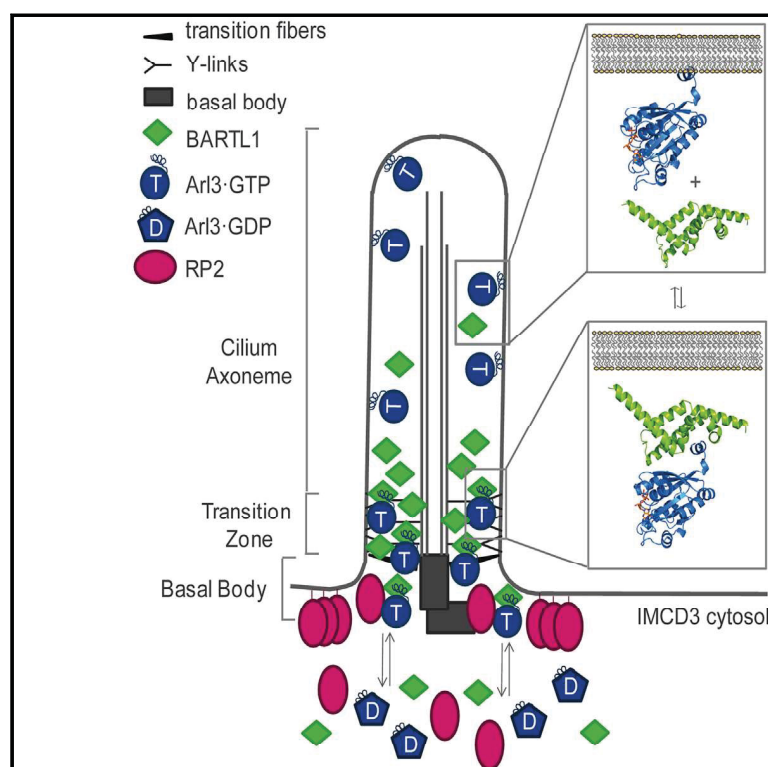
Copyright © 2015, Elsevier, Creative Commons Attribution License (CC BY)

DOI: <http://dx.doi.org/10.1016/j.str.2015.08.016>

Structure

The Interaction of CCDC104/BARTL1 with Arl3 and Implications for Ciliary Function

Graphical Abstract



Authors

Mandy Lokaj, Stefanie K. Kösling, Carolin Koerner, ..., Marius Ueffing, Karsten Boldt, Alfred Wittinghofer

Correspondence

alfred.wittinghofer@mpi-dortmund.mpg.de

In Brief

Lokaj et al. biochemically and structurally characterize BARTL1 as an Arl3 effector and speculate on its function in cilia.

Highlights

- Identification of a BART-like protein, CCDC104/BARTL1, as Arl3 binding partner
- BARTL1 is a ciliary protein with transition zone localization
- Complex structure shows BARTL1 binding to conserved LLxILxxL N-term motif of Arl3
- N-terminal amphipathic helix of Arl3 is crucial for its ciliary localization



Lokaj et al., 2015, Structure 23, 2122–2132
November 3, 2015 ©2015 The Authors
<http://dx.doi.org/10.1016/j.str.2015.08.016>

CellPress

The Interaction of CCDC104/BARTL1 with Arl3 and Implications for Ciliary Function

Mandy Lokaj,¹ Stefanie K. Kösling,¹ Carolin Koerner,¹ Sven M. Lange,¹ Sylvia E.C. van Beersum,² Jeroen van Reeuwijk,² Ronald Roepman,² Nicola Horn,³ Marius Ueffing,³ Karsten Boldt,³ and Alfred Wittinghofer^{1,*}

¹Max-Planck-Institute of Molecular Physiology, Emeritus Group, Otto-Hahn-Straße 15, 44227 Dortmund, Germany

²Department of Human Genetics and Radboud Institute for Molecular Life Sciences, Radboud University Medical Center, Geert Grooteplein Zuid 10, 6525 GA Nijmegen, the Netherlands

³Medical Proteome Center, Institute for Ophthalmic Research, University of Tübingen, Nägelsestrasse 5, 72074 Tübingen, Germany

*Correspondence: alfred.wittinghofer@mpi-dortmund.mpg.de

<http://dx.doi.org/10.1016/j.str.2015.08.016>

This is an open access article under the CC BY license (<http://creativecommons.org/licenses/by/4.0/>).

SUMMARY

Cilia are small antenna-like cellular protrusions critical for many developmental signaling pathways. The ciliary protein Arl3 has been shown to act as a specific release factor for myristoylated and farnesylated ciliary cargo molecules by binding to the effectors Unc119 and PDE6 δ . Here we describe a newly identified Arl3 binding partner, CCDC104/CFAP36. Biochemical and structural analyses reveal that the protein contains a BART-like domain and is called BARTL1. It recognizes an LLxILxxL motif at the N-terminal amphipathic helix of Arl3, which is crucial for the interaction with the BART-like domain but also for the ciliary localization of Arl3 itself. These results seem to suggest a ciliary role of BARTL1, and possibly link it to the Arl3 transport network. We thus speculate on a regulatory mechanism whereby BARTL1 aids the presentation of active Arl3 to its GTPase-activating protein RP2 or hinders Arl3 membrane binding in the area of the transition zone.

INTRODUCTION

Cilia are small, microtubule-based antennae-like protrusions of cells critical for the maintenance of cellular homeostasis and many developmental signaling pathways (Eggenschwiler and Anderson, 2007; Goetz and Anderson, 2010). Small G proteins of the Arl subfamily have been shown to be crucial to ciliogenesis and cilia maintenance. Joubert syndrome, Bardet-Biedl syndrome, and retinitis pigmentosa are so-called ciliopathies, arising from structural and/or functional defects of the G proteins Arl13B (Cantagrel et al., 2008; Thomas et al., 2015), Arl6 (Fan et al., 2004), and Arl3 (Schwahn et al., 1998; Veltel and Wittinghofer, 2009; Veltel et al., 2008a), respectively.

Arl2 and Arl3 (Arl-like) are guanosine triphosphate (GTP)-binding proteins of the Arf subfamily of the Ras superfamily. They switch between an inactive guanosine diphosphate (GDP)-bound form and an active GTP-bound form (Cox and Der, 2010; Vetter and Wittinghofer, 2001). This molecular switch is particularly striking for all (hitherto analyzed) members of the

Arl subfamily, as it involves the reorganization of the β sheet, where two strands of the sheet move by two residues along the rest of the strands when going from the inactive GDP state to the active GTP state (Gillingham and Munro, 2007; Pasqualato et al., 2001, 2002). This so-called interswitch toggle has been demonstrated by a number of three-dimensional structures to release the N-terminal (usually) amphipathic helix from its binding site on the G domain core, such that it is pointing into solution and/or is free to interact with membranes and/or other proteins (Cherfils and Zeghouf, 2013).

Arl2 and Arl3 are homologous proteins with approximately 52% sequence identity (68% similarity) and very similar structure. In addition, numerous effectors have been identified which interact with the GTP-bound form of both proteins. These are the delta subunit of the photoreceptor-specific phosphodiesterase 6 (PDE6 δ) (Linari et al., 1999), HRG4/Unc119a (Kobayashi et al., 2003), its homolog Unc119b (Wright et al., 2011), and the Arl2-binding protein (BART/Arl2BP) (Sharer and Kahn, 1999; Veltel et al., 2008b; Zhang et al., 2009). The structure of the Arl2-PDE6 δ complex showed an Arf-type conformational change. The homology to the prenyl-binding protein RhoGDI (Hanzal-Bayer et al., 2002) led to the discovery that PDE6 δ , also called PrBP, is a general prenyl-binding protein which seems to bind both farnesylated and geranylgeranylated proteins with unclear specificity (Chandra et al., 2012; Nancy et al., 2002; Zhang et al., 2004). Later it was shown that Arl2/3 and cargo binding are mutually exclusive and that Arl2/3 act as allosteric cargo-release factors by inducing a conformational change on PDE6 δ (Ismail et al., 2011). HRG4/Unc119a has a sequence and structural homology to PDE6 δ and was shown to bind myristoylated cargo such as transducin- α (Wright et al., 2011). Unc119a and Unc119b seem to be general myristoyl-binding proteins, and Arl2 and Arl3 can both act as cargo-release factors, although the conformational change leading to release of cargo is rather different from that of PDE6 δ (Ismail et al., 2012). While the structure of the Arl2-BART complex revealed a novel recognition motif of an effector (Zhang et al., 2009), where BART binds the Arl2 N-terminal helix apart from the switch region, the function of BART/Arl2BP remains to be determined.

Despite the homology in structure and biochemistry, Arl2 and Arl3 may have entirely different biological functions. It was shown very early that transfection of GTPase-negative versions (Q \rightarrow L) of Arl2/3 and the knockdown by RNAi differentially affect microtubule-dependent processes (Tian et al., 2010; Zhou et al.,

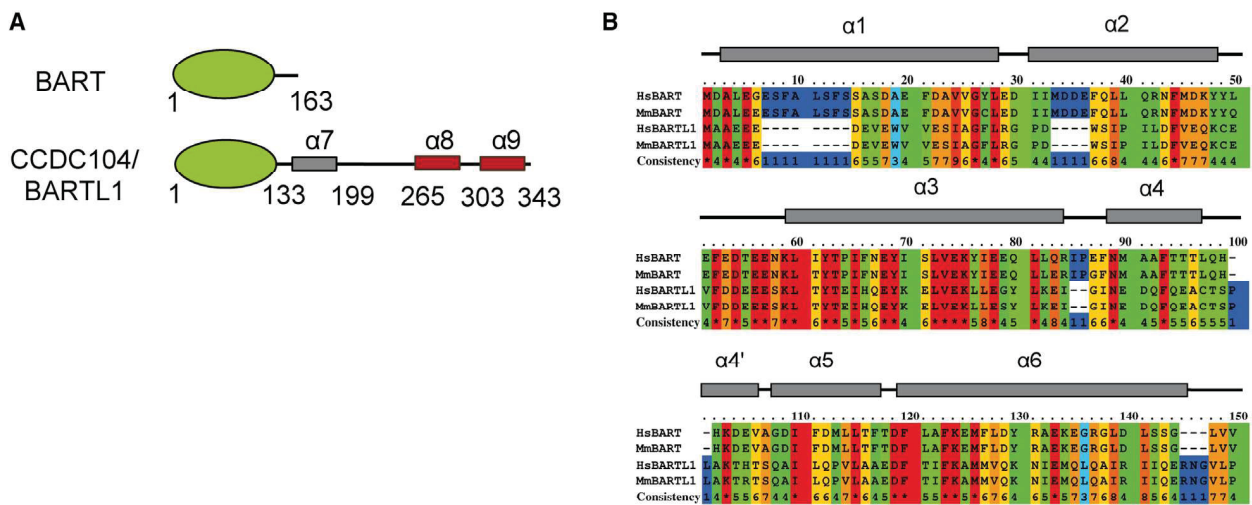


Figure 1. Domain Organization and Secondary Structure of BARTL1

(A) Domain organization of human BART and human BARTL1 with amino acid boundaries of the BART-like domain (green), random coiled coil (gray), and further α helices (red).

(B) Alignment of residues 1–133, comprising the BART-like domain, from *Homo sapiens* (Hs) and *Mus musculus* (Mm) BART and BARTL1. Dependent on their degree of conservation, residues are colored from red (highly conserved) to blue (non-conserved). The α helices of the BART-like domain are indicated above.

2006). Arl2 has been shown to bind to tubulin cofactor D, a protein necessary for folding and/or formation of the polymerization-competent α , β -tubulin dimer (Bhamidipati et al., 2000; Shern et al., 2003).

Arl3 has been identified as a ciliary protein in bioinformatics screens and localization studies (Avidor-Reiss et al., 2004). The generation of Arl3-deficient mice revealed that Arl3 is indeed involved in ciliary function affecting kidney and photoreceptor development (Schrack et al., 2006). In support of this, Arl3 has been shown to be involved in flagellum integrity in *Leishmania* (Cu villier et al., 2000). In human photoreceptor cells Arl3 is localized in the connecting cilium, a ciliary compartment important for the transport of components between inner and outer segments of photoreceptor cells (Grayson et al., 2002). Arl3, but not Arl2, can release myristoylated ciliary target proteins from their complex with Unc119 (Wright et al., 2011), and we have shown that the particular conformation of the N-terminal helix of Arl3 is responsible for this differential effect (Ismail et al., 2012). Likewise, it has been shown that the prenylated ciliary cargo protein INPP5E is released from its complex with the shuttle factor PDE6 δ by Arl3 but not Arl2 (Thomas et al., 2014). In addition, we have shown that RP2, a gene mutated in X-linked retinitis pigmentosa, is a highly active and specific GTPase-activating protein acting on Arl3 but not Arl2 (Velzel et al., 2008a). In support of the role of RP2 in ciliary trafficking, the RP2 knockout mouse shows severe defects in trafficking of prenylated and myristoylated proteins (Schwarz et al., 2012a, 2012b; Wright et al., 2011; Zhang et al., 2015).

In our search for interacting ciliary proteins, we identified CCDC104/CFAP36 as an Arl3-interacting protein with structural homology to the binder of Arl2 (BART). BART has been found to be an Arl2-interacting protein (Sharer and Kahn, 1999), which is mutated in autosomal-recessive retinitis pigmentosa (Davidson et al., 2013). Here we investigate the functional and structural properties of CCDC104/CFAP36 as a new ciliary protein and

Arl3 effector. Because of its homology to BART, we have renamed it BARTL1.

RESULTS

CCDC104/BARTL1 Contains an N-Terminal BART-like Domain

In a search for ciliary regulators (guanine nucleotide exchange factors [GEFs] and GTPase-activating proteins) for Arl3, we carried out tandem-affinity purifications (TAPs) from HEK293T cells that were transfected with constructs coding for the fast cycling mutant Arl3^{D129N} containing a C-terminal Strep-flag tag. Such a mutant is expected to associate with GEFs and effectors, as we have shown previously in the identification of plant-specific Rop-GEFs (Berken et al., 2005). We repeatedly identified peptides of CCDC104 by mass spectrometry analysis of TAP eluates (Table S1). Although CCDC104 was previously identified in a TAP using constitutively active Arl3^{Q71L} (Wright et al., 2011), we speculated, based on our findings, that CCDC104 might be a GEF for Arl3. In assessing this role, however, CCDC104 showed no GEF activity toward Arl3 (Figure S1). Bioinformatics analysis of the domain structure of CCDC104 showed the presence of an N-terminal BART-like domain followed by an extended C terminus comprising a coiled coil (α 7) and two further α helices (α 8 and α 9) (Figure 1A). The presence and similarity to BART led us to rename CCDC104 to BARTL1 (BART-like protein 1). Despite low amino acid sequence conservation between the BART-like domain of BARTL1 and BART, with only 21.4% identity and 41.4% similarity over 133 amino acids, the secondary structure prediction shows a conserved all-helical domain consisting of six α helices (Figure 1B). Thus, considering the five known common effectors of Arl2/3, we can group these into two types, where BARTL1 and BART form one group while PDE6 δ , HRG4, and Unc119b constitute the second. The latter three, despite low primary sequence conservation, have an identical

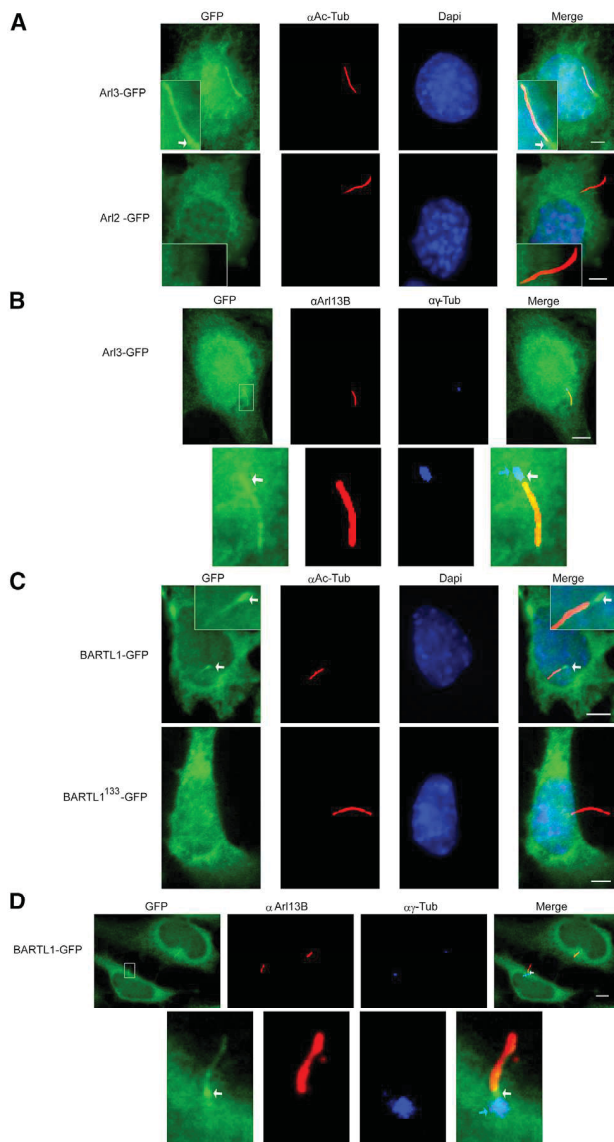


Figure 2. Localization of Arl2, Arl3, and BARTL1 in IMCD3 Cells with Induced Cilia

(A) Stably expressed, C-terminally GFP-tagged full-length mouse Arl3 or Arl2 in IMCD3 Flp-In cells were serum-starved and fixed. Apart from GFP labeling (shown in all the following figures, as indicated), the cells were immunostained for acetylated α -tubulin (AcTub) and the nucleus (DAPI). Boxed areas show enlargement of cilia. White arrows point to the base of the cilium.

(B) IMCD3 Flp-In cells stably expressing Arl3-GFP were stained for γ -tubulin (α -Tub; blue) and Arl13B (α Ar13B; red). Indicated are basal body (blue arrow) and the GFP signal between basal body and Arl13B signal (white arrow). The boxed area in the upper row (left panel) is enlarged in the lower row.

(C) IMCD3 Flp-In cells stably expressing C-terminally tagged human BARTL1-GFP and mouse BARTL1¹³³-GFP were serum-starved, fixed, and immunostained for acetylated α -tubulin (AcTub) and the nucleus (DAPI). Boxed areas show enlargement of cilia.

(D) IMCD3 Flp-In cells stably expressing BARTL1-GFP were stained for γ -tubulin (α -Tub; blue) and Arl13B (α Ar13B; red). Indicated are basal body (blue arrow) and the GFP signal between basal body and Arl13B signal (white arrow). The boxed area in the upper row (left panel) is enlarged in the lower row. Scale bars represent 5 μ m.

immunoglobulin β -sandwich fold. They form a group of guanine nucleotide dissociation inhibitor-like solubilizing factors, which are regulated by Arl2 and Arl3 small G proteins (Chandra et al., 2012; Hanzal-Bayer et al., 2002; Ismail et al., 2011, 2012). The former two can also be grouped together based on their identical all-helical fold, although the molecular functions of BART and BARTL1 are presently unknown and BARTL1 is the focus of the present study.

Arl3 and BARTL1 Localize to Cilia

The cellular localizations of Arl3 and Arl2 were analyzed in mouse inner medullary collecting duct (IMCD3) cells. In agreement with the literature (Zhou et al., 2006), we confirm the ciliary localization for Arl3 along the length of the cilium, visualized by staining against acetylated α -tubulin of the cilia axoneme (Figure 2A), in addition to the rest of the cell, in IMCD3 Flp-In cell lines stably expressing Arl3 C-terminally fused to GFP. Examination of Arl3 staining by a different fixation method combined with staining of the cilia axoneme for Arl13B, which is a protein exclusively localizing to the cilia axoneme, and for γ -tubulin, which is a marker for the basal body, shows that Arl3 is also enriched at the basal body and the transition zone additional to the length of the cilium (Figure 2B). In contrast, a corresponding Arl2 construct was excluded from the cilium and could only be found in the cytoplasm (Figure 2A). This is further supported by reports that only Arl3 and not Arl2 is found in the ciliary proteome (Avidor-Reiss et al., 2004; Efimenko et al., 2005; Pazour et al., 2005). To examine a potential role of BARTL1 in cilia, we further generated cell lines stably expressing a C-terminal fusion to GFP. Following induction of cilia by serum starvation, native BARTL1 could be detected in cilia only partly, co-localizing with the ciliary marker acetylated α -tubulin (Figure 2C). It appears that BARTL1 is enriched at the base of the cilium (close to the basal body) (Figure 2C, white arrow). A closer investigation of the staining by a different fixation method combined with staining for γ -tubulin reveals that the enrichment of BARTL1 (Figure 2D, white arrow) appears distal to the basal body (Figure 2D, blue arrow), in the transition zone. Not surprisingly BARTL1 and Arl3 can be shown to co-localize, as discussed below (Figure S5).

Interestingly, the BART-like domain of BARTL1 is not sufficient to promote its ciliary localization, as the construct BARTL1¹³³ is not found in cilia (Figure 2C). Hence, the C terminus of BARTL1 mediates and/or supports the localization to cilia by an as yet unknown mechanism. Whereas BART was reported to be localized at the basal body in photoreceptor cells (Davidson et al., 2013) and might be specifically expressed in photoreceptor cells, its localization in ciliated IMCD3 cells is variable and rarely in the cilium (data not shown). Moreover, BART has been reported to enter mitochondria and bind the adenine nucleotide transporter (Sharer et al., 2002). Based on our findings that BARTL1 and Arl3 are ciliary proteins, we postulate a role for BARTL1 in regulating the ciliary localization or function of Arl3, or vice versa.

BART-like Domain of BARTL1 Is Sufficient to Promote Interaction with Arl3

We further investigated the interaction of BARTL1 with Arl3 rather than Arl2, since the former is the focus of our studies on ciliary trafficking. Based on the elution profile of an analytical gel filtration column, we demonstrated that BARTL1 forms a tight

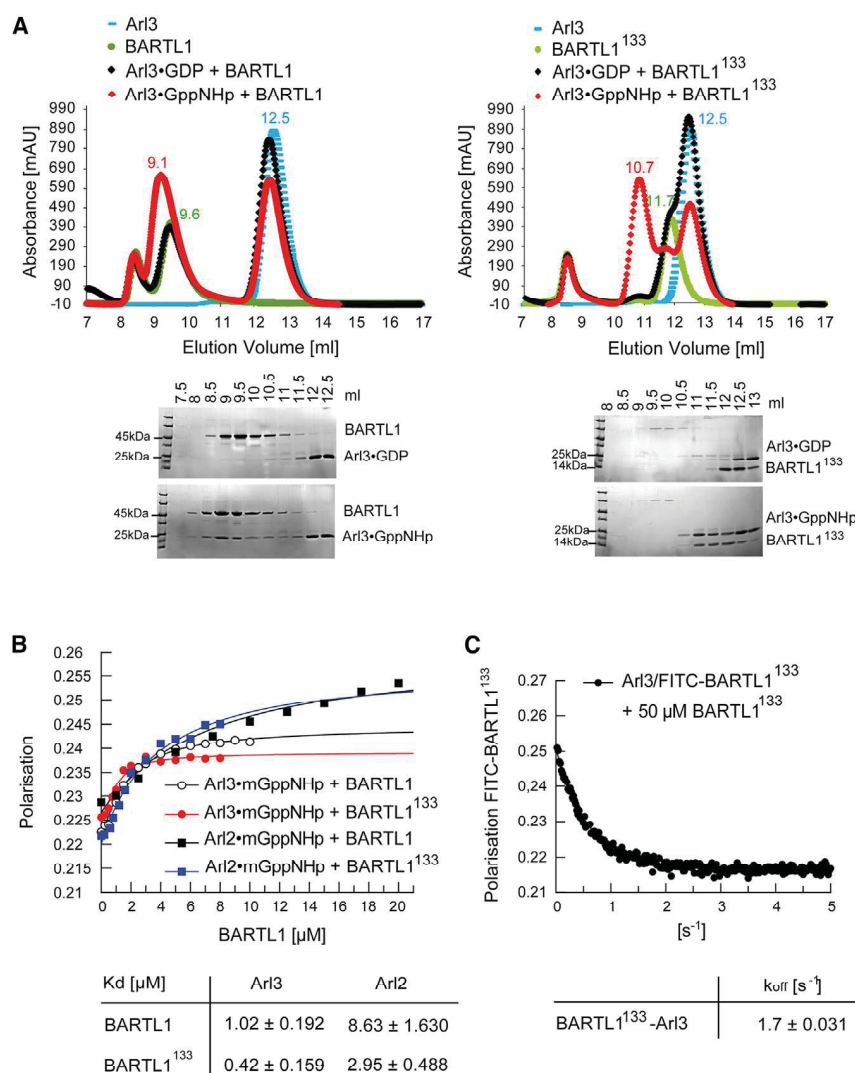


Figure 3. Biochemical Characterization of the BARTL1-Arl Interaction

(A) Analytical size-exclusion chromatography (Superdex75 10/300GL). Elution profiles of BARTL1 full-length (green, left) or BARTL1¹³³ (green, right) alone or mixed with Arl3 full-length bound to GDP (black) or GppNHp (red) as indicated. Elution profile of Arl3 alone is shown in blue. Elution fractions were analyzed by SDS-PAGE and Coomassie staining as shown below the graphs.

(B) Determination of dissociation constants (K_D) by fluorescence polarization measurements at 20°C in buffer M. 1 μM Arl3 or Arl2 full-length bound to mant-GppNHp were titrated with increasing amounts of BARTL1 full-length or BARTL1¹³³. Fitting to a quadratic equation gives the dissociation constants (and standard deviations) shown in the table below the graph.

(C) Stopped-flow fluorescence polarization at 20°C in buffer M. A preformed complex of 1 μM FITC-BARTL1¹³³ with 2 μM Arl3-GppNHp was shot together with a 50-fold excess of unlabeled BARTL1¹³³. The curve was fitted to a single exponential to determine the k_{off} rate (and SD), which is given below the graph.

BARTL1¹³³ by stopped-flow fluorescence polarization measurements employing fluorescein isothiocyanate (FITC)-labeled BARTL1. The k_{off} for the complex is 1.7 s⁻¹, which would give an association rate constant of 4×10^6 M⁻¹ s⁻¹ for the interaction between Arl3 and BARTL1, within the normal range for a protein-protein interaction (Wohlgemuth et al., 2005).

Structure of the Complex between BARTL1 and Arl3

The complex of BARTL1¹³³ with full-length Arl3 bound to the non-hydrolyzable

GTP analog GppNHp crystallized in space group P2₁2₁2₁, and diffracted to 2.2 Å resolution (Table 1; PDB: 4ZI2). The asymmetric unit contained two Arl3-GppNHp and two BARTL1¹³³ molecules (Figure S2A). BARTL1¹³³ displays the same all-helical fold as seen in BART (Zhang et al., 2009) (Figure 4A). The nomenclature of the α helices was adjusted according to the BART structure (PDB: 3DOE). Part of the BART structure in the Arl2-GTP-BART complex (PDB: 3DOE) (Zhang et al., 2009) was not visible in the electron density. However, in BARTL1¹³³ it was visible and termed helix α4', which is situated at a right angle to α4 (Figure 4A). The side chain of residue Lys89^B (superscript B stands for BARTL1, A for Arl3) from α4' forms a hydrogen bond with the backbone oxygen of Lys9^A (Figure 4A, right zoom Area1), which might explain why the α4' helix of BARTL1¹³³ as well as the N-terminal helix of Arl3 are less flexible and could thus be traced in the electron density.

To distinguish crystal packing contacts from the correct Arl3-BARTL1 interface, we compared it with the structure of Arl3-GppNHp-BARTL1¹³³ in space group P2₁, which was solved at 2.0 Å resolution (PDB: 4ZI3; Table 1 and Figure S2B).

complex with Arl3, which is dependent on its nucleotide state (Figure 3A, left panel). Arl3 in its active GppNHp-bound but not in its inactive GDP-bound state forms a complex with BARTL1, which elutes at 9.1 ml compared with 9.6 ml for BARTL1 alone. To find out whether the full-length BARTL1 is necessary for the interaction with Arl3, we tested whether BARTL1¹³³, comprising only the BART-like domain, is sufficient for binding to Arl3. Just as for full-length BARTL1, only Arl3 in its active GppNHp-bound state forms a complex (elution volume 10.7 ml of complex versus 11.7 ml of BARTL1¹³³ alone) with the truncated protein (Figure 3A, right panel).

For a more quantitative analysis, dissociation constants (K_D) were determined by titrating 1 μM Arl3 bound to mant-GppNHp with increasing amounts of effector and measuring fluorescence polarization. Complex formation increases the fluorescence polarization signal and shows that Arl3 binds to BARTL1 or BARTL1¹³³ with K_D of 1 or 0.43 μM, respectively (Figure 3B). Arl2 displays a 10-fold lower affinity to BARTL1 or BARTL1¹³³. Since affinity is usually dictated by the dissociation rate, we determined the dissociation rate constants k_{off} of Arl3 from

Table 1. Data Collection and Refinement Statistics from Molecular Replacement

	Arl3·GppNHp· CCDC104 ¹³³	Arl3·GppNHp· CCDC104 ¹³³
PDB ID	4ZI2	4ZI3
Data Collection		
Space group	P 2 ₁ 2 ₁ 2 ₁	P1 2 ₁ 1
Cell dimensions		
a, b, c (Å)	69.70, 98.60, 102.43	51.55, 67.72, 98.47
α, β, γ (°)	90.00, 90.00, 90.00	90.00, 102.65, 90.00
Resolution (Å)	29.73–2.20 (2.30–2.20)	28.95–2.00 (2.10–2.00)
R _{sym} or R _{merge}	11.0 (54.0)	5.8 (39.8)
I/σI	11.87 (3.66)	15.28 (3.72)
Completeness (%)	99.9 (99.9)	99.2 (99.1)
Redundancy	6.55 (6.80)	3.35 (3.24)
Refinement		
Resolution (Å)	2.20	2.00
No. of reflections	36,470	44,692
R _{work} /R _{free}	0.2087/0.2660	0.1893/0.2427
No. of atoms		
Total	5,442	5,335
Protein	4,993	4,995
Ligand/ion	66	66
Water	383	274
B factors	37.54	45.63
Rmsd		
Bond lengths (Å)	0.008	0.008
Bond angles (°)	1.098	1.145

Values in parentheses are for highest-resolution shell.

Comparison of these structures with that of Arl2·GTP·BART (PDB: 3DOE; Figure S2C) (Zhang et al., 2009) led us to postulate two areas contributing to the Arl3·BARTL1 interface (Figure 4A). As expected for an effector of small G proteins, BARTL1 is in contact with the switch regions of Arl3 (area 2). In addition, BARTL1 completely buries the N-terminal helix of Arl3 (area 1). This unconventional binding mode sets it apart from effectors such as PDE6δ or Unc119 and from many other effectors of the Ras superfamily proteins (Wittinghofer and Vetter, 2010). The hydrophobic side of the N-terminal amphipathic helix of Arl3 is buried in a hydrophobic groove (Figures 4 and S2D) formed by helices α3, α4, α4', and α5 of BARTL1. Leu3^A, Leu4^A, Ile6^A, Leu7^A, and Leu10^A are submerged in a hydrophobic patch made up by Lys58^B, Val61^B, Leu65^B, and Leu69^B on α3, Phe79^B and Cys83^B on α4, Ala88^B on α4', and Leu97^B, Val100^B, and Leu101^B on α5 (BARTL1 [B] and Arl3 [A]; Figures 4A area 1, and 4B). Alignment of the Arl3 N-terminal sequence of different species shows a conserved LLxILxxL motif (Figure 4C). A similar motif is found in the Arl2·GTP·BART complex. To define the contribution of these residues to the interaction, conserved residues in the ₃LLxILxxL₁₀ motif of the Arl3 N-terminal helix were mutated, and the mutated proteins analyzed in a pull-down assay. Binding to GST-BARTL1¹³³ was disrupted for the mutants Arl3^{L3D}, Arl3^{L4D}, Arl3^{L7D}, and Arl^{L10D}. Surprisingly, even though Ile6 is also pointing into the hydrophobic core of

the interface, the Arl3^{16R} mutation does not change the affinity (Figure 5A).

The second interface area is formed by switch I, switch II, and residues of the interswitch toggle of Arl3, and on the BARTL1¹³³ side by the loop connecting α2 and α3 as well as parts of the α3 and α6 helices (Figure 4A, area 2). Hydrophobic interactions involving Phe51^A and Ile53^A of β2, Trp66^A of β3, Ile74^A, Tyr81^A in switch II, and Phe106^B of α6, and Leu48^B and Thr51^B of α3 seem to be important. There are polar interactions between Thr51^B and Tyr81^A, switch I main-chain nitrogens of Gln49^A and Gly50^A with Glu45^B and Glu44^B of the α2-α3 loop with Lys45^A of β2 in the interswitch toggle and Lys35^A in the α1 helix (Figures 4A and 4B). Mutations of F51A and Y81A in Arl3 in area 2 weaken the interactions with GST-BARTL1¹³³ in a pull-down assay while Y71A seems to have no effect (Figure 5A). Introduction of single-residue mutations on the side of BARTL1¹³³ were not sufficient to disturb the interaction, so double or triple mutations had to be introduced. The simultaneous mutation of Cys83, Leu65, and Val100 in the hydrophobic groove on the surface of BARTL1 weakens the interaction with Arl3. The loss of the polar interactions by the double mutant BARTL1^{133 E44/45R} also disrupts the interaction with Arl3 (Figure 5B).

Arl3·BARTL1 Complex Compared with Arl2·BART

BARTL1 complexing with Arl3 displays similar recognition motifs as seen in the BART·Arl2 crystal structure. Arl3 and Arl2 of both structures overlay with a root-mean-square deviation (rmsd) of 0.788 Å² over 165 residues (Figure S3, left), whereas BARTL1 and BART superimpose with an rmsd of 3.521 Å² over 94 residues (Figure S3, right). Focusing on the superimposition of Arl2/3, the core G domains align nearly perfectly, with the main differences in the conformation of the N and C termini and similar relative locations of BARTL1 and BART. Whereas fewer residues of the N and C terminus of BART are visible and the region between α4 and α5 helices is not resolved, these parts of BARTL1 can be traced (Figure S3 and Figure 5C, upper), partly due to the interaction between Lys89 side chain of BARTL1 from α4' with the backbone oxygen of Lys9 of Arl3 (Figure 4A, see above). In contrast, the N-terminal helix of Arl2 seems to be anchored by an H bond of Glu74^{BART} with the backbone nitrogen of Leu3^{Arl2}, an interaction not found in the Arl3·BARTL1 complex. Further major differences in interaction area 1 are the polar interactions of Lys11^{Arl2} with Asp110^{BART}, and Lys8^{Arl2} with Thr116^{BART}, while Lys11 and Arg8 of Arl3 are not involved in any interactions (Figures 5C, upper and 5D). While in the Arl3·BARTL1 structure more hydrophobic contacts are formed by Leu10, Leu7, and Ile6 of Arl3, in the Arl2·BART structure Leu3 and Leu4 of Arl2 are involved in more hydrophobic interactions. Hence, Leu10 is more important in Arl3 and constitutes a conserved LLxILxxL motif while in Arl2 a conserved LLxIL motif is present, as was found by Zhang et al. (2009). The contact area 2 between the switch regions of Arl2/3 and BART/BARTL1 are nearly identical, as summarized in Figure 5D (lower).

N-Terminal Helix of Arl3 Is Crucial for Interaction with BARTL1 and Essential for Its Ciliary Localization

Based on the presence of a conserved N-terminal sequence in Arl3 and mutational analysis mentioned above, we hypothesized that the N-terminal helix is crucial for the interaction of Arl3 with

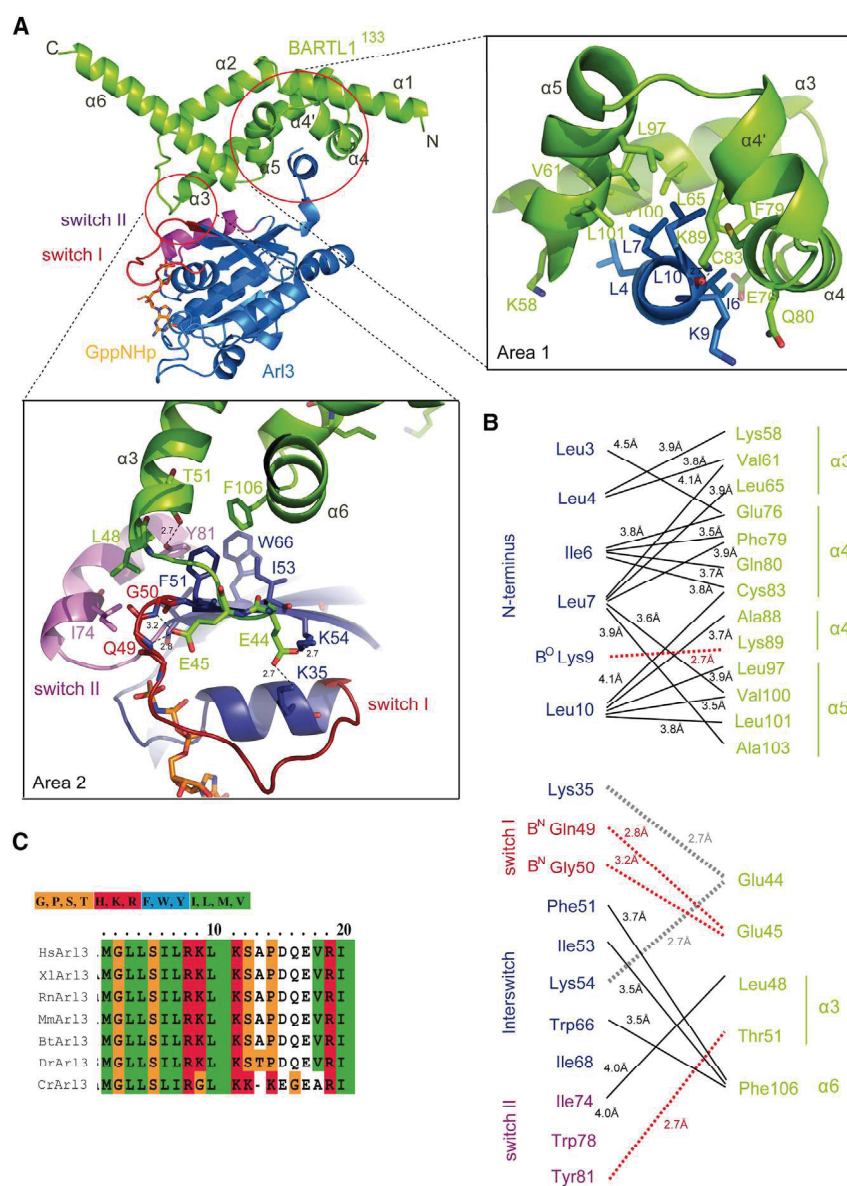


Figure 4. Structure of the Arl3-GppNHp-BARTL1¹³³ Complex

(A) Overview (left) and zoom-in of the interaction area 1 (right), with N-terminal helix of Arl3 (blue) buried in a hydrophobic groove of BARTL1¹³³ (green). Zoom-in of interaction area 2 (below) shows BARTL1¹³³ contacting switches I (red) and II (purple) of Arl3. α Helices of BARTL1¹³³ are numbered.

(B) Schematic overview of residues from BARTL1¹³³ (green) and Arl3 (blue) involved in the interaction: hydrophobic van der Waals interactions (solid black lines) involving the side chains of the residues indicated, H bonds (red dotted lines), and salt bridges (gray dotted lines). H bonds to backbone oxygen or nitrogen of residues are indicated by B^O or B^N, respectively. Distances are indicated in angstroms.

(C) Alignment of N terminus of Arl3 from different organisms, *Homo sapiens* (Hs), *Mus musculus* (Mm), *Rattus norvegicus* (Rn), *Xenopus laevis* (Xl), *Bos taurus* (Bt), *Danio rerio* (Dr), *Caenorhabditis elegans* (Ce), and *Chlamydomonas reinhardtii* (Cr), shows that the N-terminal hydrophobic LLxLLxxL motif is highly conserved in Arl3. Amino acids are colored according to the residue identity. Hydrophobic residues are shown in green.

To investigate whether the ciliary localization of Arl3 and BARTL1 is dependent on their interaction, we generated various stable IMCD3 Flp-In cell lines. Deletion of the Arl3 N-terminal helix leads to a complete loss of the ciliary localization of Arl3. A C-terminal GFP fusion construct of Arl3 Δ N compared with full-length Arl3 shows no GFP signal in cilia and lacks complete co-localization with the ciliary marker acetylated α -tubulin (Figure 7A). Hence, the N terminus of Arl3 seems to be part of or the complete ciliary localization signal. This result is surprising and raises the question why Arl2, despite 52% identity to Arl3 and only minor differences

BARTL1. Deletion of the N terminus leads to complete loss of complex formation. The elution profile of an analytical gel filtration shows no complex formation of BARTL1¹³³ with Arl3 Δ N in its active GppNHp-bound state (Figure 6A). To more quantitatively describe the effect of the mutation, we carried out fluorescence polarization measurements using Cy5-labeled BARTL1¹³³. Our results support the notion that the absence of the Arl3 N terminus leads to a K_D higher than 50 μ M, representing a more than 100-fold loss in affinity (Figure 6B). The mutation of the N-terminal residue Leu4 in Arl3 reduces affinity by 10-fold (Figure 6B), indicating that a single mutation within the hydrophobic motif $_3$ LLxLLxxL₁₀ is not enough to mimic the deletion of the whole Arl3 N terminus. Since the mutant protein Arl3^{F51A} shows a similar drastic, more than 100-fold loss of affinity, we can conclude that both contact areas make significant contributions to the affinity of the interaction.

in its N-terminal sequence, is not a ciliary protein. We generated a chimera of the Arl2 G domain fused to the N-terminal 17 amino acids of Arl3 (Arl2-3Nterm), which failed to localize to cilia (Figure 7A). We concluded that the Arl3 N terminus is not sufficient to mediate localization to cilia and that the full context of the Arl3 protein is required instead (Ismail et al., 2012). This seems to indicate that a specific retention signal is required for the ciliary localization of Arl3.

We therefore hypothesized that an effector binding to the N terminus of Arl3, such as BARTL1, is either crucial to mediate the transport of Arl3 into cilia or is important to retain Arl3 within cilia, an assumption that is supported by the co-localization of the two proteins. We thus generated cell lines stably expressing GFP-tagged Arl3^{L4D} and Arl3^{F51A} mutants, which have defects in binding to BARTL1 as demonstrated above. Arl3^{L4D} completely failed to localize to cilia (Figure 7A). Notably, the

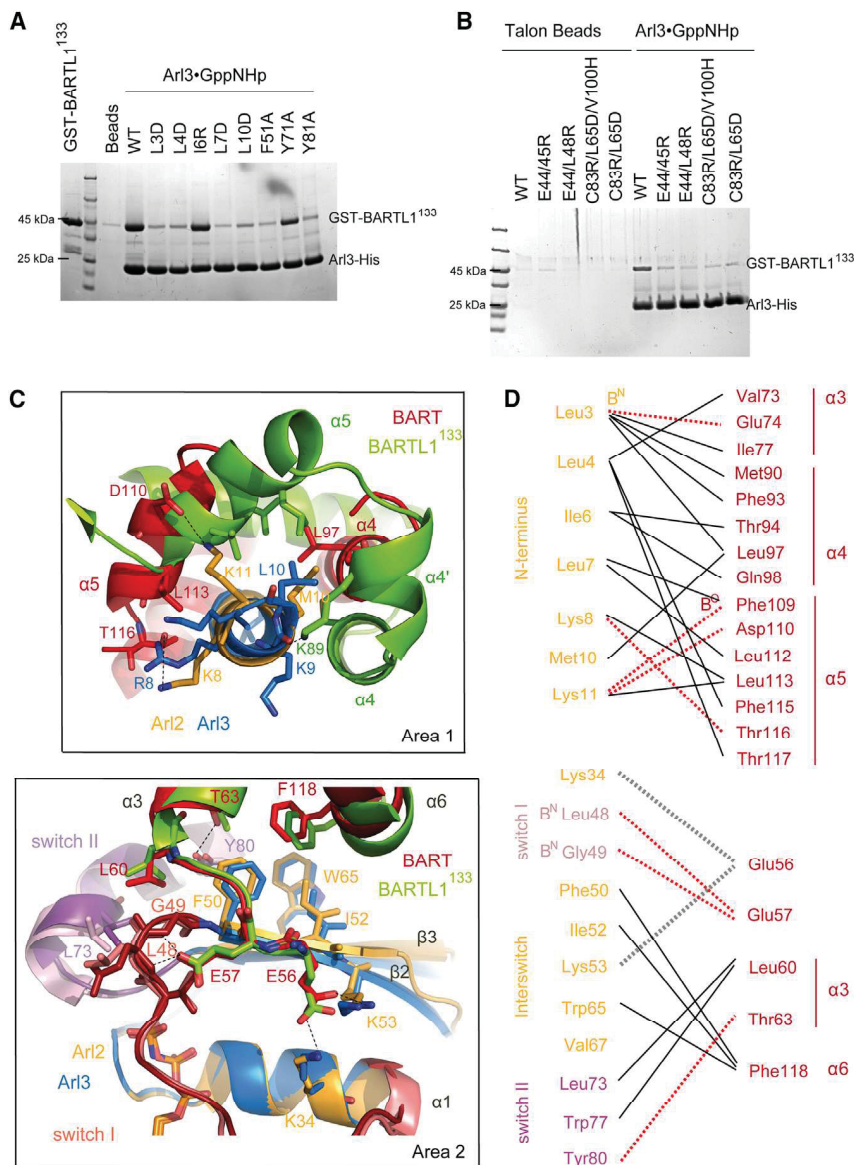


Figure 5. Biochemical Characterization of the Interface of the Arl3-GppNHp-BARTL1¹³³ Complex and Comparison with Arl2-GTP-BART

(A) Pull-down of GST-BARTL1¹³³ wild-type by either wild-type or mutant Arl3-His bound to Talon beads.

(B) Pull-down of GST-BARTL1¹³³ wild-type or mutants by Arl3-His bound to Talon beads.

(C) Interaction area 1 (upper) as in Figure 3A from the BARTL1¹³³ (green) or BART (red) complexes obtained by superimposing the N-terminal helices of Arl3 (blue) with Arl2 (orange), respectively; interaction area 2 (below) as in Figure 3A, obtained by superimposition of Arl2 and Arl3, shows contact of switches I (red) and II (purple) of Arl3 or Arl2, with BARTL1¹³³ or BART, respectively.

(D) Schematic overview of residues from BART (red) and Arl2 (orange) involved in the interaction interface as described in Figure 4B.

S4B), although it cannot be excluded that small interfering RNA (siRNA) knock-down did not result in a complete abolition of the relevant protein levels and therefore led to no observable cellular phenotype (Figure S4B).

DISCUSSION

Here, we demonstrate by X-ray structure determination that BARTL1 binds Arl3-GppNHp in a similar fashion to BART complexing Arl2-GTP (Zhang et al., 2009). It was previously shown that BART is an Arl2/3 effector (Sharer and Kahn, 1999; Veltel et al., 2008b; Zhang et al., 2009), as we demonstrate here for BARTL1. Therefore, both BART and BARTL1 form a group of Arl2/3 effectors displaying an all-helical BART domain with an unconventional recognition mode involving the binding of the N-terminal helix of Arl2/3 apart from the switches.

This binding mode is clearly different from the second group of Arl2/3 effectors formed by PDE6δ, HRG4, Unc119a, and Unc119b. These effectors display an immunoglobulin β-sandwich fold and bind to the switch regions of Arl2/3, thereby continuing the central β sheet of the Arl G protein. The structure of Arl3-Unc119a shows that the N-terminal helix of Arl3 is not contacting the effector but is important for the release of myristoylated cargo from Unc119a (Ismail et al., 2012). Biochemically we show that the N terminus of Arl2 does not affect cargo release.

Having shown that BARTL1 is a bona fide effector that binds to the GTP-bound form of Arl3 (and Arl2), we set out to speculate on the role of this interaction. We show here that both Arl3 and BARTL1 seem to be ciliary proteins with a partly overlapping localization. While Arl3 is co-staining with acetylated α-tubulin over the entire length of the cilia axoneme and seems

cilia length was also reduced in cell lines expressing Arl3^{L4D}-GFP compared with Arl3^{WT}-GFP (Figure S4A). Arl3^{L4D} decreases affinity to BARTL1 by 10-fold, so this effect could potentially be attributed to a weakened interaction. However, in contrast to our expectations, the mutant Arl3^{F51A} with a drastically reduced affinity to BARTL1 shows no defects in localization or cilia length (Figures 7A and S4A). We can thus conclude that the interaction with BARTL1 is not responsible for ciliary localization. We may also conclude, however, that the L4D mutation does disrupt the binding of Arl3 to membranes, which is heavily dependent on the N-terminal amphipathic helix (our unpublished data). For further analysis, we performed knockdown experiments. A knockdown of Arl3 had no effect on the localization of a C-terminal GFP fusion construct of BARTL1 (Figures 7B and S4B). Hence, it can be concluded that Arl3 is not regulating the localization of BARTL1. A knockdown of BARTL1 in Arl3 stable cell lines also showed no effect (Figures 7B and

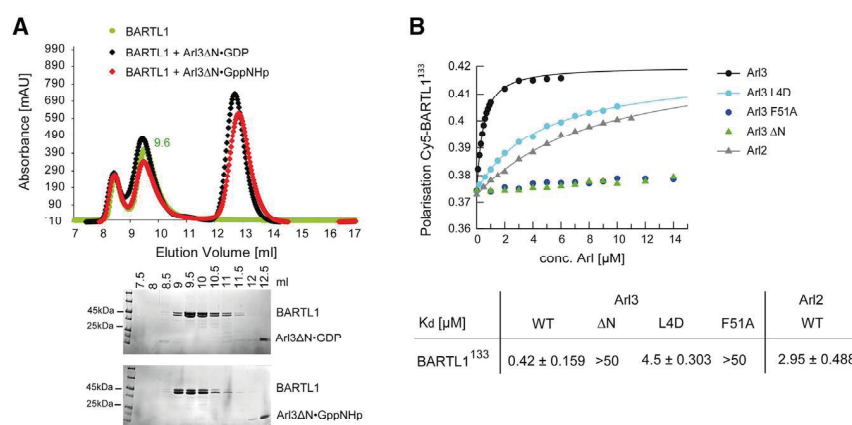


Figure 6. N-Terminal Helix of Arl3 is Crucial for the Interaction with BARTL1

(A) Analytical size-exclusion chromatography (Superdex75 10/300GL) of BARTL1 alone (green) or mixed with Arl3ΔN bound to GDP (black) or GppNHp (red) as indicated. Elution fractions were analyzed by SDS-PAGE and Coomassie staining as shown below the graph.

(B) Determination of dissociation constants (K_D) by fluorescence polarization measurements at 20°C in buffer M. 200 nM Cy5-BARTL1¹³³ was titrated with increasing amounts of Arl3^{WT}, Arl3^{L4D}, Arl3^{F51A}, Arl3^{ΔN}, and Arl2^{WT}. Fitting to a quadratic equation gives the dissociation constants (and SDs) shown in the table below the graph.

concentrated at the transition zone, BARTL1 co-localizes with Arl3 distal to the basal body, corresponding to the transition zone, localized between basal body and cilia axoneme, as shown by co-staining with γ -tubulin as a basal body marker. Staining of endogenous Arl3 in a stable cell line expressing BARTL1-GFP confirms that both proteins are present in the cilia axoneme and around the transition zone (Figure S5). In addition, we have shown here by knockdown experiments that this localization is not dependent on the presence of either of the two proteins.

We would like to propose two possible, though not necessarily mutually exclusive, roles for the Arl3-BARTL1 interaction. It has been shown by us and others that the GTP-bound form of Arl3 releases farnesylated and myristoylated ciliary cargo from the transport factors PDE6 δ and Unc119a/b. Since this is required for cargo to be transported into cilia, Arl3 is most likely localized as Arl3-GTP inside cilia. The exclusive localization of active Arl3 inside cilia is guaranteed by the Arl3-specific GTPase-activating protein RP2, which we find enriched around the basal body in IMCD3 cells (Figure S6A). We thus propose that the role of BARTL1 might be to prevent or reduce membrane interaction of Arl3-GTP and mediate the GTP hydrolysis of Arl3-GTP by RP2. We have shown that the nucleotide state and the presence of the N terminus are important for the membrane interaction of Arl3 (K.W., unpublished data). This is supported by a liposome sedimentation assay, whereby more Arl3 in its active GppNHp-bound state is precipitated than in its inactive GDP-bound state, representing the fraction bound to liposomes (Figure 8A). Addition of BARTL1¹³³ to Arl3 reduces the association of Arl3-GppNHp with liposomes.

Furthermore, superimposing the Arl3-BARTL1 (PDB: 4ZI2) structure with that of the Arl3ΔN-RP2 complex (PDB: 3BH6; Figure 8B) (Veltel et al., 2008a) shows that a triple complex between the three components can in principle be formed. Such a complex would, however, be very transient, since the addition of RP2 to an Arl3-GppNHp-BARTL1¹³³ complex leads to dissociation, as shown by fluorescence polarization using Cy5-labeled BARTL1¹³³ (Figure 8C). This experiment suggests a displacement of Arl3-GppNHp from Cy5-BARTL1¹³³ and formation of an Arl3-GppNHp-RP2 complex. An interaction between Cy5-BARTL1¹³³ and RP2 could not be observed (data not shown) although we cannot exclude that the C terminus of BARTL1 might play a role in this interaction. Addition of Arl3 to full-length

Cy5-BARTL1 showed no signal change, and therefore could not be used to test for triple complex formation (data not shown). Although BARTL1 does not influence either the intrinsic or the RP2-stimulated GTP hydrolysis of Arl3 (Figure S6B), the localization of BARTL1 on top of the RP2 domain might still mediate the exit of Arl3 as an Arl3-GTP complex from the cilium through the transition zone toward the basal body, followed by GTP hydrolysis mediated by RP2. Such a scenario might also be responsible for creating an energetic driving force for the entry of cargo into cilia, just as Ran-GTP hydrolysis is the driving force for nucleocytoplasmic transport across the nuclear pore.

EXPERIMENTAL PROCEDURES

See [Supplemental Experimental Procedures](#) for plasmids and protein purification, Cy5 and FITC labeling of BARTL1, tandem affinity purification, mass spectrometry and liposome sedimentation assay.

Crystallization

Native full-length Arl3 was purified and exchanged as previously described to be completely loaded with GppNHp (Veltel et al., 2006, 2008b). Arl3-GppNHp was mixed with BARTL1¹³³ in a molar ratio of 1.3 to 1 at 16.7 mg/ml. The sitting-drop/vapor diffusion method was used, and initial conditions were established in EasyXtal CORE II Suite (1 M LiCl, 0.1 M MES [pH 6.0], 30% polyethylene glycol [PEG] 6000) and EasyXtal PEG II Suite (1 M LiCl, 0.1 M Tris [pH 8.5], 20% PEG 4000) from Qiagen. Crystals appeared after 1–3 days and were flash-frozen after 3 days from a 96-well screen in cryosolution containing the same constituents as the crystallizing condition supplemented with 20% glycerol. Crystals from the CORE II Suite were of space group P2₁2₁2₁ and crystals from the PEG II Suite were of space group P2₁ (Table 1). Data were collected at the PXII X10SA beamline of the Swiss Light Source (SLS) and was indexed and processed with XDS (Kabsch, 1993). Molecular replacement using different Arl structures was done with MOLREP and PHASER from the CCP4 package (Collaborative Computational Project Number 4, 1994). A model of the BARTL1¹³³ sequence generated by the PHYRE threader based on BART (3DOE) was used in molecular replacement to solve the BARTL1¹³³ structure in the complex. The structure was refined using REFMAC5 (Murshudov et al., 1997) to the following resolutions (Ramachandran statistics in parentheses): Arl3-GppNHp-BARTL1¹³³ native P2₁2₁2₁ to 2.2 Å (99.0% favored, 1.0% allowed, 0% outliers) and P2₁ to 2.0 Å (97.6% favored, 2.4% allowed, 0% outliers). Structures were deposited in the RCSB PDB databank with entry codes PDB: 4ZI2 and 4ZI3, respectively. For data and refinement statistics, see Table 1. All figures were produced using PYMOL (DeLano Scientific).

Analytical Size-Exclusion Chromatography

Complex formation of Arl3 or Arl3ΔN with BARTL1 or BARTL1¹³³ was investigated by analytical size-exclusion chromatography using a Superdex200

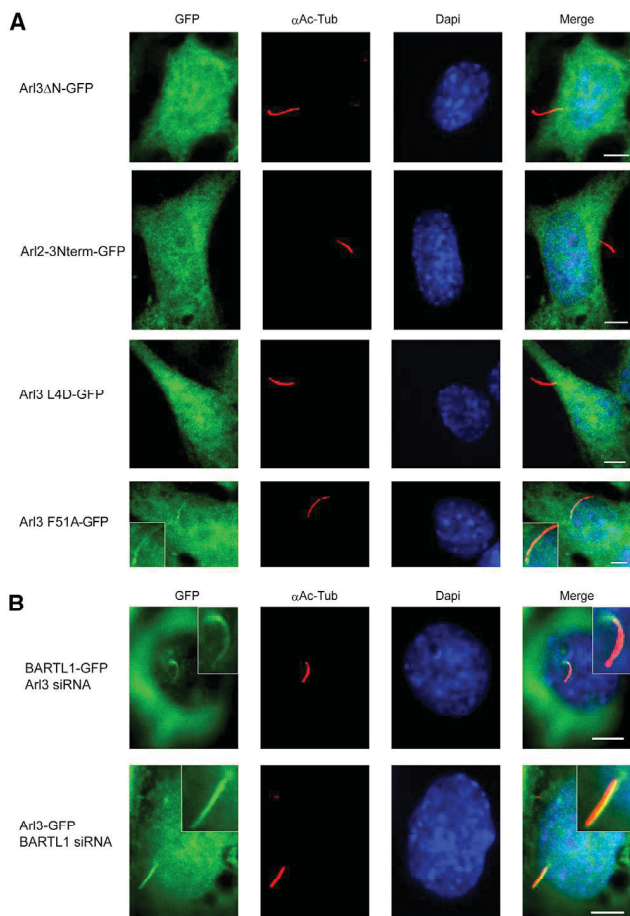


Figure 7. Localization of Arl3 Mutants in IMCD3 Cells and Knockdown of Arl3 and BARTL1, Using the Presentation Scheme as Explained in Figure 2

(A) Stably expressed, C-terminally GFP-tagged mouse Arl3^{ΔN}, Arl2^{3Nterm}, Arl3^{L4D}, and Arl3^{F51A} in IMCD3 Flp-In cells were immunostained for acetylated α -tubulin (AcTub) and the nucleus (DAPI) as indicated.

(B) Transient knockdown of BARTL1 in IMCD3 Flp-In cells stably expressing Arl3-GFP (upper panels) and knockdown of Arl3 in cells stably expressing BARTL1-GFP (lower panels). The efficiency of knockdown was analyzed by western blot of cell lysates, and is shown in Figure S4.

10/300 column (GE Healthcare). 0.5 mg of Arl3 protein was incubated with a 10-fold molar excess of GDP or GppNHp for 2 hr at room temperature. The mix was supplemented with 0.5 mg of full-length or truncated BARTL1 or BARTL1¹³³, applied to the size-exclusion chromatography column, and eluted with one column volume of buffer M. The elution profile was recorded and eluted fractions analyzed by SDS-PAGE.

Determination of Dissociation Rates by Stopped Flow

A preformed complex of 2 μ M Arl3-GppNHp with 1 μ M FITC-BARTL1¹³³ was shot together with a 50-fold excess of unlabeled BARTL1¹³³. The dissociation of the complex was followed by monitoring the polarization signal at excitation and emission wavelengths of FITC at 490 and 520 nm, respectively. Single exponential functions were fitted to the data using Grafit5 (Erithacus Software) to obtain the k_{off} values.

Affinity Measurements

Arl3^{WT}, Arl3^{L4D}, Arl3^{F51A}, and Arl2^{WT} were loaded with mant-GDP or mant-GppNHp (Pharma Waldhof) overnight at 12°C by incubation with a 1.5-fold

molar excess of nucleotide, and purified the following day on a Desalting Column in buffer M (Veltel et al., 2008b). Nucleotide loading was determined by high-performance liquid chromatography measurements on a C18 column. Polarization data were recorded with a Fluoromax-4 spectrophotometer (Jobin Yvon), with excitation and emission wavelengths of mant-nucleotides at 366 and 450 nm, respectively. Binding affinities of Arl3^{WT}, Arl3^{L4D}, Arl3^{F51A}, and Arl2^{WT} to BARTL1 and BARTL1¹³³ were measured by monitoring the polarization signal during titration of 1 μ M Arl3 loaded with the respective nucleotide with increasing amounts of the interaction partner at 20°C in buffer M. Cy5-BARTL1¹³³ was used to determine binding affinities to Arl3^{WT}, Arl3^{L4D}, Arl3^{F51A}, Arl3^{ΔN}, and Arl2^{WT} bound to GppNHp. 0.2 μ M Cy5-BARTL1¹³³ was titrated with increasing amounts of Arl proteins, and polarization data were recorded with excitation and emission wavelengths of Cy5 at 650 and 670 nm, respectively. Obtained data points were fitted to a first-order reaction using Grafit5 (Erithacus Software) to obtain the dissociation constant, K_D .

Generation of Stable Cell Lines

Mouse renal epithelial Flp-In cells from the inner medullary collecting duct (IMCD3 Flp-In; kind gift from M.V. Nachury) were cultured at 37°C and 5% CO₂ in DMEM/F12, HEPES (Life Technologies) complemented with 10% fetal bovine serum (FBS), and 1% L-glutamine. Stable cell lines were generated as previously described (Sang et al., 2011; Torres et al., 2009). In short, the parental IMCD3 Flp-In cell line contains a stably integrated FRT cassette and was co-transfected with pOG44 coding an FLP recombinase, and the appropriate construct cloned into pGLP5 vector (Addgene), coding for a C-terminal S- and GFP-tag, using Lipofectamine 2000 (Life Technologies). Selection by supplementing the media with 200 μ g/ml hygromycin (Merck) for successful stable genomic integration was carried out, and expression of the GFP fusion protein was checked by western blot using an anti-GFP antibody (1:500; Santa Cruz Biotechnology).

Knockdown

Stable IMCD3 Flp-In cell lines expressing Arl3 or CCDC104/BARTL1 were plated on poly-L-lysine-coated coverslips. After 24 hr, cells were transfected with 100 nM siRNAs directed against mouse *ARL3* or mouse *CCDC104* and a negative control siRNA, using Lipofectamine 2000 following the manufacturer's recommendations. FlexiTube siRNA oligos SI00214963 directed against *ARL3*, FlexiTube siRNA oligos SI00848855 directed against *CCDC104*, and negative control siRNA (scrambled) oligo 1027310 were used (Qiagen). 48 hr after transfection of siRNAs against *ARL3*, cells were serum-starved for 24 hr or, 24 hr after transfection of siRNAs against *CCDC104* and direct serum starvation, cells were treated for immunofluorescence microscopy as described below. Images were collected using identical settings for each sample.

Imaging by Microscopy

IMCD3 stably expressing GFP fusion proteins were plated on poly-L-lysine-coated coverslips and cilia induced by 48 hr of serum starvation. Cells were washed in PBS and fixed with 4% formaldehyde for 20 min (AcTub) or 2% formaldehyde and 50% ice-cold methanol for 15 min at 4°C (γ -Tub). Cells were permeabilized with 0.3% Triton X-100 in cytoskeletal buffer for 10 min. Cells were rinsed in 0.1% Tween 20 in PBS and blocked in 10% FBS in PBS for 30 min. For immunostaining of primary cilia, mouse 611B1 anti-acetylated α -tubulin antibody (1:5000; Sigma-Aldrich) or anti-Arl13B antibody (1:1000; Proteintech); and for basal body staining anti- γ -tubulin antibody (clone GTU-88, 1:1500; Sigma-Aldrich) and Arl3 staining anti-Arl3 antibody (1:500; Novus Biologicals) in 10% FBS in PBS were incubated overnight at 4°C. Alexa Fluor 647 or 405 anti-mouse or Alexa Fluor 647 anti-rabbit antibody (1:800; Life Technologies) was added for 45 min at room temperature. Coverslips were rinsed three times in 0.1% Tween 20 in PBS and once in PBS. Nuclei were stained with DAPI (Serva) diluted 1:10,000 in PBS for 1 min. Coverslips were fixed on glass slides with Mowiol (Merck). Images were taken using an Olympus IX81 microscope with a CCD camera and a 60 \times NA 1.35 objective. In all cases at least three independent staining experiments were carried out, and 100 cells were used for analysis.

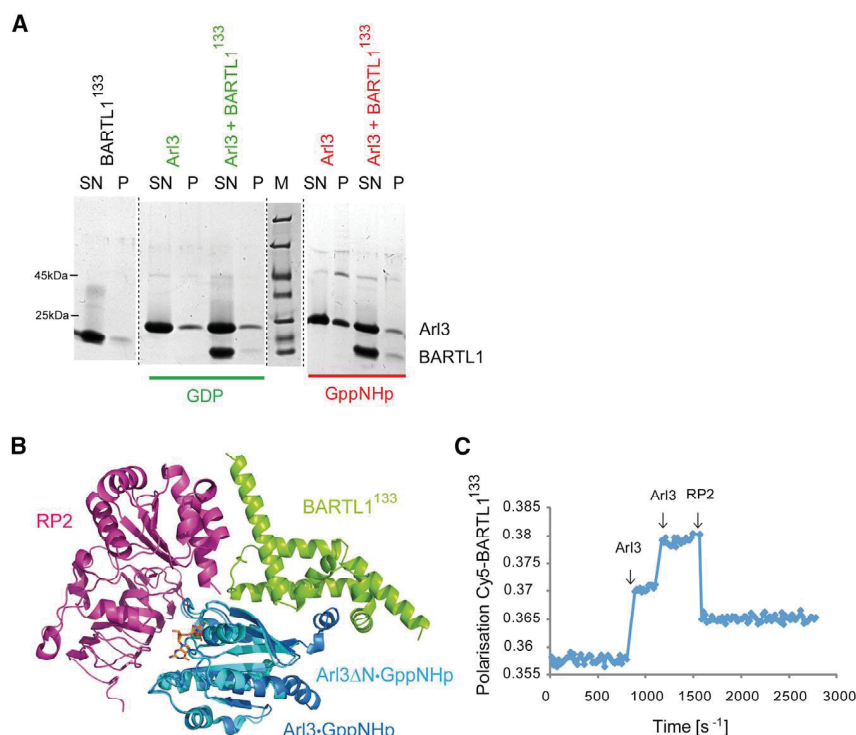


Figure 8. Investigation into Possible Function of BARTL1

(A) Liposome sedimentation assay. 2.8 mM of 200- μ m liposomes of DOPC/DOPG/DPPC/DPPG/cholesterol composition were incubated with 20 μ M Arl3 bound to GDP or GppNHp in the presence of 40 μ M BARTL1¹³³. Aliquots of the supernatant (SN) and pellet (P) compared with the marker (M) following sedimentation were analyzed by SDS-PAGE.

(B) Overlay of Arl3-GppNHp-RP2 (PDB: 3BH6) with Arl3-GppNHp-BARTL1¹³³ (PDB: 4ZI2).

(C) Fluorescence polarization measurements at 20°C in buffer M: 1 μ M Cy5-BARTL1¹³³ was titrated twice with 1 μ M Arl3-GppNHp, followed by addition of 10 μ M RP2 (as indicated by arrows).

SUPPLEMENTAL INFORMATION

Supplemental Information includes Supplemental Experimental Procedures, six figures, one table, and two 3D molecular models and can be found with this article online at <http://dx.doi.org/10.1016/j.str.2015.08.016>.

AUTHOR CONTRIBUTIONS

Protein preparation, biochemical/biophysical measurements, generation of stable cell lines, crystallization, X-ray data analysis, and manuscript preparation were carried out by M.L. C.K. cloned various constructs and helped in purifying proteins. S.K. carried out the generation of stable cell lines, knock-down experiments, immunostaining, and analysis by fluorescence microscopy. S.M.L. examined triple complex formation by polarization experiments. TAP experiments were carried out with the help of S.E.C.v.B. TAP eluates were analyzed using mass spectrometry by N.H. and K.B., and data were processed by J.v.R. under supervision of M.U. and R.R., respectively. Project design, supervision, and manuscript preparation were supervised by A.W.

ACKNOWLEDGMENTS

We would like to thank David Bier, Matthias Müller, Mandy Lokaj, and the SLS beamline staff Florian Dworkowski and Takashi Tomizaki for data collection of the crystals at the Swiss Light Source, beamline PXII-X10SA, Paul Scherer Institute, Villigen, Switzerland. This work was supported by the European Research Council (ERC) Advanced Grant (Project Title: ARCID; No. 268782) to A.W. and by the European Community's Seventh Framework Programmes FP7/2009 under grant agreement no: 241955 (SYSCILIA) to R.R. and M.U.

Received: June 9, 2015

Revised: August 26, 2015

Accepted: August 29, 2015

Published: October 8, 2015

REFERENCES

- Avidor-Reiss, T., Maer, A.M., Koundakjian, E., Polyanovsky, A., Keil, T., Subramaniam, S., and Zuker, C.S. (2004). Decoding cilia function: defining specialized genes required for compartmentalized cilia biogenesis. *Cell* 117, 527–539.
- Berken, A., Thomas, C., and Wittinghofer, A. (2005). A new family of RhoGEFs activates the Rop molecular switch in plants. *Nature* 436, 1176–1180.
- Bhamidipati, A., Lewis, S.A., and Cowan, N.J. (2000). ADP ribosylation factor-like protein 2 (Arl2) regulates the interaction of tubulin-folding cofactor D with native tubulin. *J. Cell Biol.* 149, 1087–1096.
- Cantagrel, V., Silhavy, J.L., Bielas, S.L., Swistun, D., Marsh, S.E., Bertrand, J.Y., Audollent, S., Attié-Bitach, T., Holden, K.R., Dobyns, W.B., et al. (2008). Mutations in the cilia gene ARL13B lead to the classical form of Joubert syndrome. *Am. J. Hum. Genet.* 83, 170–179.
- Chandra, A., Grecco, H.E., Pisupati, V., Perera, D., Cassidy, L., Skoulidis, F., Ismail, S.A., Hedberg, C., Hanzal-Bayer, M., Venkitaraman, A.R., et al. (2012). The GDI-like solubilizing factor PDE δ sustains the spatial organization and signalling of Ras family proteins. *Nat. Cell Biol.* 14, 148–158.
- Cherfils, J., and Zeghouf, M. (2013). Regulation of small GTPases by GEFs, GAPs, and GDIs. *Physiol. Rev.* 93, 269–309.
- Collaborative Computational Project Number 4. (1994). The CCP4 suite: programs for protein crystallography. *Acta Crystallogr. D Biol. Crystallogr.* 50, 760–763.
- Cox, A.D., and Der, C.J. (2010). Ras history. *Small GTPases* 1, 1–27.
- Cuvillier, A., Redon, F., Antoine, J.C., Chardin, P., DeVos, T., and Merlin, G. (2000). LdARL-3A, a *Leishmania* promastigote-specific ADP-ribosylation factor-like protein, is essential for flagellum integrity. *J. Cell Sci.* 113, 2065–2074.
- Davidson, A.E., Schwarz, N., Zelinger, L., Stern-Schneider, G., Shoemark, A., Spitzbarth, B., Gross, M., Laxer, U., Sosna, J., Sergouniotis, P.I., et al. (2013). Mutations in ARL2BP, encoding ADP-ribosylation-factor-like 2 binding protein, cause autosomal-recessive retinitis pigmentosa. *Am. J. Hum. Genet.* 93, 321–329.

- Efimenko, E., Bubb, K., Mak, H.Y., Holzman, T., Leroux, M.R., Ruvkun, G., Thomas, J.H., and Swoboda, P. (2005). Analysis of *xbx* genes in *C. elegans*. *Development* 132, 1923–1934.
- Eggenschwiler, J.T., and Anderson, K.V. (2007). Cilia and developmental signaling. *Annu. Rev. Cell Dev. Biol.* 23, 345–373.
- Fan, Y., Esmail, M.A., Ansley, S.J., Blacque, O.E., Boroevich, K., Ross, A.J., Moore, S.J., Badano, J.L., May-Simera, H., Compton, D.S., et al. (2004). Mutations in a member of the Ras superfamily of small GTP-binding proteins causes Bardet-Biedl syndrome. *Nat. Genet.* 36, 989–993.
- Gillingham, A.K., and Munro, S. (2007). The small G proteins of the Arf family and their regulators. *PLoS One* 2, e842.
- Goetz, S.C., and Anderson, K.V. (2010). The primary cilium: a signalling centre during vertebrate development. *Nat. Rev. Genet.* 11, 331–344.
- Grayson, C., Bartolini, F., Chapple, J.P., Willison, K.R., Bhamidipati, A., Lewis, S.A., Luthert, P.J., Hardcastle, A.J., Cowan, N.J., and Cheetham, M.E. (2002). Localization in the human retina of the X-linked retinitis pigmentosa protein RP2, its homologue cofactor C and the RP2 interacting protein Arl3. *Hum. Mol. Genet.* 11, 3065–3074.
- Hanzal-Bayer, M., Renault, L., Roversi, P., Wittinghofer, A., and Hillig, R.C. (2002). The complex of Arl2-GTP and PDE delta: from structure to function. *EMBO J.* 21, 2095–2106.
- Ismail, S.A., Chen, Y.-X., Rusinova, A., Chandra, A., Bierbaum, M., Gremer, L., Triola, G., Waldmann, H., Bastiaens, P.I.H., and Wittinghofer, A. (2011). Arl2-GTP and Arl3-GTP regulate a GDI-like transport system for farnesylated cargo. *Nat. Chem. Biol.* 7, 942–949.
- Ismail, S.A., Chen, Y.-X., Miertzschke, M., Vetter, I.R., Koerner, C., and Wittinghofer, A. (2012). Structural basis for Arl3-specific release of myristoylated ciliary cargo from UNC119. *EMBO J.* 31, 4085–4094.
- Kabsch, W. (1993). Automatic processing of rotation diffraction data from crystals of initially unknown symmetry and cell constants. *J. Appl. Crystallogr.* 26, 795–800.
- Kobayashi, A., Kubota, S., Mori, N., McLaren, M.J., and Inana, G. (2003). Photoreceptor synaptic protein HRG4 (UNC119) interacts with ARL2 via a putative conserved domain. *FEBS Lett.* 534, 26–32.
- Linari, M., Hanzal-Bayer, M., and Becker, J. (1999). The delta subunit of rod specific cyclic GMP phosphodiesterase, PDE delta, interacts with the Arf-like protein Arl3 in a GTP specific manner. *FEBS Lett.* 458, 55–59.
- Murshudov, G.N., Vagin, A.A., and Dodson, E.J. (1997). Refinement of macromolecular structures by the maximum-likelihood method. *Acta Crystallogr. D Biol. Crystallogr.* 53, 240–255.
- Nancy, V., Callebaut, I., El Marjou, A., and de Gunzburg, J. (2002). The delta subunit of retinal rod cGMP phosphodiesterase regulates the membrane association of Ras and Rap GTPases. *J. Biol. Chem.* 277, 15076–15084.
- Pasqualato, S., Ménétrey, J., Franco, M., and Cherfils, J. (2001). The structural GDP/GTP cycle of human Arf6. *EMBO Rep.* 2, 234–238.
- Pasqualato, S., Renault, L., and Cherfils, J. (2002). Arf, Arl, Arp and Sar proteins: a family of GTP-binding proteins with a structural device for “front-back” communication. *EMBO Rep.* 3, 1035–1041.
- Pazour, G.J., Agrin, N., Leszyk, J., and Witman, G.B. (2005). Proteomic analysis of a eukaryotic cilium. *J. Cell Biol.* 170, 103–113.
- Sang, L., Miller, J.J., Corbit, K.C., Giles, R.H., Brauer, M.J., Otto, E.A., Baye, L.M., Wen, X., Scales, S.J., Kwong, M., et al. (2011). Mapping the NPHP-JBTS-MKS protein network reveals ciliopathy disease genes and pathways. *Cell* 145, 513–528.
- Schrick, J.J., Vogel, P., Abuin, A., Hampton, B., and Rice, D.S. (2006). ADP-ribosylation factor-like 3 is involved in kidney and photoreceptor development. *Am. J. Pathol.* 168, 1288–1298.
- Schwahn, U., Lenzner, S., Dong, J., Feil, S., Hinzmann, B., van Duijnhoven, G., Kirschner, R., Hemberger, M., Bergen, A.A., Rosenberg, T., et al. (1998). Positional cloning of the gene for X-linked retinitis pigmentosa 2. *Nat. Genet.* 19, 327–332.
- Schwarz, N., Hardcastle, A.J., and Cheetham, M.E. (2012a). Arl3 and RP2 mediated assembly and traffic of membrane associated cilia proteins. *Vision Res.* 75, 2–4.
- Schwarz, N., Novoselova, T.V., Wait, R., Hardcastle, A.J., and Cheetham, M.E. (2012b). The X-linked retinitis pigmentosa protein RP2 facilitates G protein traffic. *Hum. Mol. Genet.* 21, 863–873.
- Sharer, J.D., and Kahn, R.A. (1999). The ARF-like 2 (ARL2)-binding protein, BART. Purification, cloning, and initial characterization. *J. Biol. Chem.* 274, 27553–27561.
- Sharer, J.D., Shern, J.F., Van Valkenburgh, H., Wallace, D.C., and Kahn, R.A. (2002). ARL2 and BART enter mitochondria and bind the adenine nucleotide transporter. *Mol. Biol. Cell* 13, 71–83.
- Shern, J.F., Sharer, J.D., Pallas, D.C., Bartolini, F., Cowan, N.J., Reed, M.S., Pohl, J., and Kahn, R.A. (2003). Cytosolic Arl2 is complexed with cofactor D and protein phosphatase 2A. *J. Biol. Chem.* 278, 40829–40836.
- Thomas, S., Wright, K.J., Le Corre, S., Micalizzi, A., Romani, M., Abhyankar, A., Saada, J., Perrault, I., Amiel, J., Litzler, J., et al. (2014). A homozygous PDE6D mutation in Joubert syndrome impairs targeting of farnesylated INPP5E protein to the primary cilium. *Hum. Mutat.* 35, 137–146.
- Thomas, S., Cantagrel, V., Mariani, L., Serre, V., Lee, J.-E., Elkhartoufi, N., de Lonlay, P., Desguerre, I., Munnich, A., Boddaert, N., et al. (2015). Identification of a novel ARL13B variant in a Joubert syndrome-affected patient with retinal impairment and obesity. *Eur. J. Hum. Genet.* 23, 621–627.
- Tian, G., Thomas, S., and Cowan, N.J. (2010). Effect of TBCD and its regulatory interactor Arl2 on tubulin and microtubule integrity. *Cytoskeleton (Hoboken)* 67, 706–714.
- Torres, J.Z., Miller, J.J., and Jackson, P.K. (2009). High-throughput generation of tagged stable cell lines for proteomic analysis. *Proteomics* 9, 2888–2891.
- Veltel, S., and Wittinghofer, A. (2009). RPGR and RP2: targets for the treatment of X-linked retinitis pigmentosa? *Expert Opin. Ther. Targets* 13, 1239–1251.
- Veltel, S., Schlichting, I., and Wittinghofer, A. (2006). Crystal structure of the human retinitis pigmentosa 2 protein and its interaction with Arl3. *Structure* 14, 367–378.
- Veltel, S., Gasper, R., Eisenacher, E., and Wittinghofer, A. (2008a). The retinitis pigmentosa 2 gene product is a GTPase-activating protein for Arf-like 3. *Nat. Struct. Mol. Biol.* 15, 373–380.
- Veltel, S., Kravchenko, A., Ismail, S., and Wittinghofer, A. (2008b). Specificity of Arl2/Arl3 signaling is mediated by a ternary Arl3-effector-GAP complex. *FEBS Lett.* 582, 2501–2507.
- Vetter, I.R., and Wittinghofer, A. (2001). The guanine nucleotide-binding switch in three dimensions. *Science* 294, 1299–1304.
- Wittinghofer, A., and Vetter, I.R. (2010). structure-function relationships of the G Domain, a canonical switch motif. *Annu. Rev. Biochem.* 80, 943–971.
- Wohlgemuth, S., Kiel, C., Krämer, A., Serrano, L., Wittinghofer, F., and Herrmann, C. (2005). Recognizing and defining true Ras binding domains I: biochemical analysis. *J. Mol. Biol.* 348, 741–758.
- Wright, K.J., Baye, L.M., Olivier-Mason, A., Mukhopadhyay, S., Sang, L., Kwong, M., Wang, W., Pretorius, P.R., Sheffield, V.C., Sengupta, P., et al. (2011). An ARL3-UNC119-RP2 GTPase cycle targets myristoylated NPHP3 to the primary cilium. *Genes Dev.* 25, 2347–2360.
- Zhang, H., Liu, X., Zhang, K., Chen, C.-K., Frederick, J.M., Prestwich, G.D., and Baehr, W. (2004). Photoreceptor cGMP phosphodiesterase delta subunit (PDEdelta) functions as a prenyl-binding protein. *J. Biol. Chem.* 279, 407–413.
- Zhang, T., Li, S., Zhang, Y., Zhong, C., Lai, Z., and Ding, J. (2009). Crystal structure of the ARL2-GTP-BART complex reveals a novel recognition and binding mode of small GTPase with effector. *Structure* 17, 602–610.
- Zhang, H., Hanke-Gogokhia, C., Jiang, L., Li, X., Wang, P., Gerstner, C.D., Frederick, J.M., Yang, Z., and Baehr, W. (2015). Mistrafficking of prenylated proteins causes retinitis pigmentosa 2. *FASEB J.* 29, 932–942.
- Zhou, C., Cunningham, L., Marcus, A.I., Li, Y., and Kahn, R.A. (2006). Arl2 and Arl3 regulate different microtubule-dependent processes. *Mol. Biol. Cell* 17, 2476–2487.

Structure, Volume 23

Supplemental Information

The Interaction of CCDC104/BARTL1 with Arl3 and Implications for Ciliary Function

Mandy Lokaj, Stefanie K. Kösling, Carolin Koerner, Sven M. Lange, Sylvia E.C. van Beersum, Jeroen van Reeuwijk, Ronald Roepman, Nicola Horn, Marius Ueffing, Karsten Boldt, and Alfred Wittinghofer

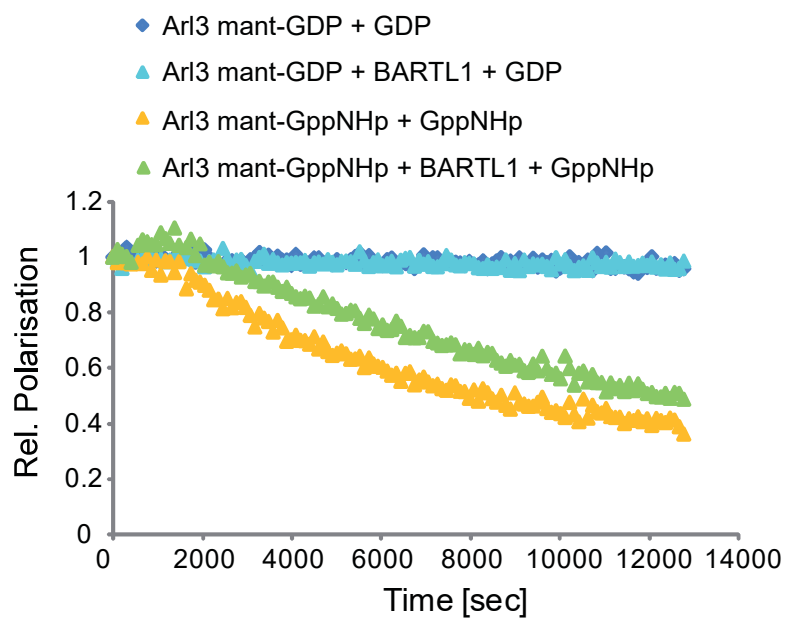
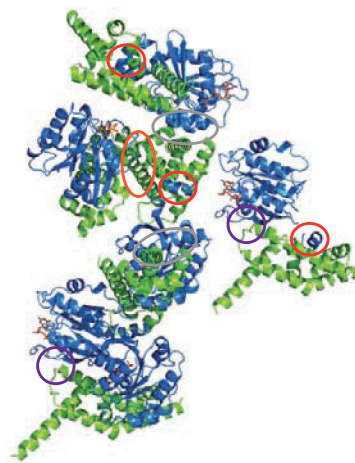
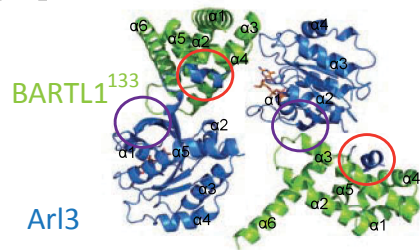
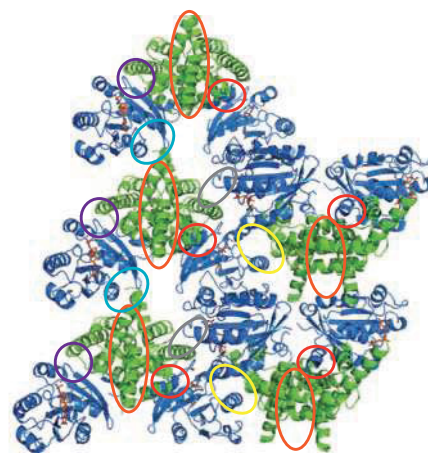
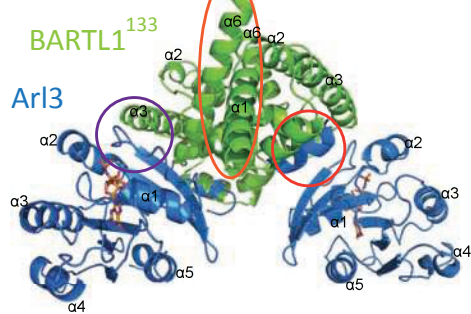


Figure S1

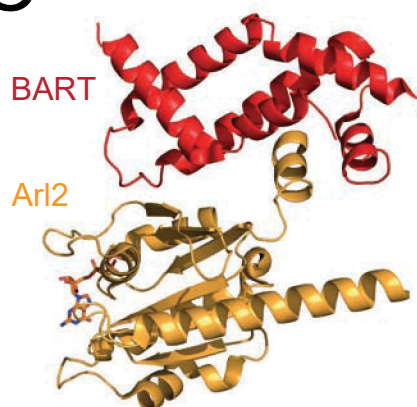
A P2₁2₁2₁



B P₁2₁



C



D

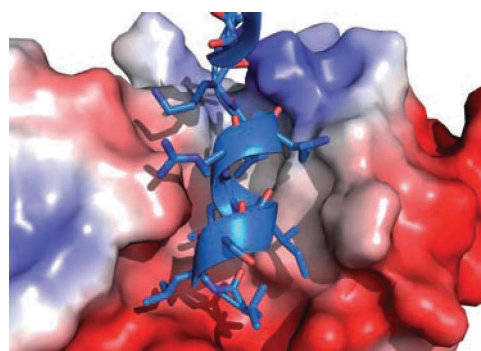


Figure S2

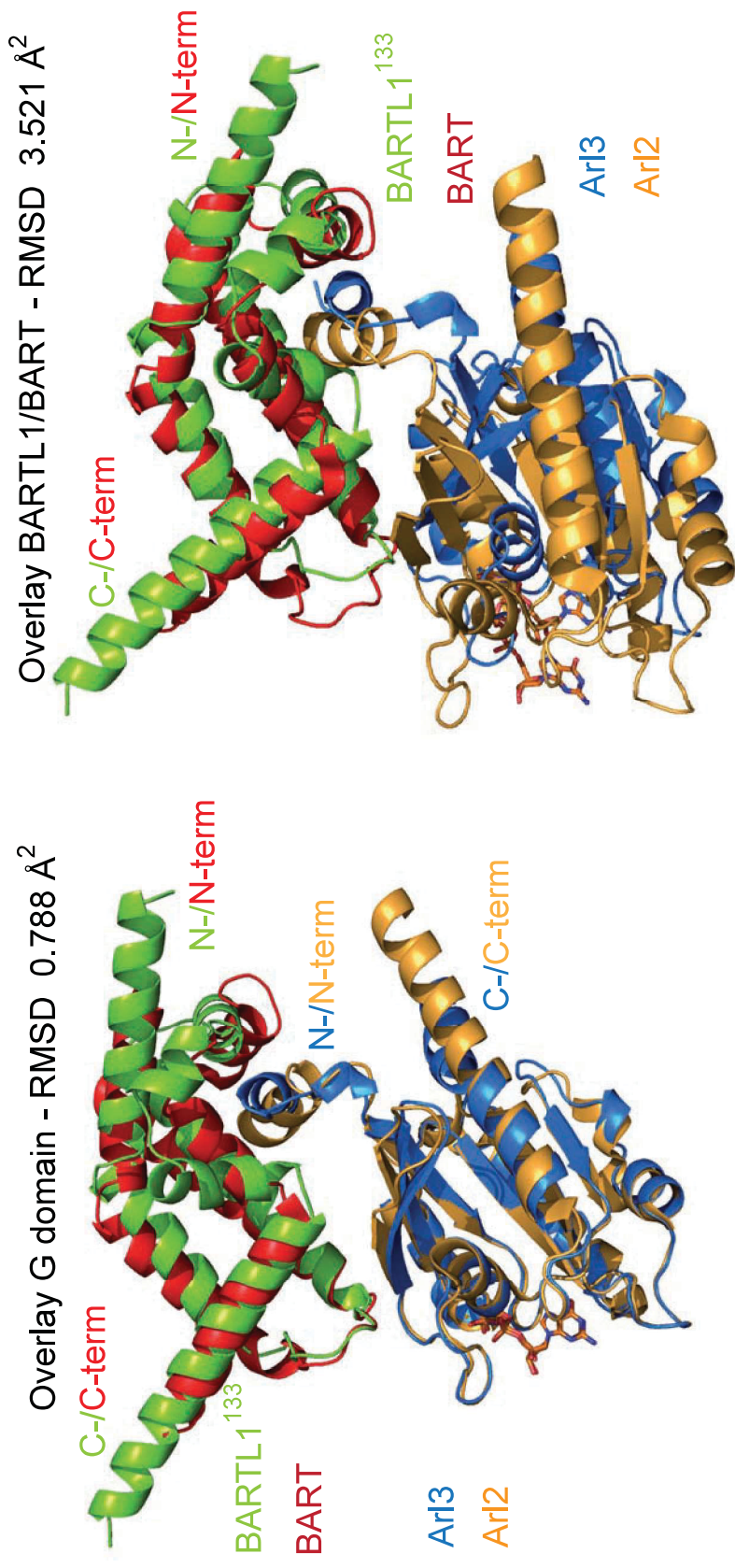
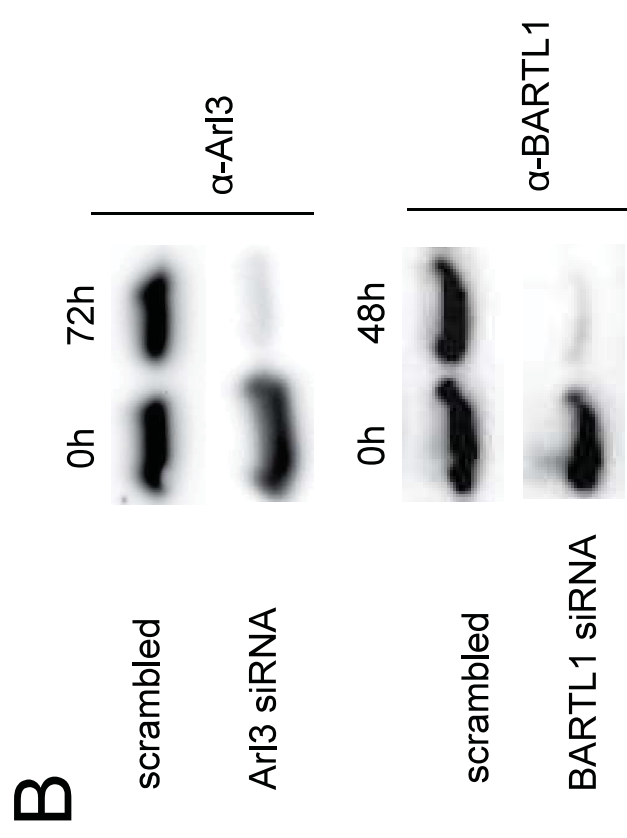
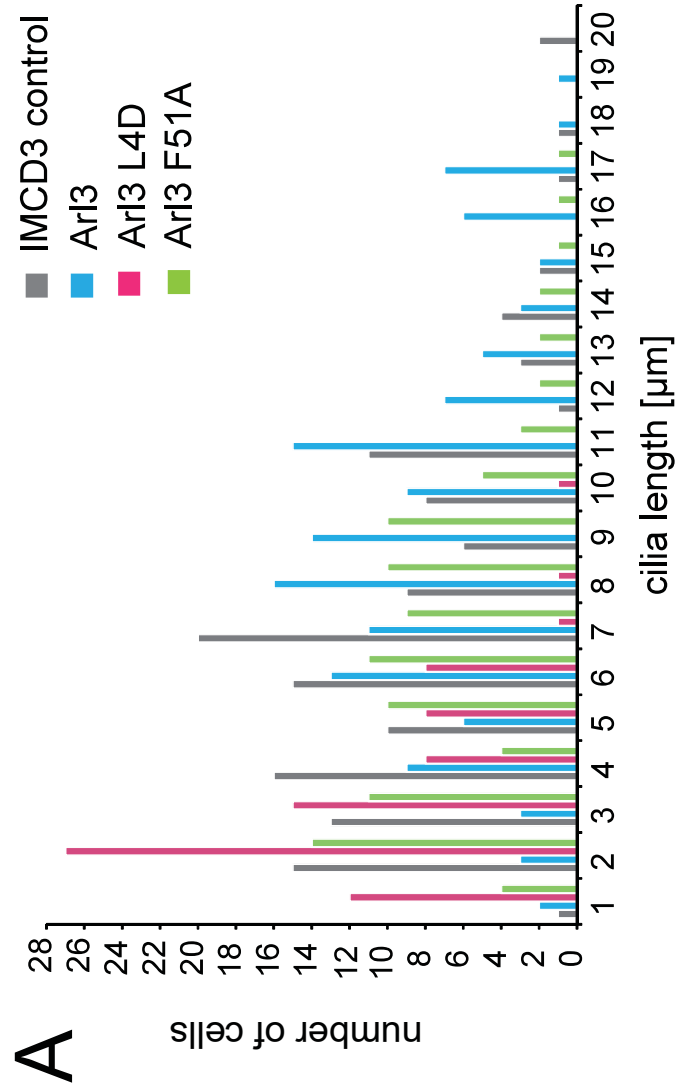


Figure S3



cell line	average cilia length [μm]	% ciliated cells
IMCD3	7	73
Arl3	9	75
Arl3 L4D	3	73
Arl3 F51A	6	76

Figure S4

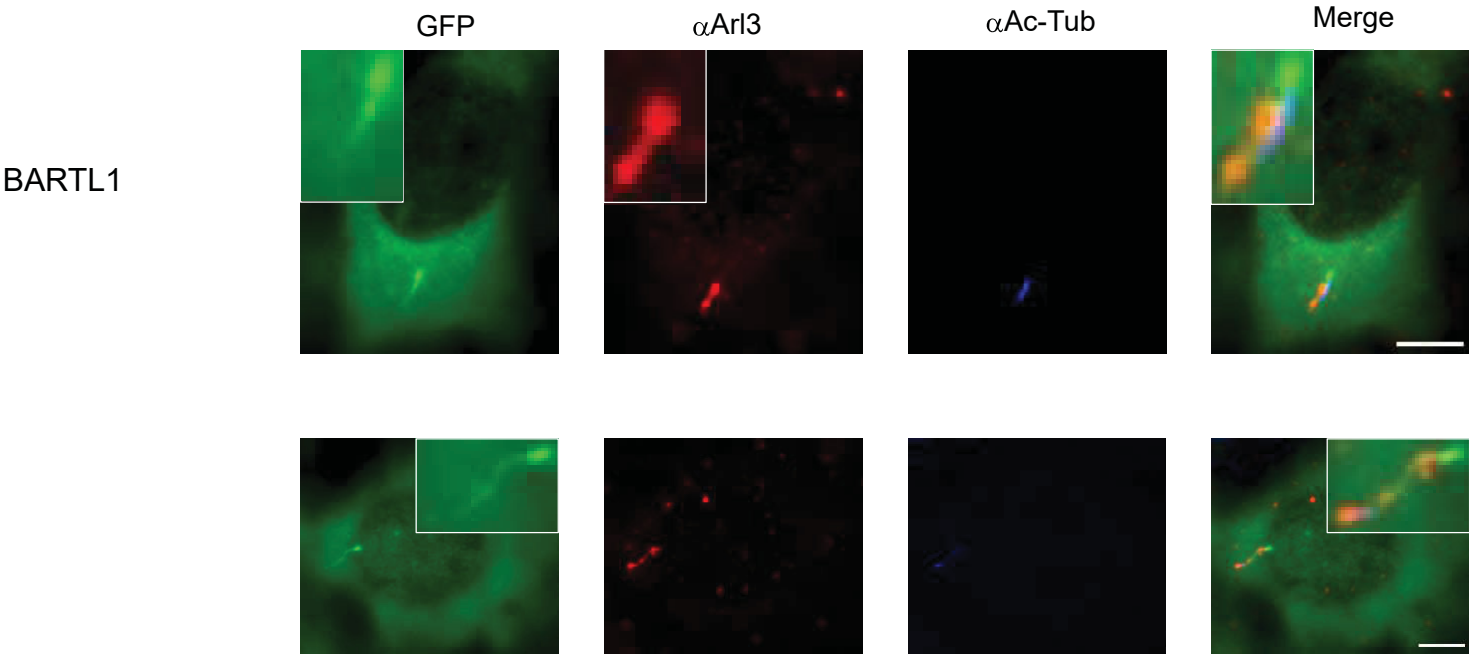
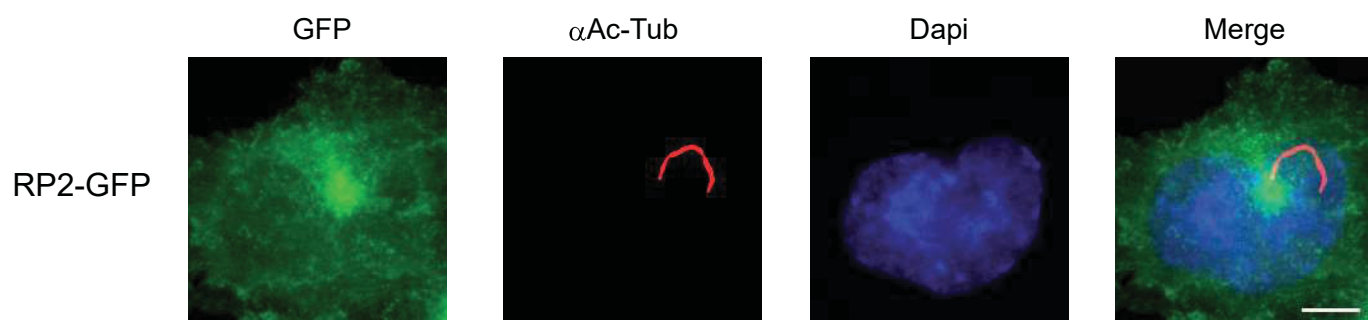
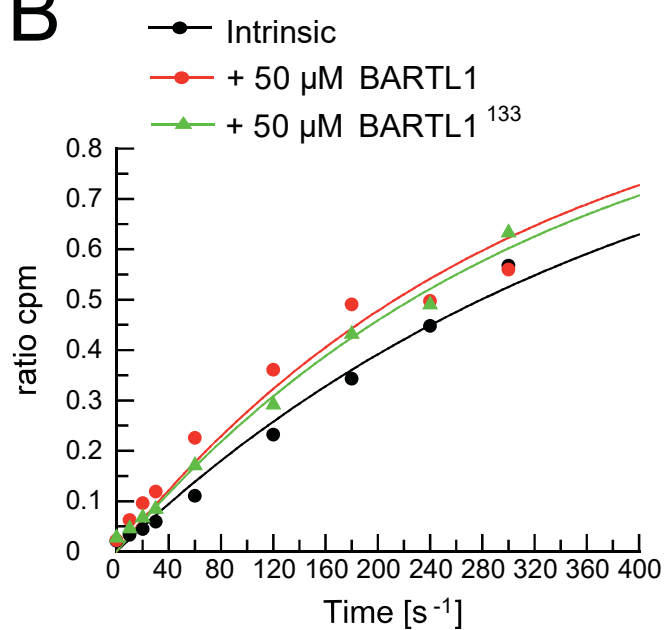


Figure S5

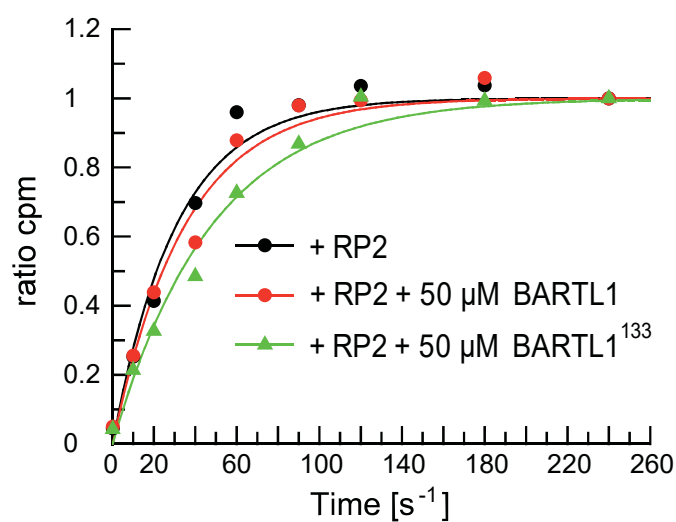
A



B



	Rate constants cpm/s ⁻¹
Arl3 intrinsic	$0.0025 \pm 9.16 \cdot 10^{-5}$
+ BARTL1	$0.0032 \pm 2.00 \cdot 10^{-4}$
+ BARTL1 ¹³³	$0.0031 \pm 9.23 \cdot 10^{-5}$



	Rate constants cpm/s ⁻¹
Arl3	
+ RP2	0.0325 ± 0.0028
+ RP2 + BARTL1	0.0286 ± 0.0024
+ RP2 + BARTL1 ¹³³	0.0209 ± 0.0014

Figure S6

Figure S1, Related to Figure 3. CCDC104/BARTL1 is an effector but no GEF for Arl3.

Fluorescence polarisation measurements to test for GEF activity of BARTL1. Relative fluorescence polarisation values were plotted against the time. Nucleotide exchange was induced by addition of 100-fold excess of unlabelled GDP or GppNHp, respectively to 1 μ M Arl3 bound to either mant-GDP or mant-GppNHp in the presence and absence of BARTL1.

Figure S2, Related to Figure 4. Crystal Contacts. (A) The Arl3•GppNHp•BARTL1¹³³ complex (pdb: 4ZI2) crystallized in space group P2₁2₁2₁ and the asymmetric unit contained two Arl3 (blue) and two BARTL1¹³³ (green) molecules (left panel). Two biological assemblies via interaction Area 1 (red circle) and 2 (lilac circle) (see main text) can be found. Crystal contacts are formed via dimer formation of BARTL1¹³³ involving its α 2, α 5 and α 6 helices (orange circle). The α 5 helix of Arl3 is forming further crystal contacts to the α 2 and α 6 helices of a neighbouring BARTL1¹³³ molecule (grey circle). (B) The Arl3•GppNHp•BARTL1¹³³ complex (pdb: 4ZI3) crystallized in space group P12₁ and the asymmetric unit contained two Arl3 (blue) and two BARTL1¹³³ (green) molecules (left panel). Within the asymmetric unit BARTL1¹³³ is forming a dimer involving its α 2, α 5 and α 6 helices (orange circle) and each BARTL1¹³³ is contacting Arl3 via interaction Area 1 (red circle) and 2 (lilac circle) (see main text). Crystal contacts are formed by the α 6 helices of both BARTL1¹³³ molecules contacting α 3 and the loop between β 2- β 3 of Arl3 (cyan circle). The α 3 helix of BARTL1¹³³ contacts the loop between α 4- β 4 of a further Arl3 molecule (grey circle). Additional, the α 2 and α 3 helices of Arl3 are contacting α 3 and α 1 of a neighbouring BARTL1¹³³ molecule (yellow circle). (C) The complex of Arl2•GTP•BART (pdb: 3DOE) crystallized in space group P2₁ (Zhang et al., 2009). The asymmetric unit contained only one Arl2 (orange) and one BART (red) molecule representing the biological assembly. (D) Surface representation of BARTL1 (red – acidic, blue – basic, white – hydrophobic patches) showing the groove in which N-term of Arl3 (blue) is buried.

Figure S3, Related to Figure 5. Overlay of Arl2•BART (pdb: 3DOE) and Arl3•BARTL1 (pdb: 4ZI2). Superimposition of the G domain of Arl2 (orange) and Arl3 (blue) (left panel) and BART (red) and BARTL1 (green) (right panel) of both structures. N- and C-termini of proteins and rmsd values are indicated.

Figure S4, Related to Figure 7. Further analysis of stable cell lines. (A) Quantification of cilia number and length for IMCD3 control cells and cells stably expressing Arl3^{WT}; Arl3^{L4D} and Arl3^{F51A}. The cilia length of 100 cells was plotted according to the determined cilia length. (B) Samples of siRNA treated stable cell lines used for imaging (see Figure 7) compared to cells treated with scrambled control siRNA were subjected to SDS-PAGE and analysed by Western Blot: anti-Arl3 antibody (1:500; Novus Biologicals) and anti-CCDC104/BARTL1 antibody (1:500, Abnova).

Figure S5, Related to Figure 2. Co-Staining of Arl3 and BARTL1. Two representative IMCD3 cells stably expressing BARTL1-GFP in which endogenous Arl3 and acetylated α -tubulin were stained following serum starvation and fixation. White bar indicates 5 μ m.

Figure S6, Related to Figure 8. GTP hydrolysis measurement. (A) IMCD3 cells stably expressing, C-terminally tagged full-length human RP2-GFP were and immunostained for acetylated α -tubulin (AcTub) and the nucleus (DAPI). White bar indicates 5 μ m. (B) Intrinsic (left panel) or RP2 stimulated (right panel) GTP hydrolysis of either 10 μ M Arl3 loaded with 60 nM ³²P-GTP/10 μ M GTP alone or in presence of 0.1 μ M RP2 and/or 50 μ M BARTL1 or BARTL1¹³³. Rough observed rate constants (and standard deviations) are indicated below in the table.

Proteins identified by mass spectrometry from tandem affinity proteomics experiments in HEK293T cells		SwissProt_2013_02_Accession	Arl3_D129N_C-TAP_Exp1	Arl3_D129N_C-TAP_Exp2		
EntrezGeneSymbol	EntrezGeneFullName		unique peptides	sequence coverage	unique peptides	sequence coverage
ABHD10	abhydrolase domain containing 10	Q9NUJ1	4	0.19	4	0.16
AIFM1	apoptosis-inducing factor, mitochondrion-associated, 1	O95831	15	0.36	24	0.48
ARL2BP	ADP-ribosylation factor-like 2 binding protein	Q9Y2Y0	5	0.39	6	0.37
ARL3	ADP-ribosylation factor-like 3	P36405	12	0.68	10	0.67
C20orf194	chromosome 20 open reading frame 194	Q5TEA3	34	0.41	35	0.43
CFAP36	cilia and flagella associated protein 36	Q96G28	3	0.13	9	0.37
PDE6D	phosphodiesterase 6D, cGMP-specific, rod, delta	O43924	5	0.35	5	0.35
RPL23	ribosomal protein L23	P62829	2	0.11	2	0.16
UBB	ubiquitin B	P0CG47	4	0.17		
UNC119	unc-119 homolog (C. elegans)	Q13432	7	0.44	8	0.53
UNC119B	unc-119 homolog B (C. elegans)	A6NIH7	17	0.84	17	0.82
YWHA8	tyrosine 3-monooxygenase/tryptophan 5-monooxygenase activation protein P31946		5	0.45	5	0.58
YWHA9	tyrosine 3-monooxygenase/tryptophan 5-monooxygenase activation protein P61981		4	0.32	6	0.49
YWHAH	tyrosine 3-monooxygenase/tryptophan 5-monooxygenase activation protein Q04917		2	0.18	4	0.35
YWHAQ	tyrosine 3-monooxygenase/tryptophan 5-monooxygenase activation protein P27348		7	0.40	11	0.56
YWHAZ	tyrosine 3-monooxygenase/tryptophan 5-monooxygenase activation protein P63104		7	0.47	14	0.64

Table S1. SF-TAP analysis with over-expressed C-terminally SF-TAP-tagged Arl3_D129N in HEK293T cells. Shown are the number of unique identified peptides as well as the sequence coverage for each protein detected by mass spectrometry in 2 experiments. Proteins identified in the SF-TAP analysis of empty vector control experiments were removed.

Exp1

Q96G28 (100%), 39.447,1 Da

Coiled-coil domain-containing protein 104 OS=Homo sapiens GN=CCDC104 PE=1 SV=2

3 exclusive unique peptides, 3 exclusive unique spectra, 3 total spectra, 46/342 amino acids (13% coverage)

MAAEEDEVE WVVESIAGFL R G P D W S I P I L D F V E Q K C E V F D D E E S K L T Y T E I H Q E Y K E L V E K L L E G Y L K E I G I N E D Q F Q
EACTSPLAKT HTSQA ILQPV LAAEDFTIFK AMMVQKN IEM Q L Q A I R I I Q E R N G V L P D C L T D G S D V V S D L E H E E M K I L R E V
LRKSK E E Y D Q E E E R K R K K Q L S E A K T E E P T V H S S E A A I M N N S Q G D G E H F A H P P S E V K M H F A N Q S I E P L G R K V E R S E T S S L P
QKDLK I P G L E H A S I E G P I A N L S V L G T E E L R Q R E H Y L K Q K R D K L M S M R K D M R T K Q I Q N M E Q K G K P T G E V E E M T E K P E M T A E
E K Q T L L K R R L L A E K L K E E V I N K

Exp2

Q96G28 (100%), 39.447,1 Da

Coiled-coil domain-containing protein 104 OS=Homo sapiens GN=CCDC104 PE=1 SV=2

9 exclusive unique peptides, 9 exclusive unique spectra, 9 total spectra, 128/342 amino acids (37% coverage)

MAAEEDEVE WVVESIAGFL R G P D W S I P I L D F V E Q K C E V F D D E E S K L T Y T E I H Q E Y K E L V E K L L E G Y L K E I G I N E D Q F Q
EACTSPLAKT HTSQA ILQPV LAAEDFTIFK AMMVQKN IEM Q L Q A I R I I Q E R N G V L P D C L T D G S D V V S D L E H E E M K I L R E V
LRKSK E E Y D Q E E E R K R K K Q L S E A K T E E P T V H S S E A A I M N N S Q G D G E H F A H P P S E V K M H F A N Q S I E P L G R K V E R S E T S S L P
QKDLK I P G L E H A S I E G P I A N L S V L G T E E L R Q R E H Y L K Q K R D K L M S M R K D M R T K Q I Q N M E Q K G K P T G E V E E M T E K P E M T A E
E K Q T L L K R R L L A E K L K E E V I N K

Supplementary Experimental Procedures

Plasmids and protein purification BARTL1 was amplified by PCR from a cDNA library from a mouse spleen cDNA and a human W38 cDNA library. In this work human full length BARTL1 (UNP:Q96G28) and a shortened mouse BARTL1 (UNP:Q8C6E0) comprising amino acids 1 to 133 were used. Full length BARTL1 was cloned into pProExHTa containing an N-terminal His tag and BARTL1¹³³ into pGexET (derivative of pGex4T-1) containing an N-terminal Glutathione-S-transferase fusion followed by a thrombin, TEV and precession cleavage site (order as mentioned). Arl3 (UNP:Q9WUL7) and Arl2 (UNP:Q9D0J4) full length in pET20 as well as Arl3 Δ N and Arl2 Δ N in pGex4T-1 (Veltel et al., 2008b) were already available. Respective BARTL1 mutants and Arl mutants were generated by mutagenesis PCR. All proteins were expressed in BL21 DE3 codon plus RIL cells at 25°C following induction with 100 μ M IPTG at 18°C overnight. Purification was done using GSH-sepharose columns (Amersham/GE Healthcare) which were washed with Wash-Buffer (75 mM Hepes pH 7.5, 300 mM KCl, 5mM MgCl₂, 3 mM β -mercaptoethanol and 10 % glycerol). The GST-fusion proteins were eluted with Elution-Buffer (Wash Buffer + 20 mM reduced glutathione). Following cleavage with precession protease overnight residual GST was removed by size exclusion chromatography using a Superdex 200 16/60 (Amersham/GE Healthcare). Arl3 and Arl2 proteins and mutants containing a C-terminal His-tag were purified as previously described (Veltel et al., 2008b). The proteins were stored in buffer M containing 25 mM Hepes pH 7.5, 150 mM KCl, 5 mM MgCl₂, 1 mM DTE and 5 % glycerol. The nucleotide content of all G proteins was determined by HPLC measurements. All proteins used displayed full nucleotide loading. Plasmids used for the generation of stable cell lines can be found below in the respective section.

Cy5, FITC Labelling of BARTL1 For BARTL1¹³³ the mutant C83A/E59C was constructed for labelling. 1 mg of protein was exchanged into 1 x PBS, 1 mM TCEP and incubated with a

50-fold molar excess of Cy5 or FITC in DMSO, respectively for 3 hours at room temperature and further incubation overnight at 4°C. Following day the excess label was removed by a Desalting Column. The ratio of protein:label was determined 1:3, i.e. 30 % efficiency.

Liposome Sedimentation Assay The phospholipids 1,2-dioleoyl-sn-glycero-3-phosphocholine (DOPC), 1,2-dioleoyl-sn-glycero-3-phospho-(1'-rac-glycerol) sodium salt (DOPG), 1,2-dipalmitoyl-snglycero-3-phospho-(1'-rac-glycerol) sodium salt (DPPG), and 1,2-dipalmitoyl-sn-glycero-3-phosphocholine (DPPC) were purchased from Avanti Polar Lipids (Alabaster, AL). Cholesterol (Chol) was from Sigma-Aldrich.

DOPC:DOPG:DPPC:DPPG:Cholesterol were mixed in a molar ratio of 4:25:5:50:25 and vacuum dried. The dried lipid mix was resuspended in a buffer containing 20 mM Tris pH7.5, 20 mM NaCl, 5 mM MgCl₂, 1 mM DTE (buffer L) to a final concentration of 2.8 mM and sonicated at 65 °C for 15 min and subsequently subjected to nine freeze-thaw-vortex cycles. Afterwards, unilamellar vesicles of homogeneous sizes were obtained by using an extruder (Avanti Polar Lipids, Alabaster, AL) with polycarbonate membranes of 200 nm pore size at 65 °C in presence of 40 µM GDP or GppNHp in buffer L. 2.8 mM of 200 µM liposomes were incubated with 20 µM Arl3 bound to GDP or GppNHp, respectively in the presence of 40 µM BARTL1¹³³ for 30 min at room temperature. Liposomes were pelleted at 125,000 × g for 1 h 30 min at 10°C in a TLA-45 rotor. The pellets were resuspended in buffer L, up to the same volume as the supernatant. Equal amounts of the supernatants and resuspended pellets volumes were analyzed by SDS-PAGE.

Measurement of GTP hydrolysis by [γ -³²P]GTP charcoal method This was performed as described (Brinkmann et al., 2002; Miertzschke et al., 2011). Briefly, a mix of 10 µM GTP and 60 nM [γ -³²P]GTP in Buffer M was supplemented with 10 µM Arl3 bound to GppCH₂p to start the intrinsic GTPase reaction at 25°C. For investigation of RP2-stimulated GTP-

hydrolysis, 0.1 μ M RP2 was added to start the reaction. The intrinsic and RP2 stimulated GTP-hydrolysis was measured in absence and presence of 50 μ M BARTL1 or BARTL1¹³³. Aliquots of 10 μ l were taken at certain time points and mixed with 400 μ l of charcoal solution (50 g*1-l charcoal in 20 mM phosphoric acid) to stop the reaction. The charcoal was pelleted and the amount of free ³²Pi in the supernatant determined by scintillation counting. Data was plotted by showing the ratio of specific counts of supernatant over total counts of sample at each point. Data points were fitted to a first-order reaction to obtain rough kobs.

Tandem affinity purification. HEK293T (human embryonic kidney, ATCC) cells were transfected for 48 hours with SF-TAP-Arl3^{D129N} using polyethyleneimine (PEI, Polysciences) as a transfection reagent. Following transfection, cells were lysed in lysis buffer containing 30 mM Tris-HCl (pH 7.4), 150 mM NaCl, 0.5% Nonidet-P40 (NP40), freshly supplemented with protease inhibitor cocktail (Roche), phosphatase inhibitor cocktail II and III (Sigma), for 20 minutes at 4°C. The Streptavidin- and FLAG-based tandem affinity purification steps were performed as previously described (Boldt et al., 2009; Gloeckner et al., 2007). 5% of the final eluate was evaluated by SDS-PAGE followed by silver staining, according to standard protocols, while the remaining 95% were subjected to protein precipitation with chloroform and methanol. Protein precipitates were subsequently subjected to mass spectrometry analysis and peptide identification as previously described (Texier et al., 2014). For one step Strep purifications, SF-TAP-tagged proteins and associated protein complexes were purified essentially as described earlier (Gloeckner et al., 2009a). HEK293T cells, transiently expressing the SF-TAP-tagged constructs were lysed in lysis buffer, containing 0.5% Nonidet-P40, protease inhibitor cocktail (Roche) and phosphatase inhibitor cocktails II and III (Sigma-Aldrich) in TBS (30 mM Tris-HCl (pH 7.4), 150 mM NaCl), for 20 minutes at 4°C. After sedimentation of nuclei at 10,000 x g for 10 minutes, the protein concentration was determined by a Bradford assay, before equal amounts of each lysate were transferred to

Strep-Tactin-Superflow beads (IBA) and were incubated for one hour at 4°C on an end-over-end shaker. Then, the resin was washed three times with wash buffer (TBS containing 0.1% NP-40, phosphatase inhibitor cocktail II and III). The protein complexes were eluted by incubation for 10 minutes in Strep-elution buffer (IBA). The eluted samples were concentrated using 10 kDa cut-off VivaSpin 500 centrifugal devices (Sartorius Stedim Biotech) and pre-fractionated using SDS-Page. Afterwards, the samples were subjected to in-gel tryptic cleavage as described elsewhere (Gloeckner et al., 2009b).

Mass spectrometry and data analysis. LC-MS/MS analysis was performed on an Ultimate3000 nano RSLC system (Thermo Scientific) coupled to a LTQ Orbitrap Velos mass spectrometer (Thermo Scientific) by a nano spray ion source. Tryptic peptide mixtures were automatically injected and loaded at a flow rate of 6 µl/min in 0.1% trifluoroacetic acid in HPLC-grade water onto a nano trap column (75 µm i.d. × 2 cm, packed with Acclaim PepMap100 C18, 3 µm, 100 Å; Thermo Scientific). After 5 minutes, peptides were eluted and separated on the analytical column (75 µm i.d. × 25 cm, Acclaim PepMap RSLC C18, 2µm, 100 Å; Thermo Scientific) by a linear gradient from 2% to 35% of buffer B (80% acetonitrile and 0.08% formic acid in HPLC-grade water) in buffer A (2% acetonitrile and 0.1% formic acid in HPLC-grade water) at a flow rate of 300 nl/min over 80 minutes. Remaining peptides were eluted by a short gradient from 35% to 95% buffer B in 5 minutes. The eluted peptides were analyzed by a LTQ Orbitrap Velos mass spectrometer. From the high resolution MS pre-scan with a mass range of 300 to 1500, the ten most intense peptide ions were selected for fragment analysis in the linear ion trap if they exceeded an intensity of at least 200 counts and if they were at least doubly charged. The normalized collision energy for CID was set to a value of 35 and the resulting fragments were detected with normal resolution in the linear ion trap. The lock mass option was activated; the background signal with a mass of 445.12003

was used as lock mass. Every ion selected for fragmentation, was excluded for 20 seconds by dynamic exclusion.

MS/MS data were analyzed, using Mascot (version 2.4.1, Matrix Science, Boston, MA, USA). Mascot was set up to search the human subset of the Swiss Prot database (Release 2013_12, 20248 entries), assuming trypsin as the digestion enzyme. Mascot was searched with a fragment ion mass tolerance of 1 Da and a parent ion tolerance of 10.0 PPM. Oxidation of methionine and was specified as variable modification, iodoacetamide derivative of cysteine as fixed. The Mascot results were loaded in Scaffold (version Scaffold_4.4.1.1, Proteome Software Inc., Portland, OR) to validate MS/MS based peptide and protein identifications. Peptide identifications were accepted if they could be established at greater than 95.0% probability as specified by the Peptide Prophet algorithm (Keller et al., 2002). Protein identifications were accepted if they could be established at greater than 95.0% probability and contained at least 2 identified peptides. Protein probabilities were assigned by the Protein Prophet algorithm (Nesvizhskii et al., 2003). Proteins, which contained similar peptides and could not be differentiated based on MS/MS analysis alone, were grouped to satisfy the principles of parsimony.

Quantification of cilia number and length

Cilia length quantification of parental IMCD3 FlpIn cells and stable Arl3 WT, Arl3 L4D, Arl3 F51A cell lines was performed using Fiji software. After setting the scale, the length was measured by hand using the segmented line tool. For each cell line, approximately 100 cells were analyzed. Data were illustrated in Microsoft Excel plotting rounded cilia length values (μm) against the number of corresponding cells and average length values were calculated for each cell line.

References

Boldt, K., van Reeuwijk, J., Gloeckner, C.J., Ueffing, M., and Roepman, R. (2009). Tandem affinity purification of ciliopathy-associated protein complexes. *Methods Cell Biol.* 91, 143–160.

Brinkmann, T., Daumke, O., Herbrand, U., Kühlmann, D., Stege, P., Ahmadian, M.R., and Wittinghofer, A. (2002). Rap-specific GTPase activating protein follows an alternative mechanism. *J Biol Chem* 277, 12525–12531.

Gloeckner, C.J., Boldt, K., Schumacher, A., Roepman, R., and Ueffing, M. (2007). A novel tandem affinity purification strategy for the efficient isolation and characterisation of native protein complexes. *Proteomics* 7, 4228–4234.

Gloeckner, C.J., Boldt, K., and Ueffing, M. (2009a). Strep/FLAG tandem affinity purification (SF-TAP) to study protein interactions. *Curr. Protoc. Protein Sci. Chapter 19*, Unit19.20.

Gloeckner, C.J., Boldt, K., Schumacher, A., and Ueffing, M. (2009b). Tandem affinity purification of protein complexes from mammalian cells by the Strep/FLAG (SF)-TAP tag. *Methods Mol. Biol.* 564, 359–372.

Keller, A., Nesvizhskii, A.I., Kolker, E., and Aebersold, R. (2002). Empirical statistical model to estimate the accuracy of peptide identifications made by MS/MS and database search. *Anal. Chem.* 74, 5383–5392.

Miertzschke, M., Koerner, C., Vetter, I.R., Keilberg, D., Hot, E., Leonardy, S., Søgaaard-Andersen, L., and Wittinghofer, A. (2011). Structural analysis of the Ras-like G protein MglA and its cognate GAP MglB and implications for bacterial polarity. *EMBO J.* 30, 4185–4197.

Nesvizhskii, A.I., Keller, A., Kolker, E., and Aebersold, R. (2003). A statistical model for identifying proteins by tandem mass spectrometry. *Anal. Chem.* *75*, 4646–4658.

Texier, Y., Toedt, G., Gorza, M., Mans, D.A., van Reeuwijk, J., Horn, N., Willer, J., Katsanis, N., Roepman, R., Gibson, T.J., et al. (2014). Elution profile analysis of SDS-induced subcomplexes by quantitative mass spectrometry. *Mol. Cell. Proteomics* *13*, 1382–1391.

Zhang, T., Li, S., Zhang, Y., Zhong, C., Lai, Z., and Ding, J. (2009). Article Crystal Structure of the ARL2-GTP-BART Complex Reveals a Novel Recognition and Binding Mode of Small GTPase with Effector. *Struct. Des.* *17*, 602–610.

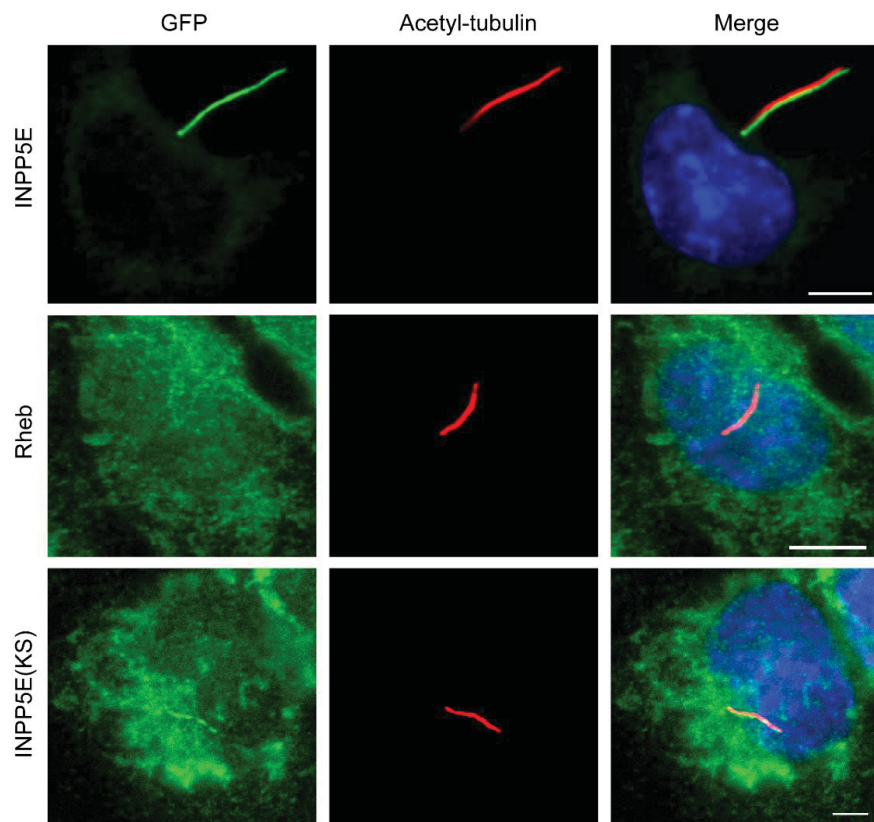
These were the main conclusions from this publication

- Arl3 localizes to the cytosol and to primary cilia of IMCD3 cells, where it is enriched at the basal body and in the transition zone.
- The N-terminal amphipathic helix of Arl3 is the main determinant for its ciliary localization in contrast to the non-ciliary Arl2 and is essential but not sufficient for ciliary localization.
- The Arl3 GAP RP2 is excluded from cilia of IMCD3 cells.
- CCDC104 is a ciliary protein that accumulates in the transition zone. Its BART-like domain alone is not sufficient to localize to cilia.
- The ciliary localization of Arl3 does not directly depend on CCDC104 or vice versa.
- The interaction of CCDC104 and Arl3 might support the creation of a driving force for the entry of lipidated cargo proteins of PDE6 δ /Unc119a/b to cilia.

3 Publication II

PDE6 δ -mediated sorting of INPP5E into the cilium is determined by cargo-carrier affinity

Eyad K. Fansa*, **Stefanie K. Kösling***, Eldar Zent, Alfred Wittinghofer and Shehab Ismail (2016). *Nature Communications* 7:11366, 1-9. (* Co-first authors)



These were the questions to be answered by this publication

- What determines the sorting of farnesylated cargo of PDE6 δ to different membrane compartments?
- Which role do PDE6 δ and the GTP-specific releasing factors Arl2 and Arl3 play for the sorting of farnesylated PDE6 δ interacting proteins?
- Exemplary: Both farnesylated proteins INPP5E and Rheb interact with PDE6 δ , but why does Rheb localize to endomembranes, whereas INPP5E localizes to primary cilia?
- Why does INPP5E almost exclusive localize to cilia?

Contribution of 45 %

- Plasmid generation and mutagenesis for transfection of IMCD3 cells.
- Cell cultivation, generation of stable GFP cell lines (INPP5E, INPP5E(KS), Rheb, Rheb(SI)), validation by western blotting.
- Cell fixation, IF staining, fluorescence microscopy of the cell lines above, image processing
- Quantification of the fold of ciliary enrichment of Rheb(SI).
- RNAi knockdown study of Arl3 in the INPP5E cell line, validation by western blotting and quantification of the fold of ciliary enrichment of INPP5E.
- Writing of the methods section in the manuscript regarding IMCD3 cell experiments.

Declaration: Reprinted (adapted) with permission from Nature Communications

Copyright © 2016, Springer Nature, Creative Commons Attribution License (CC BY)

DOI: 10.1038/ncomms11366

ARTICLE

Received 2 Sep 2015 | Accepted 18 Mar 2016 | Published 11 Apr 2016

DOI: 10.1038/ncomms11366

OPEN

PDE6 δ -mediated sorting of INPP5E into the cilium is determined by cargo-carrier affinity

Eyad Kalawy Fansa^{1,*}, Stefanie Kristine Kösling^{1,*}, Eldar Zent¹, Alfred Wittinghofer¹ & Shehab Ismail²

The phosphodiesterase 6 delta subunit (PDE6 δ) shuttles several farnesylated cargos between membranes. The cargo sorting mechanism between cilia and other compartments is not understood. Here we show using the inositol polyphosphate 5'-phosphatase E (INPP5E) and the GTP-binding protein (Rheb) that cargo sorting depends on the affinity towards PDE6 δ and the specificity of cargo release. High-affinity cargo is exclusively released by the ciliary transport regulator Arl3, while low-affinity cargo is released by Arl3 and its non-ciliary homologue Arl2. Structures of PDE6 δ /cargo complexes reveal the molecular basis of the sorting signal which depends on the residues at the -1 and -3 positions relative to farnesylated cysteine. Structure-guided mutation allows the generation of a low-affinity INPP5E mutant which loses exclusive ciliary localization. We postulate that the affinity to PDE6 δ and the release by Arl2/3 in addition to a retention signal are the determinants for cargo sorting and enrichment at its destination.

¹Max Planck Institute of Molecular Physiology, Otto-Hahn-Strasse 11, 44227 Dortmund, Germany. ²CR-UK Beatson Institute, Garscube Estate Switchback Road, Glasgow G61 1BD, UK. * These authors contributed equally to this work. Correspondence and requests for materials should be addressed to A.W. (email: alfred.wittinghofer@mpi-dortmund.mpg.de) or to S.I. (email: s.ismail@beatson.gla.ac.uk).

Primary cilia are antenna-like microtubule-based cell surface protrusions which can be found on eukaryotic cells and serve as sensory organelles. Genetic disorders affecting structure or function of cilia result in a large number of diseases collectively termed ciliopathies^{1,2}. While the cilium appears as a protrusion in the plasma membrane that is open to the cell body, the ciliary content and membrane composition are different than that of the cell body and plasma membrane^{3,4}. This is in part achieved by the presence of a diffusion and transport barrier, where entry and exit decisions of ciliary components have to be taken^{5,6}.

PDE6 δ is a prenyl-binding protein that was originally discovered as the delta subunit of rod photoreceptor-specific phosphodiesterase PDE6 (ref. 7). It was found as a solubilizing factor for the prenylated subunits of this enzyme and was later shown to be a general prenyl-binding protein (hence also called PrBP/PDE6 δ)^{8–11}. PDE6 δ was shown to bind prenylated peptides or proteins of the Ras subfamily with approximately micromolar affinity^{12,13} and to play a critical role in their cellular distribution^{14–16}. Since it is believed to be crucial for the localization and thus the activity of the oncoprotein Ras, inhibitors of the Ras-PDE6 δ complex were actually considered as promising Ras drug candidates¹⁷.

INPP5E belongs to the inositol polyphosphate 5'-phosphatase family that hydrolyzes the 5'-phosphate of phosphatidylinositols and localizes to primary cilia^{18,19}. The importance of the 5'-phosphatase activity for ciliary function is underscored by the finding that *INPP5E* is mutated in Joubert syndrome, a ciliopathy characterized by motor and intellectual disabilities^{18–20}, and that the gene mutated in the OCRL (Oculocerebrorenal) or Lowe syndrome also encodes an inositol polyphosphate 5'-phosphatase^{21,22}. INPP5E contains a C-terminal CaaX motif where the C-terminal residue Cys644 is farnesylated²³. A mutation encoding a stop codon near to the CaaX motif (Q627) of INPP5E was identified in a family with MORM syndrome¹⁸, a ciliopathy characterized by intellectual disability, obesity, retinal dystrophy and micropenis²⁴. This mutation was shown to affect INPP5E ciliary localization, which in combination with other reports²⁵ indicates the importance of the C-terminus and its farnesylation for the ciliary localization of INPP5E (ref. 18).

Recently, PDE6 δ was co-purified with INPP5E and siRNA-mediated knockdown of *PDE6 δ* resulted in impaired ciliary localization of INPP5E (ref. 26). Moreover, a *PDE6 δ* deletion mutation, which was identified in Joubert syndrome, was shown to impair the targeting of farnesylated INPP5E protein to the primary cilium²⁵. Knockdown of *PDE6 δ* also impeded the transport of GRK1 and PDE6 catalytic subunits to photoreceptor outer segments, which are considered specialized forms of cilia^{27,28}.

The homologous small Arf-like GTP-binding proteins Arl2 and Arl3 have been shown to act as nucleotide-dependent-specific release factors of farnesylated cargo from PDE6 δ *in vitro* and *in vivo*. Structural and kinetic analyses have shown that Arl2/3 act allosterically to increase the dissociation rate constants for cargo-carrier complexes^{13,15,29,30}. In contrast, it was shown recently by pull-down experiments with cellular extracts that Arl3 but not Arl2 can efficiently release INPP5E from its complex with PDE6 δ (ref. 25).

In analogy to nuclear localization signals a number of different ciliary localization signals have been identified for different transmembrane proteins^{31–33}. However, not much is known about the molecular mechanism of how these signals are recognized and how decisions on ciliary entry based on these signals are made. For certain membrane-associated, post-translationally modified proteins carrying an N-terminal myristoyl or a C-terminal prenyl motif, it has been shown that

the import into cilia is dependent on the carrier proteins PDE6 δ , UNC119a and UNC119b and on Arl3 as displacement factor^{13,25,28,30,34}. However, it has been extensively documented that Ras proteins as well as Rheb require PDE6 δ for their proper localization at the plasma membrane or internal membranes, but do not appear to be localized in cilia^{15,16}.

This begs the question about the mechanism of PDE6 δ -mediated sorting of farnesylated cargo between the cilium and other cellular compartments. Thus, we set out to investigate the molecular basis of farnesylated cargo sorting using ciliary INPP5E and non-ciliary Rheb as an example. Here, we show that a 100-fold difference in the binding affinity of farnesylated cargo with PDE6 δ and the specific release of high-affinity cargo by activated Arl3•GTP determines cargo sorting into cilia, while low-affinity cargo can be released by both Arl3•GTP and Arl2•GTP and stays outside the cilium. Moreover, we show by structural, biochemical and cell biological approaches, how and why the binding affinity is dependent on the residues at the –1 and –3 positions preceding the farnesylated cysteine and that sorting of farnesylated cargo can be manipulated by changing the affinity to PDE6 δ .

Results

INPP5E and Rheb localization and binding affinity to PDE6 δ .

Using IMCD3 cells stably expressing either *INPP5E* or *Rheb* fused to a localization and tandem affinity purification (LAP) tag³⁵, we can show that INPP5E localizes almost exclusively to the primary cilium with very small fraction in the cell body (Fig. 1a; upper), which is consistent with previous reports^{18,19,26}. In contrast, Rheb mainly localizes to endomembranes (Fig. 1a; lower), this observation is consistent with previous reports^{13,36}. Given that the prenyl-binding protein PDE6 δ is the shuttle factor mediating the localization of INPP5E and Rheb^{13,16,18,25,26}, we set out to characterize the interaction of PDE6 δ with INPP5E and Rheb. Previously we have shown that farnesylated C-terminal peptides derived from Rheb or KRas bind to PDE6 δ in exactly the same way and with similar affinities as the full-length farnesylated proteins^{12,13}. Hence, we used a fluorescently labelled C-terminal farnesylated and carboxy-methylated peptide of INPP5E (residues 637–644) and Rheb (residues 175–181) to measure the affinity to PDE6 δ by fluorescence polarization. Figure 1b (left) shows that PDE6 δ binds to INPP5E peptide with low nanomolar affinity ($K_d = 3.7 \text{ nM} \pm 0.2$, \pm indicates s.d., $n = 9$). In contrast, the affinity between PDE6 δ and the farnesylated C-terminal peptide of Rheb falls into the submicromolar range ($K_d = 445 \pm 83 \text{ nM}$, \pm indicates s.d., $n = 10$) (Fig. 1b; right), which is in the same range with the previously described values^{12,13}. These data raised the question, whether the almost 100-fold higher affinity of INPP5E towards PDE6 δ as compared to Rheb is involved in the sorting mechanism of these two proteins to different destinations.

High-affinity cargo is specifically released by Arl3•GTP.

Towards an explanation for the possible sorting mechanism that leaves some PDE6 δ -cargo in the cell body but allows others to be enriched in the cilia we turned to the release activities of Arl2 and Arl3. Both GTP-binding proteins in their active conformation have been shown to be responsible for releasing cargo from PDE6 δ . While Arl2 is a non-ciliary protein, Arl3 localizes along the length of the cilium³⁷. Using fluorescence polarization, we measured the release of INPP5E and Rheb peptides from PDE6 δ by the addition of Arl2 or Arl3 bound to the non-hydrolysable GTP analogue GppNHp. The data show that Rheb peptide can be released by both Arl2•GppNHp and Arl3•GppNHp (Fig. 2a), supporting earlier observations¹³. In contrast, INPP5E peptide can only be released by Arl3•GppNHp under the same conditions

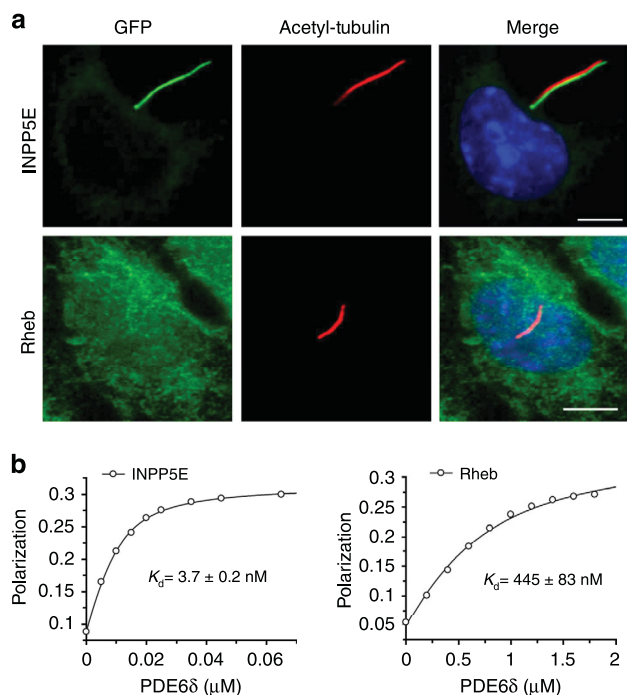


Figure 1 | Localization of INPP5E and Rheb and their affinity to PDE6δ.

(a) Localization of INPP5E and Rheb in IMCD3 cells. Stably expressed GFP-INPP5E colocalizes with acetylated tubulin, as shown by immunostaining of acetylated tubulin (red) and GFP fluorescence (LAP-tagged) (green), while GFP-Rheb (green) localizes to endomembranes and is almost absent from cilia. White bar indicates 5 μm. (b) 0.01 μM TAMRA-labelled farnesylated peptide (SQNSSTIC(Far)-OMe) from INPP5E (left) and 0.5 μM FITC-labelled peptide (SQGKSSC(Far)-OMe) from Rheb (right) were titrated with increasing concentrations of PDE6δ and the increase in fluorescence polarization was plotted against the PDE6δ concentration. The data were fitted to a quadratic equation giving the indicated dissociation constants (K_d). ± indicates s.d. ($n \geq 9$).

(Fig. 2b). To compare the cargo release kinetics of Arl2•GppNHp and Arl3•GppNHp, we measured the dissociation rate constants of INPP5E and Rheb peptides from PDE6δ in the presence and absence of Arl3•GppNHp or Arl2•GppNHp, by adding a large excess of unlabelled peptide to silence the back reaction. In the absence of Arl2/3, Rheb showed an intrinsic dissociation rate ($k_{\text{off}} = 0.95 \pm 0.004 \text{ s}^{-1}$, ± indicates s.d., $n = 4$), while no measurable dissociation rate could be observed for INPP5E in a reasonable time window. This observation is in line with the almost 100-fold difference in the binding affinity between both peptides determined from the steady state equilibrium measurements. The presence of Arl3•GppNHp or Arl2•GppNHp has a similar acceleration effect on the dissociation rate of Rheb peptide from PDE6δ ($k_{\text{off}} = 27.2 \pm 0.7$ and $15.3 \pm 0.3 \text{ s}^{-1}$, respectively, ± indicates s.d., $n = 4$) (Fig. 2c,d). However, the release of INPP5E peptide in the presence of Arl3•GppNHp shows an estimated 10,000-fold acceleration ($k_{\text{off}} = 10.7 \pm 0.2 \text{ s}^{-1}$, ± indicates s.d., $n = 4$), while release by Arl2•GppNHp ($k_{\text{off}} = 0.018 \pm 0.0005 \text{ s}^{-1}$, ± indicates s.d., $n = 4$) is almost 600-fold slower (Fig. 2e,f). Taken together, our data suggest that high-affinity farnesylated cargo can be specifically released by Arl3, while low-affinity cargo can be released similarly by both Arl2 and Arl3.

Role of Arl3 N-terminal helix in the release mechanism. Previously we have shown that the N-terminal helix of Arl3 is

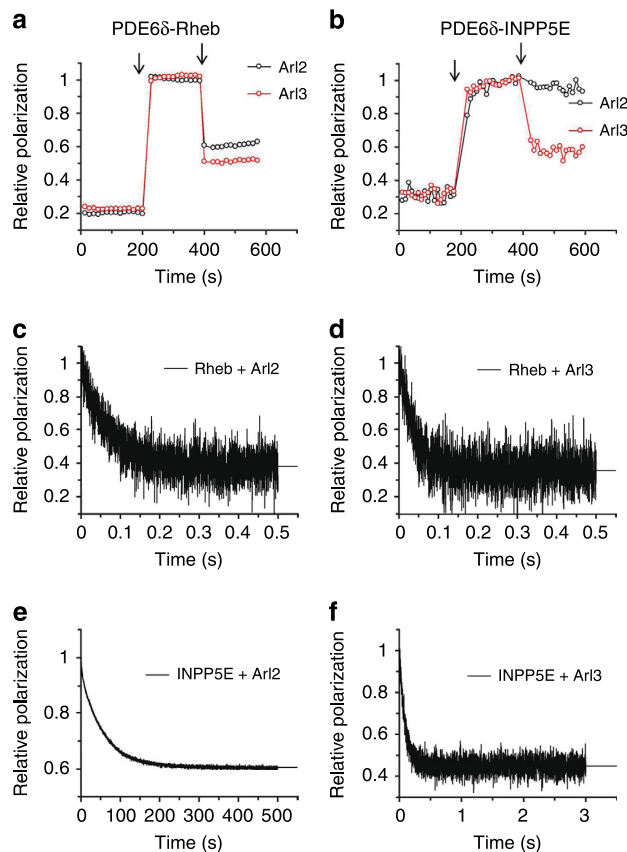


Figure 2 | INPP5E release from PDE6δ by Arl2•GppNHp and Arl3•GppNHp.

(a) Fluorescence polarization measurements of 0.5 μM FITC-labelled Rheb peptide followed by addition of 0.5 μM PDE6δ and the addition of 5 μM Arl2•GppNHp or Arl3•GppNHp (arrow). (b) Fluorescence polarization measurements of 0.2 μM TAMRA-labelled INPP5E peptide followed by the addition of 0.2 μM PDE6δ (arrow) and 5 μM Arl2•GppNHp or Arl3•GppNHp (arrow). (c–f) Stopped-flow fluorescence polarization kinetic experiment where complexes of 1 μM PDE6δ with either 0.2 μM of FITC-labelled Rheb peptide (c,d) or TAMRA-labelled farnesylated INPP5E peptide (e,f) were mixed with 100-fold excess of unlabelled peptide and 10 μM of Arl2 (c,e) or Arl3 (d,f) as indicated.

important to release myristoylated cargo from a complex with the shuttle factor UNC119 (ref. 30). To find out whether the N-terminus of Arl3 and/or Arl2 has a similar if any role in the interaction with PDE6δ, fluorescence polarization measurements using full-length Arl3 (Arl3^{fl}) or an N-terminal truncated form (Arl3^{ΔN}) were performed. Supplementary Fig. 1 shows that Arl3^{ΔN} is unable to release the INPP5E peptide from PDE6δ as compared with Arl3^{fl}. To investigate the role of the N-terminal helix of Arl3 in the release mechanism, we measured association and dissociation rate constants to determine the affinity of PDE6δ towards Arl2 and Arl3 in both full-length and N-terminal truncated forms. Association rate constants between the four proteins Arl3^{fl}, Arl3^{ΔN}, Arl2^{fl} and Arl2^{ΔN} are rather similar although association is almost twice as fast for full-length Arl3 as compared with Arl2 (Fig. 3a,b). In contrast, determination of the dissociation rate constants shows large differences. While the difference in k_{off} between full-length protein Arl2^{fl} and N-terminal deleted Arl2^{ΔN} is only threefold, Arl3^{fl} shows a 26-fold higher residence time with PDE6δ, as compared with Arl3^{ΔN} (Fig. 3c–e). By calculating the equilibrium dissociation constants ($K_d = k_{\text{off}}/k_{\text{on}}$), Arl3^{ΔN}, Arl2^{fl} and Arl2^{ΔN} exhibit affinities in the submicromolar range (217 ± 4.3 , 149 ± 19 and

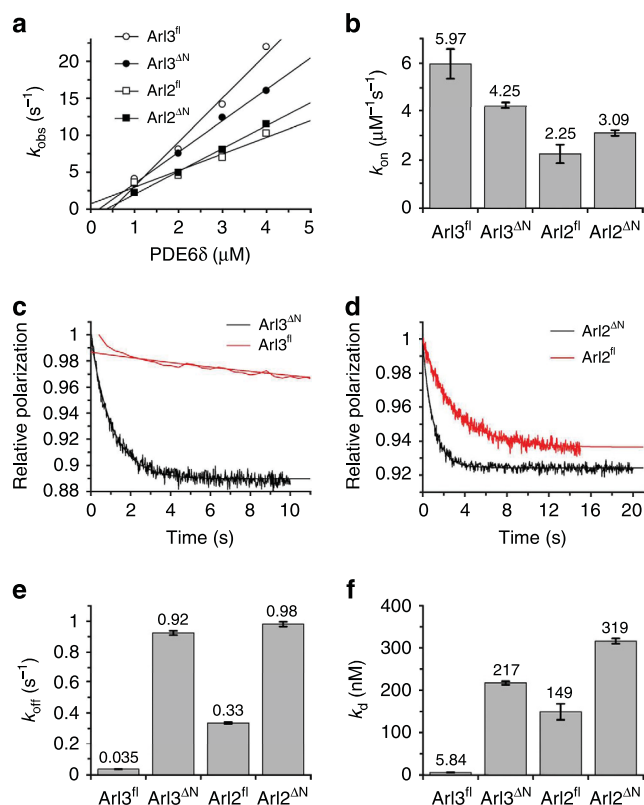


Figure 3 | Contribution of the N-terminal helix of Arl3 to the binding affinity with PDE6 δ . (a) Stopped-flow fluorescence polarization kinetic measurements of the association of 0.2 μM mantGppNHP loaded Arl proteins with increasing concentrations of PDE6 δ . The observed pseudo-first order rate constants (k_{obs}) are plotted against PDE6 δ concentration. (b) Bar charts of the association rate constants (k_{on}) determined in a. (c,d) Stopped-flow fluorescence polarization kinetic experiments where complexes of 2 μM PDE6 δ with 0.2 μM of full-length (Arl^{fl}) or N-terminally deleted (Arl^{ΔN}) mantGppNHP loaded Arl proteins as indicated were mixed with 200-fold excess of unlabelled Arl proteins to determine k_{off} . (e) Bar charts of the dissociation rate constants (k_{off}) from experiments in c,d. (f) Bar charts of the equilibrium dissociation constants (K_d) of complexes between PDE6 δ and Arl proteins as determined from the kinetic constants in c,e. Error bars indicate s.d., $n = 4$.

316 \pm 6.3 nM, respectively, \pm indicates s.d., $n = 4$), whereas Arl3^{fl} has an affinity in the low nanomolar range ($K_d = 5.8 \pm 0.5$ nM, \pm indicates s.d., $n = 4$) (Fig. 3f). The K_d values for Arl2^{fl} and Arl3^{fl} differ from previously determined values³⁸, likely because of the different techniques used.

Our data suggest that the N-terminal helix of Arl3 makes a significant contribution to the interaction with PDE6 δ and increases the affinity between the proteins by 37-fold. This additional input of Arl3 compared with Arl2 is probably a major factor in the ability of Arl3 to release high-affinity farnesylated cargo from PDE6 δ . A similar effect was shown for the Arl3/UNC119 complex where in contrast to Arl2 (and any other Arf protein), the N-terminal helix of Arl3 did not detach from the surface of the protein after the GDP-GTP conformational change and actively participates in the release mechanism in the closed position³⁰.

The sorting signal of PDE6 δ -related farnesylated cargo. To investigate the nature of the affinity difference between INPP5E and Rheb peptides towards PDE6 δ in more details, we solved the

crystal structure of the INPP5E peptide in complex with PDE6 δ at 1.85 Å resolution (data collection and refinement statistics summarized in Supplementary Table 1). Superimposition of the INPP5E peptide/PDE6 δ complex with the structure of PDE6 δ in complex with Rheb (PDB code: 3T5G) shows that the immunoglobulin-like β -sandwich folds of PDE6 δ overlay well with an r.m.s. deviation of 0.5731 Å. The proteins show a hydrophobic cavity, where the farnesyl moieties of INPP5E and Rheb are inserted (Fig. 4a; upper). The prenyl groups overlay well and make an identical interaction pattern with the surrounding hydrophobic residues of PDE6 δ (Fig. 4a; lower). However, the side chains of the residues on the -1 and -3 positions upstream of the farnesylated cysteine (the 0 position) in INPP5E and Rheb show different contacts with PDE6 δ . As shown in Fig. 4b (upper), the serine side chain of Rheb on the -1 position makes a hydrogen bond with the side chain of glutamic acid (Glu88) from PDE6 δ , whereas the hydrophobic side chain of the isoleucine of INPP5E at the equivalent position is situated in a highly hydrophobic environment mediated by five hydrophobic residues of PDE6 δ (Val80, Trp90, Met118, Leu123 and Ile128). On the other hand, the lysine side chain of Rheb at the -3 position is pointing away from the binding pocket of PDE6 δ , while the serine side chain of INPP5E at the equivalent position makes a hydrogen bond with the side chain of glutamic acid (Glu88) (Fig. 4b; lower).

Thus, we reasoned that the different contact patterns of INPP5E and Rheb peptides with PDE6 δ are responsible for the difference in affinities. To prove this, we generated two peptides, where the amino acids on the -1 and -3 positions were swapped between INPP5E and Rheb, creating INPP5E(KS) (S641K/I643S) and Rheb(SI) (K178S/S180I) peptides. Affinities of the swapped peptides to PDE6 δ were determined by titrating increasing amounts of unlabelled INPP5E(KS) and Rheb(SI) into a preformed complex of fluorescent Rheb peptide with PDE6 δ and monitoring the displacement by the decrease in fluorescence polarization. Analysis of the data with a competition model derived from the law of mass action as described^{17,39} shows that the affinities to PDE6 δ can be reversed, with a K_d values of (697 \pm 54 nM, \pm indicates s.d., $n = 14$) for INPP5E(KS) and (12 \pm 2.7 nM, \pm indicates s.d., $n = 12$) for Rheb(SI) (Fig. 4c).

To confirm the conclusion relating to the -1 and -3 positions, we measured the affinities of farnesylated peptides derived from rhodopsin kinase GRK1 and the γ -subunit of transducin GNGT1 (T γ) with PDE6 δ . It is important to note that, GRK1 carries Met and Ser at -1 and -3 positions similarly with INPP5E, whereas GNGT1 (T γ) carries Gly and Lys at -1 and -3 positions similarly with Rheb (Supplementary Fig. 2a). The results showed high binding affinity (7.2 \pm 1.3 nM, \pm indicates s.d., $n = 12$) of GRK1 and low binding affinity (6,573 \pm 477 nM, \pm indicates s.d., $n = 9$) of T γ for PDE6 δ (Supplementary Fig. 2b). These data suggest that the binding affinity between PDE6 δ and farnesylated cargo is dependent on the sequence of the farnesylated C-terminus, in particular on the -1 and -3 positions relative to the farnesylated cysteine.

Dependency of INPP5E ciliary localization on PDE6 δ and Arl3.

To test whether reducing the affinity of INPP5E to PDE6 δ is affecting its ciliary localization, we stably transfected the INPP5E(KS) mutant into IMCD3 cells and compared its localization with INPP5E(WT). Figure 5a shows that INPP5E(KS) mutant is not enriched in cilia anymore but is localized all over the cell including the cilium, while INPP5E(WT) is highly enriched in cilia with only a minor fraction in the cell body (Fig. 1a). Evaluation of mean fluorescence intensity ratio between cilia and whole cell shows that INPP5E(WT) has a 5.3-fold enrichment in

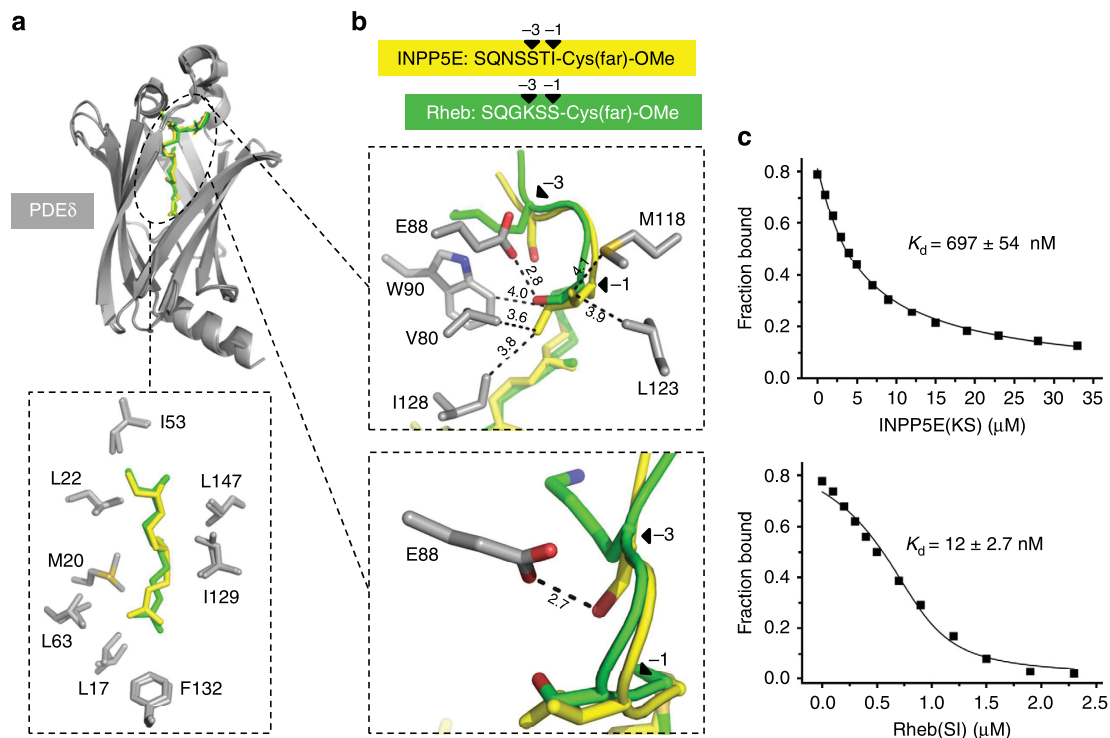


Figure 4 | Structural analysis of the interaction between PDE6 δ and farnesylated cargo. (a) Superimposition of farnesylated INPP5E peptide-PDE6 δ and Rheb-PDE6 δ (PDB code: 3T5G). The farnesyl moieties of INPP5E (yellow) and Rheb (green) insert into the hydrophobic pocket of PDE6 δ (grey) (upper) and maintain the same interaction pattern with the surrounding hydrophobic residues of PDE6 δ (lower). (b) Differences in the interaction pattern at the -1 (upper) and -3 (lower) residues from Rheb (green) and INPP5E (yellow) with PDE6 δ , bond lengths (black dashed line) are given in Å. (c) Titrations of a complex between 0.5 μ M FITC-labelled Rheb peptide and 1 μ M PDE6 δ with increasing concentrations of INPP5E(KS) (upper) and Rheb(SI) (lower) mutant peptides. Titration data were fitted with a competition model. \pm indicates s.d. ($n \geq 12$).

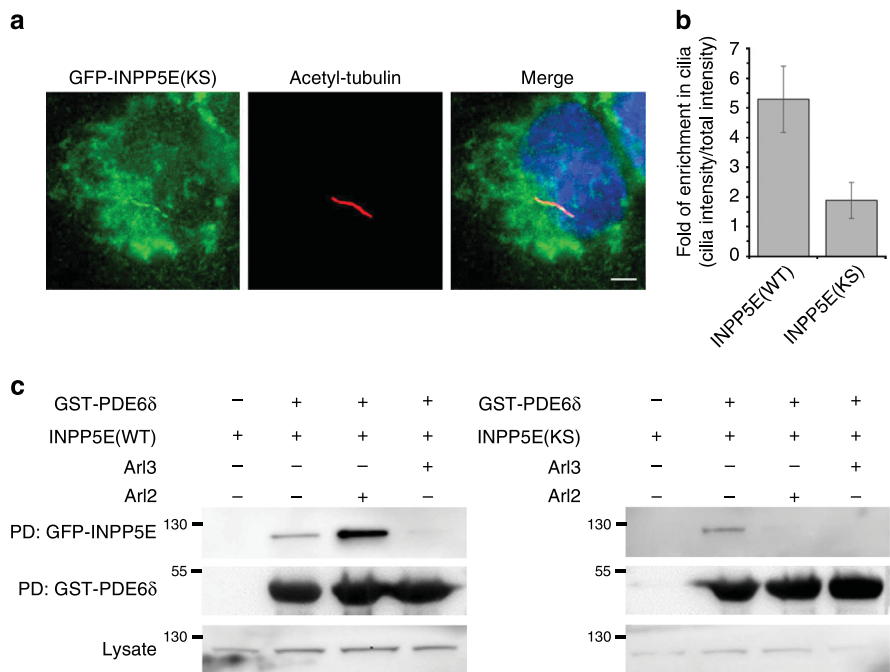


Figure 5 | INPP5E ciliary enrichment is dependent on high affinity to PDE6 δ . (a) Localization of INPP5E(KS) mutant (green) in IMCD3 cells which were stably transfected with the GFP-tagged protein. White bar indicates 5 μ m. (b) Bar chart showing ratio of GFP intensity in cilia to the total GFP intensity, indicating the enrichment of GFP-tagged protein in cilia. Data have been collected for 43 cells of INPP5E(WT) and 35 cells for INPP5E(KS) and analysis was performed using CellProfiler. Error bars indicate s.d., $n \geq 35$ ($P < 0.05$; Student's t -test). (c) GST pull-downs were performed using GST-PDE6 δ along with the IMCD3 cell lysates stably expressing INPP5E(WT) (left) or INPP5E(KS) (right). Formed complexes in the pull-down experiment were incubated with Arl2 or Arl3 as indicated. The amount of GFP-tagged interacting proteins bound to GST-PDE6 δ was detected by immunoblotting with an antibody against GFP.

the cilia, while the INPP5E(KS) mutant loses its ciliary enrichment and is more evenly distributed over the entire cell (Fig. 5b and Supplementary Fig. 3).

We propose that the mislocalization of INPP5E(KS) mutant could result from its weak affinity to PDE6 δ , which enables its release by Arl2 outside the cilium, resulting in its retention at the endomembranes. To support this assumption, we used the stably transfected IMCD3 cells expressing INPP5E(WT) or mutant INPP5E(KS) and performed a GST pull-down experiment with PDE6 δ in the presence and absence of Arl3•GppNHp or Arl2•GppNHp. The results show that the INPP5E(KS) mutant can indeed be released by both Arl2•GppNHp and Arl3•GppNHp, while INPP5E(WT) is specifically released only by Arl3•GppNHp (Fig. 5c). Confirming with this, siRNA-mediated knockdown of *Arl3* shows loss of dominant ciliary localization of INPP5E and its redistribution between cilia and cellular endomembranes (Fig. 6 and Supplementary Fig. 4).

In line with these experiments, we tested whether increasing the affinity of Rheb to PDE6 δ permits its ciliary entry. For this we stably transfected the Rheb(SI) mutant into IMCD3 cells and compared its localization to that of Rheb(WT). Rheb(SI) showed a more than fourfold increase in ciliary localization as compared with Rheb(WT) (Fig. 7). This result indicates that increasing the affinity of Rheb towards PDE6 δ shifts the equilibrium of Rheb distribution towards the cilium as compared to the entire cell. The non-exclusive ciliary localization of Rheb(SI) mutant could be explained by the absence of a Rheb specific retention signal inside the cilia.

Taken together, our data suggest that the high binding affinity between INPP5E and PDE6 δ and the specific release by Arl3•GTP are essential determinants for the ciliary localization of INPP5E.

Discussion

Consistent with our previous reports^{12,13}, here we show that non-ciliary farnesylated cargo such as Rheb binds to PDE6 δ with submicromolar affinity. Interestingly, the binding affinity between PDE6 δ and the ciliary farnesylated protein INPP5E is in the low nanomolar range. Structural analysis revealed that the residues at the –1 and –3 positions relative to the farnesylated cysteine are the determinants for the binding affinity to PDE6 δ . This finding was confirmed by mutational analysis and by the binding affinity measurements of farnesylated peptides derived from rhodopsin

kinase (GRK1) and the γ -subunit of transducin (T γ). The high binding affinity of GRK1 to PDE6 δ could explain its mislocalization in the outer segment of photoreceptor in the absence of PDE6 δ , while T γ , which has a low-affinity to PDE6 δ , is only minimally affected²⁸. The latter suggests that another farnesyl binding protein might exist to take over the role as a shuttle factor for T γ or that the ciliary entry of the heterotrimeric transducin does not rely solely on the farnesylated γ -subunit. Our findings suggest that the affinity of farnesylated cargo is an essential determinant of its PDE6 δ -mediated sorting into the ciliary compartment.

It has been reported that Arl3 is localized in the cytoplasm and inside cilia³⁷, while no ciliary localization for Arl2 has been reported so far. Considering that the complex between high-affinity cargo such as INPP5E or GRK1 with PDE6 δ can be released specifically by Arl3 and that both proteins are highly enriched in cilia, one would have to predict that the active GTP-bound form of Arl3 is only localized inside the cilium and thus is able to release cargo exclusively in this compartment. This assumption is supported by our recent study which showed that the ciliary protein Arl13B is the specific guanine nucleotide exchange factor for Arl3 (ref. 40) as well as by studies showing that retinitis pigmentosa 2 (RP2), the GTPase activating protein of Arl3, localizes at the basal body of the cilium or the preciliary region^{41,42}, so that Arl3•GTP should reside exclusively inside the cilium and would get hydrolyzed to Arl3•GDP while exiting the cilium. Confirming with this, Arl3 does not seem to take over the role of Arl2 in releasing low-affinity farnesylated cytosolic cargo, as siRNA-mediated knockdown of Arl2 was shown to be sufficient to mislocalize KRas (ref. 15). Thus, our data suggest that high-affinity farnesylated cargo is specifically released by Arl3 inside cilia and Arl2 is specific for the release of low-affinity cargo outside cilia.

Our results are apparently not in agreement with previous results^{25,26}, who showed that the transport of INPP5E is independent of Arl3. In these reports, data were analysed in terms of ciliary localization (INPP5E-positive cilia), not taking the distribution of INPP5E between cilia and the entire cell into account. Such analysis has enabled us to determine the fold enrichment of INPP5E inside cilia and how it is affected by either changing the affinity to PDE6 δ or by Arl3 knockdown. The redistribution of INPP5E in the cells, which were treated with siRNA against *Arl3*, showed similar but generally weaker effect as compared with the redistribution of the low-affinity mutant

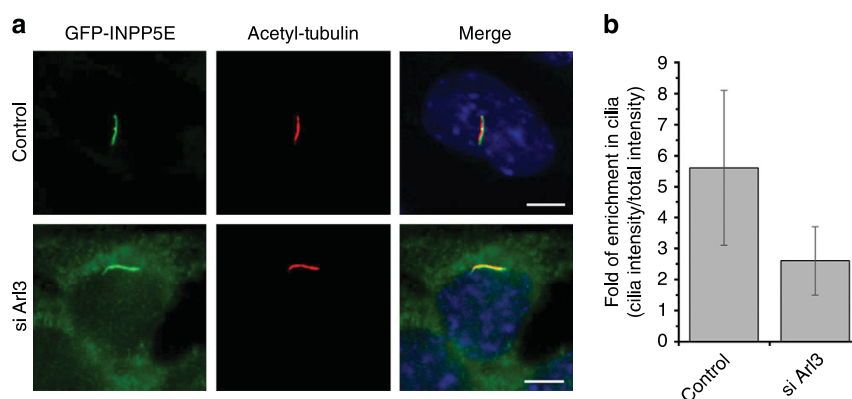


Figure 6 | INPP5E ciliary enrichment is dependent on Arl3. (a) Localization of INPP5E (green) in IMCD3 cells which were stably transfected with the LAP-tagged protein followed by the transfection with either negative control siRNA or siRNA directed against *Arl3*. White bar indicates 5 μ m. (b) Bar chart showing ratio of GFP intensity in cilia to the total GFP intensity, indicating the enrichment of GFP-tagged protein in cilia. Data have been collected for 90 cells which were treated with control siRNA and for 82 cells which were treated with siRNA against *Arl3* and analysis was performed using CellProfiler. Error bars indicate s.d., $n \geq 82$ ($P < 0.05$; Student's *t*-test).

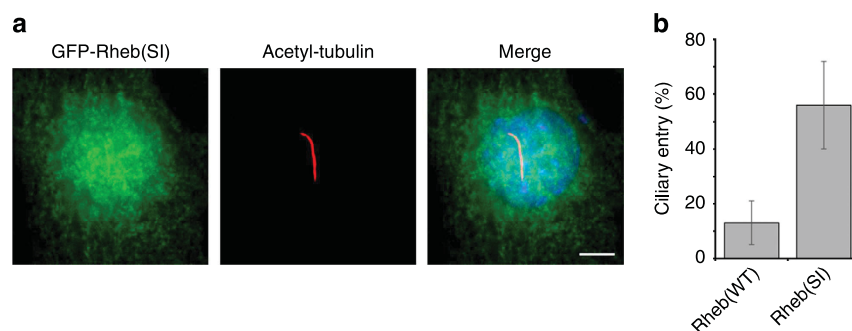


Figure 7 | Ciliary entry of Rheb is dependent on the affinity to PDE6 δ . (a) Localization of Rheb(SI) mutant (green) in IMCD3 cells which were stably transfected with the GFP-tagged protein. White bar indicates 5 μ m. (b) Bar chart showing the percentage of Rheb-positive cilia. Data were collected from two independent experiments for each Rheb(WT) (38 and 87 cells per experiment) and Rheb(SI) (92 and 126 cells per experiment). Error bars indicate s.d., $n \geq 125$ ($P < 0.05$; Student's t -test).

INPP5E(KS) (Figs 5b and 6b). The effect of Arl3 knockdown might be limited by the incomplete knockdown and by the fact that staining of INPP5E inside cilia does not differentiate between free or PDE6 δ -bound phosphatase.

Both ciliary cargo and Arl3 seem to bind to PDE6 δ with high affinities, non-ciliary cargo and Arl2 on the other hand bind to PDE6 δ with low affinities. Thus we assume that the cargo release by Arl3 inside cilia or Arl2 in the cytosol might not be complete at comparable concentrations of all components. As a consequence an additional signal would be required to drive the equilibrium to completion and to retain cargo at its destination. A retention signal could be achieved by the interaction with membrane or other interacting partners. The endomembrane system offers a large surface area and could play the role as retention signal for cytosolic farnesylated cargo such as Rheb. A possible ciliary retention signal for INPP5E could be Arl13B. The specific ciliary protein Arl13B has been shown to directly interact with INPP5E and its knockdown results in INPP5E mislocalization²⁶.

In this report, we propose a three step model for PDE6 δ -mediated sorting of farnesylated cargo into different cellular compartments. The binding affinity of farnesylated cargo to PDE6 δ is the first fundamental step in the sorting mechanism, followed by the specific release of high-affinity cargo by Arl3 inside cilia or the release of low-affinity cargo by Arl2 in the entire cell. Finally, a retention signal keeps the farnesylated cargo at its destination (Fig. 8). Interfering with any of these steps can provide valuable insights in studying the role of INPP5E in ciliopathies especially that a mutation which influences its localization to cilia is associated with MORM syndrome. Furthermore INPP5E localization studies for Arl13B patient mutations associated with Joubert syndrome will deepen our understanding of the molecular basis of ciliopathies. Finally it would be interesting to exploit available small molecules that inhibit the interaction of PDE6 δ with farnesylated cargo in studying the role of INPP5E in cilia and ciliopathies.

Methods

Plasmids. Vectors for transfection of IMCD3 Flp-In cells were generated using the Gateway cloning technology (Life technologies) following the manufacturer's recommendations. Mouse *INPP5E* and *Rheb* PCR fragments were amplified using the following primers: *INPP5E* (F-5'-ATGCCATCCAAGTCAGCTTGCTG-3', R-5'-TCAGGACACGGTGCAAACTGCACTGG-3'), *Rheb* (F-5'-ATGCCGCA GTCCAAGTCCCGGAAG-3', R-5'-TCACATCACCGAGCATGAAGACTT GCC-3'). Entry clones were obtained by integration of the PCR fragments into pCR8/GW/TOPO vector (Life technologies). Mouse *INPP5E* and *Rheb* entry clones were located to pG-LAP3 destination vector (Addgene)⁴³ by LR recombination. The pG-LAP3 vector encoded a LAP-tag (GFP-TEV-site-S-peptide) N-terminal to *INPP5E* and *Rheb*. *INPP5E* S641K/V643S (*INPP5E*(KS)) and *Rheb* K178S/S180I (*Rheb* (SI)) clones were created using *INPP5E*-pG-LAP3 and *Rheb*-pG-LAP3 as

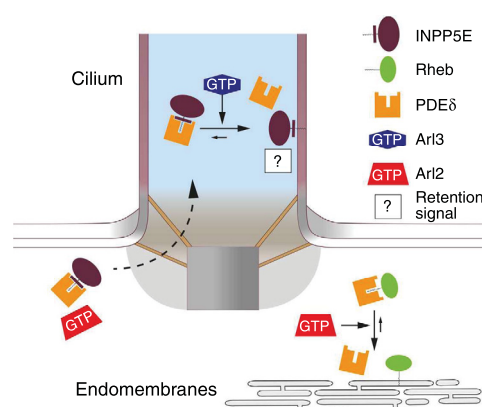


Figure 8 | Model of PDE6 δ -mediated sorting of farnesylated cargo. High-affinity cargo such as INPP5E can be specifically released from PDE6 δ by Arl3•GTP in the cilium, but not by Arl2•GTP in the cytosol. In contrast, low-affinity cargo such as Rheb can be released by Arl2•GTP. As a consequence, PDE6 δ -free INPP5E can be specifically retained and thus be enriched in the ciliary compartment while PDE6 δ -free Rheb is retained at endomembranes and stays outside the cilia.

template and following single mutagenesis primers: *INPP5E* V643S (F-5'-GCCAG AGCTCCAGTGCAAGTTGCACCGTGTCTCGTAAAGGGCG-3'), *INPP5E* S641K (F-5'-GCCAGAGCTCCAAAGCAGTTTGACCCGTGTCTGAAAGGGCG-3'), *Rheb* K178S (F-5'-GGGGCAGCTTCACAAGGCTCGTCTTCATGCTCGG TGATG-3'), *Rheb* S180V (F-5'-GCTTCACAAGGCTCGTCTGTATGCTCGG TGATGTGAAAGG-3').

Proteins. All proteins were expressed in *Escherichia coli* strain BL21-Codon-Plus(DE3)-RIL. Cells were induced at OD ~ 0.6 with 100 μ M IPTG and incubated at 20 $^{\circ}$ C overnight. Cells were harvested and lysed in lysis buffer (25 mM Tris-HCl, pH 7.5, 150 mM NaCl and 1 mM b-mercaptoethanol, 1 mM PMSF) using French press. Supernatants of C-terminal histidine-tagged full-length Arl3, Arl2 and N-terminal histidine-tagged PDE6 δ were loaded onto a Ni-NTA column (QIAGEN). Proteins were eluted with elution buffer (25 mM Tris-HCl, pH 7.5, 150 mM NaCl and 1 mM b-mercaptoethanol, 250 mM imidazole), followed by gel filtration on a Superdex 75 S26/60 column using elution buffer without imidazole. Supernatants of N-terminal GST-tagged truncated Arl3 and Arl2 (aa 18-177, 17-178, respectively) were expressed, harvested and lysed similar to the histidine-tagged proteins. The supernatants were loaded onto GSH-column (Amersham Biosciences). Proteins were eluted with elution buffer (25 mM Tris-HCl, pH 7.5, 150 mM NaCl and 1 mM b-mercaptoethanol, 20 mM glutathione). The GST-fusion proteins were separated from the tag by proteolytic cleavage followed by gel filtration on a Superdex 75 S26/60 column using elution buffer without glutathione. Nucleotide exchange of the GDP bound Arl3 and Arl2 proteins was achieved by overnight incubation at 4 $^{\circ}$ C with 4 U mg $^{-1}$ alkaline phosphatase (Roche Diagnostics) and 1.5-fold excess of the non-hydrolysable GTP analogue (GppNHp) or the fluorescently labelled GppNHp (mantGppNHp) and followed by gel filtration.

Peptides. Fluorescently labelled, farnesylated and carboxy-methylated Rheb peptide (Fluorescein-SQKSSC(Far)-OMe) and INPP5E peptide (SQNSSTIC(Far)-OMe) were obtained from JPT. Farnesylated and carboxy-methylated Rheb(SI) (SQSSSIC(Far)-OMe), INPP5E(KS) (SQNSKTSC(Far)-OMe), GRK1 (SSSKSGMC(Far)-OMe) and T γ (FKELKGGC(Far)-OMe) peptides were obtained from CambridgePeptides.

Crystallization and structure determination. The INPP5E-peptide (SQNSSTIC(Far)-OMe) was dissolved in DMSO and mixed with 500 μ M solution of PDE6 δ at 1:1 molar ratio in a buffer containing 25 mM Tris-HCl (pH 7.5), 150 mM NaCl and 3 mM DTE. The crystals appeared in Protein Complex suite from Qiagen, 1.4 M sodium malonate (at 20 °C) and were flash frozen in a cryoprotectant solution that contains the mother liquor in addition to 16% (v/v) glycerol. Diffraction data set was collected at the X10SA beamline of the Suisse Light Source, Villigen. XDS program was used for data processing. The structure was solved by molecular replacement using Molrep from CCP4 (suite) and PDE6 δ from the PDE6 δ -farnesylated Rheb complex (PDB code: 3T5G) as a search model. The farnesylated INPP5E peptide was built using WinCoot and refinement was done with REFMAC5. Refinement and data collection statistics are summarized in Supplementary Table 1. Structure coordinates were deposited in the Protein Data Bank (PDB code 5F2U). A stereo image of a portion of the electron density map is displayed in Supplementary Fig. 5.

Fluorescence polarization measurements. All fluorescence polarization measurements were performed at 20 °C in a buffer containing 25 mM Tris-HCl (pH 7.5), 50 mM NaCl and 3 mM DTE. For the titration measurement, data were recorded with Fluoromax-4 spectrophotometer (HORIBA Jobin Yvon, Munich, Germany) with excitation and emission wavelengths at 530 and 580 nm for TAMRA-labelled INPP5E peptide and at 495 and 520 nm for fluorescein-labelled Rheb peptide. The kinetic measurements were monitored by a stopped-flow apparatus (Applied Photophysics) in the polarization mode using an excitation wavelength of 366 nm and filter with 420 nm cutoff for mantGppNHp bound Arl protein, excitation wavelength of 495 nm and filter with 520 nm cutoff for fluorescein-labelled Rheb peptide and excitation wavelength of 530 nm and filter with 570 nm cutoff for TAMRA-labelled INPP5E peptide. Data analysis was done with GraFit 5.0 program (Erithacus Software). Concentrations used for each experiment are indicated in the corresponding figure legend.

Cell culture and stable cell line generation. Mouse renal epithelial cells from the inner medullary collecting duct containing a stably integrated FRT cassette (IMCD3 FLP-In, kind gift from M.V. Nachury lab; FLP-In cell line technology by Life technologies) were cultured at 37 °C and 5% CO₂ in DMEM/F-12, HEPES (Life technologies) complemented with 10% fetal bovine serum and 2 mM L-Glutamine. Stable cell lines were generated as previously described^{43,44}. Briefly, IMCD3 cells were seeded in six-well plates at a density of 100,000 cells per well. On the following day the cells with a confluence of 40–60% were cotransfected with the pG-LAP3 vector (Addgene) containing the gene of interest and pOG44 vector (Life technologies) encoding the FLP recombinase using Lipofectamine 2,000 (Life technologies). Transfected cells were selected with hygromycin in a concentration of 100–200 μ g ml⁻¹ complemented culture medium. Expression of the respective proteins was proven by immunoblotting with an anti-GFP antibody (1:500; Santa Cruz Biotechnology sc-9996).

Immunostaining and microscopy. IMCD3 cells stably expressing GFP-tagged protein were plated on poly-L-lysine coated coverslips in six-well plates, each well containing 100,000 cells. Twenty-four hours later, cilia were induced by 48 h serum starvation. Cells were washed in PBS and fixed with 4% formaldehyde in cytoskeletal buffer (2.75 M NaCl, 100 mM KCl, 25 mM Na₂HPO₄, 8 mM KH₂PO₄, 40 mM MgCl₂, 40 mM EGTA, 100 mM PIPES, 100 mM Glucose, pH 6.0) for 20 min. After two washes with PBS cells were permeabilized with 0.3% Triton X100 in cytoskeletal buffer for 10 min. Cells were rinsed in 0.1% Tween20 in PBS and blocked in 10% FBS in PBS for 30 min. For immunostaining of primary cilia, mouse 6-11B-1 anti-acetylated tubulin antibody (1:5,000; Sigma T6793) in 10% FBS in PBS was incubated overnight at 4 °C. Alexa Fluor 647 anti-mouse secondary antibody (1:800; Life technologies A-31571) was added for 45 min at room temperature after washing four times with 0.1% Tween20 in PBS. Coverslips were rinsed three times in 0.1% Tween20 in PBS and afterwards in PBS. Nuclei were stained with DAPI (Serva), diluted 1:10,000 in PBS for 1 min. After three washes with PBS, coverslips were fixed on glass slides with Mowiol (Merck). Images were taken using an Olympus IX81 microscope with a CCD camera and a 60x NA 1.35 oil immersion objective.

Knockdown experiment. The INPP5E(WT) stable cell line was plated on poly-L-lysine coated coverslips in six-well plates at a density of 100,000 cells per well. After 24 h cells were transiently transfected with Lipofectamine 2,000 with siRNAs directed against mouse Arl3 and a negative control siRNA, following the manufacturer's recommendations. The siRNAs against Arl3 and for a negative control were provided from Qiagen with the following sequences: for Arl3

(sense: 5'-GGGUCAGGAACUACGGAATT-3', antisense: 5'-UUCGUGUAGU UCCUGACCCGT-3'); for negative control (sense: 5'-UUCUCCGAACGUGUC ACGUdTdT-3', antisense: 5'-ACGUGACACGUUCGAGAAAdTdT-3'). Eighty-four hours later, cells were serum-starved for 24 h and subsequently treated for immunofluorescence microscopy as described before. Image collection was performed utilizing identical settings for every sample.

GST pull-down assay. IMCD3 cells stably expressing GFP-INPP5E(WT) or GFP-INPP5E(KS) were lysed in lysis buffer containing 75 mM Hepes pH 7.5, 150 mM KCl, 1.5 mM EGTA, 1.5 mM MgCl₂, 15% glycerol, 0.2% NP-40 and one protease inhibitor cocktail tablet (Roche). Cell lysates were cleared and supernatants were incubated for 1 h at 4 °C with 100 μ l GSH-beads conjugated with 20 μ M GST-PDE6 δ . For the release assay, 20 μ M of either Arl2 or Arl3 were added to the previous mixture and incubated for further 1 h at 4 °C. After 5 times washing with the lysis buffer, the complexes were analysed by western blotting using anti-GFP antibody (1:500; Santa Cruz Biotechnology sc-9996) and anti GST (1:5,000; home source). Full scans of western blots are provided in Supplementary Fig. 6.

References

1. Badano, J. L., Mitsuma, N., Beales, P. L. & Katsanis, N. The ciliopathies: an emerging class of human genetic disorders. *Annu. Rev. Genomics Hum. Genet.* **7**, 125–148 (2006).
2. Novarino, G., Akizu, N. & Gleeson, J. G. Modeling human disease in humans: the ciliopathies. *Cell* **147**, 70–79 (2011).
3. Emmer, B. T., Maric, D. & Engman, D. M. Molecular mechanisms of protein and lipid targeting to ciliary membranes. *J. Cell Sci.* **123**, 529–536 (2010).
4. Tyler, K. M. *et al.* Flagellar membrane localization via association with lipid rafts. *J. Cell Sci.* **122**, 859–866 (2009).
5. Nozawa, Y. I., Lin, C. & Chuang, P. T. Hedgehog signaling from the primary cilium to the nucleus: an emerging picture of ciliary localization, trafficking and transduction. *Curr. Opin. Genet. Dev.* **23**, 429–437 (2013).
6. Goetz, S. C., Ocbina, P. J. & Anderson, K. V. The primary cilium as a Hedgehog signal transduction machine. *Methods Cell Biol.* **94**, 199–222 (2009).
7. Gillespie, P. G., Prusti, R. K., Apel, E. D. & Beavo, J. A. A soluble form of bovine rod photoreceptor phosphodiesterase has a novel 15-kDa subunit. *J. Biol. Chem.* **264**, 12187–12193 (1989).
8. Florio, S. K., Prusti, R. K. & Beavo, J. A. Solubilization of membrane-bound rod phosphodiesterase by the rod phosphodiesterase recombinant delta subunit. *J. Biol. Chem.* **271**, 24036–24047 (1996).
9. Zhang, H. *et al.* Photoreceptor cGMP phosphodiesterase delta subunit (PDEdelta) functions as a prenyl-binding protein. *J. Biol. Chem.* **279**, 407–413 (2004).
10. Hanzal-Bayer, M., Renault, L., Roversi, P., Wittinghofer, A. & Hillig, R. C. The complex of Arl2-GTP and PDE delta: from structure to function. *EMBO J.* **21**, 2095–2106 (2002).
11. Nancy, V., Callebaut, I., El Marjou, A. & de Gunzburg, J. The delta subunit of retinal rod cGMP phosphodiesterase regulates the membrane association of Ras and Rap GTPases. *J. Biol. Chem.* **277**, 15076–15084 (2002).
12. Chen, Y. X. *et al.* Synthesis of the Rheb and K-Ras4B GTPases. *Angew. Chem. Int. Ed. Engl.* **49**, 6090–6095 (2010).
13. Ismail, S. A. *et al.* Arl2-GTP and Arl3-GTP regulate a GDI-like transport system for farnesylated cargo. *Nat. Chem. Biol.* **7**, 942–949 (2011).
14. Zhang, H., Constantine, R., Frederick, J. M. & Baehr, W. The prenyl-binding protein PrBP/delta: a chaperone participating in intracellular trafficking. *Vision. Res.* **75**, 19–25 (2012).
15. Schmick, M. *et al.* KRas localizes to the plasma membrane by spatial cycles of solubilization, trapping and vesicular transport. *Cell* **157**, 459–471 (2014).
16. Chandra, A. *et al.* The GDI-like solubilizing factor PDEdelta sustains the spatial organization and signalling of Ras family proteins. *Nat. Cell Biol.* **14**, 148–158 (2012).
17. Zimmermann, G. *et al.* Small molecule inhibition of the KRAS-PDEdelta interaction impairs oncogenic KRAS signalling. *Nature* **497**, 638–642 (2013).
18. Jacoby, M. *et al.* INPP5E mutations cause primary cilium signaling defects, ciliary instability and ciliopathies in human and mouse. *Nat. Genet.* **41**, 1027–1031 (2009).
19. Bielas, S. L. *et al.* Mutations in INPP5E, encoding inositol polyphosphate-5-phosphatase E, link phosphatidyl inositol signaling to the ciliopathies. *Nat. Genet.* **41**, 1032–1036 (2009).
20. Travaglini, L. *et al.* Phenotypic spectrum and prevalence of INPP5E mutations in Joubert syndrome and related disorders. *Eur. J. Hum. Genet.* **21**, 1074–1078 (2013).
21. Pirruccello, M. & De Camilli, P. Inositol 5-phosphatases: insights from the Lowe syndrome protein OCRL. *Trends Biochem. Sci.* **37**, 134–143 (2012).
22. Conduit, S. E., Dyson, J. M. & Mitchell, C. A. Inositol polyphosphate 5-phosphatases; new players in the regulation of cilia and ciliopathies. *FEBS Lett.* **586**, 2846–2857 (2012).

23. De Smedt, F., Boom, A., Pesesse, X., Schiffmann, S. N. & Erneux, C. Post-translational modification of human brain type I inositol-1,4,5-trisphosphate 5-phosphatase by farnesylation. *J. Biol. Chem.* **271**, 10419–10424 (1996).
24. Hampshire, D. J. *et al.* MORM syndrome (mental retardation, truncal obesity, retinal dystrophy and micropenis), a new autosomal recessive disorder, links to 9q34. *Eur. J. Hum. Genet.* **14**, 543–548 (2006).
25. Thomas, S. *et al.* A homozygous PDE6D mutation in Joubert syndrome impairs targeting of farnesylated INPP5E protein to the primary cilium. *Hum. Mutat.* **35**, 137–146 (2014).
26. Humbert, M. C. *et al.* ARL13B, PDE6D, and CEP164 form a functional network for INPP5E ciliary targeting. *Proc. Natl Acad. Sci. USA* **109**, 19691–19696 (2012).
27. Zhang, H. *et al.* Mistrafficking of prenylated proteins causes retinitis pigmentosa 2. *FASEB J.* **29**, 932–942 (2014).
28. Zhang, H. *et al.* Deletion of PrBP/delta impedes transport of GRK1 and PDE6 catalytic subunits to photoreceptor outer segments. *Proc. Natl Acad. Sci. USA* **104**, 8857–8862 (2007).
29. Watzlich, D. *et al.* The interplay between RPGR, PDEdelta and ARL2/3 regulate the ciliary targeting of farnesylated cargo. *EMBO. Rep.* **14**, 465–472 (2013).
30. Ismail, S. A. *et al.* Structural basis for ARL3-specific release of myristoylated ciliary cargo from UNC119. *EMBO J.* **31**, 4085–4094 (2012).
31. Nachury, M. V., Seeley, E. S. & Jin, H. Trafficking to the ciliary membrane: how to get across the periciliary diffusion barrier? *Annu. Rev. Cell Dev. Biol.* **26**, 59–87 (2010).
32. Hsiao, Y. C., Tuz, K. & Ferland, R. J. Trafficking in and to the primary cilium. *Cilia* **1**, 4 (2012).
33. Garcia-Gonzalo, F. R. & Reiter, J. F. Scoring a backstage pass: mechanisms of ciliogenesis and ciliary access. *J. Cell Biol.* **197**, 697–709 (2012).
34. Wright, K. J. *et al.* An ARL3-UNC119-RP2 GTPase cycle targets myristoylated NPHP3 to the primary cilium. *Genes Dev.* **25**, 2347–2360 (2011).
35. Cheeseman, I. M. & Desai, A. A combined approach for the localization and tandem affinity purification of protein complexes from metazoans. *Sci. STKE* **2005**, pl1 (2005).
36. Buerger, C., DeVries, B. & Stambolic, V. Localization of Rheb to the endomembrane is critical for its signaling function. *Biochem. Biophys. Res. Commun.* **344**, 869–880 (2006).
37. Zhou, C., Cunningham, L., Marcus, A. I., Li, Y. & Kahn, R. A. ARL2 and ARL3 regulate different microtubule-dependent processes. *Mol. Biol. Cell* **17**, 2476–2487 (2006).
38. Veltel, S., Kravchenko, A., Ismail, S. & Wittinghofer, A. Specificity of ARL2/ARL3 signaling is mediated by a ternary ARL3-effector-GAP complex. *FEBS Lett.* **582**, 2501–2507 (2008).
39. Roehrl, M. H., Wang, J. Y. & Wagner, G. A general framework for development and data analysis of competitive high-throughput screens for small-molecule inhibitors of protein-protein interactions by fluorescence polarization. *Biochemistry* **43**, 16056–16066 (2004).
40. Gotthardt, K. *et al.* A G-protein activation cascade from ARL13B to ARL3 and implications for ciliary targeting of lipidated proteins. *Elife* **4**, e11859 (2015).
41. Evans, R. J. *et al.* The retinitis pigmentosa protein RP2 links pericentriolar vesicle transport between the golgi and the primary cilium. *Hum. Mol. Genet.* **19**, 1358–1367 (2010).
42. Hurd, T. *et al.* The retinitis pigmentosa protein RP2 interacts with polycystin 2 and regulates cilia-mediated vertebrate development. *Hum. Mol. Genet.* **19**, 4330–4344 (2010).
43. Torres, J. Z., Miller, J. J. & Jackson, P. K. High-throughput generation of tagged stable cell lines for proteomic analysis. *Proteomics* **9**, 2888–2891 (2009).
44. Sang, L. *et al.* Mapping the NPHP-JBTS-MKS protein network reveals ciliopathy disease genes and pathways. *Cell* **145**, 513–528 (2011).

Acknowledgements

The funding was supported by the European Research Council (ERC Grant 268782), Sonderforschungsbereich-DFG (SFB 642) and CRUK core funding award to S.I. (A19257). We thank C. Körner and J.A. Seidel for expert technical assistance. We thank the staff of the beamline X10SA at the Swiss Light Source for their support and Prof E. Hofmann, Dr R. Gasper-Schönenbrücher and S. Terheyden for help with the data collection. We thank G. Zimmermann for labelling the INPP5E peptide with TAMRA.

Author contributions

E.K.F. and S.K.K. performed all the experiments and their analysis and contributed to their design; S.I. strongly supported crystallization and structure determination; E.Z. established the analysis of the microscopic data and contributed to the design of the experiments; and A.W. and S.I. supervised the work and advised about the design of the experiments and wrote the manuscript with E.K.F.

Additional information

Accession codes: The X-ray crystallographic coordinates for structures reported in this study have been deposited at the Protein Data Bank (PDB), under the accession code 5F2U.

Supplementary Information accompanies this paper at <http://www.nature.com/naturecommunications>

Competing financial interests: The authors declare no competing financial interests.

Reprints and permission information is available online at <http://npg.nature.com/reprintsandpermissions/>

How to cite this article: Fansa, E. K. *et al.* PDE6δ-mediated sorting of INPP5E into the cilium is determined by cargo-carrier affinity. *Nat. Commun.* **7**:11366 doi: 10.1038/ncomms11366 (2016).

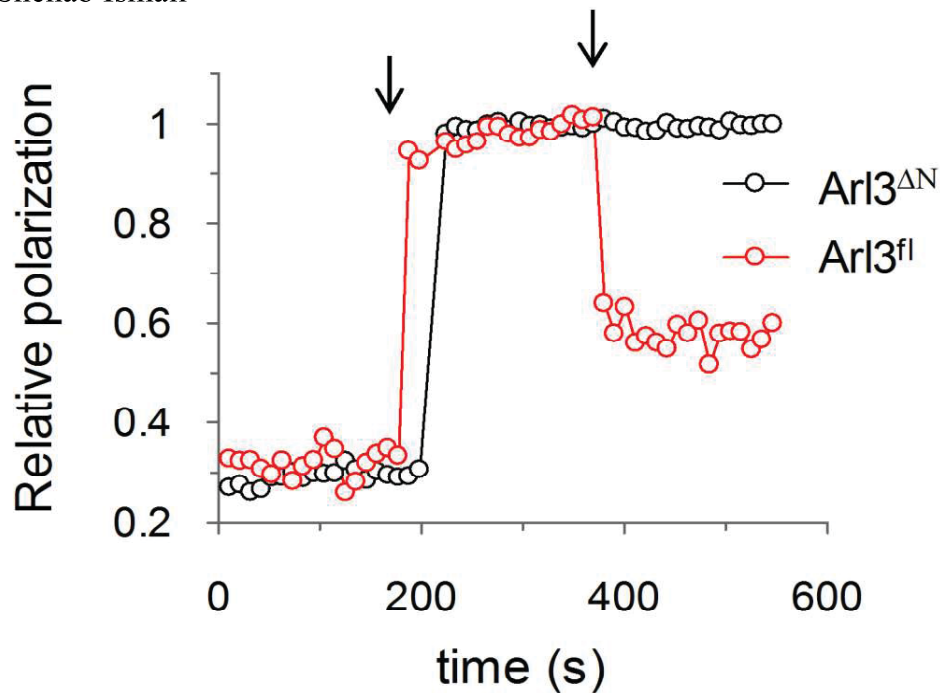


This work is licensed under a Creative Commons Attribution 4.0 International License. The images or other third party material in this article are included in the article's Creative Commons license, unless indicated otherwise in the credit line; if the material is not included under the Creative Commons license, users will need to obtain permission from the license holder to reproduce the material. To view a copy of this license, visit <http://creativecommons.org/licenses/by/4.0/>

Supplementary Information

PDE6 δ -mediated sorting of INPP5E into the cilium is determined by cargo-carrier affinity

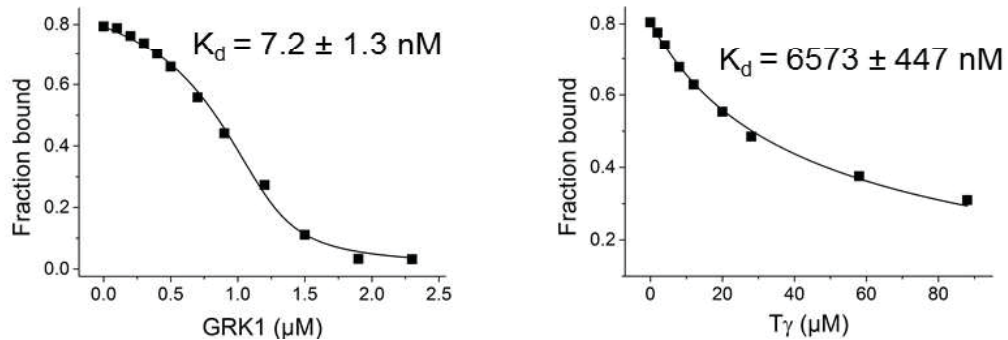
Eyad Kalawy Fansa*, Stefanie Kristine Kösling*, Eldar Zent, Alfred Wittinghofer & Shehab Ismail



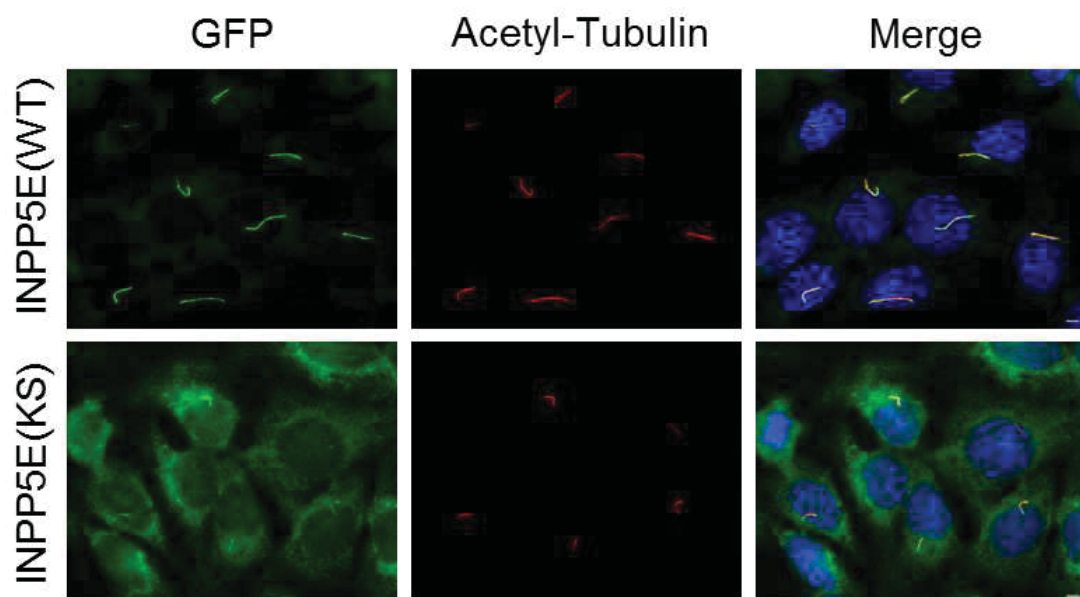
Supplementary Figure 1: INPP5E release is dependent on the N-terminal helix of Arl3•GTP. Fluorescence polarization measurements of 0.2 μ M TAMRA-labeled INPP5E peptide followed by addition of 0.2 μ M PDE6 δ (arrow) and the addition of 5 μ M Arl3^{fl} or Arl3 ΔN (arrow).

a

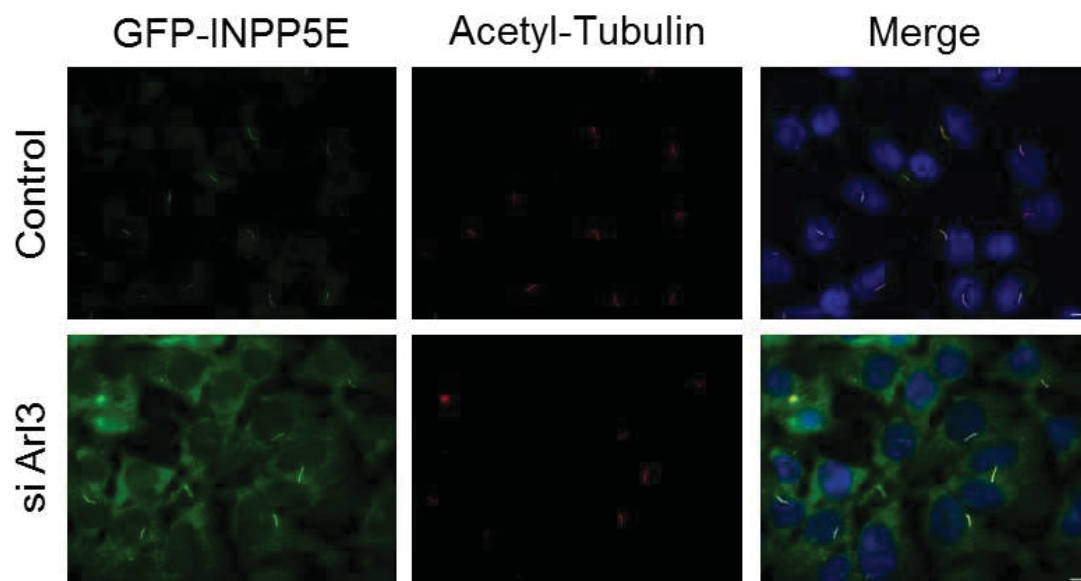
<u>Protein</u>	<u>Upstream sequence</u>	<u>CaaX-motif</u>
INPP5E	LQSQNSSTI	CSVS
GRK1	SSSSSKSGM	CLVS
Rheb	GAASQGKSS	CSVM
NGT1(T γ)	NPFKELKGG	CVIS

b**Supplementary Figure 2: Affinity of GRK1 and T γ farnesylated peptides to PDE6 δ .**

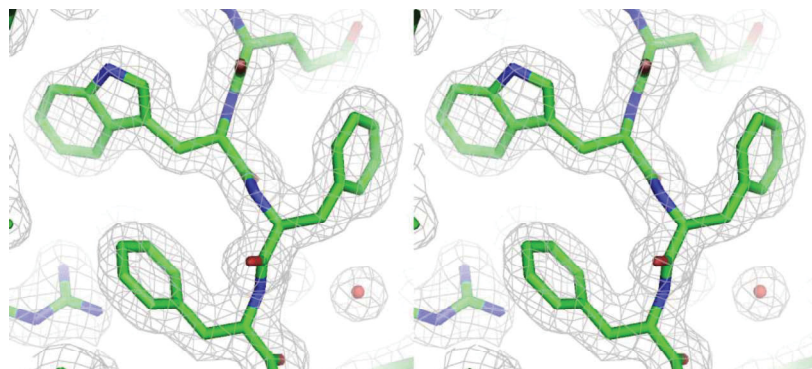
(a) Sequence alignment of C-terminal part of PDE6 δ high affinity binding partners (INPP5E and GRK1) and low affinity binding partner (Rheb and T γ). The prenylated cysteine is highlighted in black; residues at the -1 and -3 positions upstream of the cysteine are highlighted in red **(b)** Titrations of a complex between 0.5 μ M FITC-labeled Rheb peptide and 1 μ M PDE6 δ with increasing concentrations of GRK1 (left) and T γ (right) peptides. Titration data were fitted with a competition model.



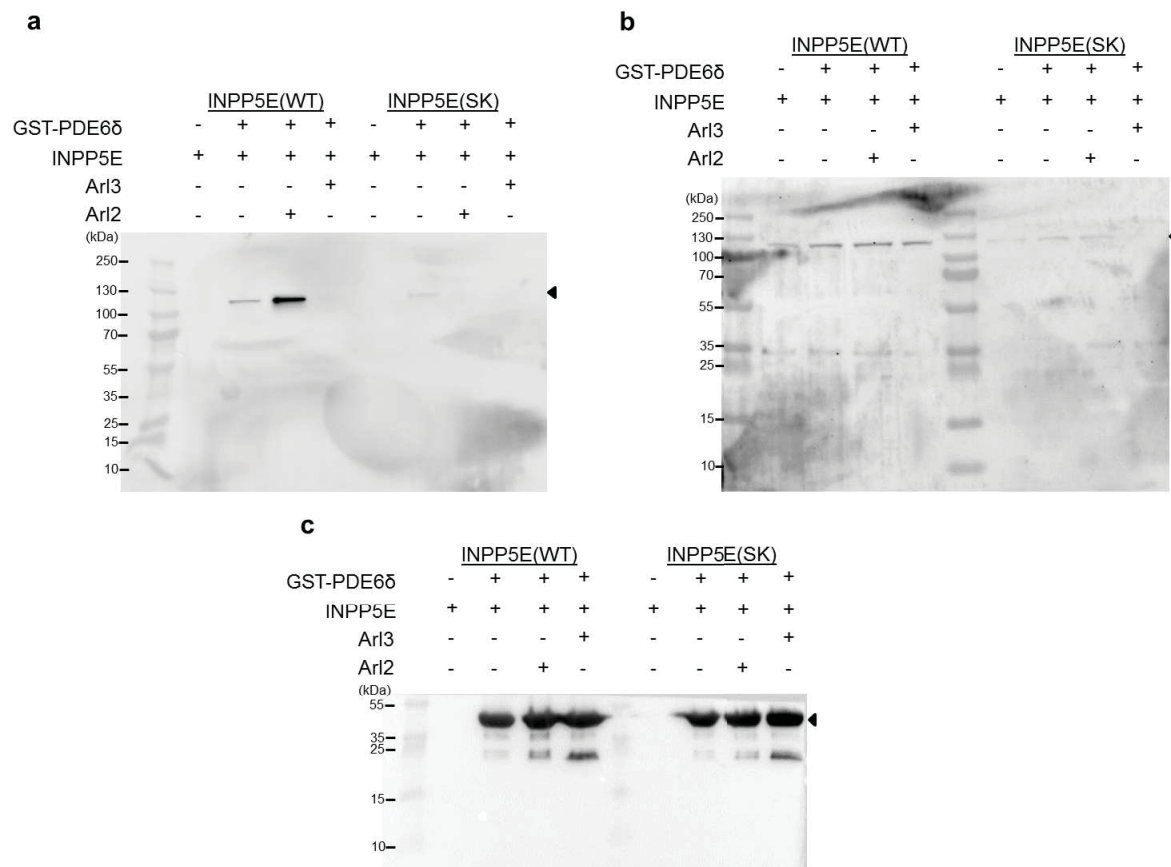
Supplementary Figure 3: Mislocalization of low affinity mutant of INPP5E towards PDE6 δ . Localization of either INPP5E(WT) or INPP5E(KS) (green) in IMCD3 cells which were stably transfected with the GFP-tagged proteins. White bar indicates 5 μ m.



Supplementary Figure 4: Ciliary enrichment of INPP5E is dependent on Arl3. Localization of INPP5E (green) in IMCD3 cells which were stably transfected with the GFP-tagged protein followed by the transfection with either control siRNA or siRNA directed against *Arl3*. White bar indicates 5 μ m



Supplementary Figure 5: A stereo image of a portion of the 2F_o-F_c electron density map. Representative electron density, as a cross-eyed stereo pair at 1 σ level around Try90, Phe91 and Phe92 of F-INPP5E-peptide•PDE6 δ complex structure.



Supplementary Figure 6: Full scans of western blots used in the main figure. (a) Blot against GFP-INPP5E from the GST pull-down. **(b)** Blot against GFP-INPP5E from the total cell lysate. **(c)** Blot against GST-PDE6δ from the GST pull-down. Black arrows indicate the target proteins.

Supplementary table 1: Data collection and refinement statistics (molecular replacement).

	F-INPP5E-peptide•PDE6δ
Data collection	
Space group	$C222_1$
Cell dimensions	
a, b, c (Å)	77.47, 81.20, 117.21
α, β, γ (°)	90.00, 90.00, 90.00
Resolution (Å)	19.53-1.85 (1.9-1.85)
R_{sym} or R_{merge}	9.7 (67.2)
$I / \sigma I$	10.42 (3.09)
Completeness (%)	99.8 (100.0)
Redundancy	6.39 (6.58)
R_{meas}	10.5 (69.1)
R_{pim}	4.1 (26.0)
Refinement	
Resolution (Å)	19.53-1.85 (1.9-1.85)
No. reflections	31895 (2396)
No. collected reflections	203615 (15773)
$R_{\text{work}} / R_{\text{free}}$	17.3/20.7 (24.0/29.6)
No. atoms	
Protein	2434
Ligand/ion	112
Water	89
B -factors	
Protein	34.0
Ligand/ion	39.66
Water	39.84
R.m.s. deviations	
Bond lengths (Å)	0.0201
Bond angles (°)	2.0109
Ramachandran plot statistics	
Favoured region (%)	98.3

Allowed region (%)	1.7
Outlier region (%)	0.0
PDB code	5F2U

Numbers in parentheses represent the highest-resolution bin.

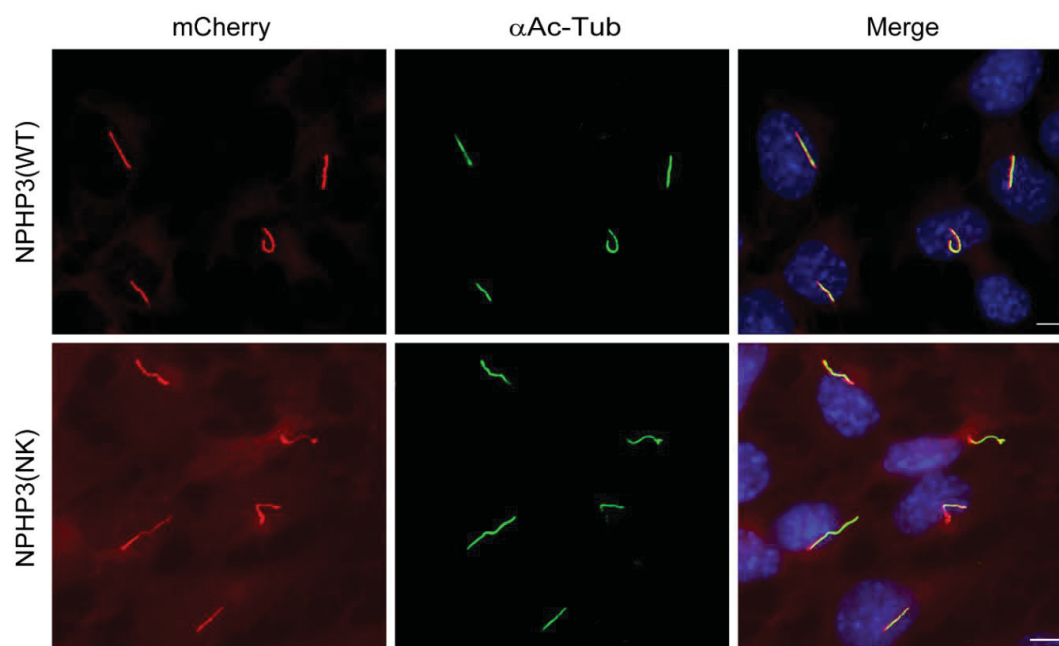
These were the main conclusions from this publication

- INPP5E localizes to cilia of IMCD3 cells, whereas Rheb localizes to endomembranes.
- The ciliary localization of INPP5E depends on PDE6 δ and on Arl3.
- The affinity towards PDE6 δ determines the sorting of farnesylated cargo: High affinity cargo such as INPP5E localizes to cilia, where it is released by Arl3•GTP, whereas low affinity cargo localizes to other inner membranes, where it is released by Arl2•GTP.
- The -1 and -3 positions relative to the farnesylated cysteine of INPP5E, which are the main determinants of the high affinity to PDE6 δ , are suggested as ciliary sorting signals.

4 Publication III

Novel biochemical and structural insights into the interaction of myristoylated cargo with Unc119 protein and their release by Arl2/3

Mamta Jaiswal*, Eyad K. Fansa*, **Stefanie K. Kösling**, Tom Mejuch, Herbert Waldmann, and Alfred Wittinghofer (2016). *The Journal of Biological Chemistry* 291(39), 20766-20778.
(* Co-first authors)



These were the questions to be answered by this publication

- Unc119a/b and PDE6 δ are homologs and shuttle lipidated proteins to different membrane compartments - Is there a similar sorting principle of myristoylated cargo of Unc119a/b as it was shown for the sorting of farnesylated PDE6 δ cargo?
- What determines the sorting of myristoylated NPHP3 to primary cilia and which role do Unc119a/b play?

Contribution of 20 %

- Plasmid generation and mutagenesis for transfection of IMCD3 cells.
- Cell cultivation, generation of stable mCherry cell lines (NPHP3(1-203/WT), NPHP3(NK)), validation by western blotting.
- Cell fixation, IF staining, fluorescence microscopy of the cell lines above, image processing.
- Quantification of the fold of ciliary enrichment of NPHP3(WT) and NPHP3(NK).
- Writing of the methods section in the manuscript regarding IMCD3 cell experiments.

Declaration: Reprinted (adapted) with permission from The Journal of Biological Chemistry
Copyright © 2016, American Society for Biochemistry and Molecular Biology
DOI: 10.1074/jbc.M116.741827

Novel Biochemical and Structural Insights into the Interaction of Myristoylated Cargo with Unc119 Protein and Their Release by Arl2/3*

Received for publication, June 6, 2016, and in revised form, July 29, 2016. Published, JBC Papers in Press, August 1, 2016, DOI 10.1074/jbc.M116.741827

Mamta Jaiswal^{†1}, Eyad K. Fansa^{†1}, Stefanie K. Kösling[‡], Tom Mejuch[§], Herbert Waldmann[§], and Alfred Wittinghofer^{†2}

From the [†]Structural Biology Group and the [§]Department of Chemical Biology, Max Planck Institute of Molecular Physiology, Otto-Hahn-Strasse 11, 44227 Dortmund, Germany

Primary cilia are highly specialized small antenna-like cellular protrusions that extend from the cell surface of many eukaryotic cell types. The protein content inside cilia and cytoplasm is very different, but details of the sorting process are not understood for most ciliary proteins. Recently, we have shown that prenylated proteins are sorted according to their affinity to the carrier protein PDE6 δ and the ability of Arl3 but not Arl2 to release high affinity cargo inside the cilia (Fansa, E. K., Kösling, S. K., Zent, E., Wittinghofer, A., and Ismail, S. (2016) *Nat. Commun.* 7, 11366). Here we address the question whether a similar principle governs the transport of myristoylated cargo by the carrier proteins Unc119a and Unc119b. We thus analyzed the binding strength of N-terminal myristoylated cargo peptides (GNAT1, NPHP3, Cystin1, RP2, and Src) to Unc119a and Unc119b proteins. The affinity between myristoylated cargo and carrier protein, Unc119, varies between subnanomolar and micromolar. Peptides derived from ciliary localizing proteins (GNAT1, NPHP3, and Cystin1) bind with high affinity to Unc119 proteins, whereas a peptide derived from a non-ciliary localizing protein (Src) has low affinity. The peptide with intermediate affinity (RP2) is localized at the ciliary transition zone as a gate keeper. We show that the low affinity peptides are released by both Arl2-GppNHp and Arl3-GppNHp, whereas the high affinity peptides are exclusively released by only Arl3-GppNHp. Determination of the x-ray structure of myristoylated NPHP3 peptide in complex with Unc119a reveals the molecular details of high affinity binding and suggests the importance of the residues at the +2 and +3 positions relative to the myristoylated glycine for high and low affinities. The mutational analysis of swapping the residues at the +2 and +3 positions between high and low affinity peptides results in reversing their affinities for Unc119a and leads to a partial mislocalization of a low affinity mutant of NPHP3.

The existence of cilia in higher organisms was discovered a century ago, but research to explore the functional importance

of cilia has only recently intensified. Cilia are highly specialized small antenna-like cellular protrusions that extend from the cell surface of almost all eukaryotic cell types. Primary cilia as sensory organelles are important for many cellular functions. They work as control centers of developmental signaling pathways, such as Hedgehog, or the induction of left-right asymmetry (2–4). Ciliary dysfunction leads to a range of diseases like Meckel-Gruber syndrome, Joubert syndrome, Bardet-Biedl syndrome, nephronophthisis, and polycystic kidney disease, which are commonly identified as ciliopathies (5).

Although the ciliary membrane is the extension of plasma membrane, the lipid composition is different from that of the plasma membrane (6). The composition and concentrations of proteins inside this compartment are also very different from the entire cell (7). A membrane barrier between cilia and the rest of the cell formed by a septin ring has been postulated such that the entry of transmembrane and membrane-associated proteins is tightly regulated (8–10). This renders the ciliary membrane a very specialized compartment of the cell, which orchestrates proteins to achieve spatially controlled signaling pathways. However, the regulation of entry into and retention inside cilia and signals for such processes are still incompletely understood. It has been proposed that partition of proteins between cilium and cell body is directed by steric hindrance and/or cytoskeletal structures (11) or binding affinities between proteins and cytoplasmic elements (12).

We and others have previously shown that proteins with a C-terminal CaaX box motif, which are post-translationally modified with a farnesyl or geranylgeranyl moiety, are transported via the δ subunit of phosphodiesterase 6 (PDE6 δ) (1, 13–15). PDE6 δ is a structural homologue to RhoGDI. It forms a β -sandwich fold with a deep hydrophobic pocket, which binds the prenylated cysteine and the adjacent three amino acid residues, two of which determine the affinity of the interaction. We have shown recently that the sorting of cargo between cilia and the rest of the cell depends on the affinity between cargo and PDE6 δ , such that cargo with high affinity is destined for cilia, whereas low affinity cargo stays in the rest of the cell or is no longer exclusively retained inside the cilium (1).

Unc119a (uncoordinated), also known as HRG4 (human retina gene 4) and Unc119b share 58% sequence identity and are homologous to PDE6 δ . The C termini of Unc119a/b share the PDE δ -like β -sandwich domain, whereas they are considerably

* This work was supported by European Research Council (ERC) Grant 268782 and Sonderforschungsbereich-DFG Grant SFB 642. The authors declare that they have no conflicts of interest with the contents of this article. The atomic coordinates and structure factors (code 5L7K) have been deposited in the Protein Data Bank (<http://www.pdb.org/>).

[†] Both authors contributed equally to this work.

² To whom correspondence should be addressed. Tel.: 49-231-133-2990; Fax: 49-231-133-2199; E-mail: alfred.wittinghofer@mpi-dortmund.mpg.de.

divergent in the N-terminal part. Unc119a has been shown to be localized at the basal body of the cilium, whereas the homologous Unc119b localizes to the transition zone and proximal cilium of RPE cells (16). Unc119a is also found in the eye and highly enriched in photoreceptor cells, in both rods and cones (17), supporting the notion that photoreceptors are considered as a specialized version of cilia (18–21). Unc119a has been shown to be expressed in eosinophils, T-cells, lung fibroblasts, adrenal glands, cerebellum, and kidney (22–25). Numerous studies have shown the involvement of Unc119a in the function of Src family kinases, Lyn, Fyn, Lck, and Hck, or as an inhibitor of Abl family tyrosine kinases, although the nature of such interactions had remained obscure (23–28).

N-terminal myristoylation of proteins facilitates their reversible membrane binding activity (29). The mechanism by which myristoylated proteins are recruited to the proper membrane of cellular organelles remains unclear. Unc119a/b have been shown to bind specifically to N-terminal myristoylated proteins (30), and biochemical studies have shown that Unc119a/b proteins are involved in binding and shuttling of N-myristoylated proteins (16, 30–32), suggesting that the early findings on the involvement of Unc119 in Src kinase function can be related to that observation. The determination of a structure between Unc119a and a lauroylated N-terminal peptide from the α subunit of transducin has shown that Unc119a forms a β -sandwich structure very similar to that of PDE6 δ (32, 33). Unc119a forms a hydrophobic pocket that accommodates a lipid moiety and a number of N-terminal residues of the peptide. Thus, like PDE6 δ , Unc119a/b work as a carrier of these post-translationally modified membrane-associated proteins. These proteins can also be considered chaperones that shield the lipid from the solvent (16, 32–34).

Previous studies have revealed a number of myristoylated proteins that interact with Unc119 (16, 31, 32). Binding of Unc119a/b to their interacting partners has been analyzed either qualitatively via yeast two-hybrid screening and *in vitro* pull-down assays or quantitatively through isothermal titration calorimetry (32) and polarization measurements (31). Previous studies have measured the affinities of either Unc119a or Unc119b with the N-terminal myristoylated peptides of GNAT1, NPHP3, and Src (16, 30–32). It has also been shown for Cystin1 and NPHP3 that the cargo is released from Unc119a only by Arl3-GTP and not Arl2-GTP (16, 31). Recently, we have shown that high affinity binding between farnesylated cargo INPP5E and PDE6 δ leads to INPP5E recruitment to the ciliary membrane, and its release from PDE6 δ by Arl3 exclusively in cilia, whereas low affinity binding between farnesylated Rheb and PDE6 δ results in Rheb localization to the cytosol (1).

Here we have set out to perform a comparative more comprehensive analysis of the interaction between Unc119a/b and different myristoylated proteins, the interaction with Arl2 and Arl3, and finally the release of cargo by Arl2 and Arl3. The myristoylated proteins analyzed in this study are NPHP3, Cystin1, GNAT1, RP2, and Src. We find different affinities of Unc119a/b for Arl2 and Arl3 and for cargo peptides and differences in cargo release by Arl2/3. By structure-guided mutational analysis, we show how the difference in affinities can be

manipulated between high and low affinity cargo. Our results suggest that similar to the transport of prenylated cargo into cilia, the import of myristoylated cargo might be determined by the cargo-carrier binding affinity and the cargo release specificity mediated by Arl2 and Arl3.

Results

Binding of N-terminal Myristoylated Peptides to Unc119a and Unc119b—Using fluorescence polarization, we measured the binding affinity of both Unc119a and Unc119b to N-terminal myristoylated peptides derived from transducin- α (GNAT1), NPHP3, Cystin1, RP2, and Src, which were labeled with fluorescein at the C terminus. Preliminary experiments had suggested that some of the affinities were too high to be reliably measured by equilibrium methods (data not shown; also see below). Thus, we used kinetic measurements via stopped flow instead to determine association and dissociation rate constants and obtain K_D (Fig. 1). Fig. 1A shows the association of 1 μ M fluorescein-labeled N-terminal myristoylated GNAT1 peptide with increasing concentrations of Unc119a. The association of the myristoylated GNAT1 peptide with Unc119a (0.2–20 μ M) leads to the increase in fluorescence polarization. Plotting of the observed rate constants (k_{obs}) against the concentration of Unc119a resulted in the determination of the association rate constant (k_{on}) of the reaction (Fig. 1B). The association rate constant (k_{on}) for Unc119a is 4.6 μ M⁻¹ s⁻¹ and is very similar to Unc119b (6.3 μ M⁻¹ s⁻¹) measured under the same conditions (Fig. 1B). Association rate measurements were also measured for the N-terminal myristoylated peptides from NPHP3, Cystin1, RP2, and Src under similar experimental conditions, and the association rate constants (k_{on}) obtained are shown as a bar diagram in Fig. 1C and numerically in Table 1. These values are very similar and range from 3.4 to 12 μ M⁻¹ s⁻¹. Association of myristoylated cargo is generally slightly faster for Unc119b than for Unc119a.

The dissociation rate constants were determined by incubating a complex of C-terminal fluorescein labeled N-terminal myristoylated peptides with Unc119a/b in the presence of a 100-fold excess of unlabeled peptides, as shown for the GNAT1 peptide (Fig. 1D). In contrast to k_{on} , the k_{off} values vary considerably among the different peptides over a 900-fold range from 0.0002 to 1.74 s⁻¹ (Fig. 1E and Table 1). NPHP3 and Cystin1 show the slowest release from Unc119a with 0.002 and 0.006 s⁻¹, whereas Src peptide has the fastest off rate close to 1 s⁻¹. The rate for RP2 is intermediate between very slow and very fast rates. The dissociation rate constants of Unc119a and -b for NPHP3, Cystin1, RP2, and Src are rather similar, but for GNAT1, there is a >10-fold difference between Unc119a and Unc119b, with k_{off} values of 0.0023 and 0.035 s⁻¹, respectively.

The equilibrium dissociation constants (K_D) for the complexes between Unc119a/b and myristoylated peptides were calculated as the ratio of k_{off}/k_{on} (Fig. 1F and Table 1). The data revealed three different categories of affinity: (i) the very tight binding with subnanomolar affinities for Cystin1 and NPHP3 and low nanomolar affinity for GNAT1, (ii) the intermediate binding affinity in the two-digit nanomolar range for RP2, and

N-terminal Myristoylated Cargo Interaction with Unc119a/b

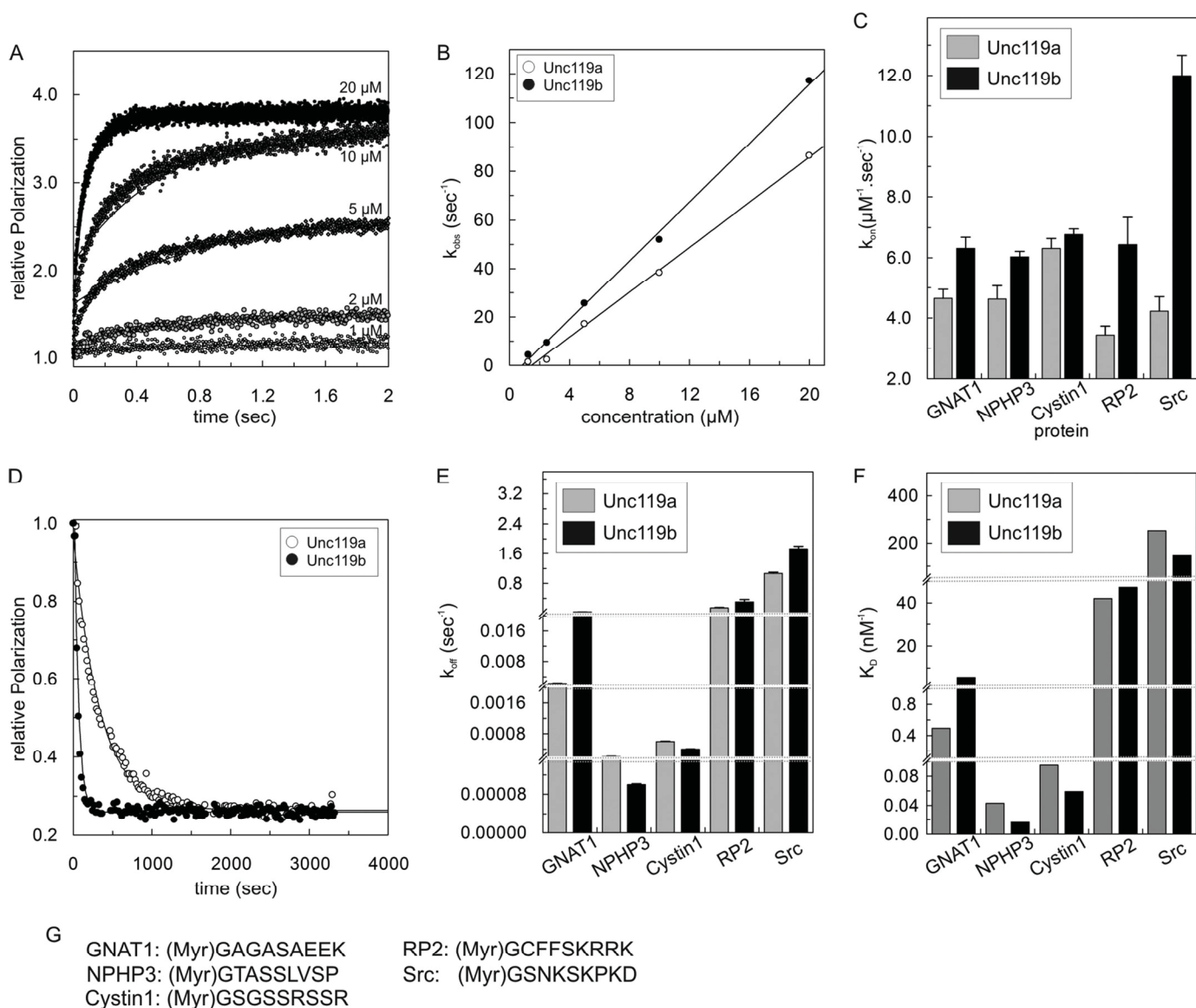


FIGURE 1. Interaction of Unc119a/b with N-terminal myristoylated peptides. *A*, kinetics of association between fluorescently labeled GNAT1 peptide (1 μ M) and different concentrations (1–20 μ M) of Unc119a. Rates were measured as change in fluorescence polarization using a stopped flow instrument. Reactions were carried out at 25 °C in buffer A. Observed rate constants (k_{obs}) of associations were obtained by single exponential fitting of individual curves. *B*, the observed association rate constants k_{obs} for interaction of Unc119a and Unc119b with N-terminal myristoylated cargo peptide (GNAT1) obtained as in *A* were plotted against the concentration of Unc119a and Unc119b. The association rate (k_{on}) is represented by the slope. The k_{on} values for all N-terminal myristoylated cargo peptides (GNAT1, NPHP3, Cystin1, RP2, and Src) are summarized in a bar diagram (*C*) and in Table 1. *D*, dissociation of cargo was measured at 25 °C in buffer A by monitoring the decrease of fluorescence polarization after incubating a complex of fluorescein labeled peptide with Unc119 (1 μ M) with a 100-fold excess (100 μ M) of unlabeled peptide. Dissociation rate constants (k_{off}) were obtained by single exponential fitting of the data. All k_{off} values are summarized in a bar diagram (*E*) and in Table 1. *F*, equilibrium dissociation constants (K_D) were calculated as ratios, k_{off}/k_{on} , and the values are plotted as a bar diagram and summarized in Table 1. *G*, the sequences of N-terminal myristoylated peptides used in this study. For labeled peptides, fluorescein fluorophore was attached at the C terminus of N-myristoylated peptides. All bar graphs show the average of 5–7 measurements for the experiments performed by stopped flow instruments and an average of three measurements for the experiments performed by the Fluoromax instrument. Error bars, S.D., for (*C*) $n = 5$ –7 and for (*E*) $n = 3$.

(iii) the low affinity in the submicromolar range for Src (145–252 nM) (Fig. 1*F* and Table 1). The affinities of Unc119a and Unc119b for myristoylated peptides are similar except for GNAT1, which shows >10-fold higher affinity for Unc119a as compared with Unc119b, exclusively due to the different dissociation rates. The affinities determined here by kinetics are different from those determined earlier by an equilibrium method (31). As indicated above, equilibrium binding assays are not quite suitable for such high affinities (picomolar or sub-nanomolar) because such affinity measurements by titration result

in straight lines that look like active site titrations and only give upper limits for the K_D .

Binding Affinity of Unc119a and Unc119b to Arl Proteins— We have shown previously that Unc119a and PDE6 δ bind to Arl2/3 with high affinity (1, 35, 36). We showed that the binding affinities of Unc119a and PDE6 δ are 20–30-fold higher for Arl3 as compared with Arl2 (1, 36) because of the additional contribution by the N-terminal helix of Arl3 to the interaction. To verify whether the same holds true for Unc119b and to compare with Unc119a, we measured the kinetics of interaction using

TABLE 1

N terminus-myristoylated peptide binding properties for Unc119 proteins

Protein	GNAT1	NPHP3	Cystin1	RP2	Src
Association constants (k_{on}) of Unc119a/b for N terminus-myristoylated peptides ($s^{-1} \mu M^{-1}$)					
Unc119a	4.64	4.26	6.31	3.44	4.23
Unc119b	6.32	6.04	6.77	6.44	11.99
Dissociation rates (k_{off}) by 100× non-labeled peptide (s^{-1})					
Unc119a	0.0023	0.0002	0.0006	0.145	1.07
Unc119b	0.0364	0.0001	0.0004	0.304	1.74
Equilibrium dissociation constants (K_D) of Unc119a/b for N-terminal myristoylated peptides (nM)					
Unc119a	0.49	0.043	0.095	42.1	252.96
Unc119b	5.76	0.02	0.059	47.2	145.12
Dissociation rates (k_{off}) by 10× Arl3 in the presence of 100× non-labeled peptide (s^{-1})					
Unc119a	2.8	1.72	5.2	0.61	2.73
Unc119b	5.6	2.5	11.3	0.52	2.82
Dissociation rates (k_{off}) by 10× Arl2 in the presence of 100× non-labeled peptide (s^{-1})					
Unc119a	0.045	0.018	0.002	0.56	2.83
Unc119b	0.658	0.032	0.001	0.38	3.99

full-length Arl2/3 labeled with mant-GppNHp³ (fluorescent, non-hydrolyzable analog of GTP). The association rates with increasing concentrations of Unc119a and -b were measured with fluorescence polarization using a stopped flow instrument (Fig. 2). Association rate constants for Arl2/3-GppNHp were obtained as described above by plotting the observed rate constants of association against the concentration of Unc119a/b (Fig. 2A). The results are shown as a bar diagram in Fig. 2B and in numerical form in Table 2. The association rate constants (k_{on}) are on the order of $1-3 \mu M^{-1} s^{-1}$. The association rates are >3-fold higher for Arl3 than for Arl2 in the case of Unc119b, whereas it is only 2-fold in the case of Unc119a. Dissociation rates were measured by incubating the fluorescent complex of Unc119a/b and Arl2/3-mant-GppNHp with a 100-fold excess of unlabeled Arl2/3-GppNHp, as shown for Arl2 and Unc119a/b (Fig. 2, C and D). The dissociation rate constants (k_{off}) are shown as a bar diagram in Fig. 2E and numerically in Table 2. The dissociation rate constants (k_{off}) are slower for Arl3 than Arl2 for both Unc119a and Unc119b. The equilibrium dissociation constants for Unc119a/b toward full-length Arl2-GppNHp and Arl3-GppNHp were calculated as the ratio of k_{off}/k_{on} (Fig. 2F and Table 2). The kinetic data suggested the binding affinities of Arl3 toward both Unc119a and -b are higher as compared with Arl2. Whereas, the 14-fold difference in affinity between Arl3 and Arl2 toward Unc119a is mediated only by the dissociation rates, the difference for Unc119b is due to a combination of different association and dissociation rates.

Release of Myristoylated Cargo by Arl2/3 Proteins—The Arl-like small GTP-binding proteins Arl2 and Arl3 act as displacement factors for lipid-modified proteins bound to the GDI-like solubilizing factor PDE68 as well as to Unc119a/b (15, 31, 33, 34). Previously, it has been shown that Arl3, but not Arl2,

allosterically regulates the release of ciliary proteins from Unc119a/b (16, 31). We thus analyzed the specificity of Arl2- and Arl3-mediated release of the high and low affinity peptides analyzed above for both Unc119a and Unc119b (Fig. 3). Arl2-GppNHp or Arl3-GppNHp was added to the preformed complex of fluorescent peptides from GNAT1, NPHP3, Cystin1, RP2, and Src with Unc119a and Unc119b. The release of peptide from the complex is scored as a decrease in fluorescence polarization. Under the conditions used, Arl3-GppNHp was able to disrupt the complex of Unc119a with all five peptides (Fig. 3, A and C). In contrast, Arl2-GppNHp was only able to disrupt the complex of Unc119a with the low or intermediate affinity RP2 or Src peptides, whereas the high affinity GNAT1, Cystin1, and NPHP3 peptides were fully resistant to release by Arl2 under the conditions used (Fig. 3, B and D). The results were consistent with the previous studies, which used GNAT1 and NPHP3 bound to Unc119a (16, 31). When comparing Unc119a and -b, similar results were obtained for the specificity of Arl2 and Arl3 (Fig. 3, A and B versus C and D). These results indicate that the high affinity cargos GNAT1/NPHP3/Cystin1 are only released by Arl3-GppNHp, whereas Arl2-GppNHp can release only the low affinity cargo RP2 and Src. Myristoylated GNAT1 was partially released by Arl2-GppNHp when bound to Unc119b but not Unc119a, possibly due to the 10-fold affinity difference observed above (Fig. 3D).

Because these data were obtained under equilibrium conditions and are somewhat difficult to compare quantitatively, we determined the Arl2/3-GppNHp cargo release acceleration from Unc119a/b in the presence of excess unlabeled peptides. The effects of Arl3-GppNHp and Arl2-GppNHp on the dissociation rates were determined in the presence of a 100-fold excess of unlabeled peptides to silence the back-reaction and were measured as a decrease in polarization in a stopped flow instrument. The data for the release of GNAT1 peptide from either Unc119a or -b are shown in Fig. 4, A and B, respectively, and the dissociation rates for release of GNAT1, NPHP3, Cystin1, RP2, and Src are summarized in Table 1. The presence of Arl3 increases the off rates for high affinity peptides GNAT1 (2.8

³ The abbreviations used are: mant-GppNHp, 2'-[3-O-(N-methyl-anthraniloyl)-guanosine-5'-[(β,γ)-imidoditriphosphate, triethylammonium salt; GppNHp, 5'-guanylyl imidodiphosphate; PDB, Protein Data Bank; GAP, GTPase-activating protein; DMF, N,N-dimethylformamide; DCM, dichloromethane; DIPEA, diisopropylethylamine; HCTU, [O-(6-chloro-1H-benzotriazol-1-yl)-N,N,N',N'-tetramethyluronium hexafluorophosphate].

N-terminal Myristoylated Cargo Interaction with Unc119a/b

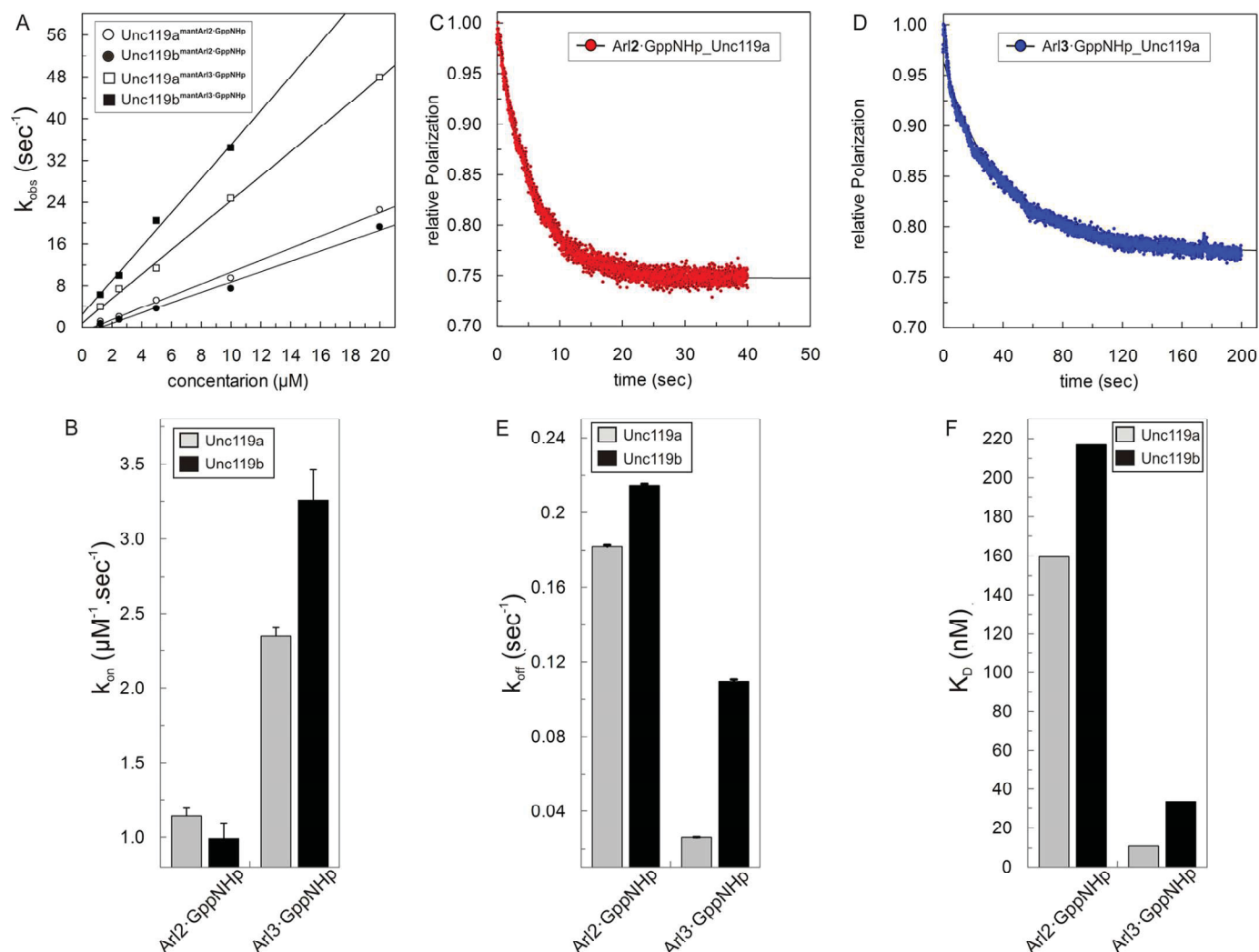


FIGURE 2. Interaction of Unc119a/b with Arl2/3. A, observed association rate constants between $0.5 \mu\text{M}$ mant-GppNHp-loaded Arl2 and Arl3 and different concentrations ($1\text{--}20 \mu\text{M}$) of Unc119a and Unc119b measured with fluorescence polarization using a stopped flow instrument as described in the legend to Fig. 1A at 25°C in buffer A. The association rate constants (k_{on}) of Unc119a (open circles/squares) and Unc119b (closed circles/squares) for Arl2-GppNHp (open/closed circles) and Arl3-GppNHp (open/closed squares) binding were calculated from the slope of the linear regression of the k_{obs} values plotted against the concentration of Unc119a and Unc119b proteins. All k_{on} values are plotted as a bar diagram (B) and appear in Table 2. C and D, the dissociations of full-length Arl2-GppNHp and Arl3-GppNHp from a complex with Unc119a/b ($0.5 \mu\text{M}$) at 25°C in buffer A were measured as decreases of fluorescence polarization after the addition of a 100-fold excess ($50 \mu\text{M}$) of unlabeled Arl2/3-GppNHp. E, observed dissociation rate constants (k_{off}) were obtained by single exponential fitting of the data. All k_{off} values are plotted as a bar diagram and summarized in Table 2. F, equilibrium dissociation constants (K_D) were calculated as ratios of k_{off}/k_{on} , and the values here are plotted as a bar diagram and appear in Table 2. All bar graphs show the average of 5–7 measurements for the experiments performed by stopped flow instruments and an average of three measurements for the experiments performed by the Fluoromax instrument. Error bars, S.D., $n = 5\text{--}7$.

TABLE 2
Arl2 and Arl3 binding properties for Unc119 proteins

	Unc119a	Unc119b
Association constants (k_{on}) ($\text{s}^{-1} \mu\text{M}^{-1}$)		
Arl2-GppNHp	1.14	0.99
Arl3-GppNHp	2.35	3.26
Dissociation rates (k_{off}) (s^{-1})		
Arl2-GppNHp	0.18	0.21
Arl3-GppNHp	0.026	0.11
Equilibrium dissociation constants (K_D) (nM)		
Arl2-GppNHp	159.36	216.82
Arl3-GppNHp	11.02	33.61

s^{-1}), NPHP3 (1.72 s^{-1}), and Cystin1 (5.2 s^{-1}) 1217-, 8600-, and 8667-fold, respectively, for Unc119a such that these rates are now very similar, on the order of $2\text{--}5 \text{ s}^{-1}$. There is a similar pattern of release from the Unc119b complex by Arl3; the only significant difference is the >2 -fold faster release for Cystin1,

which amounts to an almost 19,000-fold acceleration of the dissociation. The release rates for the intermediate affinity RP2 peptide (0.61 s^{-1}) and low affinity Src peptide (2.73 s^{-1}) are only marginally increased by Arl3-GppNHp, by 4.3- and 2.5-fold for RP2 and Src, respectively. The presence of Arl2-GppNHp has a much smaller effect on the release rates for high affinity peptides, which are increased 19-, 90-, and 3-fold for GNAT1, NPHP3, and Cystin1 peptides, respectively. There is no major difference between Unc119a and Unc119b complexes, except for GNAT1. The latter has a weaker affinity to Unc119b and is also much more effectively released, such that the dissociation in the presence of Arl2-GppNHp is 0.66 s^{-1} . The allosteric effect on the release of intermediate (RP2) and low (Src) affinity peptide is, however, very similar for both Arl3 and Arl2. In comparison, the dissociation rates of the high affinity peptides GNAT1, NPHP3, and Cystin1 are increased

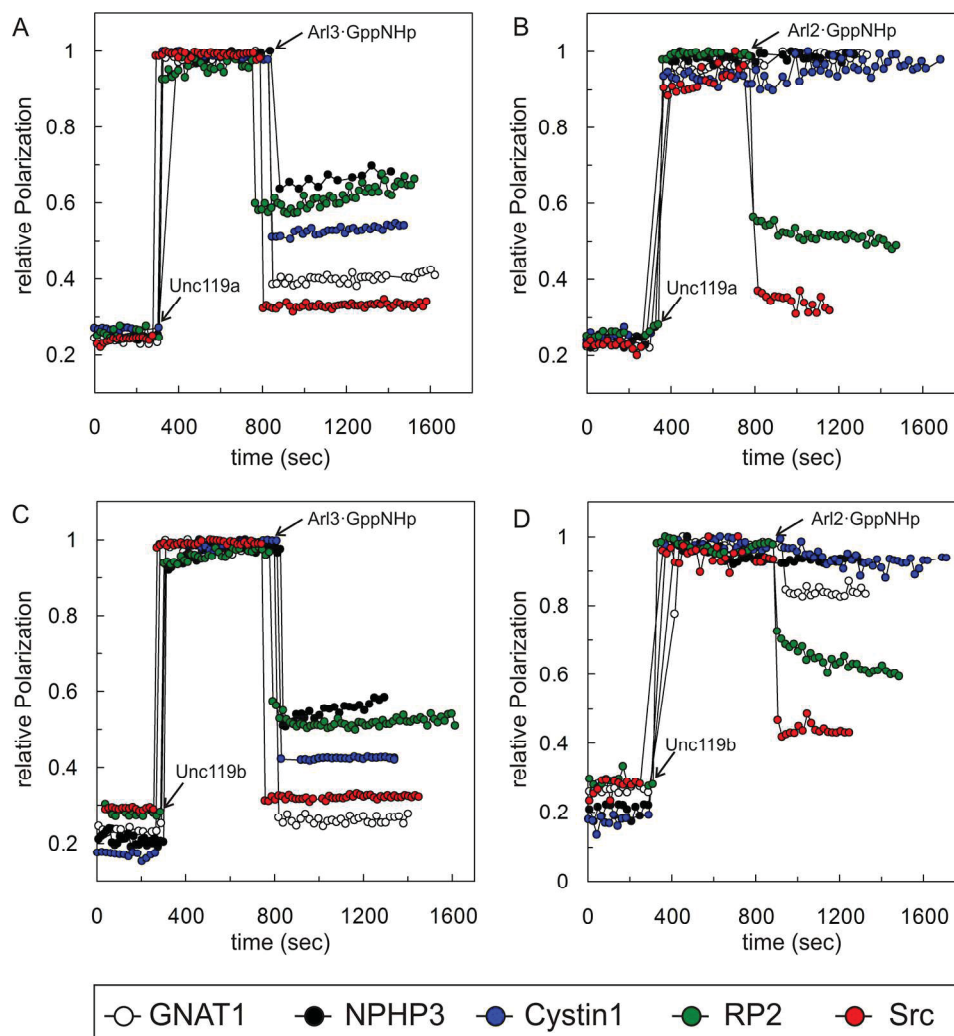


FIGURE 3. Cargo release from Unc119a/b by Arl2 and Arl3 proteins. The cargo release by Arl proteins was observed by fluorescence polarization at 25 °C in buffer A. 0.2 μ M Unc119a (A and B) or Unc119b (C and D) was added to a solution of 0.1 μ M fluorescein-labeled N-terminal myristoylated GNAT1 (open circles), NPHP3 (black, closed circles), Cystin1 (blue, closed circles), RP2 (green, closed circles), and Src (red, closed circles) peptides followed by the addition of a 10-fold excess (2 μ M) full-length Arl3-GppNHp (A and C) or Arl2-GppNHp (B and D). The addition time points are indicated by arrows. All experiments were repeated three times independently.

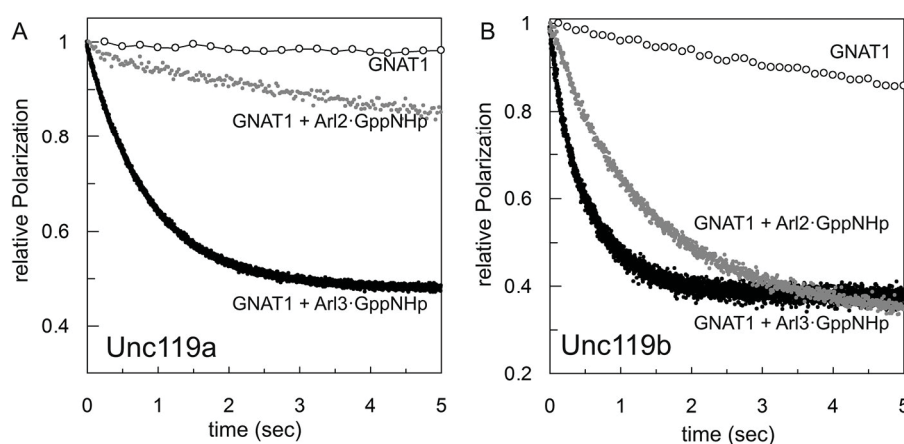


FIGURE 4. Dissociation rates of cargo from Unc119a/b in the presence and absence of Arl proteins. The dissociation rates of cargo release in the presence and absence of Arl proteins were measured by a stopped flow instrument in the fluorescence polarization mode at 25 °C in buffer A. 1 μ M preformed complex of Unc119a (A) or Unc119b (B) with fluorescein-labeled N-terminal myristoylated GNAT1 peptide was mixed with a 100-fold excess of unlabeled N-terminal myristoylated GNAT1 peptide in the presence or absence of a 10-fold excess of Arl2/3-GppNHp proteins as indicated. The kinetics of dissociation was monitored, and dissociation rate constants were calculated using first order rate equations. All bar graphs show the average of 5–7 measurements.

N-terminal Myristoylated Cargo Interaction with Unc119a/b

TABLE 3

Data collection and refinement statistics (molecular replacement)

Numbers in parentheses represent the highest resolution bin.

	Unc119a(58–240)·Myr-NPHP3 peptide (myrGTASSL)
Data collection	
Space group	$I4_1$
Cell dimensions	
a, b, c (Å)	82.27, 82.27, 105.94
α, β, γ (degrees)	90.00, 90.00, 90.00
Resolution (Å)	28.53–2.10
R_{sym} or R_{merge}	12.3 (74.6)
$I/\sigma I$	13.47 (3.38)
Completeness (%)	99.9 (100)
Redundancy	11.3 (13.6)
Refinement	
Resolution (Å)	2.10
No. of reflections	22,466
$R_{\text{work}}/R_{\text{free}}$	22.11/27.82
No. of atoms	
Protein	2425
Ligand/ion	118
Water	116
B-factors	
Protein	31.85
Ligand/ion	37.58
Water	41.47
Root mean square deviations	
Bond lengths (Å)	0.018
Bond angles (degrees)	1.925
PDB code	5L7K

10–20-fold by Arl2 but up to 1000–10,000-fold by Arl3. However, for intermediate RP2 or low affinity Src peptides, the dissociation rates are similarly increased 2–4-fold by both Arl2 and Arl3.

Crystallization and Structural Analysis of Unc119a-NPHP3 Complex—To gain molecular insights and to understand the nature of the binding affinity difference between low and high affinity myristoylated peptides toward Unc119a/b, we aimed to solve the crystal structure of peptides in complex with Unc119a or Unc119b. Using full-length Unc119a/b and myristoylated GNAT1, NPHP3, RP2, and Src peptides of 10-residue length, we did not obtain any suitable crystals. The sequence alignment of Unc119a and Unc119b reveals that they share 58% sequence identity. The N-terminal 50 residues of Unc119b are the most variable region. Because the first 57 residues of Unc119a do not have any effect on peptide binding (16, 33), we deleted these residues of Unc119a. However, the complex of the truncated Unc119a with peptides did not crystallize either. Finally, we used myristoylated peptides of 6-residue length and in addition added limited amounts of both trypsin and chymotrypsin to the crystallization setup. With this strategy, we were able to obtain crystals and solve the crystal structure of myristoylated NPHP3 peptide in complex with Unc119a at 2.1 Å resolution (data collection and refinement statistics summarized in Table 3). Trypsin and chymotrypsin protease were used for *in situ* proteolysis. The flexible loop of Unc119a, which is located at the entry of the myristoylated peptide, is cleaved by trypsin and chymotrypsin and apparently facilitates crystal packing. Superimposition of the NPHP3 peptide-Unc119a complex with the previously solved structure of Unc119a in complex with lauroylated GNAT1 peptide (PDB code 3RBQ) shows that the β -sandwich fold of Unc119a in both complexes superimposes well with a root mean square deviation of 0.9 Å (Fig. 5A, left). The myr-

istoyl moiety of NPHP3 inserts into the hydrophobic cavity of Unc119a in a very similar pattern as the lauroyl moiety of GNAT1. The two additional carbon atoms of the myristoyl moiety are suited inside the hydrophobic cavity by a higher level of ramification and slightly deeper insertion. Nevertheless, both moieties maintain an identical interaction pattern with the surrounding hydrophobic residues of Unc119a (Fig. 5A, left).

The myristoyl-glycine ester bond makes hydrophilic interactions with Tyr-131 and Glu-163 (Fig. 5A, right). As in the structure with the GNAT1 peptide, the first residues of NPHP3 also form helical turns. The interaction of the carbon chain with the pocket involves the hydrophobic residues Ile-93, Val-143, Phe-175, Tyr-194, Tyr-134, Phe-91, Phe-137, and Phe-196. Fig. 5B shows that the alanine and serine side chain of the NPHP3 peptide at positions +2 and +3 after the myristoylated glycine (the 0 position) are situated in a tightly structured environment. Comparing the equivalent +2 and +3 residues from the other peptides analyzed here, we observe that the high affinity Unc119 binders (GNAT1, NPHP3, and Cystin1) have small size side chain residues, such as alanine, serine, or glycine (Fig. 5B). In contrast, the low or intermediate affinity Unc119 binders (Src and RP2) possess residues with bigger side chains, such as lysine, phenylalanine, or glutamine. We thus hypothesized that the residues with bigger side chains at the +2 and +3 positions would create steric clashes with Unc119a, resulting in lower binding affinities, as found for Src and RP2.

Mutational Analysis of +2 and +3 Positions—To verify our model, we generated two 10-residue mutant peptides, where the residues in the +2 and +3 positions were swapped between high (NPHP3) and low (Src) affinity binders, creating NPHP3(NK) and Src(AS) peptides. The affinities of these swapped peptides toward Unc119a were measured by titrating increasing amounts of unlabeled NPHP3(NK) (Myr-GTNK-SLVSP) and Src(AS) (Myr-GSASSKPKD) peptides into a pre-formed complex of a fluorescent RP2 peptide (0.1 μM) with Unc119a (0.2 μM) and monitoring the displacement of the fluorescent peptide by the unlabeled ones, scored as the decrease of fluorescence polarization. The data were analyzed with a competition model equation derived from the law of mass action as described before (1, 37, 38), using Origin software. The affinity of NPHP3(NK) to Unc119a decreased to a K_D of 940 ± 48 nM, whereas the affinity of Src(AS) increased to a K_D value of 6.2 ± 1.8 nM (Fig. 5C). These results clearly show that increasing the size of the amino acid side chains at the positions +2 and +3 decreases the binding affinity with Unc119a, and vice versa. Taken together, the residues at the +2 and +3 positions relative to the myristoylated glycine seem to determine the binding affinity between Unc119a and cargo.

To test whether the reduced affinity of NPHP3(NK) affects its ciliary localization, we used a fragment of NPHP3 (residues 1–203) that is very similar to one described previously for its consistent ciliary localization (16). Constructs containing wild type NPHP3 and mutant NPHP3(NK) were stably transfected into IMCD3 cells, and the ciliary localization of the proteins was measured by quantifying and comparing the fluorescence inside and outside the cilium in ciliated cells. Fig. 6 shows that NPHP3(WT) is highly enriched in cilia compared with the

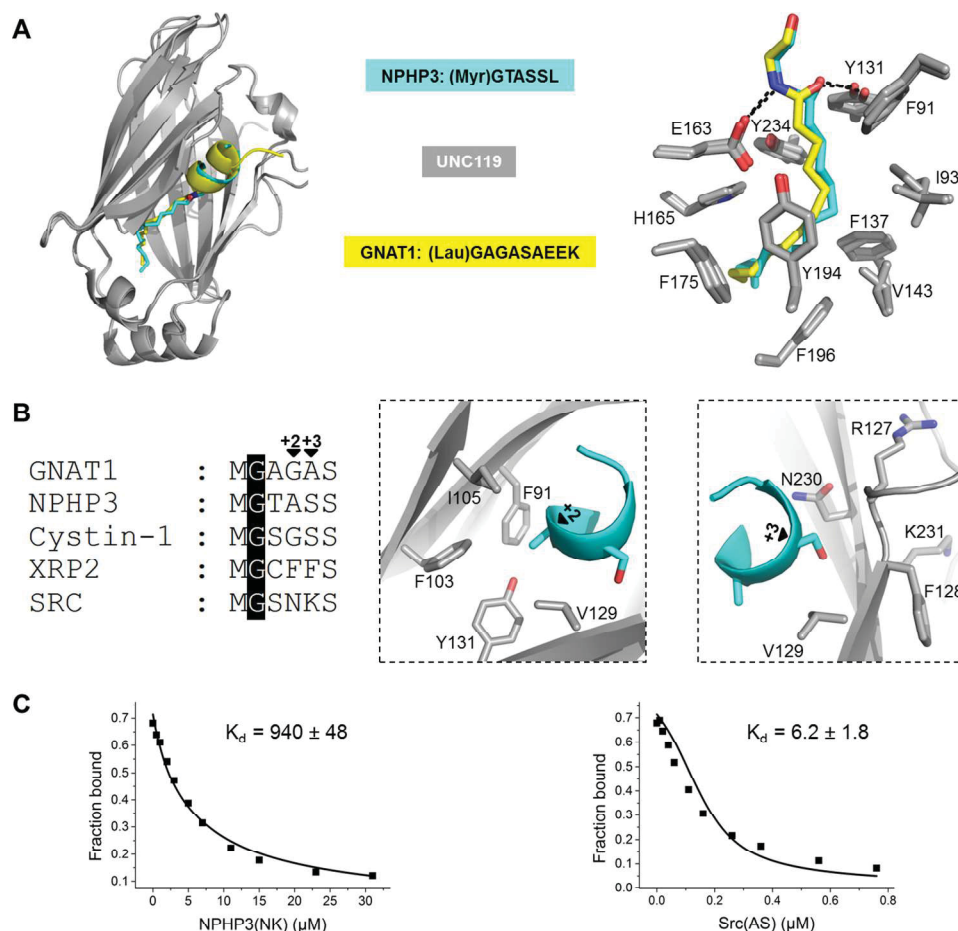


FIGURE 5. Structural analysis of a complex of Unc119a with myr-NPHP3. *A*, superimposition of the crystal structures of Unc119a-myristoylated NPHP3 and Unc119a-lauroyl-GNAT1 (PDB code 3RBQ) with the lauroyl group in yellow and myristoyl in blue (left). The right panel shows the Unc119a residues interacting with myristoylated NPHP3 and lauroylated GNAT1. *B*, sequence alignment of the N-terminal part of myristoylated proteins involved in this study (left). Residues of Unc119a around the +2 (middle) and +3 (right) positions of the myr-NPHP3 are shown. *C*, titration of a complex between 100 nM fluorescein-labeled RP2 peptide and 200 nM Unc119a with increasing concentration of NPHP3(NK) (left) and Src(AS) (right) mutant peptides leads to a decrease in fluorescence polarization. Titration data were fitted with a competition model.

cell body (Fig. 6A), whereas considerable amounts of the NPHP3(NK) mutant are localized to the rest of the cell (Fig. 6B). Quantification of the fluorescence intensity of mCherry-tagged protein was done using CellProfiler. The mean fluorescence intensity ratio between cilia and whole cell shows that the wild type protein has an 8.3-fold enrichment inside the cilia. The NPHP3(NK) mutant loses its almost exclusive ciliary localization and is more distributed over the entire cell, with only a 4.4-fold ciliary enrichment (Fig. 6C).

Discussion

Nephrocystin-3 (NPHP3) is a ciliopathy protein and localizes to primary cilia (39, 40). It has been shown to be a myristoylation-dependent binding partner of Unc119, and this myristoylation occurs at the conserved glycine at position 2 (16). Cystin1 is another cilia-associated protein (41) that has been shown to interact with Unc119 protein via myristoyl binding (16), and its N-terminal myristoylation is required for its proper ciliary membrane localization (42). Myristoylated transducin- α (GNAT1) also interacts with Unc119 protein (31, 32) and is localized in the outer segment of photoreceptor cells, a specialized form of primary cilia (43). Retinitis pigmentosa 2 (RP2) is the Arl3-specific GTPase-activating protein (GAP)

(44) that is mutated in X-linked retinitis pigmentosa (45, 46) and has been shown to be localized to the basal body or periciliary region (47, 48). Src kinases Lyn, Hck, and Src itself, non-ciliary proteins, are known to be myristoylated (34, 49), and their biology has been shown to be dependent on Unc119a/b (24–26, 28, 34, 50).

Our experiments reveal that ciliary cargo proteins NPHP3, Cystin1, and GNAT1 bind to Unc119a and Unc119b with picomolar to low nanomolar affinity, whereas the non-ciliary cargo Src has a submicromolar affinity. RP2, which has been shown to localize at the ciliary base, binds with an affinity in the 2-digit nanomolar range. As is typical for such binary interactions, the difference in affinity is mostly dictated by the dissociation rates, which differ between Unc119a and -b by a similar factor, whereas the association rates are very similar. There is no significant difference between Unc119a and -b for the binding affinities of myristoylated peptides except for GNAT1. Its interaction with Unc119a is 10-fold tighter and is determined by a 10-fold difference in the off-rate. Unc119a was originally found as a retina-specific gene named *HRG4*. It is highly expressed in photoreceptor cells, a specialized form of cilia, and the protein is reported to be localized in the inner segments and photore-

N-terminal Myristoylated Cargo Interaction with Unc119a/b

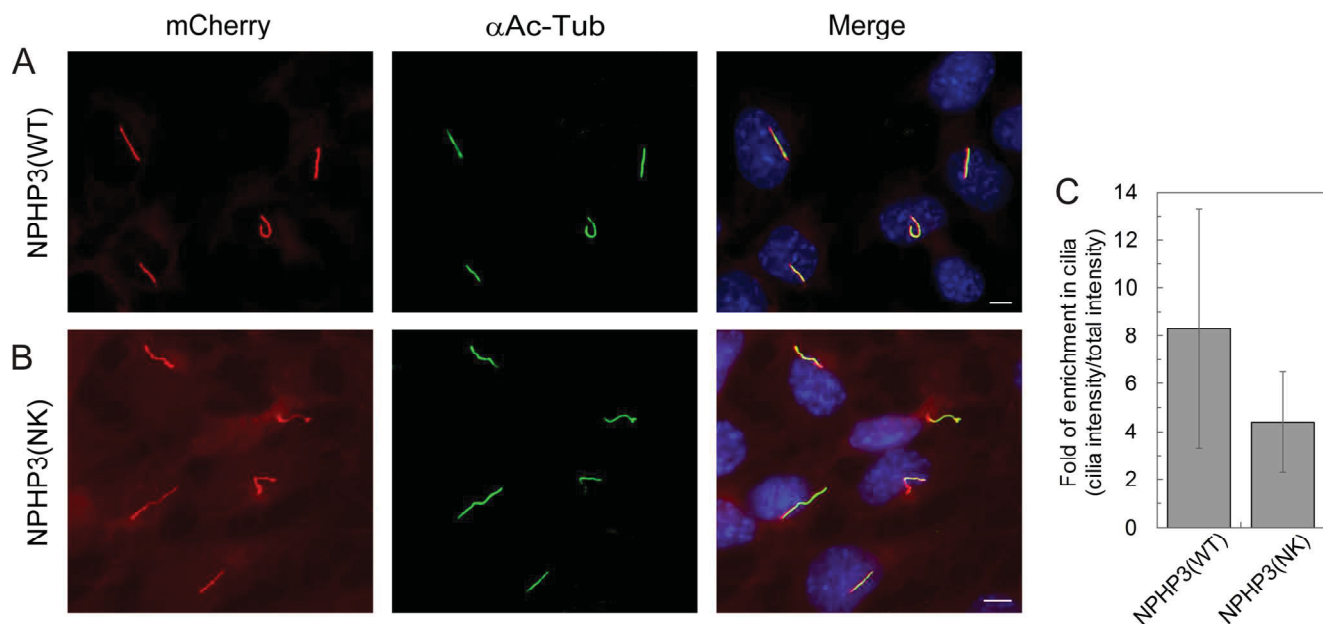


FIGURE 6. Localization of NPHP3(WT)-mCherry and NPHP3(NK)-mCherry in IMCD3 cells. A, mCherry fluorescence (LAP-tagged) (red) shows stably expressed NPHP3(WT)-mCherry almost exclusively localizing to primary cilia, which are immunostained with an antibody against acetylated tubulin (green). B, NPHP3(NK)-mCherry localizes both to primary cilia and to the rest of the cell. White bar, 5 μ m. C, ciliary enrichment of NPHP3(WT)-mCherry was compared with that of the NPHP3(NK) mutant. The bar graph shows the ratios of the mCherry fluorescence intensity in cilia relative to the total mCherry intensity outside the cilium. Ratios indicate the enrichment of mCherry-tagged NPHP3 inside the cilia. Data analysis of 40 ciliated cells each stably expressing wild type or mutant was accomplished using CellProfiler. Error bars, S.D., $n = 40$ ($p < 0.05$; Student's t test).

ceptor synapses (51). Our quantitative and comparative study for Unc119a/b binding to myristoylated cargo suggests that the binding affinity between cargo and Unc119a/b seems to be very important for the Unc119a/b-mediated sorting into the ciliary compartment. This is a scenario similar to what we have recently demonstrated for the sorting of prenylated cargo, such as INPP5E, into cilia (1). The cell biology experiments show the mislocalization of the mutant NPHP3 construct, which is no longer highly enriched in cilia but is now visible over the whole cell. We propose that this mislocalization results from its reduced affinity to Unc119 protein. The fact that the localization cannot be completely reversed by reducing the affinity argues for an additional retention signal operating inside cilia, something that has also been proposed for the localization of prenylated proteins (1).

Although Arl2 and Arl3 share several GTP-dependent interacting partners like the GDI-like solubilizing factors Unc119a, Unc119b, and PDE6 δ , in addition to BART and BARTL1 (52), their cellular functions are distinct. Our data show that high affinity myristoylated cargoes (GNAT1, NPHP3, and Cystin1) bound to Unc119a/b are specifically released only by Arl3, whereas lower affinity cargo is released by both Arl2 and Arl3. One exception is GNAT1, which can be partially released from its complex with Unc119b but not with Unc119a by Arl2, possibly due to the 10-fold lower affinity of GNAT1 to Unc119b as compared with Unc119a. We have previously shown that the Arl3-specific GEF Arl13B (53) is exclusively localized inside cilia, whereas RP2, the Arl3-specific GAP (44), localizes to the base of cilia and the periciliary region (47, 48, 52), thus making cilia an Arl3-GTP-enriched compartment. This suggests that Arl3 can release NPHP3 and Cystin1 cargo only inside the cilia and GNAT1 in the outer segment of photo-

receptors, whereas Arl2 is capable of releasing intermediate affinity (RP2) and low affinity cargo (Src) outside cilia. Our data support the notion that (i) Unc119a/b proteins regulate the trafficking of myristoylated transducin α subunit (GNAT1), NPHP3, and Cystin1 into the cilia, and (ii) Arl2/3 proteins regulate the sorting of myristoylated cargo into the cilia. The fact that the affinities of Unc119 for its ciliary myristoylated cargo are higher than for Arl3 suggests a very high concentration of activated Arl3 inside the cilium and/or that, in addition to the release mechanism by Arl3, a retention signal for cargo proteins must be in operation to drive the equilibrium toward full release. Such retention could be achieved by the interaction with the ciliary membrane or other ciliary interacting partners.

Unc119a has been shown to localize to the centrosome at the ciliary base, whereas Unc119b localizes to the transition zone and proximal cilium of RPE cells (16). Unc119a and Unc119b proteins share a 58% identity. The sequence comparison of Unc119a and -b shows that the N terminus (residues 1–55) is the most variable region and is not involved in the binding to myristoylated proteins. However, the N terminus might be important and responsible for the different localization of the orthologues. The crystal structure revealed that Unc119a forms a hydrophobic pocket to accommodate the myristoyl moiety that is formed by the residues Phe-91, Ile-93, Tyr-131, Phe-137, Val-143, Glu-163, His-165, Phe-175, Tyr-194, Phe-196, and Tyr-234 of Unc119a (Fig. 5A). The sequence comparison between Unc119a and -b shows that these residues are conserved in Unc119b (Fig. 7), suggesting a similar mode of interaction between Unc119a/b and myristoylated cargo.

N-terminal Myristoylated Cargo Interaction with Unc119a/b

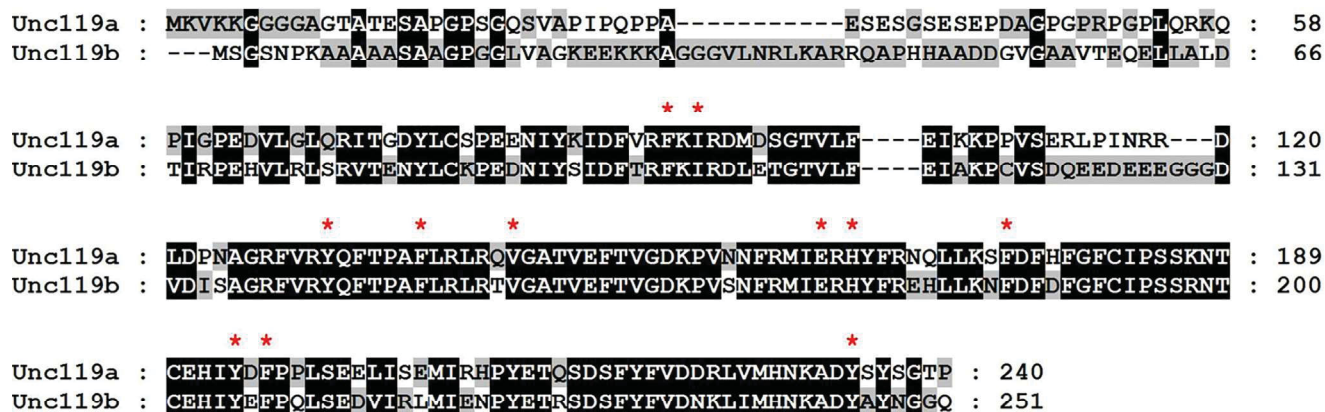


FIGURE 7. **Sequence comparison of Unc119 isoforms.** Sequence alignment of Unc119 isoforms Unc119a and Unc119b was generated by using ClustalW program. The residues involved in the interaction of Unc119a and the myristoyl moiety are marked by an asterisk and are conserved between Unc119a and -b.

Experimental Procedures

Plasmids and Proteins—Constructs of full-length human Unc119a and Unc119b were cloned into the pGEX-4T3 and pET28a vectors containing an N-terminal GST and His₆ tag, respectively. The construct of Unc119a(58–240) in pGEX-2T we received as a gift from the laboratory of Prof. Baehr and was later recloned in pET28 vector. The C-terminal His₆ tag full-length constructs of Arl2 and Arl3 in pET20b vector were already available in the laboratory. All proteins were expressed as GST or His₆ fusion proteins from *Escherichia coli* BL21(DE3) CodonPlusRIL, isolated in a first step by affinity chromatography on a glutathione-Sepharose and Talon column respectively, and purified after proteolytic cleavage of GST in a second step by size exclusion chromatography (Superdex S75), as described before (35, 44, 54). After purification, both Arl2 and Arl3 full-length proteins were bound to GDP, as detected via HPLC. The exchange for the GTP analog GppNHP and to mant fluorophore-labeled mant-GppNHP was done as described before (35, 54). The amount of protein-bound nucleotide was analyzed and quantified by C18 reversed-phase column with HPLC.

Plasmids for Cell Culture—Plasmids for transfection of IMCD3 Flp-In cells were created using Gateway cloning technology (Life Technologies), following the manufacturer's recommendations. Full-length human NPHP3 was amplified by PCR from a human Wi38 cDNA library, using the following primers: 5'-GAGAGCTAGCGCCGGTCCGATGGGGACCGCCTCGTCGCTCG-3' (forward) and 5'-GAGTGTGCGACTACCTTTGTCCTTGCTGAAGG-3' (reverse). It was located to a modified pACEBac1 vector (ATG Biosynthetics) by restriction enzyme cloning and used as a template for the Gateway entry clone. The entry clone was obtained by PCR using the primers 5'-ATGGGGACCGCCTCGTCGCTCGTG-3' (forward) and 5'-CCTTTGTCCTTGCTGAAGGAAAAC-3' (reverse), and the PCR fragment was integrated into the pCR8/GW/TOPO vector (Life Technologies) and located to a pG-LAP5 destination vector (Addgene) (55) by LR recombination. The pG-LAP5 vector originally encoded a LAP tag (S-peptide-PreScission site-GFP) C-terminal to the gene of interest where the region encoding GFP was exchanged against mCherry by restriction enzyme cloning. The C-terminal truncated con-

struct NPHP3(1–203) (NPHP3(WT)) was generated using NPHP3-pG-LAP5-mCherry as a template and the following primers: 5'-ATGGGGACCGCCTCGTCGCTCGTG-3' (forward) and 5'-CTGAGCCTGTAGCCTCTGAAGTTTGC-3' (reverse). Mutant NPHP3(1–203) A4N/S5K (NPHP3(NK)) was created using NPHP3(1–203) (WT)-pG-LAP5-mCherry as template and the following mutagenesis primer: 5'-CCG-AATTCGCCCTTATGGGGACCAACAAGTCGCTCGTGAGCCCCGCGG-3' (forward).

Peptides—The N-terminal myristoylated peptides GNAT1 (Myr-GAGASAEK) and NPHP3 (Myr-GTASSLVSP), unlabeled and labeled with fluorescein at the C terminus, were obtained from AltaBioscience. C-terminal fluorescein-labeled and -unlabeled N-terminal myristoylated Cystin1 (Myr-GSGSSRSSR), NPHP3(NK) (Myr-GTNKSLVSP), and Src(AS) (Myr-GSASSKPKD) were obtained by CambridgePeptides. The C-terminal fluorescein-labeled and unlabeled N-terminal myristoylated RP2 (Myr-GCFFSKRRK) and Src peptides (Myr-GSNKSKPKD) were prepared as described below.

For crystallization, 6-amino acid length N-terminal myristoylated peptides of GNAT1 (Myr-GAGASA), NPHP3 (Myr-GTASSL), Cystin1 (Myr-GSGSSR), RP2 (Myr-GCFFSK), and Src (Myr-GSNKSK) were obtained from Cambridge Peptides.

Synthesis of the Peptides—Solid phase peptide synthesis was carried out on a 0.1-mmol scale using a CEM-Liberty peptide synthesizer equipped with a CEM-Discover microwave. Washing steps between coupling and deprotection were carried out in DMF and DCM using 1 ml of solvent per 100 mg of resin. The Fmoc protecting group was removed with a solution of piperidine in DMF (20%, v/v), 1 min at 30 °C (intensity = 40 watts), and 5 min at 70 °C (intensity = 40 watts). All amino acid couplings were performed in DMF and repeated twice. Typically, Fmoc-Xaa-OH (4 eq, 0.2 M), HCTU (4 eq), and DIPEA (8 eq) were reacted for 10 min at 80 °C (intensity = 20 watts). Upon the completion of the automated synthetic cycles, the resin was washed with DCM (5 ml × 5), DMF (5 ml × 5), and DCM (5 ml × 5). The C-terminal allyl group was removed with a mixture of Pd(PPh₃)₄ (20 mol %), PhSiH₃ (14 eq) in dry THF (3 ml for 0.1 mmol of peptide on the resin) under an argon atmosphere for 12 h to deprotect them. Upon the completion of the reaction, the resin was filtered under vacuum and washed with

N-terminal Myristoylated Cargo Interaction with Unc119a/b

dry THF (5 ml \times 5), DCM (5 ml \times 5), DMF (5 ml \times 5), and DCM (5 ml \times 5). Fmoc-(PEG3)-NH₂ (4 eq with regard to the resin loading) was dissolved in dry DMF (0.2 M). [O-(6-chloro-1*H*-benzotriazol-1-yl)-*N,N,N',N'*-tetramethyluronium hexafluorophosphate] (HCTU) (4 eq) and diisopropylethylamine (DIPEA) (8 eq) were subsequently added, and the resulting mixture was shaken for 5 min. The peptide-containing resin was shaken with the reaction mixture for 4 h at the ambient temperature. The resin was filtered under vacuum and washed with DCM (5 ml \times 5), DMF (5 ml \times 5), and DCM (5 ml \times 5). The coupling and the washing step were repeated twice. The Fmoc group was removed by shaking the resin with piperidine (20% in DMF, 5 ml) for 40 min at the ambient temperature twice. The resin was washed with DMF (5 ml \times 5). Fluorescein isothiocyanate (5 eq) and DIPEA (5 eq) were dissolved in dry DMF (0.2 M), and the resin was shaken with the mixture for 4 h at the ambient temperature. The resin was washed with DCM (5 ml \times 5), DMF (5 ml \times 5) and DCM (5 ml \times 5). The coupling and the washing steps were repeated twice. The peptides were fully deprotected and cleaved from the resin with 5 ml of the mixture of DCM/TFA/TES (50:25:25). The resin was shaken with the deprotection mixture for 2 h and filtered into a round bottom flask. The resin was washed with DCM (5 ml \times 3), DCM/MeOH (1:1, 5 ml \times 3), and MeOH (5 ml \times 3). The combined liquids were diluted with toluene (10 ml) and concentrated under reduced pressure. The resulting slurry was diluted again in toluene (10 ml) and co-evaporated again. The co-evaporation was repeated three times. The resulting crude products were purified by preparative HPLC using a C4 column and characterized by HRMS. The purity of the peptides exceeded 95%.

Fluorescence Measurements—All fluorescence polarization measurements were performed in buffer containing 30 mM HEPES, pH 7.5, 5 mM MgCl₂, 100 mM NaCl, and 3 mM DTE (buffer A) at 20 °C. The kinetic measurements were performed with a stopped flow instrument (Applied Photophysics, Leatherhead, UK) in the polarization mode, and fluorescence polarization experiments were performed with a Fluoromax-2 spectrophotometer instrument (Horiba Jobin Yvon, Munich, Germany). The excitation wavelengths were 366 nm for mant and 490 nm for fluorescein fluorophore, whereas the emission wavelengths used for mant and fluorescein fluorophore were 450 and 520 nm, respectively. Emission in stopped flow was detected through a cut-off filter (Schott glass) of 420 and 500 nm for mant and fluorescein, respectively. Data were analyzed using GraFit version 5.0 (Erithacus Software).

Crystallization and Structure Determination—The myristoylated N-terminal peptide of NPHP3 (Myr-GTASSL) was dissolved in 100% DMSO to make 50 mM stock solution. 500 μ M solution of Unc119a(58–240) was mixed with N-terminal myristoylated NPHP3 peptide at a 1:1 molar ratio in a buffer containing 25 mM Tris-HCl (pH 7.5), 150 mM NaCl and 3 mM DTE. *In situ* proteolysis was applied prior to the screening at 20 °C by the addition of both proteases, trypsin and chymotrypsin (at a 1:1000 (w/w) ratio each), as described before (56). The crystals appeared in several conditions containing ammonium sulfate. The final crystallization condition that was optimized was 1.75 M (NH₄)₂SO₄, 0.1 M CAPS (pH 10.0), and 0.2 M Li₂SO₄. Cryoprotectant solution containing the mother liquor in addition to

20% (v/v) glycerol was used for flash freezing the crystals. X-ray diffraction data were collected at the X10SA beamline of the Suisse Light Source, Villigen. Data were processed by the XDS program. Molecular replacement was carried out using Molrep from the CCP4 suite and Unc119a from the Unc119a-N-terminal lauroylated transducin- α -mimicking peptide complex (PDB code 3RBQ) used as a search model. The model was further built by WinCoot, and the refinement was done with REFMAC5. Refinement and data collection statistics are summarized in Table 3.

Cell Culture and Generation of Stable Cell Lines—Mouse renal epithelial cells from the inner medullary collecting duct (IMCD3) were cultured at 37 °C and 5% CO₂ in DMEM/F-12, HEPES complemented with 10% fetal bovine serum and 2 mM L-Glutamine (Life Technologies). The genome of the IMCD3 cells contained a stably integrated FRT cassette (IMCD3 FLP-In, a kind gift from M. V. Nachury; FLP-In cell line technology by Life Technologies), which enabled the generation of stable cell lines as described previously (55, 57). Briefly, IMCD3 FLP-In cells were seeded in 6-well plates at a density of 100,000 cells/well. On the next day, the cells reached a confluence of 40–60% and were cotransfected with the following two vectors: (i) the modified pG-LAP5-mCherry vector containing the gene of interest, a flippase recognition target site, and a hygromycin resistance gene and, (ii) the pOG44 vector (Life Technologies) encoding the FLP recombinase. Transfection was accomplished using Lipofectamine 2000 (Life Technologies). Beginning 2 days after transfection, cells were selected with 100–200 mg/ml hygromycin in the complemented culture medium. Expression of the respective mCherry-tagged proteins was verified by immunoblotting with an antibody against mCherry (1:2000; MPI-CBG antibody facility).

Immunostaining and Microscopy—IMCD3 FLP-In cells stably expressing the respective mCherry-tagged protein were plated on poly-L-lysine-coated coverslips in 6-well plates. Each well contained 100,000 cells. On the following day, cilia were induced by serum starvation for 48 h. After washing in PBS, cells were fixed with 4% formaldehyde in cytoskeletal buffer (2.75 M NaCl, 100 mM KCl, 25 mM Na₂HPO₄, 8 mM KH₂PO₄, 40 mM MgCl₂, 40 mM EGTA, 100 mM PIPES, 100 mM glucose, pH 6.0) for 20 min. Cells were washed twice in PBS and permeabilized with 0.3% Triton X-100 in cytoskeletal buffer for 10 min. After rinsing in 0.1% Tween 20 in PBS, cells were incubated in 10% FBS in PBS for 30 min for blocking. To immunostain primary cilia, mouse 6-11B-1 anti-acetylated tubulin antibody (1:5000; Sigma T6793) in 10% FBS in PBS was incubated overnight at 4 °C. After washing four times with 0.1% Tween 20 in PBS, Alexa Fluor 488 anti-mouse secondary antibody (1:800; Life Technologies A-11001) was added for 45 min at room temperature. Coverslips were rinsed three times in 0.1% Tween 20 in PBS and once in PBS. Nuclei were stained with DAPI (Serva) for 1 min, diluted 1:10,000 in PBS. Cells were washed three times in PBS, and the coverslips were fixed on glass slides using Mowiol (Merck). Images were taken using an Olympus IX81 microscope with a CCD camera and a 60 \times oil immersion objective with a numerical aperture of 1.35 using identical settings for each image to ensure comparability.

Author Contributions—M. J., E. K. F., and A. W. designed the experiments and wrote the manuscript. M. J., E. K. F., S. K. K., and T. M. performed the experiments. H. W. critically reviewed the manuscript. All authors read and approved the manuscript.

Acknowledgments—We thank C. Koerner for cloning the *Unc119b* construct and J. A. Seidel, M. Lokaj, and K. Gotthardt for helping in generating the plasmids used for the generation of stable cell lines. We are also very thankful to Prof. Wolfgang Baehr and Prof. M. V. Nachury for providing the *Unc119a* plasmid and *IMCD3 Flp-In* system, respectively.

References

- Fansa, E. K., Kösling, S. K., Zent, E., Wittinghofer, A., and Ismail, S. (2016) PDE6delta-mediated sorting of INPP5E into the cilium is determined by cargo-carrier affinity. *Nat. Commun.* **7**, 11366
- Veland, I. R., Awan, A., Pedersen, L. B., Yoder, B. K., and Christensen, S. T. (2009) Primary cilia and signaling pathways in mammalian development, health and disease. *Nephron Physiol.* **111**, p39–p53
- Corbit, K. C., Shyer, A. E., Dowdle, W. E., Gaulden, J., Singla, V., Chen, M. H., Chuang, P. T., and Reiter, J. F. (2008) Kif3a constrains β -catenin-dependent Wnt signalling through dual ciliary and non-ciliary mechanisms. *Nat. Cell Biol.* **10**, 70–76
- Berbari, N. F., O'Connor, A. K., Haycraft, C. J., and Yoder, B. K. (2009) The primary cilium as a complex signaling center. *Curr. Biol.* **19**, R526–R535
- Waters, A. M., and Beales, P. L. (2011) Ciliopathies: an expanding disease spectrum. *Pediatr. Nephrol.* **26**, 1039–1056
- Tyler, K. M., Fridberg, A., Toriello, K. M., Olson, C. L., Cieslak, J. A., Hazlett, T. L., and Engman, D. M. (2009) Flagellar membrane localization via association with lipid rafts. *J. Cell Sci.* **122**, 859–866
- Nachury, M. V. (2014) How do cilia organize signalling cascades? *Philos. Trans. R. Soc. Lond. B Biol. Sci.* 10.1098/rstb.2013.0465
- Hu, Q., Milenkovic, L., Jin, H., Scott, M. P., Nachury, M. V., Spiliotis, E. T., and Nelson, W. J. (2010) A septin diffusion barrier at the base of the primary cilium maintains ciliary membrane protein distribution. *Science* **329**, 436–439
- Caudron, F., and Barral, Y. (2009) Septins and the lateral compartmentalization of eukaryotic membranes. *Dev. Cell* **16**, 493–506
- Kim, S. K., Shindo, A., Park, T. J., Oh, E. C., Ghosh, S., Gray, R. S., Lewis, R. A., Johnson, C. A., Attie-Bittach, T., Katsanis, N., and Wallingford, J. B. (2010) Planar cell polarity acts through septins to control collective cell movement and ciliogenesis. *Science* **329**, 1337–1340
- Najafi, M., Maza, N. A., and Calvert, P. D. (2012) Steric volume exclusion sets soluble protein concentrations in photoreceptor sensory cilia. *Proc. Natl. Acad. Sci. U.S.A.* **109**, 203–208
- Najafi, M., and Calvert, P. D. (2012) Transport and localization of signaling proteins in ciliated cells. *Vision Res.* **75**, 11–18
- Thomas, S., Wright, K. J., Le Corre, S., Micalizzi, A., Romani, M., Abhyankar, A., Saada, J., Perrault, I., Amiel, J., Litzler, J., Filhol, E., Elkhartoufi, N., Kwong, M., Casanova, J. L., Boddaert, N., et al. (2014) A homozygous PDE6D mutation in Joubert syndrome impairs targeting of farnesylated INPP5E protein to the primary cilium. *Hum. Mutat.* **35**, 137–146
- Chandra, A., Grecco, H. E., Pisupati, V., Perera, D., Cassidy, L., Skoulidis, F., Ismail, S. A., Hedberg, C., Hanzal-Bayer, M., Venkitaraman, A. R., Wittinghofer, A., and Bastiaens, P. I. (2012) The GDI-like solubilizing factor PDE8 sustains the spatial organization and signalling of Ras family proteins. *Nat. Cell Biol.* **14**, 148–158
- Zhang, H., Constantine, R., Frederick, J. M., and Baehr, W. (2012) The prenyl-binding protein PrBP/δ: a chaperone participating in intracellular trafficking. *Vision Res.* **75**, 19–25
- Wright, K. J., Baye, L. M., Olivier-Mason, A., Mukhopadhyay, S., Sang, L., Kwong, M., Wang, W., Pretorius, P. R., Sheffield, V. C., Sengupta, P., Slusarski, D. C., and Jackson, P. K. (2011) An ARL3-UNC119-RP2 GTPase cycle targets myristoylated NPHP3 to the primary cilium. *Genes Dev.* **25**, 2347–2360
- Kobayashi, A., Kubota, S., Mori, N., McLaren, M. J., and Inana, G. (2003) Photoreceptor synaptic protein HRG4 (UNC119) interacts with ARL2 via a putative conserved domain. *FEBS Lett.* **534**, 26–32
- Allen, R. A. (1965) Isolated cilia in inner retinal neurons and in retinal pigment epithelium. *J. Ultrastruct. Res.* **12**, 730–747
- Christensen, S. T., Pedersen, L. B., Schneider, L., and Satir, P. (2007) Sensory cilia and integration of signal transduction in human health and disease. *Traffic* **8**, 97–109
- Singla, V., and Reiter, J. F. (2006) The primary cilium as the cell's antenna: signaling at a sensory organelle. *Science* **313**, 629–633
- Wolfrum, U., and Schmitt, A. (2000) Rhodopsin transport in the membrane of the connecting cilium of mammalian photoreceptor cells. *Cell Motil. Cytoskeleton* **46**, 95–107
- Swanson, D. A., Chang, J. T., Campochiaro, P. A., Zack, D. J., and Valle, D. (1998) Mammalian orthologs of *C. elegans* unc-119 highly expressed in photoreceptors. *Invest. Ophthalmol. Vis. Sci.* **39**, 2085–2094
- Vepachedu, R., Karim, Z., Patel, O., Goplen, N., and Alam, R. (2009) UNC119 protects from Shigella infection by inhibiting the Abl family kinases. *PLoS One* **4**, e5211
- Cen, O., Gorska, M. M., Stafford, S. J., Sur, S., and Alam, R. (2003) Identification of UNC119 as a novel activator of SRC-type tyrosine kinases. *J. Biol. Chem.* **278**, 8837–8845
- Gorska, M. M., Stafford, S. J., Cen, O., Sur, S., and Alam, R. (2004) Unc119, a novel activator of Lck/Fyn, is essential for T cell activation. *J. Exp. Med.* **199**, 369–379
- Gorska, M. M., Liang, Q., Karim, Z., and Alam, R. (2009) Uncoordinated 119 protein controls trafficking of Lck via the Rab11 endosome and is critical for immunological synapse formation. *J. Immunol.* **183**, 1675–1684
- Gorska, M. M., Cen, O., Liang, Q., Stafford, S. J., and Alam, R. (2006) Differential regulation of interleukin 5-stimulated signaling pathways by dynamin. *J. Biol. Chem.* **281**, 14429–14439
- Lee, Y., Chung, S., Baek, I. K., Lee, T. H., Paik, S. Y., and Lee, J. (2013) UNC119a bridges the transmission of Fyn signals to Rab11, leading to the completion of cytokinesis. *Cell Cycle* **12**, 1303–1315
- Resh, M. D. (1999) Fatty acylation of proteins: new insights into membrane targeting of myristoylated and palmitoylated proteins. *Biochim. Biophys. Acta* **1451**, 1–16
- Mejuch, T., van Hattum, H., Triola, G., Jaiswal, M., and Waldmann, H. (2015) Specificity of lipoprotein chaperones for the characteristic lipidated structural motifs of their cognate lipoproteins. *Chembiochem* **16**, 2460–2465
- Ismail, S. A., Chen, Y. X., Miertzschke, M., Vetter, I. R., Koerner, C., and Wittinghofer, A. (2012) Structural basis for Arl3-specific release of myristoylated ciliary cargo from UNC119. *EMBO J.* **31**, 4085–4094
- Zhang, H., Constantine, R., Vorobiev, S., Chen, Y., Seetharaman, J., Huang, Y. J., Xiao, R., Montelione, G. T., Gerstner, C. D., Davis, M. W., Inana, G., Whitby, F. G., Jorgensen, E. M., Hill, C. P., Tong, L., and Baehr, W. (2011) UNC119 is required for G protein trafficking in sensory neurons. *Nat. Neurosci.* **14**, 874–880
- Ismail, S. A., Chen, Y. X., Rusinova, A., Chandra, A., Bierbaum, M., Gremer, L., Triola, G., Waldmann, H., Bastiaens, P. I., and Wittinghofer, A. (2011) Arl2-GTP and Arl3-GTP regulate a GDI-like transport system for farnesylated cargo. *Nat. Chem. Biol.* **7**, 942–949
- Constantine, R., Zhang, H., Gerstner, C. D., Frederick, J. M., and Baehr, W. (2012) Uncoordinated (UNC)119: coordinating the trafficking of myristoylated proteins. *Vision Res.* **75**, 26–32
- Veltel, S., Kravchenko, A., Ismail, S., and Wittinghofer, A. (2008) Specificity of Arl2/Arl3 signaling is mediated by a ternary Arl3-effector-GAP complex. *FEBS Lett.* **582**, 2501–2507
- Kapoor, S., Fansa, E. K., Möbitz, S., Ismail, S. A., Winter, R., Wittinghofer, A., and Weise, K. (2015) Effect of the N-terminal helix and nucleotide loading on the membrane and effector binding of Arl2/3. *Biophys. J.* **109**, 1619–1629
- Roehrl, M. H., Wang, J. Y., and Wagner, G. (2004) A general framework for development and data analysis of competitive high-throughput screens for small-molecule inhibitors of protein-protein interactions by fluorescence polarization. *Biochemistry* **43**, 16056–16066

N-terminal Myristoylated Cargo Interaction with Unc119a/b

38. Zimmermann, G., Papke, B., Ismail, S., Vartak, N., Chandra, A., Hoffmann, M., Hahn, S. A., Triola, G., Wittinghofer, A., Bastiaens, P. I., and Waldmann, H. (2013) Small molecule inhibition of the KRAS-PDE δ interaction impairs oncogenic KRAS signalling. *Nature* **497**, 638–642
39. Olbrich, H., Fliegau, M., Hoefele, J., Kispert, A., Otto, E., Volz, A., Wolf, M. T., Sasmaz, G., Trauer, U., Reinhardt, R., Sudbrak, R., Antignac, C., Gretz, N., Walz, G., Schermer, B., *et al.* (2003) Mutations in a novel gene, NPHP3, cause adolescent nephronophthisis, tapeto-retinal degeneration and hepatic fibrosis. *Nat. Genet.* **34**, 455–459
40. Shiba, D., Manning, D. K., Koga, H., Beier, D. R., and Yokoyama, T. (2010) Inv acts as a molecular anchor for Nphp3 and Nek8 in the proximal segment of primary cilia. *Cytoskeleton* **67**, 112–119
41. Hou, X., Mrug, M., Yoder, B. K., Lefkowitz, E. J., Kremmidiotis, G., D'Eustachio, P., Beier, D. R., and Guay-Woodford, L. M. (2002) Cystin, a novel cilia-associated protein, is disrupted in the cpk mouse model of polycystic kidney disease. *J. Clin. Invest.* **109**, 533–540
42. Tao, B., Bu, S., Yang, Z., Siroky, B., Kappes, J. C., Kispert, A., and Guay-Woodford, L. M. (2009) Cystin localizes to primary cilia via membrane microdomains and a targeting motif. *J. Am. Soc. Nephrol.* **20**, 2570–2580
43. Lerea, C. L., Bunt-Milam, A. H., and Hurley, J. B. (1989) α -Transducin is present in blue-, green-, and red-sensitive cone photoreceptors in the human retina. *Neuron* **3**, 367–376
44. Veltel, S., Gasper, R., Eisenacher, E., and Wittinghofer, A. (2008) The retinitis pigmentosa 2 gene product is a GTPase-activating protein for Arf-like 3. *Nat. Struct. Mol. Biol.* **15**, 373–380
45. Schwahn, U., Lenzner, S., Dong, J., Feil, S., Hinzmann, B., van Duijnhoven, G., Kirschner, R., Hemberger, M., Bergen, A. A., Rosenberg, T., Pinckers, A. J., Fundele, R., Rosenthal, A., Cremers, F. P., Ropers, H. H., and Berger, W. (1998) Positional cloning of the gene for X-linked retinitis pigmentosa 2. *Nat. Genet.* **19**, 327–332
46. Avidor-Reiss, T., Maer, A. M., Koundakjian, E., Polyakov, A., Keil, T., Subramaniam, S., and Zuker, C. S. (2004) Decoding cilia function: defining specialized genes required for compartmentalized cilia biogenesis. *Cell* **117**, 527–539
47. Evans, R. J., Schwarz, N., Nagel-Wolfrum, K., Wolfrum, U., Hardcastle, A. J., and Cheetham, M. E. (2010) The retinitis pigmentosa protein RP2 links pericentriolar vesicle transport between the Golgi and the primary cilium. *Hum. Mol. Genet.* **19**, 1358–1367
48. Hurd, T., Zhou, W., Jenkins, P., Liu, C. J., Swaroop, A., Khanna, H., Martens, J., Hildebrandt, F., and Margolis, B. (2010) The retinitis pigmentosa protein RP2 interacts with polycystin 2 and regulates cilia-mediated vertebrate development. *Hum. Mol. Genet.* **19**, 4330–4344
49. Silverman, L., Sudol, M., and Resh, M. D. (1993) Members of the src family of nonreceptor tyrosine kinases share a common mechanism for membrane binding. *Cell Growth Differ.* **4**, 475–482
50. Gorska, M. M., and Alam, R. (2012) Consequences of a mutation in the UNC119 gene for T cell function in idiopathic CD4 lymphopenia. *Curr. Allergy Asthma Rep.* **12**, 396–401
51. Higashide, T., McLaren, M. J., and Inana, G. (1998) Localization of HRG4, a photoreceptor protein homologous to Unc-119, in ribbon synapse. *Invest. Ophthalmol. Vis. Sci.* **39**, 690–698
52. Lokaj, M., Kösling, S. K., Koerner, C., Lange, S. M., van Beersum, S. E., van Reeuwijk, J., Roepman, R., Horn, N., Ueffing, M., Boldt, K., and Wittinghofer, A. (2015) The interaction of CCDC104/BARTL1 with Arl3 and implications for ciliary function. *Structure* **23**, 2122–2132
53. Gotthardt, K., Lokaj, M., Koerner, C., Falk, N., Giessl, A., and Wittinghofer, A. (2015) A G-protein activation cascade from Arl13B to Arl3 and implications for ciliary targeting of lipidated proteins. *Elife* **4**, 10.7554/eLife.11859
54. Jaiswal, M., Dubey, B. N., Koessmeier, K. T., Gremer, L., and Ahmadian, M. R. (2012) Biochemical assays to characterize Rho GTPases. *Methods Mol. Biol.* **827**, 37–58
55. Torres, J. Z., Miller, J. J., and Jackson, P. K. (2009) High-throughput generation of tagged stable cell lines for proteomic analysis. *Proteomics* **9**, 2888–2891
56. Dong, A., Xu, X., Edwards, A. M., Midwest Center for Structural Genomics, Structural Genomics Consortium, Chang, C., Chruszcz, M., Cuff, M., Cymborowski, M., Di Leo, R., Egorova, O., Evdokimova, E., Filippova, E., Gu, J., Guthrie, J., *et al.* (2007) *In situ* proteolysis for protein crystallization and structure determination. *Nat. Methods* **4**, 1019–1021
57. Sang, L., Miller, J. J., Corbit, K. C., Giles, R. H., Brauer, M. J., Otto, E. A., Baye, L. M., Wen, X., Scales, S. J., Kwong, M., Huntzicker, E. G., Sfakianos, M. K., Sandoval, W., Bazan, J. F., Kulkarni, P., *et al.* (2011) Mapping the NPHP-JBTS-MKS protein network reveals ciliopathy disease genes and pathways. *Cell* **145**, 513–528

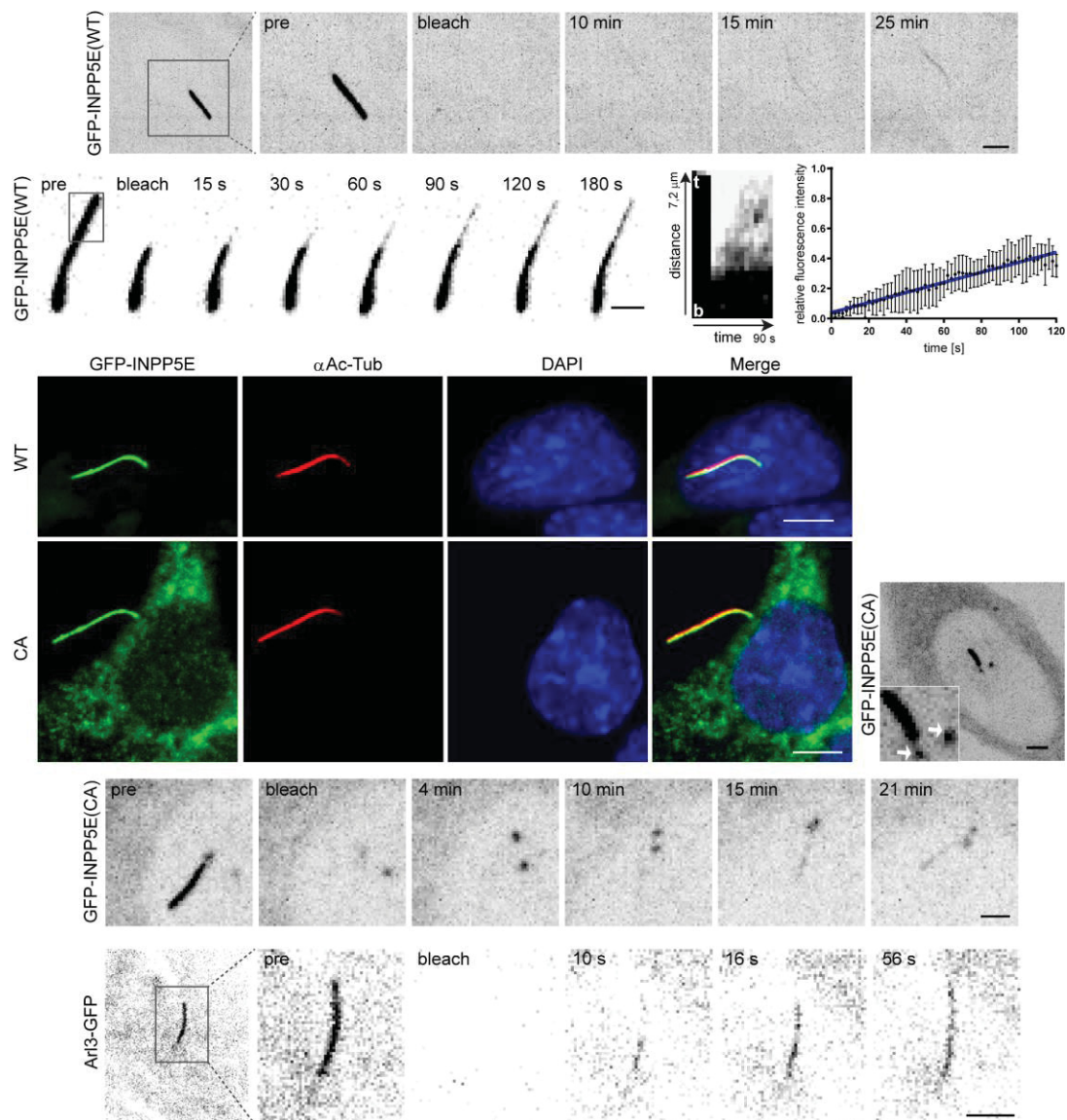
These were the main conclusions from this publication

- The sorting principle of myristoylated cargo proteins of Unc119a/b is similar to that of farnesylated cargo by PDE6 δ .
- The affinity towards Unc119a/b determines the sorting of myristoylated cargo: High affinity cargo such as NPHP3 localizes to cilia, where it is released by Arl3•GTP, low affinity cargo is excluded from cilia and is released by Arl2•GTP.
- The +2 and +3 positions relative to the myristoylated glycine of the cargo protein determine the affinity towards Unc119a/b and might act as ciliary sorting signals of NPHP3.

5 Publication IV

Mechanism and dynamics of INPP5E transport into and inside the ciliary compartment

Stefanie K. Kösling, Eyad K. Fansa, Stefano Maffini* and Alfred Wittinghofer* (2018). *Biological Chemistry* 399(3), 277-292. (* Co-corresponding authors)



These were the questions to be answered by this publication

- Analyzed in living cells, does INPP5E exclusively localize to cilia?
- What is the mechanism of INPP5E targeting to and entry into cilia? What are the roles of PDE6 δ and the dynein/IFT system?
- Does INPP5E move within cilia and if yes, how is the innerciliary transport regulated? Are PDE6 δ or the IFT system involved?
- What is the role of the farnesylation of INPP5E for ciliary localization, targeting, entry and innerciliary transport?
- How does Arl3 move in the cytosol, into and within cilia? Does it depend on active transport?

Contribution of 90 %

- Plasmid generation and mutagenesis for transfection of IMCD3 cells.
- Cell cultivation, generation of stable GFP cell lines (INPP5E, INPP5E(CA)), validation by western blotting.
- Cell fixation, IF staining and fluorescence microscopy of the cell lines above, image processing.
- Quantification of the fold of ciliary enrichment of INPP5E and INPP5E(CA).
- Confocal fluorescence microscopy for live cell imaging, FRAP experiments of the cell lines above and of the Arl3-GFP cell line, inhibitor experiments (ciliobrevin D, Deltazinone 1), image and video processing.
- For FRAP: Quantification of the fluorescence intensity values of signal recovery after bleaching, kymograph analysis and velocity determination of GFP signal recovery.
- Writing of the manuscript.

Declaration: Reprinted (adapted) with permission from Biological Chemistry

Copyright © 2018, Walter de Gruyter GmbH

DOI: <https://doi.org/10.1515/hsz-2017-0226>

Stefanie Kristine Kösling, Eyad Kalawy Fansa, Stefano Maffini* and Alfred Wittinghofer*

Mechanism and dynamics of INPP5E transport into and inside the ciliary compartment

<https://doi.org/10.1515/hsz-2017-0226>

Received August 24, 2017; accepted November 3, 2017; previously published online November 15, 2017

Abstract: The inositol polyphosphate 5'-phosphatase E (INPP5E) localizes to cilia. We showed that the carrier protein phosphodiesterase 6 delta subunit (PDE6 δ) mediates the sorting of farnesylated INPP5E into cilia due to high affinity binding and release by the ADP-ribosylation factor (Arf)-like protein Arl3-GTP. However, the dynamics of INPP5E transport into and inside the ciliary compartment are not fully understood. Here, we investigate the movement of INPP5E using live cell fluorescence microscopy and fluorescence recovery after photobleaching (FRAP) analysis. We show that PDE6 δ and the dynein transport system are essential for ciliary sorting and entry of INPP5E. However, its innerciliary transport is regulated solely by the intraflagellar transport (IFT) system, independent from PDE6 δ activity and INPP5E farnesylation. By contrast, movement of Arl3 into and within cilia occurs freely by diffusion and IFT-independently. The farnesylation defective INPP5E CaaX box mutant loses the exclusive ciliary localization. The accumulation of this mutant at centrioles after photobleaching suggests an affinity trap mechanism for ciliary entry, that in case of the wild type is overcome by the interaction with PDE6 δ . Collectively, we postulate a three-step mechanism regulating ciliary localization of INPP5E, consisting of farnesylation- and PDE6 δ -mediated targeting, INPP5E-PDE6 δ complex diffusion into the cilium with transfer to the IFT system, and retention inside cilia.

Keywords: Arl3; cilium; farnesylation; FRAP; Joubert syndrome; PDE6 δ .

Introduction

Primary cilia are hair-like organelles that protrude from the surface of most eukaryotic cells (Wheatley, 1995; Pazour and Witman, 2003) and serve multiple functions in various differentiated and growth-arrested cell types in vertebrates (Wheatley, 1995; Wheatley et al., 1996; Eggenschwiler and Anderson, 2007). They exhibit various sensory functions (Pazour and Witman, 2003) and are essential for a number of developmental signaling pathways (Eggenschwiler and Anderson, 2007; Goetz and Anderson, 2010), such as Hedgehog (Huangfu et al., 2003; Corbit et al., 2005; Liu et al., 2005), platelet-derived growth factor receptor α (Schneider et al., 2005), Wnt signaling (Cano et al., 2004; Simons et al., 2005; May-Simera and Kelley, 2012) and Gli transcription factor processing (Haycraft et al., 2005; Liu et al., 2005).

Defects in the structure and function of cilia cause a large number of congenital human diseases, called ciliopathies (Badano et al., 2006; Novarino et al., 2011; Waters and Beales, 2011). The scaffold of a cilium, the axoneme, is built by nine doublets of microtubules that are anchored to the mother centriole derived basal body (De Robertis, 1956; Sorokin, 1968; Berbari et al., 2009) (Figure 1). The ciliary lumen and its surrounding membrane differ from the plasma membrane and cellular cytosol in its protein and lipid composition (Bloodgood, 1984; Rohatgi and Snell, 2010; Garcia-Gonzalo et al., 2015). Protein entry to and exit from the ciliary compartment are strictly regulated by a ciliary gate that separates the ciliary lumen from the cytosol (Hu and Nelson, 2011; Williams et al., 2011; Jensen et al., 2015). Sorting and retention of proteins to and within the cilium are determined by various apparently unrelated ciliary targeting sequences (CTS) suggesting different molecular mechanisms for entry into the compartment (Nachury et al., 2010). Within the cilium, proteins are transported by the IFT system, that is driven by the motor proteins heterotrimeric kinesin-2 and homodimeric kinesin-2 (Kif17/OSM-3), which move along the axonemal microtubules in anterograde or plus-end direction from the base to the tip (Cole et al., 1993, 1998; Kozminski et al., 1993, 1995; Ou et al., 2005), and the AAA+ ATPase IFT-dynein, which moves in retrograde or minus-end direction (Gibbons and Rowe, 1965; Rosenbaum and

***Corresponding authors: Stefano Maffini**, Department of Mechanistic Cell Biology, Max Planck Institute of Molecular Physiology, Otto-Hahn-Straße 11, D-44227 Dortmund, Germany, e-mail: stefano.maffini@mpi-dortmund.mpg.de; and **Alfred Wittinghofer**, Structural Biology Group, Max Planck Institute of Molecular Physiology, Otto-Hahn-Straße 11, D-44227 Dortmund, Germany, e-mail: alfred.wittinghofer@mpi-dortmund.mpg.de

Stefanie Kristine Kösling and Eyad Kalawy Fansa: Structural Biology Group, Max Planck Institute of Molecular Physiology, Otto-Hahn-Straße 11, D-44227 Dortmund, Germany

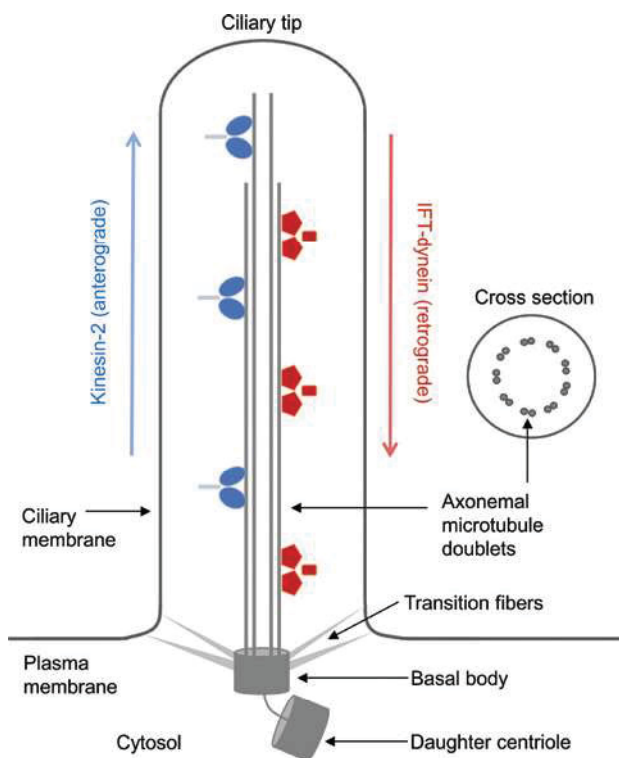


Figure 1: The cilium.

The axoneme is the scaffold of the cilium and is built by nine doublets of microtubules (9+0 structure of primary cilia), which are anchored to the basal body (mother centriole). The ciliary membrane surrounds the ciliary lumen, that is separated from the cytosol by the ciliary gate, which is built by transition zone and basal body associated proteins and the transition fibers. Protein transport within the cilium is regulated by the IFT system, driven by kinesin-2 in anterograde direction from the base to the tip (blue), and by IFT-dynein in retrograde direction from the tip to the base (red).

Witman, 2002; Scholey, 2003) (Figure 1). Collectively, trafficking of ciliary proteins into and inside the compartment is a complex, as yet not fully understood process.

Lipidated cargo proteins are sorted to cellular membranes by the Arl2/Arl3 system (Fansa and Wittinghofer, 2016). The Arf-like proteins Arl2 and Arl3 are homologous small GTP-binding (G) proteins (52% sequence identity, 68% similarity) and specifically interact with the homologous carrier proteins PDE6 δ (Linari et al., 1999) and Unc119a/HRG4 (uncoordinated/human retinal gene 4) and Unc119b in a nucleotide-dependent manner (Van Valkenburgh et al., 2001; Wright et al., 2011; Jaiswal et al., 2016). Through its hydrophobic pocket, PDE6 δ binds to prenylated cargoes and thereby acts as general solubilizing and shuttling factor for rod PDE6 and various small G proteins (Florio et al., 1996; Hanzal-Bayer et al., 2002; Nancy et al., 2002; Zhang et al., 2004; Chandra et al., 2012; Ismail et al., 2012) as well as different ciliary proteins,

such as INPP5E, GRK1 (rhodopsin kinase) and RPGR (retinitis pigmentosa GTPase regulator) (Zhang et al., 2007; Thomas et al., 2014; Fansa et al., 2015, 2016; Lee and Seo, 2015; Dutta and Seo, 2016). The crystal structure of PDE6 δ in complex with RheB, Ras and/or farnesylated peptides thereof have shown that only the farnesylated cysteine methyl ester and three to four additional residues insert into the hydrophobic pocket (Ismail et al., 2011; Dharmaiah et al., 2016). The regulation of Ras membrane localization is a crucial step in the biological function of Ras (Chandra et al., 2012; Schmick et al., 2014, 2015) and is considered a possible point of attack to target oncogenic Ras (Zimmermann et al., 2013; Papke et al., 2016).

In the GTP-bound form, Arl2 and Arl3 bind to their effectors PDE6 δ and Unc119a/b and allosterically release lipidated cargo proteins, thereby regulating their localization and function (Hanzal-Bayer et al., 2002; Ismail et al., 2011; Wright et al., 2011; Schmick et al., 2014; Thomas et al., 2014). Despite their similarity and overlapping function, only Arl3 but not Arl2 has been found in the primary cilium (Avidor-Reiss et al., 2004; Zhou et al., 2006; Lokaj et al., 2015). As the G protein Arl13B, which has recently been shown to be the GEF for Arl3 (Gotthardt et al., 2015), is exclusively localized to the cilium (Caspary et al., 2007; Cantagrel et al., 2008; Hori et al., 2008), it can thus be assumed that there is a high local concentration of Arl3-GTP in this compartment. Moreover, Arl3-GTP can be hypothesized to reside in the cilium because the Arl3 GAP RP2 (Veltel et al., 2008) has been observed to be excluded from cilia (Grayson et al., 2002; Blacque et al., 2005; Evans et al., 2010; Lokaj et al., 2015). Arl3-GTP enrichment is assumed to generate a driving force for the cilium-directed movement of lipidated cargoes of PDE6 δ and Unc119a/b (Gotthardt et al., 2015). The sorting of cargo has been shown to depend on the affinity between the lipidated cargo and the carrier protein. High affinity farnesylated cargo can only be released by Arl3-GTP in the cilium, while low affinity cargo, such as Rheb/Ras, are released at other cellular membranes by Arl2-GTP (Schmick et al., 2014; Fansa et al., 2016). The same principle holds true for release of myristoylated cargo from Unc119a/b (Wright et al., 2011; Fansa and Wittinghofer, 2016; Jaiswal et al., 2016).

This study focuses on the ciliary trafficking of the PDE6 δ cargo protein INPP5E, that includes a C-terminal CaaX box in which the cysteine 644 residue is farnesylated (De Smedt et al., 1996). INPP5E is an inositol polyphosphate 5'-phosphatase, which selectively removes the 5'-phosphate from the inositol ring of phosphoinositides (Astle et al., 2007) and is mutated in the ciliopathies Joubert (Bielas et al., 2009; Travaglini et al., 2013) and

MORM (mental retardation, truncal obesity, retinal dys-
trophy and micropenis) syndromes. One of the MORM-
related patient mutations misses the 18 C-terminal amino
acids, including the CaaX motif (Hampshire et al., 2006;
Jacoby et al., 2009). Thanks to the high affinity to PDE6 δ
($K_d = 3.7 \text{ nM} \pm 0.2 \text{ nM}$) (Fansa et al., 2016), INPP5E nearly
exclusively localizes to the primary cilium (Bielas et al.,
2009; Jacoby et al., 2009; Fansa et al., 2016). Ciliary localiza-
tion can in fact be severely compromised by reducing
the affinity to PDE6 δ (Fansa et al., 2016) and mutations
reducing this affinity may result in MORM syndrome
caused by the loss of the INPP5E C-terminal CaaX motif
(Hampshire et al., 2006; Jacoby et al., 2009).

A number of partially conflicting studies describe
the role played by PDE6 δ in the localization of INPP5E in
the cilium. Jacoby et al. (2009) and Thomas et al. (2014)
showed that the C-terminus of INPP5E is essential for
ciliary localization, because the above mentioned MORM
mutant loses its exclusive ciliary localization. Interest-
ingly, the latter study showed that INPP5E with the muta-
tion of the CaaX box cysteine only partially localizes to the
cilium and accumulates in the transition zone. Moreover,
this CaaX box mutant is not able to bind to PDE6 δ , con-
firming that the interaction is mediated by farnesylation.
However, a contrasting study claimed that the C-terminal
truncation of the MORM mutant INPP5E does not alter the
ciliary localization (Humbert et al., 2012). Furthermore,
a Joubert syndrome related mutation, that disrupts the
hydrophobic pocket formation of PDE6 δ , has been shown
to block ciliary localization of INPP5E and to impair
binding to Arl3-GTP. In addition, RNAi mediated knock-
down of PDE6 δ also leads to mislocalization of INPP5E
(Thomas et al., 2014). The importance of the shuttling
factor PDE6 δ for ciliary localization was strengthened
by our structural and biochemical studies revealing that
the high affinity of INPP5E towards PDE6 δ determines
its sorting to the cilium. Mutating the -1 and -3 positions
relative to the farnesylated cysteine to those found in low
affinity PDE6 δ cargo leads to mislocalization, whereby
mutant INPP5E is also found in the cytosol. This led us to
postulate that the -1 and -3 positions are a sorting signal
that is, albeit not the only signal, required for the exclusive
localization of INPP5E inside the ciliary compartment.

This study aims to advance our understanding
of INPP5E cellular sorting and ciliary transport. We
extended the existent cell biological analyses of INPP5E,
that were conducted mainly with chemically fixed cells,
to live imaging techniques using FRAP to characterize
and dissect INPP5E movement to and within the cilium.
The cilium-directed and the innerciliary movement
of the phosphatase were analyzed with a focus on the

dependency on its shuttling factor PDE6 δ and the inner-
ciliary transport system IFT.

Results

Ciliary targeting of INPP5E

INPP5E has been shown by immunofluorescence micro-
scopy to localize to primary cilia of different cell types,
such as mouse embryonic fibroblasts (Jacoby et al., 2009)
or retinal pigment epithelial (RPE) cells (Bielas et al.,
2009). We have previously shown that the fluorescence
in inner medullary collecting duct (IMCD3) cells stably
expressing GFP-INPP5E is almost exclusively localized in
the cilium of formaldehyde-fixed cells, shown by fluores-
cence microscopy (Fansa et al., 2016) (see also Figure 5A,
upper panel). Here, we used live imaging of IMCD3 cells
stably expressing GFP-INPP5E as a tool to dissect and
understand the cellular dynamics of INPP5E in living
cells. In living cells, GFP fluorescence also displayed the
almost exclusive localization of INPP5E in primary cilia
observed in fixed material, validating the functionality of
our GFP-INPP5E fusion (Figures 2A and 4A). We employed
this cellular tool to characterize INPP5E cellular sorting
and ciliary transport. To do so, we performed FRAP exper-
iments in which the fluorescence signal of a single cilium
was bleached either completely, to examine the move-
ment from the cytosol into the primary cilium, or partially,
to observe the innerciliary mobility.

To analyze the targeting and entry of cytosolic INPP5E
into the cilium, FRAP experiments were started by bleach-
ing the entire ciliary fluorescence signal and monitor the
signal recovery over time. The recovery in cilia, which was
first observable 10–15 min after the bleach, was weak but
still observable after 25 min, and to a level comparable
to that of the cytosolic compartment (Figure 2A, Supple-
mentary Video 1). The significantly reduced recovery was
to be expected, as the main portion of fluorescent mate-
rial localized in the cilium and the remaining unbleached
cytosolic fraction was minimal. This observation suggests
that there is a constant low-level transport of INPP5E from
the cell body to the primary cilium.

To analyze the entry mechanism for INPP5E into the
cilium, we asked whether dynein, which is involved in
IFT, also participates in loading of INPP5E. FRAP analysis
was performed as in Figure 2A, but in this case cells were
treated with an inhibitor for dynein. Ciliobrevin D is an
AAA+ ATPase inhibitor that initially has been shown to
block specifically cytoplasmic dynein, as well as ciliary

IFT-dynein (Firestone et al., 2012). In contrast to untreated cells, which show low but observable INPP5E levels in cilia after complete bleaching of the ciliary signal, pretreatment with ciliobrevin D completely abolished any signal recovery in cilia within the 25 min observation window (Figure 2B, Supplementary Video 2). Thus, transport of INPP5E from the cytosol and/or entry to the cilium depend on dynein activity. However, further experimental support will be required to clarify if this observation depends on cytoplasmic or IFT mediated dynein activity.

We then dissected the transport mechanism in relation to the function played by PDE6 δ in shuttling INPP5E to the cilium. To analyze the PDE6 δ dependency for INPP5E ciliary targeting in living cells, PDE6 δ was inhibited with Deltazinone 1, a pyrazolopyridazinone that binds to the prenyl-binding pocket of PDE6 δ with high affinity in the low nanomolar range (Papke et al., 2016). After treatment of cells with Deltazinone 1 and total bleach of the ciliary fluorescence, the recovery was fully abrogated within 25 min (Figure 2C, Supplementary Video 3). Control cells for the FRAP experiments with inhibitors were treated with equal volumes of DMSO and a signal recovery was observed as for the completely untreated cells shown in Figure 2A (DMSO data not shown). These observations strongly agree with the study by Thomas et al., who showed that both PDE6 δ and the farnesylation of INPP5E are required for correct ciliary localization of INPP5E (Thomas et al., 2014), and with our previous study (Fansa et al., 2016). Moreover, our results can be related to the study by Jacoby et al., revealing the essentiality of the farnesylated INPP5E C-terminus for its localization to cilia (Jacoby et al., 2009), at which it

is now known that the INPP5E-PDE6 δ interaction is mediated by the farnesyl moiety (Thomas et al., 2014; Fansa et al., 2016). Our results highlight that PDE6 δ is an essential component for the targeting of INPP5E to primary cilia, at least for the initial phases of the process (in this case the 25 min observation time window).

Ciliary targeting of Arl3

The small G protein Arl3 plays a critical role in the PDE6 δ -INPP5E network and we wondered about its movement. Because of its small size of 20 kDa we expected Arl3 to be able to freely move across the transition zone. We and others have demonstrated that Arl3, but not Arl2 is localized inside the cilium, but is also found in the rest of the cell (Avidor-Reiss et al., 2004; Zhou et al., 2006; Lokaj et al., 2015). Arl3 has been shown by immunofluorescence microscopy to occur in the connecting cilium of rod and cone photoreceptor cells (Grayson et al., 2002), in primary cilia of NIH3T3 (Zhou et al., 2006) and by GFP and immunofluorescence in IMCD3 cells (Lokaj et al., 2015). However, all these studies have been conducted using formaldehyde-fixed cells. Here, we analyzed the mobility of Arl3-GFP (48 kDa) by live imaging FRAP analysis. GFP fluorescence in living cells also indicated an even distribution of Arl3 between cilia and cytosol. After bleaching the whole ciliary fluorescence, the fluorescent signal recovered rapidly within a few seconds (Figure 3A, Supplementary Video 4). We then tested if the IFT machinery is involved in the loading of Arl3 to the cilium

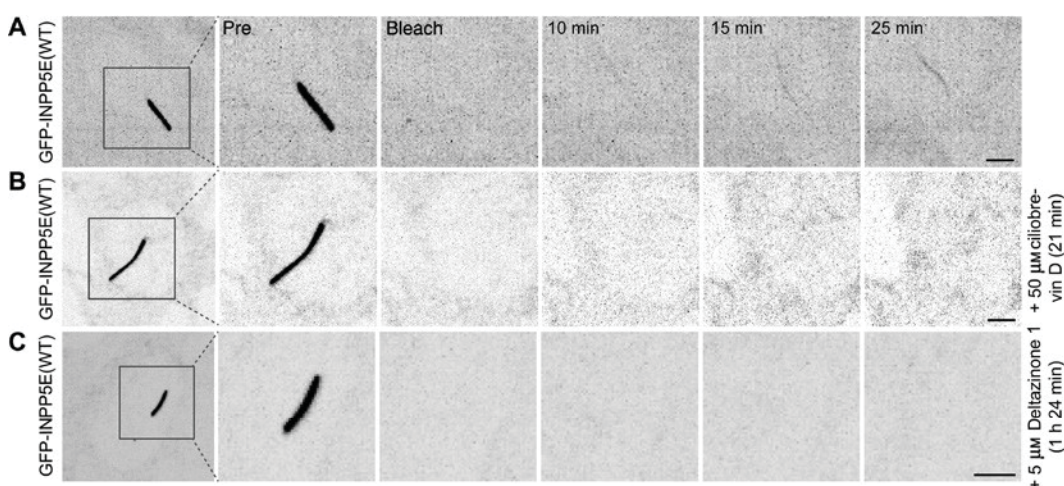


Figure 2: Ciliary targeting of INPP5E.

FRAP experiments in IMCD3 cells after bleaching the complete ciliary fluorescence of GFP-INPP5E(WT). Gray indicates GFP fluorescence of inverted images in all figures and gray boxes with dashed lines show zoomed area. Time lapse of recovery of (A) untreated cells, (B) after 21 min preincubation of cells with 50 μ M ciliobrevin D or (C) after 1 h 24 min preincubation with 5 μ M Deltazinone 1. Scale bars indicate 3 μ m.

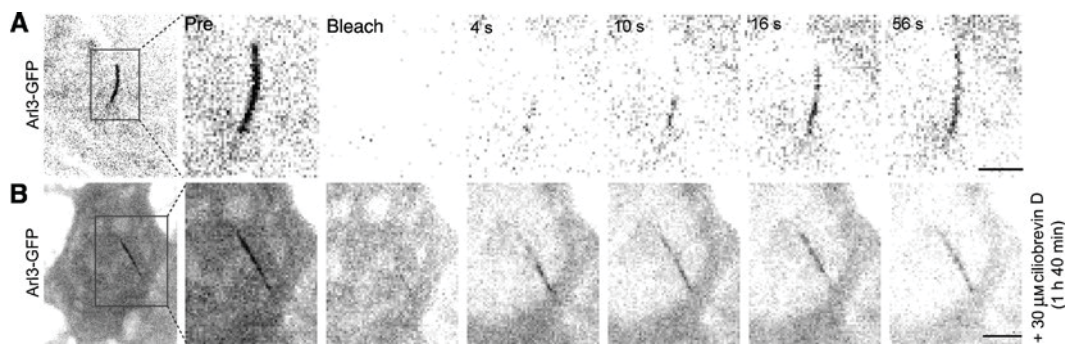


Figure 3: Ciliary targeting of Arl3.

FRAP experiments after bleaching the complete ciliary fluorescence of Arl3-GFP. Time lapse of recovery of (A) untreated cells or (B) after 1 h 40 min preincubation with 30 μM ciliobrevin D. Scale bars indicate 3 μm . Images in all figures represent raw data and are not corrected for photobleaching.

and its subsequent innerciliary transport, as shown for INPP5E. Interestingly, dynein inhibition by ciliobrevin D did not affect the fast recovery of the Arl3-GFP fluorescence (Figure 3B, Supplementary Video 5). Together, these experiments lead us to conclude that Arl3 moves freely within the cell and through the ciliary gate and that also its innerciliary movement does not seem to depend on dynein, whereas sorting to and localization of INPP5E in the cilium are regulated by dynein and PDE6 δ .

Innerciliary transport of INPP5E

Very little is known about how INPP5E moves within primary cilia after its entry. Therefore, following the analysis of INPP5E targeting to the cilium, we set out to characterize its motility within the cilium. To address this question, we focused our bleaching experiments on specific regions of the cilium, such as the region at the base or at the tip. The base could be distinguished from the tip based on the morphology of the cilia, which is broader in this region than in the tip (Reiter et al., 2012). Bleaching of the base region displays the fluorescence recovery in retrograde direction, whereas bleaching of the tip region illustrates the anterograde recovery. When bleached individually, both the tip and the base region displayed relatively fast recovery of the GFP-INPP5E signal in the photobleached region within several seconds (Figure 4A and D, Supplementary Video 6) and as expected from the above, did not regain its initial intensity.

Fluorescence recovery originated from the unbleached region of the cilium, suggesting it was the consequence of directional movement of INPP5E. This directionality is clearly visualized in the kymograph of Figure 4B, in which fluorescence intensity of the

bleached area is plotted over time. This observation led us to the assumption that the innerciliary movement of INPP5E may depend on active transport. The only known transport system within cilia is the IFT system, which is driven by kinesin-2 to generate anterograde directed transport, and by dynein to generate retrograde directed motion. To test this possibility, we determined the velocity of the fluorescence signal directional recovery. Velocity quantification in the photobleached region (Figure 4B and C) revealed an average speed of $0.29 \mu\text{m/s} \pm 0.07 \mu\text{m/s}$ in anterograde direction. To compare retrograde and anterograde velocities in the same cilium, we performed FRAP experiments by bleaching the middle region of the cilia (Supplementary Figure 1A). Resultant average velocities for this middle region were $0.20 \mu\text{m/s} \pm 0.10 \mu\text{m/s}$ in anterograde direction and $0.23 \mu\text{m/s} \pm 0.07 \mu\text{m/s}$ in retrograde direction, showing no significant velocity differences between the two opposite directional fluorescence recoveries. These calculated velocities of signal recovery after bleaching are compatible with the rates reported for active transport for kinesin-2 ($0.20\text{--}2.4 \mu\text{m/s}$) and IFT-dynein ($0.14\text{--}5.60 \mu\text{m/s}$) driven active transport (Lehtreck, 2015). Moreover, in a study that was also conducted in IMCD3 cells, the IFT transport marker IFT88-EYFP displayed velocities of $0.3 \mu\text{m/s}$ in anterograde and $0.6 \mu\text{m/s}$ in retrograde direction (Besschetnova et al., 2009). Using GFP-IFT88 in the same cell line, Ye et al. found velocities in a similar range with values of $0.63 \mu\text{m/s}$ for anterograde directed motion and $0.36 \mu\text{m/s}$ in the retrograde direction (Ye et al., 2013). This resemblance between observed and reported velocities led us to hypothesize that INPP5E transport within primary cilia might be associated with IFT.

To test this hypothesis, we measured INPP5E innerciliary movement in cells treated with the dynein inhibitor

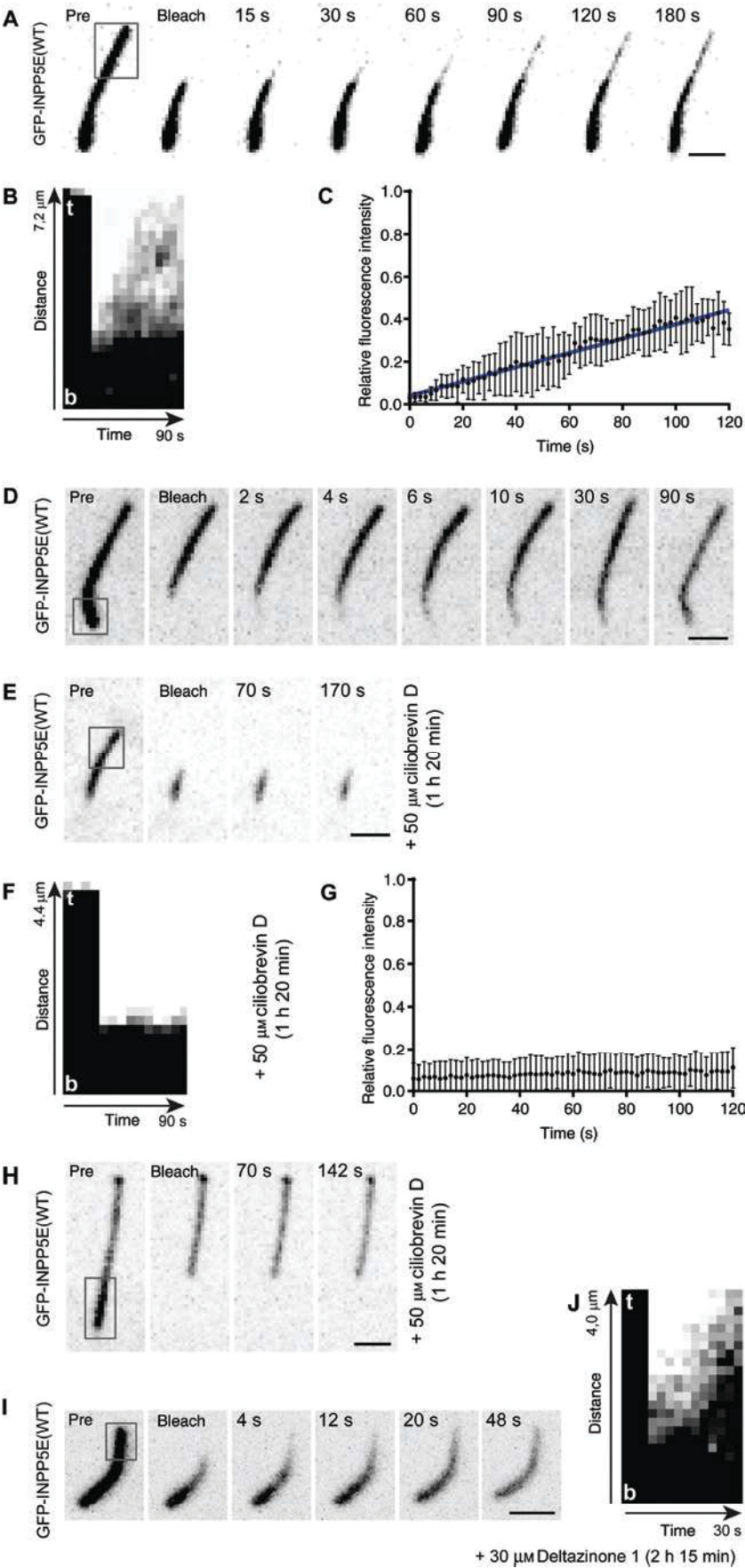


Figure 4: Innerciliary transport of INPP5E.

Fluorescence recovery after partial bleach of the ciliary fluorescence of GFP-INPP5E(WT). (A) Time lapse after bleaching the signal at the tip of untreated cells, (B) corresponding kymograph in which fluorescence intensity of the bleached area is plotted over time (t = tip, b = base) and (C) graph illustrating the relative fluorescence intensity over time. Relative fluorescence intensity of 1.0 equates to average intensity before bleaching. (D) Time lapse after bleaching the signal at the base of untreated cells. (E) Time lapse after bleaching the signal at the tip and 1 h 20 min preincubation with 50 μ M ciliobrevin D, (F) corresponding kymograph and (G) graph illustrating the relative fluorescence intensity over time. (H) Time lapse after bleaching the signal at the base after 1 h 20 min preincubation with 50 μ M ciliobrevin D. (I) Experiment as in A, B, however after 2 h 15 min preincubation with 30 μ M Deltazinone 1, (J) corresponding kymograph. Gray boxes mark bleached cilium area and scale bars indicate 2 μ m.

ciliobrevin D. In contrast to untreated or DMSO treated control cells, treatment with 50 μ M ciliobrevin D completely abrogated the recovery of the GFP-INPP5E fluorescent signal in the retrograde direction (Figure 4H). It has been previously reported that in IMCD3 cells prolonged treatment with 30–50 μ M ciliobrevin D also results in the inhibition of anterograde directed active transport, possibly because dynein might be required to load onto the ciliary base cytoplasmic IFT complexes and kinesin-2 for anterograde directed transport (Ye et al., 2013). To exploit this time-related effect of ciliobrevin D treatments, we looked at the effects of different incubation times. In line with this, our FRAP experiments in the presence of ciliobrevin D also revealed different effects of the inhibitor on anterograde directed recovery, depending on the treatment time. As expected, treatment with ciliobrevin D for a short time (3–7 min) was sufficient to abrogate retrograde directed fluorescence recovery (Supplementary Figure 2B). Moreover, the inhibition of retrograde transport was consistent during the following 1 h 20 min after ciliobrevin D addition (Figure 4H, Supplementary Video 7). Interestingly, short treatment with ciliobrevin D did not affect anterograde directed recovery of fluorescence (Supplementary Figure 2A), whereas longer treatments (≥ 20 min) significantly abrogated the recovery in the anterograde direction (Figure 4E–G). Thus, ciliobrevin D can be used as inhibitor of IFT in both directions after long preincubation (Supplementary Figure 1B). These experiments confirm that INPP5E transport within cilia is regulated by the IFT system.

Dynein is therefore important for the loading of INPP5E into the cilium and for its innerciliary transport. Moreover, our data show a crucial role of the shuttling factor PDE6 δ for ciliary entry. Because PDE6 δ has been found to localize to the ciliary transition zone and the proximal cilium (Thomas et al., 2014), we tested whether it might also be actively involved in the innerciliary transport of INPP5E. Therefore, we inhibited PDE6 δ by treating the cells with Deltazinone 1 and performed FRAP analysis on the tip region of a cilium. FRAP measurements and subsequent kymograph analysis revealed that the

fluorescence directional recovery, which was observed in untreated and DMSO treated control cells, was not impaired in PDE6 δ inhibited cells (Figure 4I and J, Supplementary Video 8). Thus, it can be assumed that the IFT-related movement of INPP5E within the cilium does not depend on PDE6 δ .

The INPP5E CaaX box mutant

Farnesylated INPP5E almost exclusively localizes to cilia (Bielas et al., 2009; Jacoby et al., 2009; Fansa et al., 2016) (Figure 5A, upper panel). To elucidate the specific role and importance of farnesylation and the interaction of INPP5E with PDE6 δ , we employed a cell line stably expressing GFP-INPP5E in which the CaaX box cysteine 644 was mutated to alanine [INPP5E(C644A)] to prevent farnesylation. Similarly to a previous report (Thomas et al., 2014), we observe in chemically fixed cells that the cilium levels of the CaaX box mutant are significantly lower than in the wild type. Moreover, the mutant showed a localization to endomembranes, including the ER (Figure 5A, lower panel), that was not observed for the wild type. To illustrate the loss of ciliary enrichment of the mutant compared to the wild type protein, we measured the ratio of the GFP fluorescence intensity within cilia relative to the intensity in the residual cell body. As we reported previously, wild type INPP5E is 5.3-fold \pm 1.1 enriched in primary cilia (Fansa et al., 2016). However, here we show that the ciliary enrichment of the CaaX box mutant is only 2.0-fold \pm 0.8 (Figure 5B). We conclude that the C-terminal farnesylation of INPP5E is indeed essential to promote the nearly exclusive ciliary localization of INPP5E. Live imaging of the mutant also revealed a significant cytosolic mislocalization besides the ciliary localization. Interestingly, and in contrast to the wild type protein, the mutant is additionally located both at the mother centriole, which in this ciliated cell forms the basal body, and the daughter centriole (Figure 5C). This centriolar enrichment could not be found in fixed cells, because according to our observation, centriolar structures cannot be visualized after formaldehyde

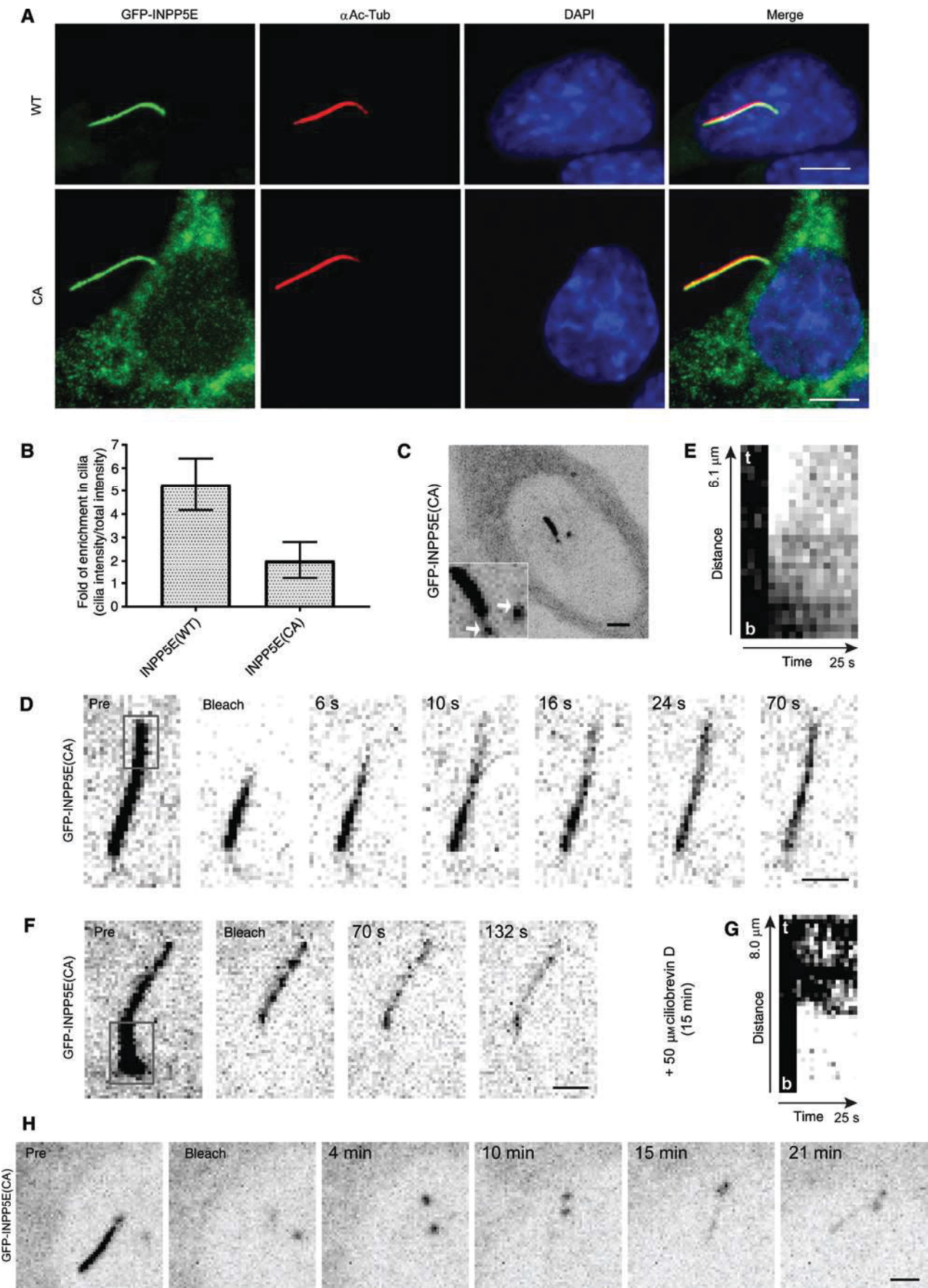


Figure 5: The INPP5E CaaX box mutant.

(A) Localization of INPP5E(WT) (upper panel) and CaaX box mutant INPP5E(C644A) (lower panel), shown by GFP fluorescence (green) of formaldehyde-fixed cells. Cilia were immunostained with an antibody against acetylated tubulin (red) and nuclei were stained with DAPI (blue). Scale bars indicate 5 μm . (B) Corresponding bar chart representation illustrates the enrichment of wild type and mutant INPP5E in cilia relative to the fluorescence in the cell body, analyzed using CellProfiler. Standard deviation is indicated by error bars, $n=43$ cells for INPP5E(WT) and 37 cells for INPP5E(C644A), $p \leq 0.05$ (Student's *t*-test). The cell lines have similar expression levels of either wild type or mutant INPP5E (see Supplementary Figure 4). (C) Localization of the CaaX box mutant in living cells. Inlet shows a zoom and white arrows indicate centriolar enrichment. Scale bar indicates 3 μm . (D–H) FRAP experiments with the CaaX box mutant. (D) Time lapse after bleaching the GFP-INPP5E(C644A) fluorescence at the ciliary tip of untreated cells and the corresponding kymograph (E). (F) Time lapse after bleaching the fluorescence at the base after 15 min preincubation with 50 μM ciliobrevin D and the corresponding kymograph (G). (H) Time lapse after bleaching the complete ciliary fluorescence of untreated cells. Scale bars in panels (D), (F), (H) indicate 2 μm .

treatment and thus impairs INPP5E localization at centrioles.

Next, we set out to understand how INPP5E is transported within the cilium in the absence of farnesylation. To do so, we performed FRAP analyses on different cilium regions of cells expressing GFP-INPP5E(C644A). Innerciliary directional movement of the mutant was observed after bleaching either the base or the tip region, with dynamics slightly faster than that of the wild type (Figure 5D and E; Supplementary Video 9; data of bleaching the base not shown). To test if the IFT-driven innerciliary movement of INPP5E depends on farnesylation, we performed dynein inhibition, followed by FRAP measurements of the mutant in the base region of the cilium. Similarly to the wild type protein, the fluorescent signal of the mutant did not show any directional recovery (Figure 5F and G; Supplementary Video 10; data of control cells not shown). We conclude that, like for the wild type protein, the innerciliary transport of the CaaX box mutant is regulated by the IFT system, indicating that the connection of INPP5E to IFT does not require farnesylation.

We then investigated if mutation in the CaaX box of INPP5E could affect its entry and transport from the cell body to the cilium. We observed that in contrast to farnesylated INPP5E, the CaaX box mutant localizes to the basal body and the daughter centriole (Figure 5C). Our FRAP measurements of GFP-INPP5E(C644A) recovery after bleaching the complete ciliary region showed a slow recovery along the axoneme, with levels and dynamics similar to the recovery of the wild type protein (Figure 5H, Supplementary Video 11). However, we observed that, unlike the wild type, the fluorescence signal of the CaaX box mutant accumulated at both centrioles. Similar to the wild type, bleaching of both centrioles together with the entire axoneme resulted in a slow and only minor recovery of the pre-FRAP intensity levels of the mutant in the axonemal region (Figure 5H). Unlike the axonemal region, the signal recovery at the basal body was rapid (within approximately 3 min) and complete (Figure 5H,

4 min panel). These high levels of the mutant at centrioles persisted for several minutes before the fluorescence signal recovery started to appear along the axoneme. We conclude that the absence of farnesylation does not completely inhibit the entry of INPP5E into the cilium, but rather causes the mutant to accumulate at the basal body before it enters the cilium.

Discussion

In this study, we addressed the sorting of INPP5E to the cilium and its subsequent innerciliary transport with a focus on the role played by PDE6 δ and the IFT system. To elucidate the role of farnesylation in this context, we analyzed the INPP5E CaaX box mutant. Furthermore, we investigated the cellular motility of Arl3. We employed live cell fluorescence microscopy using FRAP to analyze the mobility of GFP-tagged proteins.

As demonstrated by bleaching the complete ciliary fluorescence, INPP5E slowly reenters the cilium. PDE6 δ inhibition using Deltazinone 1 fully abrogates the recovery, highlighting the importance of PDE6 δ for sorting of INPP5E to and entry into cilia. Furthermore, this shows that Deltazinone 1 is able to displace from PDE6 δ not only the low affinity cargoes but also the high affinity ones, such as INPP5E, in living cells. So far, Deltazinone 1 has only been shown to displace prenylated KRas, which binds with low affinity to PDE6 δ (Papke et al., 2016). Inhibition of dynein by ciliobrevin D also leads to an abolition of fluorescence recovery. We assume that INPP5E does not simply diffuse through the ciliary gate to enter the cilium, but needs to be in complex with PDE6 δ and might need active transport mechanisms. As dynein is implicated in IFT transport, an intact IFT system might be required, although we cannot exclude that cytoplasmic dynein is also, albeit indirectly, involved in the transport of INPP5E to the cilium. An accumulation of INPP5E in the cell body

after treatment with Deltazinone 1 or ciliobrevin D could not be observed. Due to the very low amount of remaining fluorescent protein after bleaching the ciliary fraction, a detection of such an accumulation would technically be difficult.

Previous studies have shown in IMCD3 cells that passive diffusion of proteins decreases sharply with the increase of their size, indicating a sieve-like behavior of the ciliary transition zone, and that proteins larger than approximately 100 kDa are restricted from entering cilia. In living cells, the small protein Arl3 (20 kDa, here 48 kDa including GFP-tag) is distributed within cytosol and cilium, but the active Arl3-GTP is assumed to localize exclusively to the latter (Gotthardt et al., 2015; Fansa and Wittinghofer, 2016). By bleaching the total ciliary fluorescence, we observed a fast recovery within a few seconds after bleaching. The loading and innerciliary movement of Arl3 appeared to be independent of dynein or the IFT system, as shown by addition of ciliobrevin D. Thus, we conclude that the small-sized proteins such as Arl3 move freely between cytosol and cilia by diffusion across the ciliary transition zone, confirming earlier reports (Breslow et al., 2013; Lin et al., 2013). However, the bigger size of INPP5E (72 kDa, here 100 kDa including GFP-tag), which recovered in a range of 10–20 min and appears to be unable to fast and freely move between compartments, makes the need for active transport mechanisms to pass the ciliary gate more likely. Indeed, this is confirmed by the abrogation of INPP5E recovery after dynein inhibition. Our findings about the fast Arl3 diffusion into cilia and the slow entry of the larger INPP5E protein are supported by a model of the ciliary gate as sieve-like barrier, which can be passed by molecules at different rates according to their size (Lin et al., 2013).

By bleaching the GFP fluorescence at the base or tip region, we first demonstrated that INPP5E behaves dynamically within cilia, as shown by a directional recovery in both cases. The dynamic distribution of INPP5E along the whole axoneme might be essential for its function as inositol polyphosphate 5'-phosphatase, as it has been described as a modulator of the ciliary membrane composition by dephosphorylating PIPs (Chávez et al., 2015; Garcia-Gonzalo et al., 2015). Our kymograph analysis revealed velocities of recovery between 0.20 $\mu\text{m/s}$ and 0.29 $\mu\text{m/s}$ for anterograde directed motion and 0.23 $\mu\text{m/s}$ for retrograde directed motility of INPP5E, values that are in agreement with earlier measurements with IFT components (Besschetnova et al., 2009; Ye et al., 2013).

After inhibition of IFT by long preincubation with ciliobrevin D, movement of INPP5E in both directions was significantly abrogated. In agreement with studies on IFT

components (Ye et al., 2013), we also observed a dependency of INPP5E movements on the preincubation time with ciliobrevin D. Retrograde movement was exclusively blocked after short preincubation of 3 min, whereas anterograde transport was not affected, but was abolished after 20 min or longer preincubation. It is agreed that long preincubation with ciliobrevin D inhibits IFT in both directions demonstrating that the innerciliary anterograde and retrograde transport of INPP5E are regulated by the IFT system, although from our data we cannot exclude a minor contribution of diffusion. We suppose that the interaction between INPP5E and IFT components might be indirect and mediated by other ciliary proteins that link INPP5E to IFT proteins. For instance, such a task could be performed by a linking protein like Arl13B, which has been shown to interact with both INPP5E (Humbert et al., 2012) and the IFT components IFT46/56 (Nozaki et al., 2016). As Deltazinone 1 did not show any effect on INPP5E movement within cilia, we conclude that INPP5E innerciliary transport does not depend on PDE6 δ .

Analyses of the CaaX box mutant in chemically fixed and living cells clearly showed that farnesylation of INPP5E is essential for proper ciliary localization. Indeed, in chemically fixed cells, the 5.3-fold enrichment of farnesylated INPP5E in cilia was reduced to 2.0-fold and its levels at endomembranes were increased upon mutation of the CaaX box. The localization pattern shown here is in agreement with previous studies by Jacoby et al. and Thomas et al. (Jacoby et al., 2009; Thomas et al., 2014; Fansa et al., 2016), but not in line with the study by Humbert et al. (Humbert et al., 2012). Loss of farnesylation and thus of interaction with PDE6 δ might lead to an impaired ciliary sorting mechanism or a defective retention in the ciliary membrane due to loss of the lipid anchor and thus decrease of membrane affinity. As a similar localization pattern has been shown for the mutant with low affinity to PDE6 δ (Fansa et al., 2016), which retains the lipid anchor, we suggest that farnesylation is mostly required for the sorting of INPP5E and import into the cilium by interaction with PDE6 δ .

After partial bleach of the ciliary fluorescence, a slightly faster recovery of the mutant than that of the wild type was observed and after inhibition of IFT, the recovery was completely abrogated. This indicates that non-farnesylated INPP5E is still transported by IFT within cilia and that the IFT-dependent transport of the wild type does not depend on the farnesylation. The slightly slower recovery of wild type compared to mutant INPP5E can be explained with the increased membrane affinity of farnesylated INPP5E. While being transported via IFT, farnesylated INPP5E might move slower due to ciliary

membrane attachment. Nevertheless, the importance of the CaaX modification and PDE6 δ is supported by our observation that the CaaX box mutant, in contrast to the wild type, is enriched at the basal body (the mother centriole) and the daughter centriole and shows reduced axonemal localization. Notably, non-farnesylated INPP5E still has a certain membrane affinity, as shown by the localization at endomembranes, including the ER. Our findings about the localization of the CaaX box mutant, which does not interact with PDE6 δ , is at least partly compatible with the observation by Thomas et al. (2014), showing in PDE6 δ mutated Joubert syndrome patient tissues that in the absence of functional PDE6 δ and thus PDE6 δ -INPP5E interaction, INPP5E accumulates at the apical pole of epithelial tubule cells without entering the cilia.

After bleaching the total ciliary and basal body fluorescence of the CaaX box mutant, the axonemal signal recovered with a comparable speed to that of the wild type, but recovery at the basal body was very fast. We assume that the mutant diffuses into cilia and is then transferred to the IFT system. It might appear inconsistent that wild type INPP5E does not enter cilia after inhibition of PDE6 δ , whereas the mutant, which also does not interact with PDE6 δ , is at least partially able to enter cilia. This might be due to a trapping of farnesylated INPP5E at inner membranes in the absence of PDE6 δ which has been shown to function as a solubilizing protein (Florio et al., 1996; Hanzal-Bayer et al., 2002; Nancy et al., 2002; Zhang et al., 2004; Chandra et al., 2012; Ismail et al., 2012). Based on the basal body enrichment of the mutant and the similar speed of ciliary entry of wild type and mutant INPP5E, we postulate an affinity trap mechanism to be responsible for retention of the mutant at the base before entry. The affinity trap might be due to an enhanced affinity to centriolar protein(s) which in case of farnesylated INPP5E is overcome by the interaction with PDE6 δ . In support of this, the wild type protein is never seen accumulating at the basal body, most likely due to its high affinity to PDE6 δ . Thus, the main driving force for the sorting of INPP5E to cilia, which is due to the Arl3-GTP compartment acting on high affinity cargo of PDE6 δ , does not affect non-farnesylated INPP5E and leads to its defective sorting. Taken together, we show clearly that loss of farnesylation and thus impaired interaction with PDE6 δ interferes with the ciliary sorting mechanism of INPP5E, as indicated by the decrease of ciliary enrichment and the prolonged destination at the centrioles of the CaaX box mutant. This behavior of the mutant could be due to either the defective retention in the ciliary membrane or the increase in solubility due to loss of the lipid anchor, resulting in a different pathway of ciliary sorting and entry.

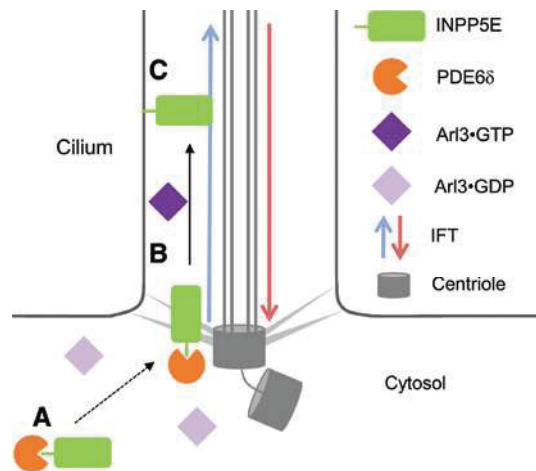


Figure 6: Model of the three-step mechanism leading to INPP5E ciliary localization.

(A) INPP5E binds to PDE6 δ and the complex is transported to the ciliary base. (B) The complex diffuses into the cilium. After entry, INPP5E is transferred to the IFT system, released from PDE6 δ by Arl3-GTP and the farnesyl moiety attaches INPP5E to the ciliary membrane. Within the cilium, INPP5E is transported by the IFT system. (C) INPP5E is retained inside the cilium.

Collectively, we propose a three-step mechanism leading to the almost exclusive ciliary localization of INPP5E. The first step is binding to PDE6 δ and the complex is transported to the ciliary base, which might also involve a ciliary targeting signal. Secondly, the complex might diffuse from the base into the cilium and be transferred to the IFT system. After entry, Arl3-GTP releases INPP5E from PDE6 δ and the farnesyl moiety anchors INPP5E to the ciliary membrane. The subsequent innerciliary transport of INPP5E is regulated by the IFT machinery and is independent of farnesylation or PDE6 δ . The third step is retention within cilia, mediated by the interaction with the IFT system, Arl13B, the ciliary membrane, or other unknown factors (Figure 6).

Materials and methods

Plasmids

Plasmids used to transfect IMCD3 Flip-In cells were created utilizing the Gateway cloning technology (Life Technologies/Thermo Fisher Scientific, Carlsbad, USA) according to the manufacturer's advices. The mouse *INPP5E* polymerase chain reaction (PCR) fragment was amplified applying subsequent primers: F-5'-ATG CCA TCC AAG TCA GCT TGC CTG-3', R-5'-TCA GGA CAC GGT GCA AAC TGC ACT GG-3'. The *INPP5E* entry clone was generated by PCR fragment integration into the pCR8/GW/TOPO vector (Life Technologies/Thermo Fisher Scientific, Carlsbad, USA) and following LR recombination reaction transferred it to the pG-LAP3 destination vector (Addgene, Cambridge,

USA) (Torres et al., 2009). The pG-LAP3 plasmid encoded an N-terminal to *INPP5E* located localization and affinity purification (LAP)-tag (GFP-TEV-site-S-peptide). Mutated *INPP5E*(C644A) was achieved by mutagenesis PCR using *INPP5E*-pG-LAP3 as template and the following mutagenesis primer: F-5'-GCC AGA GCT CCA GTG CAG TTG CCA CCG TGT CCT GAA AGG GCG-3'. Mouse *Ar13* PCR fragment was cloned using the primers: F-5'-ATG GGC TTG CTC TCT ATT TTG CGC-3', R-5'-TTT CTT CTT TGC GTT GAC ATT CTT GC-3', and *Ar13* in pET20 vector as template which was available in our lab. To obtain the *Ar13* entry clone, the PCR fragment was integrated into the pCR8/GW/TOPO vector. Similar to the cloning of *INPP5E*, LR recombination relocated the *Ar13* sequence to the pG-LAP5 destination vector (Addgene, Cambridge, USA) (Torres et al., 2009), which encodes a LAP-tag (S-peptide-Precision-site-GFP) C-terminal to *Ar13*.

Cell culture and generation of stable cell lines

Mouse IMCD3 cells were originally isolated from the mouse kidney (Rauchman et al., 1993) and contained a flippase (Flp) recombination target (FRT) cassette that was stably integrated. The IMCD3 Flp-In cell line was a kind gift from Prof. Dr. M. V. Nachury (Flp-In technology by Life Technologies/Thermo Fisher Scientific, Carlsbad, USA). The cells were cultured in DMEM/F-12, HEPES medium (Life Technologies/Thermo Fisher Scientific, Carlsbad, USA) that was supplemented with 10% fetal bovine serum and 2 mM L-glutamine (Life Technologies/Thermo Fisher Scientific, Carlsbad, USA) at 37°C and 5% CO₂. Development of stable cell lines has been conducted as reported previously (Torres et al., 2009; Sang et al., 2011). Shortly, approximately 100 000 cells were plated in 35 mm dishes and cultivated for 24 h to reach a confluence of 40–60%. The cells were cotransfected with the appropriate gene of interest integrated in the pG-LAP3 or pG-LAP5 vector (Addgene) and the pOG44 vector (Life Technologies/Thermo Fisher Scientific, Carlsbad, USA) that encoded the FLP recombinase utilizing the transfection reagent Lipofectamine 2000 (Life Technologies/Thermo Fisher Scientific, Carlsbad, USA). The selection of the transfected cells was facilitated by 100–200 mg hygromycin B (Merck, Darmstadt, Germany) per 1 ml culture medium. Respective protein expression was verified by immunoblotting using an antibody against GFP (1:500; Santa Cruz Biotechnology, Dallas, USA, sc-9996).

Immunostaining and microscopy of fixed cells

IMCD3 cells stably expressing the appropriate protein coupled to GFP were plated on coverslips, which were previously coated with poly-L-lysine (Sigma-Aldrich, St. Louis, USA), in 35 mm dishes. Each dish contained circa 100 000 cells that were cultivated in supplemented medium for 24 h to become approximately 50% confluent. To induce ciliogenesis, cells were incubated under serum deprivation for further 48 h. The cells on coverslips were washed in phosphate buffered solution (PBS) and fixed by 20 min incubation in a solution of 4% formaldehyde in cytoskeletal buffer (2.75 M NaCl, 100 mM KCl, 100 mM PIPES, 100 mM Glucose, 40 mM MgCl₂, 40 mM EGTA, 25 mM Na₂HPO₄, 8 mM KH₂PO₄, pH 6.0). After two PBS washes, the cell membranes were permeabilized during a 10 min incubation in cytoskeletal buffer containing 0.3% Triton X100. Before blocking in 10% fetal bovine serum (FBS) in PBS for 30 min, cells were rinsed in PBS with 0.1% Tween20. Mouse 6-11B-1 anti-acetylated tubulin antibody (1:5000; Sigma-Aldrich, St. Louis, USA, T6793), diluted in 10% FBS in PBS was

added for immunostaining of primary cilia and incubated overnight at 4°C. After four washes with 0.1% Tween 20 in PBS, anti-mouse secondary antibody coupled to Alexa Fluorophor 647 (1:800; Life Technologies/Thermo Fisher Scientific, Carlsbad, USA, A-31571) was incubated for 45 min at room temperature. The coverslips were rinsed three times in PBS complemented with 0.1% Tween 20 and subsequently in pure PBS. Nuclear DNA was stained with a 1:10 000 DAPI (Serva, Heidelberg, Germany) solution in PBS for 1 min and excess was removed by three washes in PBS. Mounting of coverslips on glass slides was conducted with a Mowiol (Merck, Darmstadt, Germany) solution. Images were obtained working with an Olympus (Tokyo, Japan) IX81 microscope, equipped with a 60×NA 1.35 oil immersion objective and a CCD camera.

Live cell microscopy and FRAP experiments

IMCD3 cells stably expressing the particular GFP-tagged protein were seeded with a number of 60 000 cells in 35 mm glass bottom μ -dishes or with a number of 12 000 cells per well in 8-well glass bottom μ -slides (ibidi, Planegg, Germany). Previously, the glass surfaces were coated with poly-L-lysine. Cells were cultivated in supplemented culture medium for 24 h to become approximately 50–60% confluent. To promote ciliary growth, cells were serum starved for 48 h in DMEM/F-12, HEPES medium complemented with 2 mM L-glutamine. Before imaging, the cells were washed in PBS and the medium was changed to CO₂ Independent Medium (Life Technologies/Thermo Fisher Scientific, Carlsbad, USA) complemented with 2 mM L-glutamine. Images and videos of cells that were placed in a heated chamber at 37°C were obtained using a 3i Marianas system (Intelligent Imaging Innovations, Inc., Denver, USA) provided with an Advanced Marianas™ Microscope with a 3i Axio Observer Z1 and a Plan-Apochromat 63×/1.4 NA oil immersion objective, M27 with DIC III Prism (Zeiss, Oberkochen, Germany). Spinning disc confocal images were recorded with an Orca Flash 4.0 sCMOS Camera (Hamamatsu Photonics, Hamamatsu, Japan) and imaging was supported by the Slidebook Software 5.5 (Intelligent Imaging Innovations, Inc., Denver, USA).

For the FRAP experiments, the FRAP tool of the Slidebook Software was used. To bleach the total ciliary GFP signal, the bleached area was selected manually, whereas for a bleach of ciliary parts a spherical area was chosen. Three-dimensional (3D) time lapse images of GFP fluorescence were taken of five planes and 0.6 μ m step size in 2 s or 3 s intervals for half cilium FRAP or 30 s for the total bleach and an exposition time of 100–250 ms. FRAP analysis was performed on maximum intensity projections of the z-stack. The total duration of each time-lapse was 3 min (90 time points) for partial cilium FRAP and 30 min (60 time points) for a total bleach. Pre-bleaching intensity was calculated based on the average of 2–4 time points acquired before bleaching. Bleaching of the selected area was conducted with 10 ms pulses from a 488 nm laser.

For the analysis of dynein-dependent movements, dynein inhibitor ciliobrevin D (Merck Calbiochem, Darmstadt, Germany) was dissolved in DMSO, diluted in CO₂ Independent Medium complemented with 2 mM L-glutamine to final concentrations of 30–50 μ M (concentration previously reported and validated by Firestone et al., 2012, and Ye et al., 2013) and added to the cells for varying incubation times between 3 min and 1 h 40 min. Varying concentrations between 30 μ M and 50 μ M ciliobrevin D and preincubation times between 20 min and 1 h 40 min were tested to have the same effects on the

behavior of GFP-INPP5E and Arl3-GFP in living cells. PDE6 δ inhibitor Deltazinone 1, dissolved in DMSO, was diluted in CO₂ Independent Medium with 2 mM L-glutamine to final concentrations of 5–30 μ M and added to the cells 30 min to 2 h 15 min prior to imaging. These variations in preincubation times and concentrations of Deltazinone 1 were tested to have similar effects on GFP-INPP5E in cells.

Analysis of microscopy data

Analysis of fluorescence microscopic images of immunostained cells was performed using CellProfiler (Carpenter et al., 2006) (Cambridge, USA; <http://cellprofiler.org>). Ratios of the GFP intensity in cilia relative to the mean GFP intensity in the whole cell body were calculated, which exhibit the enrichment of GFP-INPP5E(WT) or GFP-INPP5E(C644A) within the cilia. Data collection comprised 43 cells stably expressing GFP-INPP5E(WT) and 37 cells for GFP-INPP5E(C644A). Initially, cilia were stained using a primary antibody against mouse acetylated tubulin and a secondary anti-mouse antibody linked to Alexa Fluorophor 647 as described before. Single images of the cilia and the corresponding GFP fluorescence images of the GFP-tagged proteins were analyzed in CellProfiler using a macro which projects ciliary areas on the GFP image using the Alexa 647 fluorescence image as template. Ciliary areas were subtracted from the rest of the cell. The analysis results in relative fluorescence values for every single cilium and a mean fluorescence for the rest of the cell, which were used for the ratio calculation.

The velocity at which directional transport occurred was calculated by generating kymographs out of the bleached cilia over time. To assemble kymographs, rectangular regions of interest (ROI) comprising the entire cilia were aligned and plotted over time using Fiji/ImageJ (Schindelin et al., 2012) (Dresden, Germany and Zürich, Switzerland; <https://fiji.sc>). The unspecific movement of the analyzed cilium due to movements of the surrounding culture medium was reduced by alignment, using the plugin 'template matching/align slices in stack' (Tseng et al., 2011) (Grenoble and Saint Martin d'Herès, France; <https://sites.google.com/site/qingzongtseng/template-matching-ij-plugin>). A segmented line with a thickness of seven pixel was drawn along the cilium and by using the 'reslice' function the kymograph was generated. The velocity of the recovering signal was analyzed using the kymograph and the 'velocity measurement macro'. A straight line was drawn along the slope that resulted from the recovering fluorescence signal over time and the program revealed the velocity as number of pixel per time frame. This value, the pixel size and the time frame that was set in the experiment were used to calculate the final velocity in μ m per second. Eleven single cilia were analyzed to calculate the average velocity.

For the determination of the recovery rate the aligned file was used, generated as described above. Rectangular ROIs of the same size were placed on the aligned image at three different positions: at the ciliary GFP fluorescence signal in the bleached area, a non-bleached ciliary area and a background area outside of the cells. Using the ROI manager, all three ROIs were selected and mean gray values were measured for each time point. Raw data was processed in Excel (Microsoft Office, Redmond, USA), using the formula described in Supplementary Figure 3, including an internal control for photobleaching correction and additional baseline subtraction, modified from Chen and Huang (2001). The final relative fluorescence values were plotted against the time using the GraphPad Prism software (San Diego, USA).

Acknowledgments: AW acknowledges funding by the European Research Council (ERC Grant 268782) and Sonderforschungsbereich-DFG (SFB 642). We cordially thank Prof. Dr. A. Musacchio for the support provided throughout the project. We thank C. Koerner and J. A. Seidel for expert technical assistance, Dr. M. Lokaj for providing templates for plasmid generation and support in generation of stable cell lines, and Dr. E. Zent for CellProfiler analysis development. We are also very thankful to Prof. Dr. M. V. Nachury for providing the IMCD3 Flp-In system.

References

- Astle, M.V., Horan, K.A., Ooms, L.M., and Mitchell, C.A. (2007). The inositol polyphosphate 5-phosphatases: traffic controllers, waistline watchers and tumour suppressors? *Biochem. Soc. Symp.* **181**, 161–181.
- Avidor-Reiss, T., Maer, A.M., Koundakjian, E., Polyanovsky, A., Keil, T., Subramaniam, S., and Zuker, C.S. (2004). Decoding cilia function: defining specialized genes required for compartmentalized cilia biogenesis. *Cell* **117**, 527–539.
- Badano, J.L., Mitsuma, N., Beales, P.L., and Katsanis, N. (2006). The ciliopathies: an emerging class of human genetic disorders. *Annu. Rev. Genomics Hum. Genet.* **7**, 125–148.
- Berbari, N.F., O'Connor, A.K., Haycraft, C.J., and Yoder, B.K. (2009). The primary cilium as a complex signaling center. *Curr. Biol.* **19**, R526–R535.
- Besschetnova, T.Y., Roy, B., and Shah, J.V. (2009). Imaging intraflagellar transport in mammalian primary cilia. *Methods Cell Biol.* **93**, 331–346.
- Bielas, S.L., Silhavy, J.L., Brancati, F., Kisseleva, M.V., Al-Gazali, L., Sztriha, L., Bayoumi, R.A., Zaki, M.S., Abdel-Aleem, A., Rosti, O., et al. (2009). Mutations in the inositol polyphosphate-5-phosphatase E gene link phosphatidylinositol signaling to the ciliopathies. *Nat. Genet.* **41**, 1032–1036.
- Blacque, O.E., Perens, E.A., Boroevich, K.A., Inglis, P.N., Li, C., Warner, A., Khattri, J., Holt, R.A., Ou, G., Mah, A.K., et al. (2005). Functional genomics of the cilium, a sensory organelle. *Curr. Biol.* **15**, 935–941.
- Bloodgood, R.A. (1984). Preferential turnover of membrane proteins in the intact *Chlamydomonas* flagellum. *Exp. Cell Res.* **150**, 488–493.
- Breslow, D.K., Koslover, E.F., Seydel, F., Spakowitz, A.J., and Nachury, M.V. (2013). An in vitro assay for entry into cilia reveals unique properties of the soluble diffusion barrier. *J. Cell Biol.* **203**, 129–147.
- Cano, D.A., Murcia, N.S., Pazour, G.J., and Hebrok, M. (2004). Orpk mouse model of polycystic kidney disease reveals essential role of primary cilia in pancreatic tissue organization. *Dev. Dis.* **131**, 3457–3467.
- Cantagrel, V., Silhavy, J.L., Bielas, S.L., Swistun, D., Marsh, S.E., Bertrand, J.Y., Audollent, S., Attié-Bitach, T., Holden, K.R., Dobyns, W.B., et al. (2008). Mutations in the cilia gene ARL13B lead to the classical form of Joubert syndrome. *Am. J. Hum. Genet.* **83**, 170–179.

- Carpenter, A.E., Jones, T.R., Lamprecht, M.R., Clarke, C., Kang, I.H., Friman, O., Guertin, D.A., Chang, J.H., Lindquist, R.A., Moffat, J., et al. (2006). CellProfiler: image analysis software for identifying and quantifying cell phenotypes. *Genome Biol.* 7, R100.
- Caspary, T., Larkins, C.E., and Anderson, K.V. (2007). The graded response to sonic hedgehog depends on cilia architecture. *Dev. Cell* 12, 767–778.
- Chandra, A., Grecco, H.E., Pisupati, V., Perera, D., Cassidy, L., Skoulidis, F., Ismail, S.A., Hedberg, C., Hanzal-Bayer, M., Venkitaraman, A.R., et al. (2012). The GDI-like solubilizing factor PDE δ sustains the spatial organization and signalling of Ras family proteins. *Nat. Cell Biol.* 14, 329–329.
- Chávez, M., Ena, S., Van Sande, J., de Kerchove d'Exaerde, A., Schurmans, S., and Schiffmann, S.N. (2015). Modulation of ciliary phosphoinositide content regulates trafficking and sonic hedgehog signaling output. *Dev. Cell* 34, 338–350.
- Chen, D. and Huang, S. (2001). Nucleolar components involved in ribosome biogenesis cycle between the nucleolus and nucleoplasm in interphase cells. *J. Cell Biol.* 153, 169–176.
- Cole, D.G., Chinn, S.W., Wedaman, K.P., Hall, K., Vuong, T., and Scholey, J.M. (1993). Novel heterotrimeric kinesin-related protein purified from sea urchin eggs. *Nature* 366, 268–270.
- Cole, D.G., Diener, D.R., Himelblau, A.L., Beech, P.L., Fuster, J.C., and Rosenbaum, J.L. (1998). *Chlamydomonas* kinesin-II-dependent intraflagellar transport (IFT): IFT particles contain proteins required for ciliary assembly in *Caenorhabditis elegans* sensory neurons. *J. Cell Biol.* 141, 993–1008.
- Corbit, K.C., Aanstad, P., Singla, V., Norman, A.R., Stainier, D.Y.R., and Reiter, J.F. (2005). Vertebrate Smoothed functions at the primary cilium. *Nature* 437, 1018–1021.
- De Robertis, E. (1956). Morphogenesis of the retinal rods; an electron microscope study. *J. Biophys. Biochem. Cytol.* 2, 209–218.
- De Smedt, F., Boom, A., Pesesse, X., Schiffmann, S.N., and Erneux, C. (1996). Post-translational modification of human brain type I inositol 1,4,5-trisphosphate 5-phosphatase by farnesylation. *J. Biol. Chem.* 271, 10419–10424.
- Dharmaiah, S., Bindu, L., Tran, T.H., Gillette, W.K., and Frank, P.H. (2016). Structural basis of recognition of farnesylated and methylated KRAS4b by PDE δ . *Proc. Natl. Acad. Sci. USA* 113, E6766–E6775.
- Dutta, N. and Seo, S. (2016). RPGR, a prenylated retinal ciliopathy protein, is targeted to cilia in a prenylation- and PDE6D-dependent manner. *Biol. Open* 5, 1283–1289.
- Eggenschwiler, J.T. and Anderson, K.V. (2007). Cilia and developmental signaling. *Annu. Rev. Cell Dev. Biol.* 23, 345–373.
- Evans, R.J., Schwarz, N., Nagel-Wolfrum, K., Wolfrum, U., Hardcastle, A.J., and Cheetham, M.E. (2010). The retinitis pigmentosa protein RP2 links pericentriolar vesicle transport between the Golgi and the primary cilium. *Hum. Mol. Genet.* 19, 1358–1367.
- Fansa, E.K. and Wittinghofer, A. (2016). Sorting of lipidated cargo by the Arl2/Arl3 system. *Small GTPases* 7, 222–230.
- Fansa, E.K., O'Reilly, N.J., Ismail, S., and Wittinghofer, A. (2015). The N- and C-terminal ends of RPGR can bind to PDE6 δ . *EMBO Rep.* 16, 1583–1585.
- Fansa, E.K., Kösling, S.K., Zent, E., Wittinghofer, A., and Ismail, S. (2016). PDE6 δ -mediated sorting of INPP5E into the cilium is determined by cargo-carrier affinity. *Nat. Commun.* 7, 11366.
- Firestone, A.J., Weinger, J.S., Maldonado, M., Barlan, K., Langston, L.D., O'Donnell, M., Gelfand, V.I., Kapoor, T.M., and Chen, J.K. (2012). Small-molecule inhibitors of the AAA⁺ ATPase motor cytoplasmic dynein. *Nature* 484, 125–129.
- Florio, S.K., Prusti, R.K., and Beavo, J.A. (1996). Solubilization of membrane-bound rod phosphodiesterase by the rod phosphodiesterase recombinant δ subunit. *J. Biol. Chem.* 271, 24036–24047.
- Garcia-Gonzalo, F.R., Phua, S.C., Roberson, E.C., Garcia, G., Abedin, M., Schurmans, S., Inoue, T., and Reiter, J.F. (2015). Phosphoinositides regulate ciliary protein trafficking to modulate hedgehog signaling. *Dev. Cell* 34, 400–409.
- Gibbons, I.R. and Rowe, A.J. (1965). Dynein: a protein with adenosine triphosphatase activity from cilia. *Science* 149, 424–426.
- Goetz, S.C. and Anderson, K.V. (2010). The primary cilium: a signaling centre during vertebrate development. *Nat. Rev. Genet.* 11, 331–344.
- Gotthardt, K., Lokaj, M., Koerner, C., Falk, N., Giebl, A., and Wittinghofer, A. (2015). A G-protein activation cascade from Arl13B to Arl3 and implications for ciliary targeting of lipidated proteins. *eLife* 4, e11859.
- Grayson, C., Bartolini, F., Chapple, J.P., Willison, K.R., Bhamidipati, A., Lewis, S.A., Luthert, P.J., Hardcastle, A.J., Cowan, N.J., and Cheetham, M.E. (2002). Localization in the human retina of the X-linked retinitis pigmentosa protein RP2, its homologue cofactor C and the RP2 interacting protein Arl3. *Hum. Mol. Genet.* 11, 3065–3074.
- Hampshire, D.J., Ayub, M., Springell, K., Roberts, E., Jafri, H., Rashid, Y., Bond, J., Riley, J.H., and Woods, C.G. (2006). MORM syndrome (mental retardation, truncal obesity, retinal dystrophy and micropenis), a new autosomal recessive disorder, links to 9q34. *Eur. J. Hum. Genet.* 14, 543–548.
- Hanzal-Bayer, M., Renault, L., Roversi, P., Wittinghofer, A., and Hillig, R.C. (2002). The complex of Arl2-GTP and PDE δ : from structure to function. *EMBO J.* 21, 2095–2106.
- Haycraft, C.J., Banizs, B., Aydin-Son, Y., Zhang, Q., Michaud, E.J., and Yoder, B.K. (2005). Gli2 and Gli3 localize to cilia and require the intraflagellar transport protein polaris for processing and function. *PLoS Genet.* 1, e53.
- Hori, Y., Kobayashi, T., Kikko, Y., Kontani, K., and Katada, T. (2008). Domain architecture of the atypical Arf-family GTPase Arl13b involved in cilia formation. *Biochem. Biophys. Res. Commun.* 373, 119–124.
- Hu, Q. and Nelson, W.J. (2011). Ciliary diffusion barrier: the gatekeeper for the primary cilium compartment. *Cytoskeleton* 68, 313–324.
- Huangfu, D., Liu, A., Rakeman, A.S., Murcia, N.S., Niswander, L., and Anderson, K.V. (2003). Hedgehog signalling in the mouse requires intraflagellar transport proteins. *Nature* 426, 83–87.
- Humbert, M.C., Weihbrecht, K., Searby, C.C., Li, Y., Pope, R.M., Sheffield, V.C., and Seo, S. (2012). ARL13B, PDE6D, and CEP164 form a functional network for INPP5E ciliary targeting. *Proc. Natl. Acad. Sci. USA* 109, 19691–19696.
- Ismail, S.A., Chen, Y.-X., Rusinova, A., Chandra, A., Bierbaum, M., Gremer, L., Triola, G., Waldmann, H., Bastiaens, P.I.H., and Wittinghofer, A. (2011). Arl2-GTP and Arl3-GTP regulate a GDI-like transport system for farnesylated cargo. *Nat. Chem. Biol.* 7, 942–949.
- Ismail, S.A., Chen, Y.-X., Miertzschke, M., Vetter, I.R., Koerner, C., and Wittinghofer, A. (2012). Structural basis for Arl3-specific release of myristoylated ciliary cargo from UNC119. *EMBO J.* 31, 4085–4094.

- Jacoby, M., Cox, J.J., Gayral, S., Hampshire, D.J., Ayub, M., Blockmans, M., Pernot, E., Kisseleva, M. V, Compère, P., Schiffmann, S.N., et al. (2009). INPP5E mutations cause primary cilium signaling defects, ciliary instability and ciliopathies in human and mouse. *Nat. Genet.* 41, 1027–1031.
- Jaiswal, M., Fansa, E.K., Kösling, S.K., Mejuch, T., Waldmann, H., and Wittinghofer, A. (2016). Novel biochemical and structural insights into the interaction of myristoylated cargo with Unc119 protein and their release by Arl2/3. *J. Biol. Chem.* 291, 20766–20778.
- Jensen, V.L., Li, C., Bowie, R. V, Clarke, L., Mohan, S., Blacque, O.E., and Leroux, M.R. (2015). Formation of the transition zone by Mks5/Rpgrip1L establishes a ciliary zone of exclusion (CIZE) that compartmentalises ciliary signalling proteins and controls PIP2 ciliary abundance. *EMBO J.* 34, 2537–2556.
- Kozminski, K.G., Johnson, K.A., Forscher, P., and Rosenbaum, J.L. (1993). A motility in the eukaryotic flagellum unrelated to flagellar beating. *Cell Biol.* 90, 5519–5523.
- Kozminski, K.G., Beech, P.L., and Rosenbaum, J.L. (1995). The Chlamydomonas kinesin-like protein FLA10 is involved in motility associated with the flagellar membrane. *J. Cell Biol.* 131, 1517–1527.
- Lehtreck, K.F. (2015). IFT – cargo interactions and protein transport in cilia. *Trends Biochem. Sci.* 40, 765–778.
- Lee, J.-J. and Seo, S. (2015). PDE6D binds to the C-terminus of RPGR in a prenylation-dependent manner. *EMBO Rep.* 16, 1581–1582.
- Lin, Y.-C., Niewiadomski, P., Lin, B., Nakamura, H., Phua, S.C., Jiao, J., Levchenko, A., Inoue, T., Rohatgi, R., and Inoue, T. (2013). Chemically inducible diffusion trap at cilia reveals molecular sieve-like barrier. *Nat. Chem. Biol.* 9, 437–443.
- Linari, M., Hanzal-Bayer, M., and Becker, J. (1999). The delta subunit of rod specific cyclic GMP phosphodiesterase, PDE δ , interacts with the Arf-like protein Arl3 in a GTP specific manner. *FEBS Lett.* 458, 55–59.
- Liu, A., Wang, B., and Niswander, L.A. (2005). Mouse intraflagellar transport proteins regulate both the activator and repressor functions of Gli transcription factors. *Development* 132, 3103–3111.
- Lokaj, M., Kösling, S.K., Koerner, C., Lange, S.M., Van Beersum, S.E.C., Van Reeuwijk, J., Roepman, R., Horn, N., Ueffing, M., Boldt, K., et al. (2015). The interaction of CCDC104/BARTL1 with Arl3 and implications for ciliary function. *Structure* 23, 2122–2132.
- May-Simera, H.L. and Kelley, M.W. (2012). Cilia, Wnt signaling, and the cytoskeleton. *Cilia* 1, 1–16.
- Nachury, M.V., Seeley, E.S., and Jin, H. (2010). Trafficking to the ciliary membrane: how to get across the periciliary diffusion barrier? *Annu. Rev. Cell Dev. Biol.* 26, 59–87.
- Nancy, V., Callebaut, I., Marjou, A.El., and De Gunzburg, J. (2002). The δ subunit of retinal rod cGMP phosphodiesterase regulates the membrane association of Ras and Rap GTPases. *J. Biol. Chem.* 277, 15076–15084.
- Novarino, G., Akizu, N., and Gleeson, J.G. (2011). Modeling human disease in humans: the ciliopathies. *Cell* 147, 70–79.
- Nozaki, S., Katoh, Y., Terada, M., Michisaka, S., Funabashi, T., Takahashi, S., Kontani, K., and Nakayama, K. (2016). Regulation of ciliary retrograde protein trafficking by Joubert syndrome proteins ARL13B and INPP5E. *J. Cell Sci.* 3, 563–576.
- Ou, G., Blacque, O.E., Snow, J.J., Leroux, M.R., and Scholey, J.M. (2005). Functional coordination of intraflagellar transport motors. *Nature* 436, 583–587.
- Papke, B., Murarka, S., Vogel, H.A., Martín-Gago, P., Kovacevic, M., Truxius, D.C., Fansa, E.K., Ismail, S., Zimmermann, G., Heinelt, K., et al. (2016). Identification of pyrazolopyridazinones as PDE δ inhibitors. *Nat. Commun.* 7, 11360.
- Pazour, G.J. and Witman, G.B. (2003). The vertebrate primary cilium is a sensory organelle. *Curr. Opin. Cell Biol.* 15, 105–110.
- Rauchman, M.I., Nigam, S.K., Delpire, E., and Gullans, S.R. (1993). An osmotically tolerant inner medullary collecting duct cell line from an SV40 transgenic mouse. *Am. J. Physiol.* 265, F416–F424.
- Reiter, J.F., Blacque, O.E., and Leroux, M.R. (2012). The base of the cilium: roles for transition fibres and the transition zone in ciliary formation, maintenance and compartmentalization. *EMBO Rep.* 13, 608–618.
- Rohatgi, R. and Snell, W.J. (2010). The ciliary membrane. *Curr. Opin. Cell Biol.* 22, 541–546.
- Rosenbaum, J.L. and Witman, G.B. (2002). Intraflagellar transport. *Nat. Rev. Mol. Cell Biol.* 3, 813–825.
- Sang, L., Miller, J.J., Corbit, K.C., Giles, R.H., Brauer, M.J., Otto, E.A., Baye, L.M., Wen, X., Scales, S.J., Kwong, M., et al. (2011). Mapping the NPHP-JBTS-MKS protein network reveals ciliopathy disease genes and pathways. *Cell* 145, 513–528.
- Schindelin, J., Arganda-Carreras, I., Frise, E., Kaynig, V., Longair, M., Pietzsch, T., Preibisch, S., Rueden, C., Saalfeld, S., Schmid, B., et al. (2012). Fiji: an open-source platform for biological-image analysis. *Nat. Methods* 9, 676–682.
- Schmick, M., Vartak, N., Papke, B., Kovacevic, M., Truxius, D.C., Rossmannek, L., and Bastiaens, P.I.H. (2014). KRas localizes to the plasma membrane by spatial cycles of solubilization, trapping and vesicular transport. *Cell* 157, 459–471.
- Schmick, M., Kraemer, A., and Bastiaens, P.I.H. (2015). Ras moves to stay in place. *Trends Cell Biol.* 25, 190–197.
- Schneider, L., Clement, C.A., Teilmann, S.C., Pazour, G.J., Hoffmann, E.K., Satir, P., and Christensen, S.T. (2005). PDGFR α signaling is regulated through the primary cilium in fibroblasts. *Curr. Biol.* 15, 1861–1866.
- Scholey, J.M. (2003). Intraflagellar transport. *Annu. Rev. Cell Dev. Biol.* 19, 423–443.
- Simons, M., Gloy, J., Ganner, A., Bullerkotte, A., Bashkurov, M., Krönig, C., Schermer, B., Benzing, T., Cabello, O.A., Jenny, A., et al. (2005). Inversin, the gene product mutated in nephronophthisis type II, functions as a molecular switch between Wnt signaling pathways. *Nat. Genet.* 37, 537–543.
- Sorokin, S.P. (1968). Reconstructions of centriole formation and ciliogenesis in mammalian lungs. *J. Cell Sci.* 3, 207–230.
- Thomas, S., Wright, K.J., Le Corre, S., Micalizzi, A., Romani, M., Abhyankar, A., Saada, J., Perrault, I., Amiel, J., Litzler, J., et al. (2014). A homozygous PDE6D mutation in Joubert syndrome impairs targeting of farnesylated INPP5E protein to the primary cilium. *Hum. Mutat.* 35, 137–146.
- Torres, J.Z., Miller, J.J., and Jackson, P.K. (2009). High-throughput generation of tagged stable cell lines for proteomic analysis. *Proteomics* 9, 2888–2891.
- Travaglini, L., Brancati, F., Silhavy, J., Iannicelli, M., Nickerson, E., Elkhartoufi, N., Scott, E., Spencer, E., Gabriel, S., Thomas, S., et al. (2013). Phenotypic spectrum and prevalence of INPP5E

- mutations in Joubert syndrome and related disorders. *Eur. J. Hum. Genet.* **21**, 1074–1078.
- Tseng, Q., Wang, I., Duchemin-Pelletier, E., Azioune, A., Carpi, N., Gao, J., Filhol, O., Piel, M., Théry, M., and Balland, M. (2011). A new micropatterning method of soft substrates reveals that different tumorigenic signals can promote or reduce cell contraction levels. *Lab Chip* **11**, 2231–2240.
- Van Valkenburgh, H., Shern, J.F., Sharer, J.D., Zhu, X., and Kahn, R.A. (2001). ADP-ribosylation factors (ARFs) and ARF-like 1 (ARL1) have both specific and shared effectors: characterizing ARL1-binding proteins. *J. Biol. Chem.* **276**, 22826–22837.
- Veltel, S., Gasper, R., Eisenacher, E., and Wittinghofer, A. (2008). The retinitis pigmentosa 2 gene product is a GTPase-activating protein for Arf-like 3. *Nat. Struct. Mol. Biol.* **15**, 373–380.
- Waters, A.M. and Beales, P.L. (2011). Ciliopathies: An expanding disease spectrum. *Pediatr. Nephrol.* **26**, 1039–1056.
- Wheatley, D. (1995). Primary cilia in normal and pathological tissues. *Pathobiology* **63**, 222–238.
- Wheatley, D.N., Wang, A.M., and Strugnell, G.E. (1996). Expression of primary cilia in mammalian cells. *Cell Biol. Int.* **20**, 73–81.
- Williams, C.L., Li, C., Kida, K., Inglis, P.N., Mohan, S., Semenec, L., Bialas, N.J., Stupay, R.M., Chen, N., Blacque, O.E., et al. (2011). MKS and NPHP modules cooperate to establish basal body/transition zone membrane associations and ciliary gate function during ciliogenesis. *J. Cell Biol.* **192**, 1023–1041.
- Wright, K.J., Baye, L.M., Olivier-Mason, A., Mukhopadhyay, S., Sang, L., Kwong, M., Wang, W., Pretorius, P.R., Sheffield, V.C., Sengupta, P., et al. (2011). An ARL3-UNC119-RP2 GTPase cycle targets myristoylated NPHP3 to the primary cilium. *Genes Dev.* **25**, 2347–2360.
- Ye, F., Breslow, D.K., Koslover, E.F., Spakowitz, A.J., Nelson, W.J., and Nachury, M. V. (2013). Single molecule imaging reveals a major role for diffusion in the exploration of ciliary space by signaling receptors. *eLife* **2**, e00654.
- Zhang, H., Liu, X.H., Zhang, K., Chen, C.K., Frederick, J.M., Prestwich, G.D., and Baehr, W. (2004). Photoreceptor cGMP phosphodiesterase δ subunit (PDE δ) functions as a prenyl-binding protein. *J. Biol. Chem.* **279**, 407–413.
- Zhang, H., Li, S., Doan, T., Rieke, F., Detwiler, P.B., Frederick, J.M., and Baehr, W. (2007). Deletion of PrBP/ δ impedes transport of GRK1 and PDE6 catalytic subunits to photoreceptor outer segments. *Proc. Natl. Acad. Sci. USA* **104**, 8857–8862.
- Zhou, C., Cunningham, L., Marcus, A.I., Li, Y., and Kahn, R.A. (2006). ARL2 and ARL3 regulate different microtubule-dependent processes. *Mol. Biol. Cell* **17**, 2476–2487.
- Zimmermann, G., Papke, B., Ismail, S., Vartak, N., Chandra, A., Hoffmann, M., Hahn, S.A., Triola, G., Wittinghofer, A., Bastiaens, P.I.H., et al. (2013). Small molecule inhibition of the KRAS-PDE δ interaction impairs oncogenic KRAS signalling. *Nature* **497**, 638–642.

Supplemental Material: The online version of this article offers supplementary material (<https://doi.org/10.1515/hsz-2017-0226>).

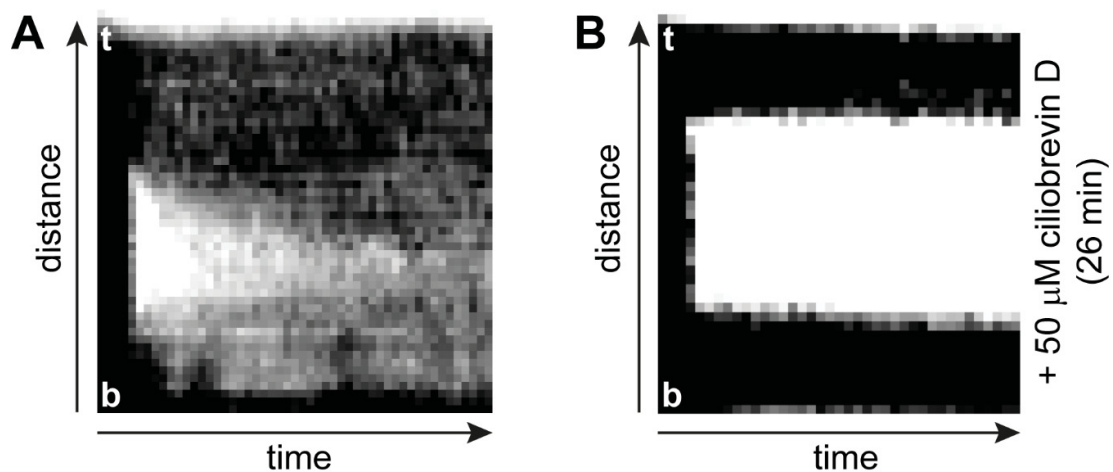
Supplementary Material

Mechanism and dynamics of INPP5E transport into and inside the ciliary compartment

Stefanie Kristine Kösling, Eyad Kalawy Fansa, Stefano Maffini and Alfred Wittinghofer

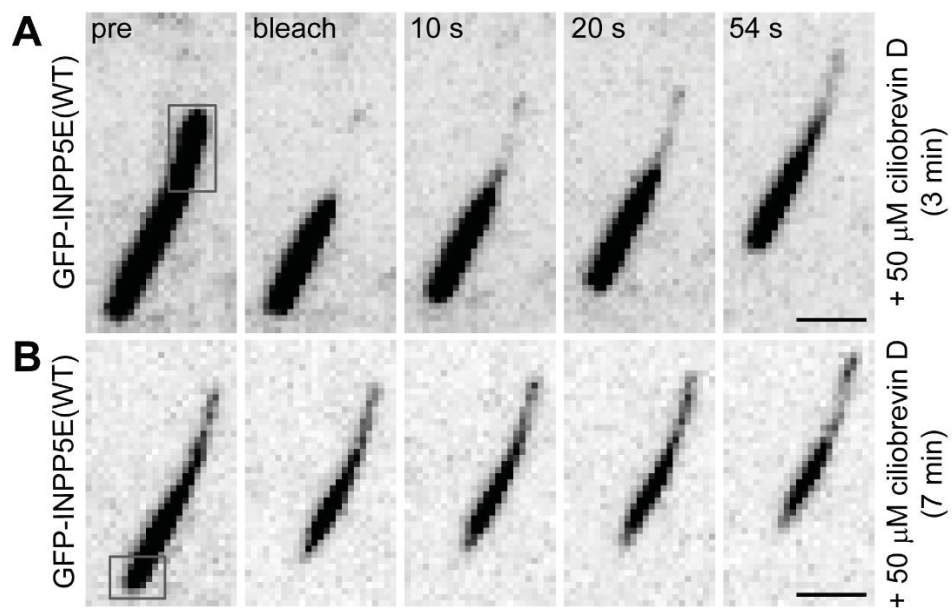
Declaration: Reprinted (adapted) with permission from
Copyright © 2018, Walter de Gruyter GmbH
<https://doi.org/10.1515/hsz-2017-0226>

Supplementary Figures



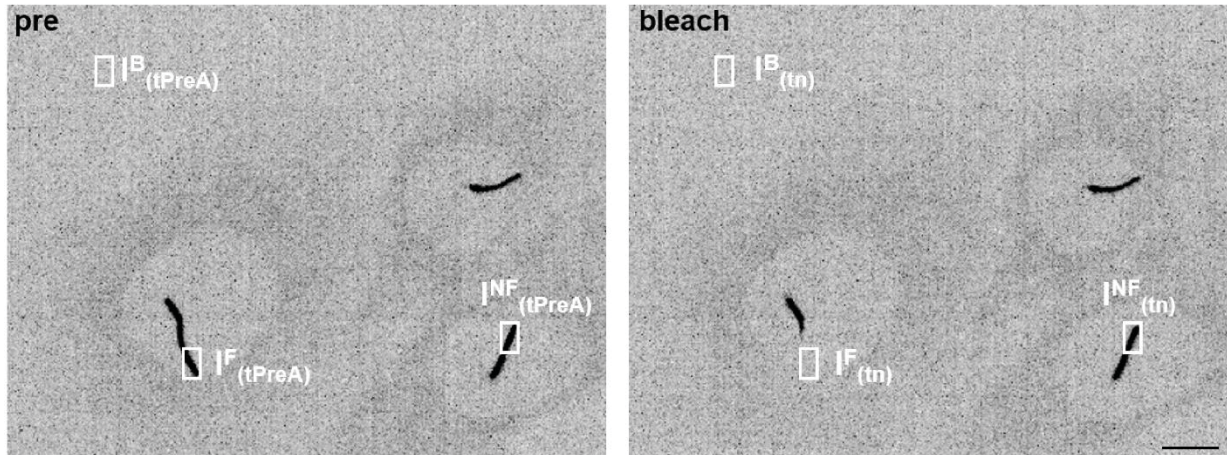
Supplementary Figure 1: Transport of INPP5E in anterograde and retrograde direction illustrated in a single cilium.

Kymographs generated from FRAP experiments after bleaching the middle region of the ciliary GFP-INPP5E(WT) fluorescence of (A) untreated cells or (B) after preincubation for 26 min with 50 μ M ciliobrevin D.



Supplementary Figure 2: Innciliary transport of INPP5E after short treatment with Ciliobrevin D.

Fluorescence recovery after partial bleach of the ciliary fluorescence of GFP-INPP5E(WT). Time lapses of the same cilium after bleaching the signal (A) at the tip and 3 min preincubation or (B) at the base and 7 min preincubation with 50 μ M ciliobrevin D. Scale bars indicate 2 μ m.



$$I_{(tn)} = ((I^F_{(tn)} - I^B_{(tn)}) / (I^{NF}_{(tn)} - I^B_{(tn)})) / ((I^F_{(PreA)} - I^B_{(PreA)}) / (I^{NF}_{(PreA)} - I^B_{(PreA)}))$$

$I_{(tn)}$ = mean fluorescence intensity for timepoint n

$I^F_{(tn)}$ = mean fluorescence intensity for the FRAPped region of interest (ROI), for timepoint n

$I^{NF}_{(tn)}$ = mean fluorescence intensity for the not FRAPped ROI, for timepoint n

$I^B_{(tn)}$ = mean fluorescence intensity for the baseline background ROI, for timepoint n

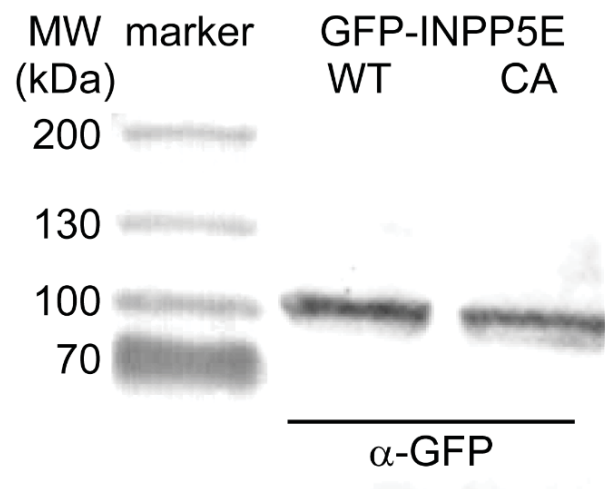
$I^F_{(PreA)}$ = mean fluorescence intensity for the FRAPped ROI before bleaching (average of 4 timepoints)

$I^{NF}_{(PreA)}$ = mean fluorescence intensity for the not FRAPped ROI before bleaching (average of 4 timepoints)

$I^B_{(PreA)}$ = mean fluorescence intensity for the baseline background ROI before bleaching (average of 4 timepoints)

Supplementary Figure 3: Analysis of FRAP data.

Exemplary image showing localization of GFP-INPP5E(WT) before (left panel) and after partial bleaching (right panel) of the ciliary fluorescence during a FRAP experiment. Scale bar indicates 5 μ m. Mean fluorescence intensities for images of the time lapse were processed according to the formula shown, including correction for photobleaching and background. The data were plotted against the time as shown in the Figures 4C,G (method modified from Chen and Huang, 2001).



Supplementary Figure 4: Expression levels of wild type and CaaX box mutant INPP5E.

Lysates of stable cell lines expressing GFP-INPP5E(WT) or GFP-INPP5E(C644A) with the same total protein concentrations were analyzed by SDS-PAGE and immunoblotting using an antibody against GFP (1:500; Santa Cruz Biotechnology sc-9996). The cell lines show similar expression levels of either wild type or mutant INPP5E.

Supplementary Video Material

Video 1: FRAP experiment in IMCD3 cells after bleaching the complete ciliary fluorescence of GFP-INPP5E(WT).

Video 2: FRAP after bleaching the complete ciliary fluorescence of GFP-INPP5E(WT), after 21 min preincubation with 50 μ M ciliobrevin D.

Video 3: FRAP after bleaching the complete ciliary fluorescence of GFP-INPP5E(WT), after 1 h 24 min preincubation with 5 μ M Deltazinone 1.

Video 4: FRAP after bleaching the complete ciliary fluorescence of Arl3-GFP.

Video 5: FRAP after bleaching the complete ciliary fluorescence of Arl3-GFP, after 1 h 40 min preincubation with 30 μ M ciliobrevin D.

Video 6: FRAP after bleaching the fluorescence of GFP-INPP5E(WT) at the ciliary tip region.

Video 7: FRAP after bleaching the fluorescence of GFP-INPP5E(WT) at the tip region, after 1 h 20 min preincubation with 50 μ M ciliobrevin D.

Video 8: GFP-INPP5E(WT) FRAP after bleaching the fluorescence at the tip region, after 2 h 15 min preincubation with 30 μ M Deltazinone 1.

Video 9: FRAP after bleaching the fluorescence of GFP-INPP5E(C644A) at the tip region.

Video 10: FRAP after bleaching the fluorescence of GFP-INPP5E(C644A) at the base region, after 15 min preincubation with 50 μ M ciliobrevin D.

Video 11: FRAP after bleaching the complete ciliary fluorescence of GFP-INPP5E(C644A).

These were the main conclusions from this publication

- A normal localization of INPP5E to cilia depends on its farnesylation, and PDE6 δ and the dynein system are crucial for ciliary sorting and entry of INPP5E.
- The innerciliary transport of INPP5E is mediated by the IFT system and independent from its farnesylation or PDE6 δ activity.
- The INPP5E CaaX box mutant accumulates at centrioles and enters cilia by an affinity trap mechanism that for the wild type is overcome by the interaction with PDE6 δ .
- A three-step mechanism was postulated to regulate INPP5E ciliary localization and consists of PDE6 δ - and farnesylation-mediated targeting, diffusion of the INPP5E-PDE6 δ complex into the cilium with transfer to the IFT system, and innerciliary retention.
- Arl3 moves into and within cilia by diffusion and independently of dynein/IFT.

6 Discussion

Transport processes of ciliary proteins are highly regulated, and their sorting and retention mechanisms mostly remain unclear. Arl2 and Arl3 act as GTP-dependent release factors for lipidated cargo proteins from PDE6 δ and Unc119a/b (Linari et al., 1999; Sharer and Kahn, 1999; Van Valkenburgh et al., 2001; Hanzal-Bayer et al., 2002; Kobayashi et al., 2003; Wright et al., 2011; Jaiswal et al., 2016) and were found to be involved in the cellular sorting of lipidated proteins. Despite Arl2 and Arl3 sharing a high degree of similarity, Arl3 exclusively localizes to the primary cilium (Avidor-Reiss et al., 2004; Zhou et al., 2006; Lokaj et al., 2015). The ciliary compartment was described as an Arl3•GTP domain due to the findings that the Arl3 GEF Arl13B is only found in the cilium, whereas the GAP RP2 is localized in the cytosol and accumulates around the basal body (my data, master thesis, 2013) (Grayson et al., 2002; Caspary et al., 2007; Veltel et al., 2008a; Gotthardt et al., 2015; Lokaj et al., 2015; Fansa and Wittinghofer, 2016).

This thesis focuses on the localization and transport processes of lipidated cargo proteins of PDE6 δ and Unc119a/b, and of Arl3, using cell biological techniques. In particular, the ciliary transport of the farnesylated PDE6 δ cargo protein INPP5E and of the myristoylated Unc119a/b cargo NPHP3 was analyzed. This work is based on four peer-reviewed publications.

6.1 The interaction of CCDC104/BARTL1 with Arl3 and implications for ciliary function

The first paper focuses on Arl3 and the CCDC104/BARTL1 protein. The ciliary and cytosolic localization of Arl3 and the exclusion of Arl2 from cilia were confirmed in IMCD3 cells, as shown by GFP fluorescence and immunofluorescence microscopy. Besides the axonemal localization, Arl3 is enriched in the ciliary transition zone and in the basal body region. The major structural difference between Arl2 and Arl3 is located in the N-terminal amphipathic helix and it was assumed that the amphipathic helix of Arl3 determines its ciliary localization. Indeed, the ciliary localization of a truncation variant of Arl3 that lacks the N-terminal helix (17 amino acid residues) was completely abrogated. However, the Arl3 helix alone was shown to be not sufficient as ciliary targeting signal, because a chimeric protein of Arl2, where the Arl2 N-terminal helix was exchanged against the Arl3 helix, did not localize to cilia (Lokaj et al., 2015). A further important difference between Arl3 and Arl2 is their membrane interaction

behavior with respect to the nucleotide loading state. Arl3 and other Arf proteins interact with membranes via their amphipathic helix, which kinks out in the GTP-bound state. However, the interaction of Arl2 with membranes is independent of the bound nucleotide. Thus, it was suggested that after activation due to exchange to GTP, Arl3 develops a new affinity to the ciliary membrane and that this might be the reason for its ciliary localization (Kapoor et al., 2015). Taken together, the N-terminal helix is essential but not sufficient for ciliary localization of Arl3. It is possible that the entire protein sequence is needed to target Arl3 to cilia, and/or that the protein contains a specific retention signal apart from the N-terminus. Further experiments are required to elucidate the determinant of Arl3 ciliary localization in contrast to Arl2 in more detail. For example, different truncation mutants of Arl3 in presence of the N-terminal helix could be analyzed according to their ciliary localization to find more ciliary targeting sequences besides the helix.

CCDC104, which was discovered as new binding partner of Arl3 (and Arl2) and as a BART-like effector (Mandy Lokaj), was identified as ciliary protein that accumulates, similar to Arl3, in the transition zone. The interaction of CCDC104 and Arl3 was examined by crystal structure determination of a complex between CCDC104 (1-133) and Arl3•GppNHp (PDB: 4ZI2), showing that the Arl3 N-terminal helix has a conserved LLxILxxL (L = leucine, I = isoleucine, x = any amino acid) motif which mediates the interaction with CCDC104. The interaction is drastically weakened when the Arl3 N-terminus is deleted. Structure alignment revealed that CCDC104 contains an N-terminal BART-like domain (amino acid residues 1-133) (Mandy Lokaj). The BART-like domain itself is not able to enter cilia, shown by GFP fluorescence of a truncated protein. This leads to the conclusion that either the complete protein structure is required for ciliary entry or that a ciliary targeting signal might be located in the middle or C-terminal region of CCDC104.

Two Arl3 mutants, L4D (L = leucine, D = aspartate) and F51A (F = phenylalanine, A = alanine), that show an interaction with CCDC104 weaker than the wild type, were analyzed for their ciliary localization. Mutation of phenylalanine 51 leads to an approximately 100-fold reduction of Arl3 affinity towards CCDC104, whereas the mutation of leucine 4 leads to a ten-fold affinity reduction (Mandy Lokaj). In cells, Arl3 L4D fails to localize to cilia, whereas the F51A mutant unexpectedly is still able to enter cilia. The mutation of leucine 4, that is part of the amphipathic helix, might disturb a possible interaction of Arl3 with membranes, which is mediated by this helix. Thus, it was concluded that the interaction between Arl3 and CCDC104 does not mediate the ciliary localization of Arl3. To analyze this in more detail, knockdown experiments using siRNAs were conducted. Arl3 knockdown did not show any effect on CCDC104 ciliary

localization. Similarly, knockdown of CCDC104 did not impact localization of Arl3. This led to the conclusion that Arl3 and CCDC104 do not depend on each other for ciliary entry (Lokaj et al., 2015). Nevertheless, it should be considered that in contrast to a knockout a knockdown is not complete and that the small remaining portion of the protein could still rescue the knockdown. Further cell biological experiments, for example using the CRISPR/Cas9 system to generate a knockout of either Arl3 or CCDC104 genes, will be required. However, an Arl3 knockout might interfere with a normal cilia formation and create difficulties to execute this experiment, as Arl3 deletion in mice was shown to lead to phenotypes which resemble that of Joubert and Bardet-Biedl syndromes (Hanke-Gogokhia et al., 2016).

Two possible not mutually exclusive functions of the Arl3-CCDC104 interaction were discussed. Arl3•GTP is expected to localize inside the ciliary compartment and it was shown before that the N-terminal helix and the loaded nucleotide decide about the binding of Arl3 to membranes. Because CCDC104 among other contact sites interacts with the N-terminus of GTP-bound Arl3, which is thought to interact with membranes, it was proposed that CCDC104 might reduce or inhibit the interaction of Arl3•GTP with membranes. This could lead to a preferential hydrolysis of Arl3-bound GTP mediated by the GAP RP2 outside of the cilium in the basal body region. A superimposition of the structure of the Arl3-CCDC104 (1-133) complex (PDB: 4ZI2) (Lokaj et al., 2015) with the structure of a complex between Arl3 D129N (D = aspartate, N = asparagine) and RP2 (PDB: 3BH6) (Veltel et al., 2008a), revealed the possibility of a triple complex formation between CCDC104, Arl3 and RP2. Because an addition of RP2 to the complex of Arl3•GppNHp and CCDC104 (1-133) resulted in complex dissociation, the assumed triple complex would probably be only transient. It was supposed that Arl3 is displaced from CCDC104 and an Arl3•GppNHp-RP2 complex is formed. It was tested that CCDC104 does not have an effect on either the RP2-mediated or the intrinsic GTP hydrolysis of Arl3 (Mandy Lokaj). However, the fact that CCDC104 localizes in the transition zone above the RP2 region around the basal body could trigger the exit of the complex of Arl3•GTP with CCDC104 from the ciliary compartment to the basal body region and subsequent RP2 assisted hydrolysis of GTP.

Assuming the ciliary compartment as an Arl3•GTP domain and the possible roles of CCDC104 described herein, the interaction of Arl3 and CCDC104 might support the creation of an energetic driving force for ciliary localization of PDE6 δ /Unc119a/b cargo proteins (Lokaj et al., 2015). Further biochemical and cell biological experiments will be required to elucidate the cellular and ciliary functions of CCDC104 and the corresponding mechanisms of the interaction with Arl3 and possible further interaction partners in more detail. For instance, phenotypic cell

analyses after a complete knockout of CCDC104 would be interesting, especially with a focus on the localization and trafficking of Arl3 and of PDE6 δ /Unc119a/b cargo proteins. The biochemical measurements and the structure determination of CCDC104, that comprise mainly the BART-like domain, could be expanded to experiments with the full length CCDC104 protein to get an insight in the role of the C-terminal domain.

6.2 PDE6 δ -mediated sorting of INPP5E into the cilium is determined by cargo-carrier affinity

The cellular sorting of farnesylated cargo proteins of PDE6 δ , either to the ciliary membrane or to other inner membranes, was analyzed with a focus on the molecular details of the cargo-carrier interaction, and the biochemical results were tested in cells (Fansa et al., 2016). It was known that both INPP5E and Rheb are farnesylated proteins that bind to the hydrophobic pocket of PDE6 δ via the farnesyl moiety (Hanzal-Bayer et al., 2002; Zhang et al., 2004; Ismail et al., 2011). However, the cargo proteins localize to different membrane compartments. INPP5E almost exclusively localizes to cilia, whereas Rheb is found at endomembranes. Because PDE6 δ is known as shuttling factor of prenylated proteins, the question about the sorting process to different membrane compartments was raised. Fluorescence polarization measurements of PDE6 δ and farnesylated peptides of INPP5E or Rheb revealed a striking difference of the affinities of 100-fold of INPP5E and Rheb towards PDE6 δ . INPP5E has a high affinity towards PDE6 δ in the low nanomolar range, whereas Rheb is a low affinity binder with an affinity in the submicromolar range (Eyad Fansa).

To understand the determinants of the affinity difference on the molecular level, crystal structures of PDE6 δ in complex with farnesylated peptides of INPP5E (PDB: 5F2U) or Rheb (PDB: 3T5G) were solved and compared. It was found, that the -1 and -3 positions relative to the farnesylated cysteine of the cargo protein were decisive for high or low affinity (Eyad Fansa). Further biochemical and cell biological experiments showed these positions and the level of affinity towards PDE6 δ to determine the sorting of the farnesylated protein. Therefore, the -1 and -3 positions might act as ciliary targeting signals, albeit further signals cannot be excluded. Swapping of the amino acids at these positions in INPP5E from high to low affinity determinants resulted in biochemically measurable lower affinity (Eyad Fansa) and to mislocalization of mutant low affinity INPP5E to the cytosol combined with a much weaker ciliary localization. Also, swapping the correspondent positions in Rheb to high affinity

residues led to a partial ciliary localization of mutated Rheb, whereas the wild type was excluded from cilia (Fansa et al., 2016). These findings are in line with experiments showing that after deletion of PDE6 δ , GRK1 with a high affinity towards PDE6 δ mislocalizes, whereas the transducin γ -subunit T γ with a low affinity shows an almost normal localization (Zhang et al., 2007).

Furthermore, it was shown by fluorescence polarization measurements that INPP5E is only released from PDE6 δ by Arl3•GTP, whereas Rheb is released by both Arl3•GTP or Arl2•GTP (Eyad Fansa). The importance of the Arl3 specific release of INPP5E to cilia was confirmed by knockdown experiments in cells stably expressing GFP-INPP5E using specific siRNAs against Arl3, resulting in a loss of the exclusive ciliary localization of INPP5E (Fansa et al., 2016). This result contrasts with results by Humbert et al. and Thomas et al., who claimed that a knockdown of Arl3 would not have any effect on INPP5E localization (Humbert et al., 2012; Thomas et al., 2014). However, these contrasting results could be explained by an analysis of INPP5E localization with different parameters. Humbert et al. and Thomas et al. only focused on INPP5E positive cilia, neglecting the cytosolic portion after the knockdown. However, an analysis of the ratio of INPP5E localization in cilia relative to the cytosolic localization as shown in Fansa et al. (2016) revealed an obvious mislocalization of INPP5E after Arl3 downregulation.

Collectively, this paper showed that INPP5E with high affinity to PDE6 δ is sorted to the ciliary compartment, where it is released by ciliary Arl3•GTP. The low affinity binder Rheb is released outside of cilia at endomembranes by cytoplasmic Arl2•GTP. The PDE6 δ -dependent sorting mechanism of farnesylated proteins to different membrane compartments was summed up in a three-step model, composed of cargo-carrier binding, specific cargo release and retention. It was postulated that this newly described sorting principle might be a general principle for the sorting of farnesylated cargo proteins to their individual membrane destination. The affinity towards PDE6 δ , the specific release by Arl2 or Arl3 and unknown retention signals were supposed to be responsible for the sorting and accumulation of farnesylated proteins at specific membranes (Fansa et al., 2016).

The results about the PDE6 δ -mediated sorting of INPP5E exhibit analogies to studies about the PDE6 δ -mediated localization of prenylated Ras proteins. It was known that PDE6 δ regulates the membrane association of Ras and Rap proteins, independently of their nucleotide state, by solubilizing them from membranes (Nancy et al., 2002). Moreover, PDE6 δ was shown to maintain the dynamic distribution of K-Ras and H-Ras over intracellular membranes. Due to

binding of the Ras protein, PDE6 δ solubilizes it and thereby increases its cytoplasmic diffusion. Polycationic Ras proteins are more effectively trapped at the plasma membrane and depalmitoylated Ras proteins are trapped at the Golgi. Thus, PDE6 δ enhances the H-/K-Ras signaling due to enrichment of Ras at the plasma membrane (Chandra et al., 2012; Philips, 2012; Schmick et al., 2014, 2015). The Arl2/3-mediated cargo release from PDE6 δ was initially shown for farnesylated Rheb and K-Ras (Ismail et al., 2011; Schmick et al., 2014).

The publication by Fansa et al. (2016) gave new insights to the sorting mechanism of INPP5E to cilia in the context of PDE6 δ and brought clarity into former discrepancies in the literature. In the study by Humbert et al. it was claimed that a C-terminal truncated MORM-related mutant INPP5E, that cannot interact with PDE6 δ , would have a normal ciliary localization (Humbert et al., 2012). However, the results by Fansa et al. are in line with two former studies by Jacoby et al. and Thomas et al. Both studies highlight the importance of the farnesylated C-terminus of INPP5E for the localization to cilia, shown by mislocalization of the MORM truncation mutant (Jacoby et al., 2009; Thomas et al., 2014). Furthermore, the INPP5E CaaX box mutant lost the ciliary enrichment and accumulated in the transition zone. These findings already suggested a connection between INPP5E ciliary localization and PDE6 δ , because INPP5E interacts with PDE6 δ via the farnesylated C-terminus. This was shown in an immunoprecipitation assay, where the CaaX box mutant fails to interact with PDE6 δ (Thomas et al., 2014).

To support the findings described here and to study the localization and role of INPP5E in cilia, it was suggested to test in living cells small molecules that might inhibit PDE6 δ and thus the interaction with farnesylated cargo, especially INPP5E. This was done with the experiments presented in the fourth publication and will be discussed there.

6.3 Novel biochemical and structural insights into the interaction of myristoylated cargo with Unc119 protein and their release by Arl2/3

Because Unc119a/b are homologs of PDE6 δ and bind to myristoylated proteins via their hydrophobic pocket, the question was if a similar or resembling principle as described for the sorting of farnesylated proteins by PDE6 δ could be found for the sorting of myristoylated proteins by Unc119a/b. To answer this question, biochemical and structural experiments were conducted (Mamta Jaiswal) and were verified by cell biological experiments (Jaiswal et al., 2016).

In former studies, affinity measurements of myristoylated NPHP3-, GNAT-1- and Src- peptides

to Unc119a or Unc119b were already performed (Wright et al., 2011; Zhang et al., 2011; Ismail et al., 2012; Mejuch et al., 2015). In the study by Jaiswal et al., myristoylated peptides of the ciliary proteins NPHP3, Cystin1 and GNAT-1 (Tao et al., 2009; Shiba et al., 2010; Zhang et al., 2011), and of the non-ciliary proteins RP2 and Src kinase were analyzed for their affinities towards Unc119 proteins. For the NPHP3, Cystin1 and GNAT-1 peptides, high affinities in the picomolar to low nanomolar range were found. However, the Src peptide has a submicromolar and thus low affinity and is not known to have any relation to the ciliary compartment (Jaiswal et al., 2016). For a myristoylated peptide of RP2, that localizes around the basal body without entering cilia, an intermediate affinity in the double-digit nanomolar range was determined (Mamta Jaiswal) (Grayson et al., 2002; Lokaj et al., 2015; Jaiswal et al., 2016). These results about Unc119a/b cargo resemble the findings about PDE6 δ cargo proteins, revealing that high affinity cargo localizes to cilia.

Furthermore, it was asked whether the Arl3•GTP specific release of high affinity ciliary proteins as observed for farnesylated proteins from PDE6 δ could also be applied to the release of myristoylated proteins from Unc119a/b. Indeed, it was shown earlier that NPHP3 and Cystin1 were specifically released from Unc119a by Arl3•GTP, but not Arl2•GTP (Wright et al., 2011; Ismail et al., 2012). Here, it was also found using fluorescence polarization that the peptides with high affinity, such as NPHP3 and Cystin1, were only released by Arl3•GTP, but low affinity peptides by both Arl2•GTP and Arl3•GTP. Excluded from this is the high affinity GNAT-1 peptide. Arl2 releases it at least partially from Unc119b, but not from Unc119a. The reason could be a lower affinity of GNAT-1 to Unc119b, which was found to be 10-fold lower with respect to that to Unc119a (Mamta Jaiswal).

Unc119 proteins bind to myristoylated ciliary proteins with higher affinities than to Arl3. Thus, for Arl3•GTP to release this cargo from Unc119a/b requires a high concentration within cilia, which is likely to persist in the exclusive localization of Arl3•GTP within this small compartment. Furthermore, a retention signal of the ciliary proteins, provided by the ciliary membrane or other ciliary proteins, might support a complete release. The differentiation between high and low affinity Unc119a/b cargo in context with the cargo localization was a novel finding and the working hypothesis of being a parallel system to PDE6 δ -mediated sorting of farnesylated proteins could be confirmed.

A crystal structure of Unc119a (58-240) with a myristoylated high affinity NPHP3 peptide (PDB: 5L7K) revealed that the +2 and +3 positions relative to the myristoylated glycine seem to determine the high affinity and might be involved in ciliary sorting (Mamta Jaiswal). This was underlined by cell biological experiments, showing a mutant NPHP3 construct, where the

+2 and +3 positions were swapped to low affinity residues. Such a construct partially mislocalized to the cytosol. That a partial ciliary localization still exists might result from unknown additional targeting or a retention signal in NPHP3, as also supposed for INPP5E before. Therefore, the +2 and +3 positions were suggested to be important in the distinction of low and high affinities of myristoylated proteins to Unc119a/b and to be decisive for ciliary sorting of high affinity cargo. A similar binding mode of Unc119a and Unc119b to myristoylated proteins can be expected, because the residues in the hydrophobic pockets of the Unc119 proteins are conserved (Jaiswal et al., 2016).

These results were an important step towards understanding the sorting principle of myristoylated proteins. However, more experiments are required to support the hypothesized mechanism leading to ciliary localization of NPHP3 and other ciliary cargo proteins in more detail. For example, structural and cell biological localization studies as shown here for Unc119a and an NPHP3 peptide, could be repeated for other ciliary cargo proteins, such as Cystin1. Moreover, localization analyses of low affinity cargo after swapping the +2 and +3 positions to that of high affinity ones, as shown for Rheb in the study by Fansa et al. (2016), could confirm the hypothesis by Jaiswal et al. It should be mentioned for NPHP3 that, besides the high affinity towards Unc119a/b mediated by the +2 and +3 positions, also the myristoylation and N-terminal coiled-coil domains of NPHP3 are known to control its ciliary targeting (Nakata et al., 2012). Furthermore, the dynamics of NPHP3 and Cystin1 could be examined in living cells, for example, if the ciliary entry and innerciliary transport depend on the IFT system as it was shown for INPP5E using ciliobrevin D (Kösling et al., 2018). Also, an inhibition of Unc119 proteins in living cells and the effects on NPHP3 and Cystin1 localization would be interesting, and a mislocalization would underline the results found by Jaiswal et al. Therefor the recently developed small molecule inhibitor for Unc119, squarunkin A, that was shown to impair the activation of Src kinase, could be used (Mejuch et al., 2017). A similar experiment could be conducted by a knockout of the Unc119a/b genes instead of protein inhibition. In *Caenorhabditis elegans*, Unc119 deletion resulted in a mislocalization of myristoylated ODR-3 and GPA-13, however leading to a complex phenotype (Zhang et al., 2011). RNAi-mediated knockdown experiments were already published, showing a mislocalization of NPHP3 after downregulation of Unc119b but not of Unc119a (Wright et al., 2011; Constantine et al., 2012), whereas knockdowns of both Unc119a or Unc119b impaired Src kinase localization (Konitsiotis et al., 2017).

The parallels between the cargo sorting systems mediated by PDE6 δ or Unc119 proteins were also illustrated in similar ciliary localization patterns of PDE6 δ and INPP5E versus Unc119b

and NPHP3 or Cystin1, showing the carrier protein in the transition zone and the lipidated cargo along the entire axoneme (Wright et al., 2011; Thomas et al., 2014). It can be assumed, that the carrier protein targets the lipidated protein to the ciliary base and the cargo-carrier complex enters the cilium. When the complex reaches the transition zone and the proximal cilium, Arl3•GTP releases the lipidated protein from the carrier. Because PDE6 δ and Unc119b were not found along the entire axoneme, but besides the transition zone also in the cytosol, the proteins might only be transiently in the cilium for cargo release, as also suggested in former publications. The release of ciliary cargo proteins was thought to trigger the entry of the carrier protein (Wright et al., 2011; Thomas et al., 2014). The GTPase reaction was proposed to be driving force for these transport processes (Gotthardt et al., 2015; Fansa and Wittinghofer, 2016).

Conclusively, the studies by Fansa et al. and Jaiswal et al. lead to the description of a general sorting principle of lipidated cargo proteins, that depends on the affinity between cargo and carrier protein and on the specificity of release by Arl2 and Arl3. This Arl2/Arl3 system is responsible for the targeting of farnesylated and myristoylated proteins to different membrane compartments, sorting high affinity cargo to the ciliary compartment with release by Arl3•GTP, whereas low affinity cargo is released by Arl2•GTP at different inner cellular membranes (Gotthardt et al., 2015; Fansa and Wittinghofer, 2016; Fansa et al., 2016; Jaiswal et al., 2016).

6.4 Mechanism and dynamics of INPP5E transport into and inside the ciliary compartment

This paper is based on the current knowledge, published by Jacoby et al. (2009), Thomas et al. (2014) and Fansa et al. (2016), about the ciliary localization and cellular trafficking of INPP5E, but is for the first time applied to living cells. It focuses on the dynamics of INPP5E transport into and inside the cilium and draws a conclusion about the correspondent transport mechanisms, by using confocal live cell imaging instead of immunofluorescence microscopy of fixed cells. Use of the FRAP technique enabled the visualization of protein movements in living cells (Kösling et al., 2018).

Measuring the speed of recovery after bleaching either the signal in the ciliary tip or base region of GFP-INPP5E expressing cells showed that INPP5E moves within cilia and revealed speed values for the innerciliary INPP5E velocity (0.20 $\mu\text{m/s}$ – 0.29 $\mu\text{m/s}$), resembling those found for IFT movement (Kösling et al., 2018). Due to the dephosphorylation of the 5' position of PIPs (and inositol phosphates), INPP5E modulates the composition of the ciliary membrane.

The observed mobility of INPP5E leading to its distribution along the entire length of the cilium might be an important component for its inositol polyphosphate 5'-phosphatase function (Chávez et al., 2015; Garcia-Gonzalo et al., 2015). An inhibition of dynein or the complete IFT system led to a total inhibition of INPP5E movement within cilia. However, inhibition of PDE6 δ did not change the innerciliary motility of INPP5E. Also, mutation of the CaaX box cysteine did not block the innerciliary movement of INPP5E. Conclusively, INPP5E is transported via IFT within the cilium and this process is independent of the interaction with PDE6 δ and independent of INPP5E farnesylation. Experiments by bleaching the entire ciliary signal showed a constant but very slow entry of INPP5E into cilia, which was impaired after inhibition of dynein/IFT or PDE6 δ . This led to the conclusion that ciliary targeting and/or entry of INPP5E depend on the dynein transport system and PDE6 δ (Kösling et al., 2018).

The results regarding the INPP5E mislocalization after inhibition of PDE6 δ are in line with studies about Ras protein trafficking defects after PDE6 δ inhibition. Initially, the inhibition of PDE6 δ by small molecules with nanomolar affinity, such as Deltarasin and Deltazinone 1, was shown to impair the interaction of PDE6 δ with Ras proteins and to lead to Ras mislocalization (Zimmermann et al., 2013; Papke et al., 2016). Newly identified inhibitors exhibiting picomolar affinity to PDE6 δ were shown to be highly selective by binding with up to seven hydrogen bonds and being less released by Arl2. These Deltasonamides were tested in K-Ras mutated cells that depend on K-Ras, where they inhibited cell growth (Martín-Gago et al., 2017). Here, it was shown for the first time that Deltazinone 1 also replaces the high affinity cargo INPP5E from PDE6 δ (Kösling et al., 2018).

An impaired localization of the INPP5E CaaX box mutant, which loses the exclusive ciliary enrichment, illustrated that the farnesylation is important for the sorting and/or entry of INPP5E to cilia. The innerciliary transport of the mutant also depends on IFT, showing that the farnesylation is not essential for the IFT-mediated transport. In living cells, the mutant was additionally enriched at the centrioles. Also, after bleaching the entire ciliary signal, the mutant accumulated fast at the basal body and daughter centriole before the signal very slowly and comparable to the wild type recovered along the axoneme. This suggested an impaired and different mechanism of ciliary entry for the CaaX box mutant with respect to the wild type protein, caused by the lack of farnesylation and thus missing interaction with PDE6 δ . Furthermore, the driving force for the sorting of lipidated proteins to the ciliary compartment, that is due to the Arl3•GTP domain acting on high affinity cargo of PDE6 δ , does not influence low affinity nonfarnesylated INPP5E and this might impair the sorting. An affinity trap

mechanism that retains the mutant at the basal body before entry was postulated. The wild type protein is thought to overcome the affinity trap by interaction with PDE6 δ . In summary, it was clearly shown that the farnesylation is crucial for a correct sorting of INPP5E to the ciliary compartment. The decreased ciliary accumulation and the centriolar enrichment of the CaaX box mutant might result from an impaired retention at the ciliary membrane or an increased solubility as result of the missing farnesylation. This could explain the modified sorting and entry of the mutant into cilia.

Collectively, for the regulation of INPP5E ciliary localization, a three-step mechanism was suggested. This mechanism takes up the above described three-step mechanism for the PDE6 δ -dependent sorting of farnesylated cargo found by Fansa et al., composed of affinity dependent cargo-carrier binding, release, and retention, and gave a deeper insight especially into the trafficking of INPP5E. Here, it was shown that INPP5E targeting to cilia is mediated by PDE6 δ and INPP5E farnesylation. After cargo-carrier binding and transport to the ciliary base, entry into the ciliary compartment occurs due to INPP5E-PDE6 δ complex diffusion, where INPP5E is then transferred to the IFT system, that transports INPP5E within the cilium (Kösling et al., 2018). The suggestion that INPP5E enters cilia in complex with PDE6 δ is supported by the partial colocalization of the proteins in the transition zone and proximal cilium which was shown by Thomas et al. (2014). Arl3•GTP releases INPP5E from the complex and the farnesyl anchor attaches it to the ciliary membrane. Ultimately, INPP5E is retained inside the ciliary compartment. Retention might be mediated by interaction with the ciliary membrane, the IFT system, other proteins such as Arl13B, the ciliary gate, or other unknown components (Fansa et al., 2016; Kösling et al., 2018).

The paper by Kösling et al. (2018) confirmed the importance of PDE6 δ for the localization of INPP5E to cilia. Before, the link between INPP5E and PDE6 δ was shown by a combination of biochemical and structural studies, and cell biological analyses of fixed cells. Here, the essentiality of the INPP5E farnesylation and the interaction with PDE6 δ for INPP5E ciliary localization was shown for the first time in living cells, and movements of INPP5E were analyzed. The live cell experiments support former results of the studies by Jacoby et al. (2009), Thomas et al. (2014) and Fansa et al. (2016) and clarify the procedures leading to the almost exclusive ciliary localization of INPP5E. As shown by mislocalization of the INPP5E CaaX box mutant, which was also observed by Thomas et al., it is now clear that the farnesylation is essential for the localization. In the contrasting study by Humbert et al. (2012) it was claimed that a C-terminal truncated INPP5E construct does not show localization defects. As described

above for the localization of INPP5E after Arl3 downregulation, Humbert et al. most probably only analyzed for mutant INPP5E positive cilia, but disregarded the ciliary signal intensity and possible cytosolic mislocalized portion of the MORM-related mutant.

Further biochemical experiments will be required to support and understand in more detail the exclusively cell biological experiments presented in this publication. For example, the connection between INPP5E and the IFT system, if it is a direct molecular interaction between INPP5E and IFT proteins, or an indirect interaction mediated by other linking proteins, requires also biochemical and structural analyses, such as binding assays, pull down assays and structure determination of protein complexes. A possible linking protein could be Arl13B, which was observed to bind to both INPP5E and IFT46/56 (Humbert et al., 2012; Nozaki et al., 2017). Moreover, to analyze the localization of INPP5E as a function of PDE6 δ , which was shown here in living cells treated with the PDE6 δ inhibitor Deltazinone 1, a knockdown of PDE6 δ using siRNAs or a knockout using the CRISPR/Cas9 system could be conducted. It was shown before, that a knockdown of PDE6 δ resulted in a mislocalization of H-Ras and N-Ras to endomembranes instead of the normal localization to the Golgi and plasma membrane (Chandra et al., 2012). Moreover, it was shown for Deltazinone 1, that it caused phenotypic effects in cells which were comparable to a PDE6 δ knockdown (Papke et al., 2016). These results suggested that a knockdown of PDE6 δ would have a similar mislocalization effect on INPP5E as observed for PDE6 δ inactivation by Deltazinone 1. A knockout of the PDE6 δ gene might have objectionable side effects leading to phenotypic effects of the cells and making the suggested experiment more difficult, as it was reported that the phenotype of photoreceptors in PDE6 δ knockout mice resembles that of retinitis pigmentosa (Baehr, 2014).

Furthermore, the localization and movement of Arl3 were analyzed in living cells and complemented the results from fixed cells (Grayson et al., 2002; Zhou et al., 2006; Lokaj et al., 2015). In contrast to INPP5E, Arl3 entered cilia rapidly and the innerciliary transport was clearly faster. Together with the result that dynein/IFT inhibition did not impact Arl3 movements, it was supposed that Arl3 diffuses through the cytosol and moves into and within cilia by diffusion (Kösling et al., 2018). This fits to the model of the ciliary gate as a size-dependent sieve-like barrier, that allows a faster diffusion for small-sized ciliary proteins (Breslow et al., 2013; Lin et al., 2013). Arl3 cycles rapidly between the Arl3•GTP compartment cilium, where the cargo is released, and the cytosol, where Arl3 is expected to be GDP-bound. The overall dynamic behavior of Arl3 might be related to its suggested function in the generation of the driving force for the release of lipidated cargo proteins from PDE6 δ and

Unc119 proteins into cilia. This system is comparable to the known driving force built by the hydrolysis of Ran•GTP for the transport between cytosol and nucleus through the nuclear pore (Görlich et al., 1996).

6.5 Summary

The following paragraphs and figure sum up the main conclusions of the publications presented in this thesis (see Figure 16). The Arl2/Arl3 system regulates the sorting of lipidated proteins that are shuttled by PDE6 δ and Unc119a/b. The sorting of lipidated cargo proteins depends on the affinity towards the carrier proteins PDE6 δ /Unc119a/b, and the specificity of the release by Arl2/3. Farnesylated proteins, such as INPP5E, or myristoylated proteins, such as NPHP3, with a high affinity to PDE6 δ or Unc119a/b, respectively, are targeted to the cilium, the cargo-carrier complex enters the ciliary compartment and the lipidated protein is released by Arl3•GTP. Within the ciliary lumen, the lipidated protein is supposed to be attached to the ciliary membrane after the release from the carrier protein. The specific release of high affinity proteins by Arl3•GTP into the ciliary compartment is established by the cilia-exclusive Arl3 GEF Arl13B. The resulting Arl3•GTP domain and its GTP hydrolysis might act as a driving force for the release of lipidated proteins into cilia.

The mechanism leading to the ciliary localization of INPP5E, was supposed to consist of three steps. First, PDE6 δ binds INPP5E and transports it to the ciliary base. The second step is diffusion of the complex into the ciliary lumen, and transfer to the IFT system, that regulates the innerciliary INPP5E transport. Arl3•GTP releases INPP5E from PDE6 δ and subsequently the farnesyl moiety anchors INPP5E to the ciliary membrane. The last step is innerciliary retention. However, low affinity proteins, such as Rheb, are sorted in complex with the carrier protein, in this case PDE6 δ , to other inner membranes, such as endomembranes, and are released there by Arl2•GTP.

CCDC104, which was identified as new binding partner of Arl3•GTP, accumulates in the transition zone and around the basal body. It binds to the N-terminal amphipathic helix of Arl3•GTP. Because this helix can attach Arl3•GTP to the ciliary membrane, it was suggested that CCDC104 reduces the Arl3•GTP membrane interaction. After exit of the CCDC104-Arl3•GTP complex from the cilium, CCDC104 might provide Arl3•GTP to its cytosolic GAP RP2 during a transient triple complex formation, followed by RP2 catalyzed hydrolysis of the Arl3-bound GTP. By this, CCDC104 might support the generation of the above described energetic driving force leading to ciliary entry of lipidated proteins.

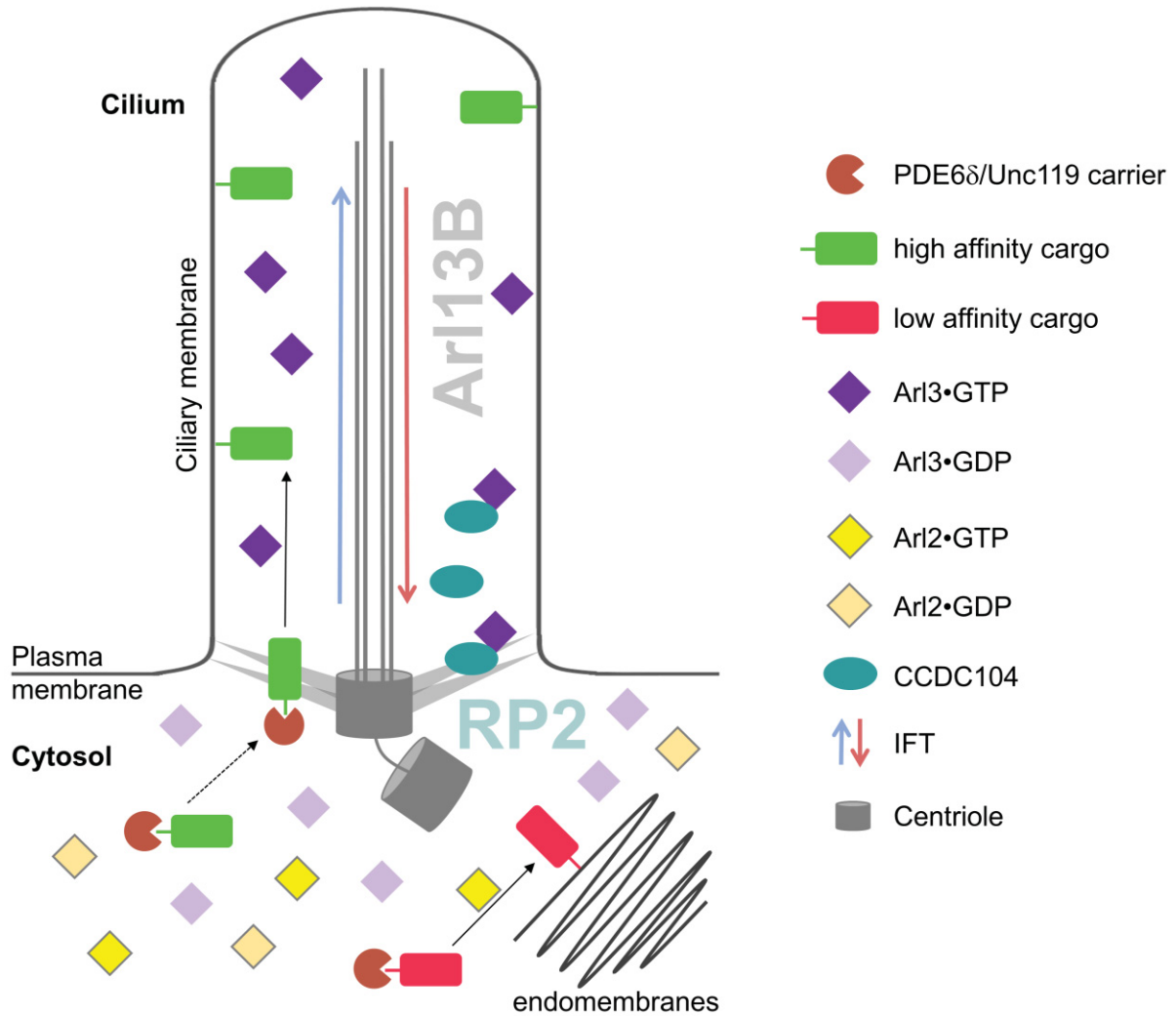


Figure 16: Model of the sorting mechanism of lipidated cargo of the carrier proteins PDE6δ and Unc119a/b, regulated by the Arl2/Arl3 system. PDE6δ shuttles farnesylated, Unc119a/b sort myristoylated proteins with a high affinity to the ciliary Arl3•GTP compartment, where the cargo protein is released after entry by Arl3•GTP. The ciliary Arl3 GEF Arl13B ensures the high Arl3•GTP concentration in the cilium. Low affinity cargo proteins are released by Arl2•GTP at other inner membranes such as the endomembrane system. For the sorting of the ciliary protein INPP5E, a three-step mechanism was supposed, that consists of (a) cargo-carrier complex building and transport to the base of the cilium, (b) complex diffusion into the cilium, transfer to the IFT system, that transports INPP5E within the cilium, cargo release and binding to the ciliary membrane, and (c) innerciliary retention. The ciliary protein CCDC104 is enriched in the transition zone and basal body region and interacts with Arl3•GTP. This complex formation might trigger the ciliary exit of Arl3•GTP and subsequent GTP hydrolysis assisted by RP2.

The results presented in this thesis and the corresponding publications lead to a better understanding of cellular and especially ciliary transport processes in the context of the Arl2/Arl3-related sorting of lipidated PDE6δ/Unc119a/b cargo proteins, such as INPP5E or NPHP3. INPP5E and PDE6δ are involved in MORM and Joubert syndrome, whereas Arl3 and Unc119a/b are implicated in rod-cone diseases and NPHP3 in nephronophthisis. Giving

consideration to the involvement of the analyzed proteins in different ciliopathies, by the new findings about their ciliary trafficking an important step to elucidate the molecular basics of the diseases was taken. Further research will be required and ultimately, this knowledge will be helpful in the development of treatments against these severe human diseases.

6.6 Zusammenfassung

Das Arl2/Arl3 System reguliert die Sortierung lipidierter Proteine, die von PDE6 δ und Unc119a/b transportiert werden. Die Sortierung dieser lipidierten Frachtproteine ist von ihrer Affinität gegenüber der Trägerproteine PDE6 δ /Unc119a/b abhängig, sowie von der Spezifität ihrer Freisetzung durch Arl2/3. Farnesylierte Proteine wie INPP5E oder myristoylierte Proteine wie NPHP3, die eine hohe Affinität zu PDE6 δ beziehungsweise zu Unc119a/b haben, werden gezielt zum Cilium hin transportiert, der Komplex aus Fracht- und Trägerprotein tritt in das ciliäre Kompartiment ein, wo das lipidierter Protein durch Arl3•GTP freigesetzt wird. Es wird angenommen, dass sich das lipidierter Protein nach der Freisetzung vom Trägerprotein im Innern des Ciliums an die ciliäre Membran anlagert. Die spezifische Freisetzung hoch affiner Proteine durch Arl3•GTP ins Cilium wird durch das ausschließlich im Cilium lokalisierte Arl3-GEF Arl13B sichergestellt. Die daraus resultierende Arl3•GTP Domäne und ihre GTP-Hydrolyse wirken vermutlich als Triebkraft für die Freisetzung der lipidierten Proteine ins Cilium.

Es wird angenommen, dass der Mechanismus, der zur Cilienlokalisierung von INPP5E führt, aus drei Schritten besteht. Zuerst bindet PDE6 δ an INPP5E und transportiert es zur Basis des Ciliums. Der zweite Schritt ist die Diffusion dieses Komplexes in das Innere des Ciliums und die Übergabe an das IFT System, das den innerciliären Transport von INPP5E übernimmt. Arl3•GTP entlässt INPP5E von PDE6 δ und anschließend verankert die Farnesylgruppe INPP5E an der Cilienmembran. Der letzte Schritt ist die innerciliäre Retention. Niedrig affine Proteine wie Rheb hingegen werden im Komplex mit dem Trägerprotein, in diesem Fall PDE6 δ , zu anderen inneren Membranen wie dem Endomembransystem sortiert und dort durch Arl2•GTP freigesetzt.

CCDC104, das als neuer Bindungspartner von Arl3•GTP entdeckt wurde, akkumuliert am Basalkörper und oberhalb dessen im Übergangsbereich des Ciliums. Es bindet an die N-terminale amphipathische Helix von Arl3•GTP. Da diese Helix Arl3•GTP an die ciliäre Membran anlagern kann, wurde vorgeschlagen, dass CCDC104 die Interaktion von Arl3•GTP mit der Membran reduziert. Nach dem Austritt des CCDC104-Arl3•GTP Komplexes aus dem Cilium wird vermutet, dass CCDC104 das GTP-gebundene Arl3 an dessen cytosolisches GAP RP2 übergibt. Dies kann während der Bildung eines kurzlebigen Dreifachkomplexes mit einer nachfolgenden RP2-katalysierten Hydrolyse des Arl3-gebundenen GTP geschehen. Dadurch kann CCDC104 die Bildung der zuvor beschriebenen energetischen Triebkraft, die zum Eintritt lipidierter Proteine ins Cilium führt, fördern.

References

- Afzelius, B. (1959). Electron microscopy of the sperm tail. *J. Biophys. Biochem. Cytol.* *5*, 269–278.
- Afzelius, B.A. (1976). A human syndrome caused by immotile cilia. *Science* *193*, 317–319.
- Ahearn, I.M., Haigis, K., Bar-Sagi, D., and Philips, M.R. (2012). Regulating the regulator: post-translational modification of RAS. *Nat. Rev. Mol. Cell Biol.* *13*, 39–51.
- Ahmadian, M.R., Stege, P., Scheffzek, K., and Wittinghofer, A. (1997). Confirmation of the arginine-finger hypothesis for the GAP-stimulated GTP-hydrolysis reaction of Ras. *Nat. Struct. Biol.* *4*, 686–689.
- Ahmadian, M.R., Zor, T., Vogt, D., Kabsch, W., Selinger, Z., Wittinghofer, A., and Scheffzek, K. (1999). Guanosine triphosphatase stimulation of oncogenic Ras mutants. *Proc. Natl. Acad. Sci. U. S. A.* *96*, 7065–7070.
- Aitken, A., and Cohen, P. (1984). Identification of N-terminal myristyl blocking groups in proteins. *Methods Enzymol.* *106*, 205–210.
- Alberts, B., Johnson, A., Lewis, J., Raff, M., Roberts, K., and Walter, P. (2008). *Molecular Biology of the Cell* (Garland Science).
- An, Y., Shao, Y., Alory, C., Matteson, J., Sakisaka, T., Chen, W., Gibbs, R.A., Wilson, I.A., and Balch, W.E. (2003). Geranylgeranyl switching regulates GDI-Rab GTPase recycling. *Structure* *11*, 347–357.
- Antonny, B., Beraud-Dufour, S., Chardin, P., and Chabre, M. (1997). N-terminal hydrophobic residues of the G-protein ADP-ribosylation factor-1 insert into membrane phospholipids upon GDP to GTP exchange. *Biochemistry* *36*, 4675–4684.
- Archer, F.L., and Wheatley, D.N. (1971). Cilia in cell-cultured fibroblasts. *J. Anat.* *109*, 277–292.
- Astle, M. V., Horan, K.A., Ooms, L.M., and Mitchell, C.A. (2007). The inositol polyphosphate 5-phosphatases: traffic controllers, waistline watchers and tumour suppressors? *Biochem. Soc. Symp.* *181*, 161–181.
- Attree, O., Olivos, I.M., Okabe, I., Bailey, L.C., Nelson, D.L., Lewis, R.A., McInnes, R.R., and Nussbaum, R.L. (1992). The Lowe's oculocerebrorenal syndrome gene encodes a protein highly homologous to inositol polyphosphate-5-phosphatase. *Nature* *358*, 239–242.
- Avidor-Reiss, T., Maer, A.M., Koundakjian, E., Polyanovsky, A., Keil, T., Subramaniam, S., and Zuker, C.S. (2004). Decoding cilia function: Defining specialized genes required for compartmentalized cilia biogenesis. *Cell* *117*, 527–539.
- Baala, L., Romano, S., Khaddour, R., Saunier, S., Smith, U.M., Audollent, S., Ozilou, C., Faivre, L., Laurent, N., Foliguet, B., et al. (2007). The Meckel-Gruber syndrome gene, MKS3, is mutated in Joubert syndrome. *Am. J. Hum. Genet.* *80*, 186–194.
- Badano, J.L., Mitsuma, N., Beales, P.L., and Katsanis, N. (2006). The ciliopathies: An emerging class of human genetic disorders. *Annu. Rev. Genomics Hum. Genet.* *7*, 125–148.
- Baehr, W. (2014). Membrane protein transport in photoreceptors: The function of PDEδ. *Investig. Ophthalmol. Vis. Sci.* *55*, 8653–8666.
- Balla, T. (2013). Phosphoinositides: tiny lipids with giant impact on cell regulation. *Physiol. Rev.* *93*, 1019–1137.
- Barnes, B.G. (1961). Ciliated secretory cells in the pars distalis of the mouse hypophysis. *J. Ultrastruct. Res.* *5*, 453–467.

- Beales, P.L., Elcioglu, N., Woolf, A.S., Parker, D., and Flinter, F.A. (1999). New criteria for improved diagnosis of Bardet-Biedl syndrome: Results of a population survey. *J. Med. Genet.* *36*, 437–446.
- Berbari, N.F., Johnson, A.D., Lewis, J.S., Askwith, C.C., and Mykityn, K. (2008). Identification of ciliary localization sequences within the third intracellular loop of G protein-coupled receptors. *Mol. Biol. Cell* *19*, 1540–1547.
- Berbari, N.F., O'Connor, A.K., Haycraft, C.J., and Yoder, B.K. (2009). The primary cilium as a complex signaling center. *Curr. Biol.* *19*, R526–R535.
- Besharse, J.C., Hollyfield, J.G., and Rayborn, M.E. (1977). Turnover of rod photoreceptor outer segments. *J. Cell Biol.* *75*, 507–527.
- Besschetnova, T.Y., Roy, B., and Shah, J. V. (2009). Imaging intraflagellar transport in mammalian primary cilia. *Methods Cell Biol.* *93*, 331–346.
- Bhamidipati, A., Lewis, S.A., and Cowan, N.J. (2000). ADP ribosylation factor-like protein 2 (Arl2) regulates the interaction of tubulin-folding cofactor D with native tubulin. *J. Cell Biol.* *149*, 1087–1096.
- Bielas, S.L., Silhavy, J.L., Brancati, F., Kisseleva, M. V, Al-Gazali, L., Sztriha, L., Bayoumi, R.A., Zaki, M.S., Abdel-Aleem, A., Rosti, O., et al. (2009). Mutations in the inositol polyphosphate-5-phosphatase E gene link phosphatidyl inositol signaling to the ciliopathies. *Nat. Genet.* *41*, 1032–1036.
- Blacque, O.E., and Sanders, A.A.W.M. (2014). Compartments within a compartment. *Organogenesis* *10*, 126–137.
- Blacque, O.E., Perens, E.A., Boroevich, K.A., Inglis, P.N., Li, C., Warner, A., Khattra, J., Holt, R.A., Ou, G., Mah, A.K., et al. (2005). Functional genomics of the cilium, a sensory organelle. *Curr. Biol.* *15*, 935–941.
- Bloodgood, R.A. (1984). Preferential turnover of membrane proteins in the intact *Chlamydomonas flagellum*. *Exp. Cell Res.* *150*, 488–493.
- Boguski, M.S., and McCormick, F. (1993). Proteins regulating Ras and its relatives. *Nature* *366*, 643–654.
- Bos, J.L. (1989). Ras oncogenes in human cancer: A review. *Cancer Res.* *49*, 4682–4689.
- Bos, J.L., Rehmann, H., and Wittinghofer, A. (2007). GEFs and GAPs: Critical elements in the control of small G proteins. *Cell* *129*, 865–877.
- Bourne, H.R., Sanders, D.A., and McCormick, F. (1990). The GTPase superfamily: A conserved switch for diverse cell functions. *Nature* *348*, 125–132.
- Bourne, H.R., Sanders, D.A., and McCormick, F. (1991). The GTPase superfamily: Conserved structure and molecular mechanism. *Nature* *349*, 117–127.
- Boyartchuk, V.L., Ashby, M.N., and Rine, J. (1997). Modulation of Ras and a-factor function by carboxyl-terminal proteolysis. *Science* *275*, 1796–1800.
- Breslow, D.K., Koslover, E.F., Seydel, F., Spakowitz, A.J., and Nachury, M. V (2013). An in vitro assay for entry into cilia reveals unique properties of the soluble diffusion barrier. *J. Cell Biol.* *203*, 129–147.
- Calvert, P.D., Schiesser, W.E., and Pugh, E.N. (2010). Diffusion of a soluble protein, photoactivatable GFP, through a sensory cilium. *J. Gen. Physiol.* *135*, 173–196.
- Camner, P., Mossberg, B., and Afzelius, B.A. (1975). Evidence of congenitally nonfunctioning cilia in the tracheobronchial tract in two subjects. *Am. Rev. Respir. Dis.* *112*, 807–809.
- Cano, D.A., Murcia, N.S., Pazour, G.J., and Hebrok, M. (2004). Orpk mouse model of

- polycystic kidney disease reveals essential role of primary cilia in pancreatic tissue organization. *Dev. Dis.* **131**, 3457–3467.
- Cantagrel, V., Silhavy, J.L., Bielas, S.L., Swistun, D., Marsh, S.E., Bertrand, J.Y., Audollent, S., Attié-Bitach, T., Holden, K.R., Dobyns, W.B., et al. (2008). Mutations in the cilia gene *ARL13B* lead to the classical form of Joubert syndrome. *Am. J. Hum. Genet.* **83**, 170–179.
- Carr, S.A., Biemann, K., Shoji, S., Parmelee, D.C., and Titani, K. (1982). n-Tetradecanoyl is the NH₂-terminal blocking group of the catalytic subunit of cyclic AMP-dependent protein kinase from bovine cardiac muscle. *Proc. Natl. Acad. Sci. U. S. A.* **79**, 6128–6131.
- Casey, P.J., Solski, P.A., Der, C.J., and Buss, J.E. (1989). p21ras is modified by a farnesyl isoprenoid. *Proc. Natl. Acad. Sci. U. S. A.* **86**, 8323–8327.
- Caspary, T., Larkins, C.E., and Anderson, K. V (2007). The graded response to Sonic hedgehog depends on cilia architecture. *Dev. Cell* **12**, 767–778.
- Cen, O., Gorska, M.M., Stafford, S.J., Sur, S., and Alam, R. (2003). Identification of Unc119 as a novel activator of Src-type tyrosine kinases. *J. Biol. Chem.* **278**, 8837–8845.
- Cevik, S., Hori, Y., Kaplan, O.I., Kida, K., Toivenon, T., Foley-Fisher, C., Cottell, D., Katada, T., Kontani, K., and Blacque, O.E. (2010). Joubert syndrome *Arl13b* functions at ciliary membranes and stabilizes protein transport in *Caenorhabditis elegans*. *J. Cell Biol.* **188**, 953–969.
- Chandra, A., Grecco, H.E., Pisupati, V., Perera, D., Cassidy, L., Skoulidis, F., Ismail, S.A., Hedberg, C., Hanzal-Bayer, M., Venkitaraman, A.R., et al. (2012). The GDI-like solubilizing factor PDE δ sustains the spatial organization and signalling of Ras family proteins. *Nat. Cell Biol.* **14**, 329–329.
- Chávez, M., Ena, S., Van Sande, J., de Kerchove d'Exaerde, A., Schurmans, S., and Schiffmann, S.N. (2015). Modulation of ciliary phosphoinositide content regulates trafficking and Sonic hedgehog signaling output. *Dev. Cell* **34**, 338–350.
- Chen, Y.X., Koch, S., Uhlenbrock, K., Weise, K., Das, D., Gremer, L., Brunsveld, L., Wittinghofer, A., Winter, R., Triola, G., et al. (2010). Synthesis of the Rheb and K-Ras4B GTPases. *Angew. Chem. Int. Ed.* **49**, 6090–6095.
- Cherfils, J., and Zeghouf, M. (2013). Regulation of small GTPases by GEFs, GAPs, and GDIs. *Physiol. Rev.* **93**, 269–309.
- Chiang, A.P., Nishimura, D., Searby, C., Elbedour, K., Carmi, R., Ferguson, A.L., Secrist, J., Braun, T., Casavant, T., Stone, E.M., et al. (2004). Comparative genomic analysis identifies an ADP-ribosylation factor-like gene as the cause of Bardet-Biedl syndrome (BBS3). *Am. J. Hum. Genet.* **75**, 475–484.
- Chun, J., Shapovalova, Z., Dejgaard, S.Y., Presley, J.F., and Melancon, P. (2008). Characterization of class I and II ADP-ribosylation factors (Arfs) in live cells: GDP-bound class II Arfs associate with the ER-Golgi intermediate compartment independently of GBF1. *Mol. Biol. Cell* **19**, 3488–3500.
- Cole, D.G., Chinn, S.W., Wedaman, K.P., Hall, K., Vuong, T., and Scholey, J.M. (1993). Novel heterotrimeric kinesin-related protein purified from sea urchin eggs. *Nature* **366**, 268–270.
- Cole, D.G., Diener, D.R., Himelblau, A.L., Beech, P.L., Fuster, J.C., and Rosenbaum, J.L. (1998). *Chlamydomonas* kinesin-II-dependent intraflagellar transport (IFT): IFT particles contain proteins required for ciliary assembly in *Caenorhabditis elegans* sensory neurons. *J. Cell Biol.* **141**, 993–1008.
- Conduit, S.E., Dyson, J.M., and Mitchell, C.A. (2012). Inositol polyphosphate 5-phosphatases; new players in the regulation of cilia and ciliopathies. *FEBS Lett.* **586**, 2846–2857.

- Constantine, R., Zhang, H., Gerstner, C.D., Frederick, J.M., and Baehr, W. (2012). Uncoordinated (UNC)119: Coordinating the trafficking of myristoylated proteins. *Vision Res.* 75, 26–32.
- Coon, B.G., Hernandez, V., Madhivanan, K., Mukherjee, D., Hanna, C.B., Barinaga-Rementería Ramirez, I., Lowe, M., Beales, P.L., and Aguilar, R.C. (2012). The Lowe syndrome protein OCRL1 is involved in primary cilia assembly. *Hum. Mol. Genet.* 21, 1835–1847.
- Corbit, K.C., Aanstad, P., Singla, V., Norman, A.R., Stainier, D.Y.R., and Reiter, J.F. (2005). Vertebrate Smoothed functions at the primary cilium. *Nature* 437, 1018–1021.
- Cox, A.D., and Der, C.J. (2010). Ras history - The saga continues. *Small GTPases* 1, 2–27.
- Cuvillier, A., Redon, F., Antoine, J.-C., Chardin, P., DeVos, T., and Merlin, G. (2000). LdARL-3A, a Leishmania promastigote-specific ADP-ribosylation factor-like protein, is essential for flagellum integrity. *J. Cell Sci.* 113, 2065–2074.
- Dai, Q., Choy, E., Chiu, V., Romano, J., Slivka, S.R., Steitz, S.A., Michaelis, S., and Philips, M.R. (1998). Mammalian prenylcysteine carboxyl methyltransferase is in the endoplasmic reticulum. *J. Biol. Chem.* 273, 15030–15034.
- Daumke, O., Weyand, M., Chakrabarti, P.P., Vetter, I.R., and Wittinghofer, A. (2004). The GTPase-activating protein Rap1GAP uses a catalytic asparagine. *Nature* 429, 197–201.
- Davidson, A.E., Schwarz, N., Zelinger, L., Stern-Schneider, G., Shoemark, A., Spitzbarth, B., Gross, M., Laxer, U., Sosna, J., Sergouniotis, P.I., et al. (2013). Mutations in ARL2BP, encoding ADP-ribosylation-factor-like 2 binding protein, cause autosomal-recessive retinitis pigmentosa. *Am. J. Hum. Genet.* 93, 321–329.
- Delous, M., Baala, L., Salomon, R., Laclef, C., Vierkotten, J., Tory, K., Golzio, C., Lacoste, T., Besse, L., Ozilou, C., et al. (2007). The ciliary gene RPGRIP1L is mutated in cerebello-oculo-renal syndrome (Joubert syndrome type B) and Meckel syndrome. *Nat. Genet.* 39, 875–881.
- Dharmaiah, S., Bindu, L., Tran, T.H., Gillette, W.K., and Frank, P.H. (2016). Structural basis of recognition of farnesylated and methylated KRAS4b by PDEδ. *Proc. Natl. Acad. Sci.* 113, E6766–E6775.
- Doxsey, S., Zimmerman, W., and Mikule, K. (2005). Centrosome control of the cell cycle. *Trends Cell Biol.* 15, 303–311.
- Dryja, T.P., McGee, T.L., Reichel, E., Hahn, L.B., Cowley, G.S., Yandell, D.W., Sandberg, M.A., and Berson, E.L. (1990). A point mutation of the rhodopsin gene in one form of retinitis pigmentosa. *Nature* 343, 364–366.
- Duijsings, D., Lanke, K.H.W., van Dooren, S.H.J., van Dommelen, M.M.T., Wetzels, R., de Mattia, F., Wessels, E., and van Kuppeveld, F.J.M. (2009). Differential membrane association properties and regulation of class I and class II Arfs. *Traffic* 10, 316–323.
- Dutta, N., and Seo, S. (2016). RPGR, a prenylated retinal ciliopathy protein, is targeted to cilia in a prenylation- and PDE6D-dependent manner. *Biol. Open* 5, 1283–1289.
- Dyson, J.M., Conduit, S.E., Feeney, S.J., Hakim, S., DiTommaso, T., Fulcher, A.J., Sriratana, A., Ramm, G., Horan, K.A., Gurung, R., et al. (2017). INPP5E regulates phosphoinositide-dependent cilia transition zone function. *J. Cell Biol.* 216, 247–263.
- Eggenchwiler, J.T., and Anderson, K. V (2007). Cilia and developmental signaling. *Annu. Rev. Cell Dev. Biol.* 23, 345–373.
- Ellis, D.S., Heckenlively, J.R., Martin, C.L., Lachman, R.S., Sakati, N., and Rimoin, D.L. (1984). Leber's congenital amaurosis associated with familial juvenile nephronophthisis and

- cone-shaped epiphyses of the hands (the Saldino-Mainzer syndrome). *Am. J. Ophthalmol.* 97, 233–239.
- Ellis, R.W., DeFeo, D., Shih, T.Y., Gonda, M.A., Young, H.A., Tsuchida, N., Lowy, D.R., and Scolnick, E.M. (1981). The p21 src genes of Harvey and Kirsten sarcoma viruses originate from divergent members of a family of normal vertebrate genes. *Nature* 292, 506–511.
- Erdmann, R., Wiebel, F.F., Flessau, A., Rytka, J., Beyer, A., Fröhlich, K.-U., and Kunau, W.-H. (1991). PAS1, a yeast gene required for peroxisome biogenesis, encodes a member of a novel family of putative ATPases. *Cell* 64, 499–510.
- Evans, R.J., Schwarz, N., Nagel-Wolfrum, K., Wolfrum, U., Hardcastle, A.J., and Cheetham, M.E. (2010). The retinitis pigmentosa protein RP2 links pericentriolar vesicle transport between the Golgi and the primary cilium. *Hum. Mol. Genet.* 19, 1358–1367.
- Fansa, E.K., and Wittinghofer, A. (2016). Sorting of lipidated cargo by the Arl2/Arl3 system. *Small GTPases* 7, 222–230.
- Fansa, E.K., O'Reilly, N.J., Ismail, S., and Wittinghofer, A. (2015). The N- and C-terminal ends of RPGR can bind to PDE6 δ . *EMBO Rep.* 16, 1583–1585.
- Fansa, E.K., Kösling, S.K., Zent, E., Wittinghofer, A., and Ismail, S. (2016). PDE6 δ -mediated sorting of INPP5E into the cilium is determined by cargo-carrier affinity. *Nat. Commun.* 7:11366, 1–9.
- Farnsworth, C.C., Kawata, M., Yoshida, Y., Takai, Y., Gelb, M.H., and Glomset, J.A. (1991). C terminus of the small GTP-binding protein smg p25A contains two geranylgeranylated cysteine residues and a methyl ester. *Proc. Natl. Acad. Sci. U. S. A.* 88, 6196–6200.
- Fawcett, D.W., and Porter, K.R. (1954). A study of the fine structure of ciliated epithelia. *J. Morphol.* 94, 221–281.
- Feistel, K., and Blum, M. (2006). Three types of cilia including a novel 9+4 axoneme on the notochordal plate of the rabbit embryo. *Dev. Dyn.* 235, 3348–3358.
- Field, C.M., Al-Awar, O., Rosenblatt, J., Wong, M.L., Alberts, B., and Mitchison, T.J. (1996). A purified *Drosophila* septin complex forms filaments and exhibits GTPase activity. *J. Cell Biol.* 133, 605–616.
- Finegold, A.A., Johnson, D.I., Farnsworth, C.C., Gelb, M.H., Judd, S.R., Glomset, J.A., and Tamanoi, F. (1991). Protein geranylgeranyltransferase of *Saccharomyces cerevisiae* is specific for Cys-Xaa-Xaa-Leu motif proteins and requires the CDC43 gene product but not the DPR1 gene product. *Proc. Natl. Acad. Sci. U. S. A.* 88, 4448–4452.
- Florio, S.K., Prusti, R.K., and Beavo, J.A. (1996). Solubilization of membrane-bound rod phosphodiesterase by the rod phosphodiesterase recombinant δ subunit. *J. Biol. Chem.* 271, 24036–24047.
- Follit, J.A., Li, X., Vucica, Y., and Pazour, G.J. (2010). The cytoplasmic tail of fibrocystin contains a ciliary targeting sequence. *J. Cell Biol.* 188, 21–28.
- Fonte, V.G., Searls, R.L., and Hilfer, S.R. (1971). The relationship of cilia with cell division and differentiation. *J. Cell Biol.* 49, 226–229.
- Freymann, D.M., Keenan, R.J., Stroud, R.M., and Walter, P. (1999). Functional changes in the structure of the SRP GTPase on binding GDP and Mg²⁺+GDP. *Nat. Struct. Biol.* 6, 793–801.
- Fry, A.M., Leaper, M.J., and Bayliss, R. (2014). The primary cilium. *Organogenesis* 10, 62–68.
- Fukumoto, Y., Kaibuchi, K., Hori, Y., Fujioka, H., Araki, S., Ueda, T., Kikuchi, A., and Takai, Y. (1990). Molecular cloning and characterization of a novel type of regulatory protein (GDI) for the rho proteins, ras p21-like small GTP-binding proteins. *Oncogene* 5, 1321–1328.

- Gallego, C., Gupta, S.K., Winitz, S., Eisfelder, B.J., and Johnson, G.L. (1992). Myristoylation of the $G\alpha_{i2}$ polypeptide, a G protein α subunit, is required for its signaling and transformation functions. *Proc. Natl. Acad. Sci. U. S. A.* *89*, 9695–9699.
- Garcia-Gonzalo, F.R., and Reiter, J.F. (2012). Scoring a backstage pass: Mechanisms of ciliogenesis and ciliary access. *J. Cell Biol.* *197*, 697–709.
- Garcia-Gonzalo, F.R., Phua, S.C., Roberson, E.C., Garcia, G., Abedin, M., Schurmans, S., Inoue, T., and Reiter, J.F. (2015). Phosphoinositides regulate ciliary protein trafficking to modulate hedgehog signaling. *Dev. Cell* *34*, 400–409.
- Geng, L., Okuhara, D., Yu, Z., Tian, X., Cai, Y., Shibazaki, S., and Somlo, S. (2006). Polycystin-2 traffics to cilia independently of polycystin-1 by using an N-terminal RVxP motif. *J. Cell Sci.* *119*, 1383–1395.
- Gibbons, I.R., and Rowe, A.J. (1965). Dynein: a protein with adenosine triphosphatase activity from cilia. *Science* *149*, 424–426.
- Gillingham, A.K., and Munro, S. (2007). The small G proteins of the Arf family and their regulators. *Annu. Rev. Cell Dev. Biol.* *23*, 579–611.
- Girotra, M., Srivastava, S., Kulkarni, A., Barbora, A., Bobra, K., Ghosal, D., Devan, P., Aher, A., Jain, A., Panda, D., et al. (2017). The C-terminal tails of heterotrimeric kinesin-2 motor subunits directly bind to α -tubulin1: possible implications for cilia-specific tubulin entry. *Traffic* *18*, 123–133.
- Goetz, S.C., and Anderson, K. V (2010). The primary cilium: a signalling centre during vertebrate development. *Nat. Rev. Genet.* *11*, 331–344.
- Goldberg, J. (1998). Structural basis for activation of ARF GTPase: Mechanisms of guanine nucleotide exchange and GTP–myristoyl switching. *Cell* *95*, 237–248.
- Görlich, D., Panté, N., Kutay, U., Aebi, U., and Bischoff, F.R. (1996). Identification of different roles for RanGDP and RanGTP in nuclear protein import. *EMBO J.* *15*, 5584–5594.
- Gotthardt, K., Lokaj, M., Koerner, C., Falk, N., Gießl, A., and Wittinghofer, A. (2015). A G-protein activation cascade from Arl13B to Arl3 and implications for ciliary targeting of lipidated proteins. *eLife* *4*:e11859, 1–16.
- Grayson, C., Bartolini, F., Chapple, J.P., Willison, K.R., Bhamidipati, A., Lewis, S.A., Luthert, P.J., Hardcastle, A.J., Cowan, N.J., and Cheetham, M.E. (2002). Localization in the human retina of the X-linked retinitis pigmentosa protein RP2, its homologue cofactor C and the RP2 interacting protein Arl3. *Hum. Mol. Genet.* *11*, 3065–3074.
- Gremer, L., Gilsbach, B., Ahmadian, M.R., and Wittinghofer, A. (2008). Fluoride complexes of oncogenic Ras mutants to study the Ras-RasGAP interaction. *Biol. Chem.* *389*, 1163–1171.
- Grillo, M.A., and Palay, S.L. (1963). Ciliated Schwann cells in the autonomic nervous system of the adult rat. *J. Cell Biol.* *16*, 430–436.
- Haim, M. (2002). The epidemiology of retinitis pigmentosa in Denmark. *Acta Ophthalmol. Scand.* *233*, 1–34.
- Hampshire, D.J., Ayub, M., Springell, K., Roberts, E., Jafri, H., Rashid, Y., Bond, J., Riley, J.H., and Woods, C.G. (2006). MORM syndrome (mental retardation, truncal obesity, retinal dystrophy and micropenis), a new autosomal recessive disorder, links to 9q34. *Eur. J. Hum. Genet.* *14*, 543–548.
- Hancock, J.F., and Hall, A. (1993). A novel role for RhoGDI as an inhibitor of GAP proteins. *EMBO J.* *1*, 91–95.
- Hancock, J.F., Magee, A.I., Childs, J.E., and Marshall, C.J. (1989). All ras proteins are polyisoprenylated but only some are palmitoylated. *Cell* *57*, 1167–1177.

- Hanke-Gogokhia, C., Wu, Z., Gerstner, C.D., Frederick, J.M., Zhang, H., and Baehr, W. (2016). Arf-like protein 3 (ARL3) regulates protein trafficking and ciliogenesis in mouse photoreceptors. *J. Biol. Chem.* 291, 7142–7155.
- Hanzal-Bayer, M., Renault, L., Roversi, P., Wittinghofer, A., and Hillig, R.C. (2002). The complex of Arl2-GTP and PDE δ : From structure to function. *EMBO J.* 21, 2095–2106.
- Haycraft, C.J., Banizs, B., Aydin-Son, Y., Zhang, Q., Michaud, E.J., and Yoder, B.K. (2005). Gli2 and Gli3 localize to cilia and require the intraflagellar transport protein polaris for processing and function. *PLOS Genet.* 1:e53, 480–488.
- Hildebrandt, F., Benzing, T., and Katsanis, N. (2011). Ciliopathies. *N. Engl. J. Med.* 364, 1533–1543.
- Hong, J.X., Lee, F.-J.S., Patton, W.A., Lin, C.Y., Moss, J., and Vaughan, M. (1998). Phospholipid- and GTP-dependent activation of cholera toxin and phospholipase D by human ADP-ribosylation factor-like protein 1 (HARL1). *J. Biol. Chem.* 273, 15872–15876.
- Hori, Y., Kobayashi, T., Kikko, Y., Kontani, K., and Katada, T. (2008). Domain architecture of the atypical Arf-family GTPase Arl13b involved in cilia formation. *Biochem. Biophys. Res. Commun.* 373, 119–124.
- Hou, Y., Qin, H., Follit, J.A., Pazour, G.J., Rosenbaum, J.L., and Witman, G.B. (2007). Functional analysis of an individual IFT protein: IFT46 is required for transport of outer dynein arms into flagella. *J. Cell Biol.* 176, 653–665.
- Hu, Q., and Nelson, W.J. (2011). Ciliary diffusion barrier: The gatekeeper for the primary cilium compartment. *Cytoskeleton* 68, 313–324.
- Huangfu, D., Liu, A., Rakeman, A.S., Murcia, N.S., Niswander, L., and Anderson, K. V. (2003). Hedgehog signalling in the mouse requires intraflagellar transport proteins. *Nature* 426, 83–87.
- Humbert, M.C., Weihbrecht, K., Searby, C.C., Li, Y., Pope, R.M., Sheffield, V.C., and Seo, S. (2012). ARL13B, PDE6D, and CEP164 form a functional network for INPP5E ciliary targeting. *Proc. Natl. Acad. Sci. U. S. A.* 109, 19691–19696.
- Ignatev, A., Kravchenko, S., Rak, A., Goody, R.S., and Pylypenko, O. (2008). A structural model of the GDP dissociation inhibitor Rab membrane extraction mechanism. *J. Biol. Chem.* 283, 18377–18384.
- Ismail, S. (2017). A GDI/GDF-like system for sorting and shuttling ciliary proteins. *Small GTPases* 8, 208–211.
- Ismail, S.A., Chen, Y.-X., Rusinova, A., Chandra, A., Bierbaum, M., Gremer, L., Triola, G., Waldmann, H., Bastiaens, P.I.H., and Wittinghofer, A. (2011). Arl2-GTP and Arl3-GTP regulate a GDI-like transport system for farnesylated cargo. *Nat. Chem. Biol.* 7, 942–949.
- Ismail, S.A., Chen, Y.-X., Miertzschke, M., Vetter, I.R., Koerner, C., and Wittinghofer, A. (2012). Structural basis for Arl3-specific release of myristoylated ciliary cargo from UNC119. *EMBO J.* 31, 4085–4094.
- Iyer, L.M., Lei, D.D., Koonin, E. V., and Aravind, L. (2004). Evolutionary history and higher order classification of AAA+ ATPases. *J. Struct. Biol.* 146, 11–31.
- Jacoby, M., Cox, J.J., Gayral, S., Hampshire, D.J., Ayub, M., Blockmans, M., Pernot, E., Kisseleva, M. V., Compère, P., Schiffmann, S.N., et al. (2009). INPP5E mutations cause primary cilium signaling defects, ciliary instability and ciliopathies in human and mouse. *Nat. Genet.* 41, 1027–1031.
- Jaiswal, M., Fansa, E.K., Kösling, S.K., Mejuch, T., Waldmann, H., and Wittinghofer, A. (2016). Novel biochemical and structural insights into the interaction of myristoylated cargo

- with Unc119 protein and their release by Arl2/3. *J. Biol. Chem.* *291*, 20766–20778.
- Jensen, V.L., and Leroux, M.R. (2017). Gates for soluble and membrane proteins, and two trafficking systems (IFT and LIFT), establish a dynamic ciliary signaling compartment. *Curr. Opin. Cell Biol.* *47*, 83–91.
- Jensen, V.L., Li, C., Bowie, R. V, Clarke, L., Mohan, S., Blacque, O.E., and Leroux, M.R. (2015). Formation of the transition zone by Mks5/Rpgrip1L establishes a ciliary zone of exclusion (CIZE) that compartmentalises ciliary signalling proteins and controls PIP2 ciliary abundance. *EMBO J.* *34*, 2537–2556.
- Jin, H., Whit, S.R., Shida, T., Schulz, S., Aguiar, M., Gygi, S.P., Bazan, J.F., and Nachury, M. V. (2010). The conserved Bardet-Biedl Syndrome proteins assemble a coat that traffics membrane proteins to cilia. *Cell* *141*, 1208–1219.
- Kapoor, S., Fansa, E.K., Möbitz, S., Ismail, S.A., Winter, R., Wittinghofer, A., and Weise, K. (2015). Effect of the N-terminal helix and nucleotide loading on the membrane and effector binding of Arl2/3. *Biophys. J.* *109*, 1619–1629.
- Kee, H.L., Dishinger, J.F., Lynne Blasius, T., Liu, C.-J., Margolis, B., and Verhey, K.J. (2012). A size-exclusion permeability barrier and nucleoporins characterize a ciliary pore complex that regulates transport into cilia. *Nat. Cell Biol.* *14*, 431–437.
- Kisseleva, M. V., Wilson, M.P., and Majerus, P.W. (2000). The isolation and characterization of a cDNA encoding phospholipid-specific inositol polyphosphate 5-phosphatase. *J. Biol. Chem.* *275*, 20110–20116.
- Kjeldgaard, M., Nyborg, J., and Clark, B.F. (1996). The GTP binding motif: Variations on a theme. *FASEB J.* *10*, 1347–1368.
- Klebe, C., Prinz, H., Wittinghofer, A., and Goody, R.S. (1995). The kinetic mechanism of Ran-nucleotide exchange catalyzed by RCC1. *Biochemistry* *34*, 12543–12552.
- Kobayashi, A., Kubota, S., Mori, N., McLaren, M.J., and Inana, G. (2003). Photoreceptor synaptic protein HRG4 (UNC119) interacts with ARL2 via a putative conserved domain. *FEBS Lett.* *534*, 26–32.
- Konitsiotis, A.D., Roßmannek, L., Stanoev, A., Schmick, M., and Bastiaens, P.I.H. (2017). Spatial cycles mediated by UNC119 solubilisation maintain Src family kinases plasma membrane localisation. *Nat. Commun.* *8*:114, 1–16.
- Kösling, S.K., Fansa, E.K., Maffini, S., and Wittinghofer, A. (2018). Mechanism and dynamics of INPP5E transport into and inside the ciliary compartment. *Biol. Chem.* *399*, 277–292.
- Kozminski, K.G., Johnson, K.A., Forscher, P., and Rosenbaum, J.L. (1993). A motility in the eukaryotic flagellum unrelated to flagellar beating. *Cell Biol.* *90*, 5519–5523.
- Kozminski, K.G., Beech, P.L., and Rosenbaum, J.L. (1995). The *Chlamydomonas* kinesin-like protein FLA10 is involved in motility associated with the flagellar membrane. *J. Cell Biol.* *131*, 1517–1527.
- Kull, F.J., Sablin, E.P., Lau, R., Fletterick, R.J., and Vale, R.D. (1996). Crystal structure of the kinesin motor domain reveals a structural similarity to myosin. *Nat. Rev. Mol. Cell Biol.* *380*, 550–555.
- Lancaster, M.A., Gopal, D.J., Kim, J., Saleem, S.N., Silhavy, J.L., Louie, C.M., Thacker, B.E., Williams, Y., Zaki, M.S., and Gleeson, J.G. (2011). Defective Wnt-dependent cerebellar midline fusion in a mouse model of Joubert syndrome. *Nat. Med.* *17*, 726–731.
- Latta, H., Maunsbach, A.B., and Madden, S.C. (1961). Cilia in different segments of the rat nephron. *J. Biophys. Biochem. Cytol.* *11*, 248–252.
- Lechtreck, K.F. (2015). IFT – cargo interactions and protein transport in cilia. *Trends Biochem.*

- Sci. 40, 765–778.
- Lee, J.-J., and Seo, S. (2015). PDE6D binds to the C-terminus of RPGR in a prenylation-dependent manner. *EMBO Rep.* 16, 1581–1582.
- Leipe, D.D., Wolf, Y.I., Koonin, E. V, and Aravind, L. (2002). Classification and evolution of P-loop GTPases and related ATPases. *J. Mol. Biol.* 317, 41–72.
- Lenzen, C., Cool, R.H., Prinz, H., Kuhlmann, J., and Wittinghofer, A. (1998). Kinetic analysis by fluorescence of the interaction between Ras and the catalytic domain of the guanine nucleotide exchange factor Cdc25 (Mm). *Biochemistry* 37, 7420–7430.
- Leonard, D., Hart, M.J., Platko, J. V., Eva, A., Henzel, W., Evans, T., and Cerione, R.A. (1992). The identification and characterization of a GDP-dissociation inhibitor (GDI) for the CDC42Hs protein. *J. Biol. Chem.* 267, 22860–22868.
- Li, Y., Wei, Q., Zhang, Y., Ling, K., and Hu, J. (2010). The small GTPases ARL-13 and ARL-3 coordinate intraflagellar transport and ciliogenesis. *J. Cell Biol.* 189, 1039–1051.
- Lidow, M.S., and Menco, B.P.M. (1984). Observations on axonemes and membranes of olfactory and respiratory cilia in frogs and rats using tannic acid-supplemented fixation and photographic rotation. *J. Ultrastruct. Res.* 86, 18–30.
- Lin, Y.-C., Niewiadomski, P., Lin, B., Nakamura, H., Phua, S.C., Jiao, J., Levchenko, A., Inoue, T., Rohatgi, R., and Inoue, T. (2013). Chemically inducible diffusion trap at cilia reveals molecular sieve-like barrier. *Nat. Chem. Biol.* 9, 437–443.
- Linari, M., Hanzal-Bayer, M., and Becker, J. (1999). The delta subunit of rod specific cyclic GMP phosphodiesterase, PDE δ , interacts with the Arf-like protein Arl3 in a GTP specific manner. *FEBS Lett.* 458, 55–59.
- Liu, A., Wang, B., and Niswander, L.A. (2005). Mouse intraflagellar transport proteins regulate both the activator and repressor functions of Gli transcription factors. *Development* 132, 3103–3111.
- Lokaj, M., Kösling, S.K., Koerner, C., Lange, S.M., Van Beersum, S.E.C., Van Reeuwijk, J., Roepman, R., Horn, N., Ueffing, M., Boldt, K., et al. (2015). The interaction of CCDC104/BARTL1 with Arl3 and implications for ciliary function. *Structure* 23, 2122–2132.
- Luo, N., West, C.C., Murga-Zamalloa, C.A., Sun, L., Anderson, R.M., Wells, C.D., Weinreb, R.N., Travers, J.B., Khanna, H., and Sun, Y. (2012). OCRL localizes to the primary cilium: A new role for cilia in Lowe syndrome. *Hum. Mol. Genet.* 21, 3333–3344.
- Mahjoub, M.R. (2013). The importance of a single primary cilium. *Organogenesis* 9, 61–69.
- Martín-Gago, P., Fansa, E.K., Klein, C.H., Murarka, S., Janning, P., Schürmann, M., Metz, M., Ismail, S., Schultz-Fademrecht, C., Baumann, M., et al. (2017). A PDE6 δ -KRas inhibitor chemotype with up to seven H-bonds and picomolar affinity that prevents efficient inhibitor release by Arl2. *Angew. Chem. Int. Ed.* 56, 2423–2428.
- Marzesco, A.M., Galli, T., Louvard, D., and Zahraoui, A. (1998). The rod cGMP phosphodiesterase δ subunit dissociates the small GTPase Rab13 from membranes. *J. Biol. Chem.* 273, 22340–22345.
- Matsunaga, H., Handa, J.T., Aotaki-Keen, A., Sherwood, S.W., West, M.D., and Hjelmeland, L.M. (1999). Beta-Galactosidase histochemistry and telomere loss in senescent retinal pigment epithelial cells. *Investig. Ophthalmol. Vis. Sci.* 40, 197–202.
- May-Simera, H.L., and Kelley, M.W. (2012). Cilia, Wnt signaling, and the cytoskeleton. *Cilia* 1:7, 1–16.
- McCormick, F., and Wittinghofer, A. (1996). Interactions between Ras proteins and their

- effectors. *Curr. Opin. Biotechnol.* **7**, 449–456.
- McGrath, J., and Brueckner, M. (2003). Cilia are at the heart of vertebrate left-right asymmetry. *Curr. Opin. Genet. Dev.* **13**, 385–392.
- McGrath, J., Somlo, S., Makova, S., Tian, X., and Brueckner, M. (2003). Two populations of node monocilia initiate left-right asymmetry in the mouse. *Cell* **114**, 61–73.
- Mejuch, T., Van Hattum, H., Triola, G., Jaiswal, M., and Waldmann, H. (2015). Specificity of lipoprotein chaperones for the characteristic lipidated structural motifs of their cognate lipoproteins. *ChemBioChem Commun.* **16**, 2460–2465.
- Mejuch, T., Garivet, G., Hofer, W., Kaiser, N., Fansa, E.K., Ehrt, C., Koch, O., Baumann, M., Ziegler, S., Wittinghofer, A., et al. (2017). Small-molecule inhibition of the UNC119-cargo interaction. *Angew. Chem. Int. Ed.* **56**, 6181–6186.
- Mikami, A., Tynan, S.H., Hama, T., Luby-Phelps, K., Saito, T., Crandall, J.E., Besharse, J.C., and Vallee, R.B. (2002). Molecular structure of cytoplasmic dynein 2 and its distribution in neuronal and ciliated cells. *J. Cell Sci.* **115**, 4801–4808.
- Milburn, M. V, Tong, L., DeVos, A.M., Brünger, A., Yamaizumi, Z., Nishimura, S., and Kim, S.H. (1990). Molecular switch for signal transduction: Structural differences between active and inactive forms of protooncogenic ras proteins. *Science* **247**, 939–945.
- Mishra, A.K., and Lambright, D.G. (2016). Small GTPases and their GAPs. *Biopolymers* **105**, 431–448.
- Mizuno, N., Toba, S., Edamatsu, M., Watai-Nishii, J., Hirokawa, N., Toyoshima, Y.Y., and Kikkawa, M. (2004). Dynein and kinesin share an overlapping microtubule-binding site. *EMBO J.* **23**, 2459–2467.
- Molla-Herman, A., Ghossoub, R., Blisnick, T., Meunier, A., Serres, C., Silbermann, F., Emmerson, C., Romeo, K., Bourdoncle, P., Schmitt, A., et al. (2010). The ciliary pocket: An endocytic membrane domain at the base of primary and motile cilia. *J. Cell Sci.* **123**, 1785–1795.
- Montoya, G., Te Kaat, K., Moll, R., Schäfer, G., and Sinning, I. (2000). The crystal structure of the conserved GTPase of SRP54 from the archaeon *Acidianus ambivalens* and its comparison with related structures suggests a model for the SRP-SRP receptor complex. *Structure* **8**, 515–525.
- Mueller, M.P., and Goody, R.S. (2016). Ras GTPases and myosin: Qualitative conservation and quantitative diversification in signal and energy transduction. *Biopolymers* **105**, 422–430.
- Munger, B.L. (1958). A light and electron microscopic study of cellular differentiation in the pancreatic islets of the mouse. *Am. J. Anat.* **103**, 275–311.
- Nachury, M.V. (2014). How do cilia organize signalling cascades? *Philos. Trans. R. Soc. London* **369:201304**, 1–9.
- Nachury, M.V., Loktev, A.V., Zhang, Q., Westlake, C.J., Peränen, J., Merdes, A., Slusarski, D.C., Scheller, R.H., Bazan, J.F., Sheffield, V.C., et al. (2007). A core complex of BBS proteins cooperates with the GTPase Rab8 to promote ciliary membrane biogenesis. *Cell* **129**, 1201–1213.
- Nachury, M.V., Seeley, E.S., and Jin, H. (2010). Trafficking to the ciliary membrane: How to get across the periciliary diffusion barrier? *Annu. Rev. Cell Dev. Biol.* **26**, 59–87.
- Najafi, M., Maza, N.A., and Calvert, P.D. (2012). Steric volume exclusion sets soluble protein concentrations in photoreceptor sensory cilia. *Proc. Natl. Acad. Sci.* **109**, 203–208.
- Nakata, K., Shiba, D., Kobayashi, D., and Yokoyama, T. (2012). Targeting of Nphp3 to the primary cilia is controlled by an N-terminal myristoylation site and coiled-coil domains.

- Cytoskeleton 69, 221–234.
- Nakatsu, F. (2015). A phosphoinositide code for primary cilia. *Dev. Cell* 34, 379–380.
- Nancy, V., Callebaut, I., Marjou, A. El, and De Gunzburg, J. (2002). The δ subunit of retinal rod cGMP phosphodiesterase regulates the membrane association of Ras and Rap GTPases. *J. Biol. Chem.* 277, 15076–15084.
- Nassar, N., Hoffman, G.R., Manor, D., Clardy, J.C., and Cerione, R.A. (1998). Structures of Cdc42 bound to the active and catalytically compromised forms of Cdc42GAP. *Nat. Struct. Biol.* 5, 1047–1052.
- Nauli, S.M., Alenghat, F.J., Luo, Y., Williams, E., Vassilev, P., Li, X., Elia, A.E.H., Lu, W., Brown, E.M., Quinn, S.J., et al. (2003). Polycystins 1 and 2 mediate mechanosensation in the primary cilium of kidney cells. *Nat. Genet.* 33, 129–137.
- Neal, S.E., Eccleston, J.F., and Webb, M.R. (1990). Hydrolysis of GTP by p21NRAS, the NRAS protooncogene product, is accompanied by a conformational change in the wild-type protein: Use of a single fluorescent probe at the catalytic site. *Proc. Natl. Acad. Sci. U. S. A.* 87, 3562–3565.
- Nigg, E.A. (2006). A licence for duplication. *Nature* 442, 874–875.
- Nomanbhoy, T.K., and Cerione, R.A. (1996). Characterization of the interaction between RhoGDI and Cdc42Hs using fluorescence spectroscopy. *J. Biol. Chem.* 271, 10004–10009.
- Nomanbhoy, T.K., Erickson, J.W., and Cerione, R.A. (1999). Kinetics of Cdc42 membrane extraction by Rho-GDI monitored by real-time fluorescence resonance energy transfer. *Biochemistry* 38, 1744–1750.
- Nonaka, S., Tanaka, Y., Okada, Y., Takeda, S., Harada, A., Kanai, Y., Kido, M., and Hirokawa, N. (1998). Randomization of left-right asymmetry due to loss of nodal cilia generating leftward flow of extraembryonic fluid in mice lacking KIF3B motor protein. *Cell* 95, 829–837.
- Novarino, G., Akizu, N., and Gleeson, J.G. (2011). Modeling human disease in humans: The ciliopathies. *Cell* 147, 70–79.
- Nozaki, S., Katoh, Y., and Terada, M. (2017). Regulation of ciliary retrograde protein trafficking by Joubert syndrome proteins ARL13B and INPP5E. *J. Cell Sci.* 130, 563–576.
- Obar, R.A., Collins, C.A., Hammarback, J.A., Shpetner, H.S., and Vallee, R.B. (1990). Molecular cloning of the microtubule-associated mechanochemical enzyme dynamin reveals homology with a new family of GTP-binding proteins. *Nature* 347, 256–261.
- Orozco, J.T., Wedaman, K.P., Signor, D., Brown, H., Rose, L., and Scholey, J.M. (1999). Movement of motor and cargo along cilia. *Nature* 398, 674.
- Ostrowski, L.E., Blackburn, K., Radde, K.M., Moyer, M.B., Schlatzer, D.M., Moseley, A., and Boucher, R.C. (2002). A proteomic analysis of human cilia: Identification of novel components. *Mol. Cell. Proteomics* 1, 451–465.
- Otto, E.A., Schermer, B., Obara, T., O'Toole, J.F., Hiller, K.S., Mueller, A.M., Ruf, R.G., Hoefele, J., Beekmann, F., Landau, D., et al. (2003). Mutations in INVS encoding inversin cause nephronophthisis type 2, linking renal cystic disease to the function of primary cilia and left-right axis determination. *Nat. Genet.* 34, 413–420.
- Ou, G., Blacque, O.E., Snow, J.J., Leroux, M.R., and Scholey, J.M. (2005). Functional coordination of intraflagellar transport motors. *Nature* 436, 583–587.
- Pai, E.F., Kabsch, W., Krengel, U., Holmes, K.C., John, J., and Wittinghofer, A. (1989). Structure of the guanine-nucleotide-binding domain of the Ha-ras oncogene product p21 in the triphosphate conformation. *Nature* 341, 209–214.

- Pai, E.F., Krengel, U., Petsko, G.A., Goody, R.S., Kabsch, W., and Wittinghofer, A. (1990). Refined crystal structure of the triphosphate conformation of H-ras p21 at 1.35 Å resolution: Implications for the mechanism of GTP hydrolysis. *EMBO J.* 9, 2351–2359.
- Pan, J., and Snell, W. (2007). The primary cilium: Keeper of the key to cell division. *Cell* 129, 1255–1257.
- Di Paolo, G., and De Camilli, P. (2006). Phosphoinositides in cell regulation and membrane dynamics. *Nature* 443, 651–657.
- Papke, B., Murarka, S., Vogel, H.A., Martín-Gago, P., Kovacevic, M., Truxius, D.C., Fansa, E.K., Ismail, S., Zimmermann, G., Heinelt, K., et al. (2016). Identification of pyrazolopyridazinones as PDEδ inhibitors. *Nat. Commun.* 7:11360, 1–9.
- Paridaen, J.T.M.L., Wilsch-Bräuninger, M., and Huttner, W.B. (2013). Asymmetric inheritance of centrosome-associated primary cilium membrane directs ciliogenesis after cell division. *Cell* 155, 333–344.
- Parisi, M.A., Bennett, C.L., Eckert, M.L., Dobyns, W.B., Gleeson, J.G., Shaw, D.W.W., McDonald, R., Eddy, A., Chance, P.F., and Glass, I.A. (2004). The NPHP1 gene deletion associated with juvenile nephronophthisis is present in a subset of individuals with Joubert syndrome. *Am. J. Hum. Genet.* 75, 82–91.
- Pasqualato, S., Ménétrey, J., Franco, M., and Cherfils, J. (2001). The structural GDP / GTP cycle of human Arf6. *Mol. Biol.* 2, 234–238.
- Pasqualato, S., Renault, L., and Cherfils, J. (2002). Arf, Arl, Arp and Sar proteins: A family of GTP-binding proteins with a structural device for “front-back” communication. *EMBO Rep.* 3, 1035–1041.
- Pazour, G.J., and Witman, G.B. (2003). The vertebrate primary cilium is a sensory organelle. *Curr. Opin. Cell Biol.* 15, 105–110.
- Pazour, G.J., Agrin, N., Leszyk, J., and Witman, G.B. (2005). Proteomic analysis of a eukaryotic cilium. *J. Cell Biol.* 170, 103–113.
- Pedersen, L.B., Veland, I.R., Schröder, J.M., and Christensen, S.T. (2008). Assembly of primary cilia. *Dev. Dyn.* 237, 1993–2006.
- Perrone, C.A., Triticchler, D., Taulman, P., Bower, R., Yoder, B.K., and Porter, M.E. (2003). A novel dynein light intermediate chain colocalizes with the retrograde motor for intraflagellar transport at sites of axoneme assembly in *Chlamydomonas* and mammalian cells. *Mol. Biol. Cell* 14, 2372–2384.
- Philips, M.R. (2012). Ras hitchhikes on PDE6δ. *Nat. Cell Biol.* 14, 128–129.
- Phua, S.C., Chiba, S., Suzuki, M., Su, E., Roberson, E.C., Pusapati, G. V, Setou, M., Rohatgi, R., Reiter, J.F., Ikegami, K., et al. (2017). Dynamic remodeling of membrane composition drives cell cycle through primary cilia excision. *Cell* 168, 264–279.
- Pigino, G., Geimer, S., Lanzavecchia, S., Paccagnini, E., Cantele, F., Diener, D.R., Rosenbaum, J.L., and Lupetti, P. (2009). Electron-tomographic analysis of intraflagellar transport particle trains in situ. *J. Cell Biol.* 187, 135–148.
- Plotnikova, O. V, Pugacheva, E.N., and Golemis, E.A. (2009). Primary cilia and the cell cycle. *Methods Cell Biol.* 94, 137–160.
- Poole, C.A., Flint, M.H., and Beaumont, B.W. (1985). Analysis of the morphology and function of primary cilia in connective tissues: A cellular cybernetic probe? *Cell Motil.* 5, 175–193.
- Porter, K.R. (1957). The submicroscopic morphology of protoplasm. *Harvey Lect.* 51, 175–228.

- Praetorius, H.A., and Spring, K.R. (2001). Bending the MDCK cell primary cilium increases intracellular calcium. *J. Membr. Biol.* 184, 71–79.
- Pylypenko, O., Rak, A., Durek, T., Kushnir, S., Dursina, B.E., Thomae, N.H., Constantinescu, A.T., Brunsveld, L., Watzke, A., Waldmann, H., et al. (2006). Structure of doubly prenylated Ypt1:GDI complex and the mechanism of GDI-mediated Rab recycling. *EMBO J.* 25, 13–23.
- Qin, H., Diener, D.R., Geimer, S., Cole, D.G., and Rosenbaum, J.L. (2004). Intraflagellar transport (IFT) cargo: IFT transports flagellar precursors to the tip and turnover products to the cell body. *J. Cell Biol.* 164, 255–266.
- Qin, H., Burnette, D.T., Bae, Y.K., Forscher, P., Barr, M.M., and Rosenbaum, J.L. (2005). Intraflagellar transport is required for the vectorial movement of TRPV channels in the ciliary membrane. *Curr. Biol.* 15, 1695–1699.
- Qin, Y., Polacek, N., Vesper, O., Staub, E., Einfeldt, E., Wilson, D.N., and Nierhaus, K.H. (2006). The highly conserved LepA is a ribosomal elongation factor that back-translocates the ribosome. *Cell* 127, 721–733.
- Rauchman, M.I., Nigam, S.K., Delpire, E., and Gullans, S.R. (1993). An osmotically tolerant inner medullary collecting duct cell line from an SV40 transgenic mouse. *Am. J. Physiol.* 265, F416–F424.
- Resh, M.D. (1996). Regulation of cellular signalling by fatty acid acylation and prenylation of signal transduction proteins. *Cell. Signal.* 8, 403–412.
- Resh, M.D. (2013). Covalent lipid modifications of proteins. *Curr. Biol.* 23, R431–R435.
- Reuther, G.W., and Der, C.J. (2000). The Ras branch of small GTPases: Ras family members don't fall far from the tree. *Curr. Opin. Cell Biol.* 12, 157–165.
- Rittinger, K., Walker, P.A., Eccleston, J.F., Smerdon, S.J., and Gamblin, S.J. (1997). Structure at 1.65 Å of RhoA and its GTPase-activating protein in complex with a transition-state analogue. *Nature* 389, 758–762.
- De Robertis, E. (1956). Morphogenesis of the retinal rods; An electron microscope study. *J. Biophys. Biochem. Cytol.* 2, 209–218.
- Roberts, A.J., Kon, T., Knight, P.J., Sutoh, K., and Burgess, S. a (2013). Functions and mechanics of dynein motor proteins. *Nat. Rev. Mol. Cell Biol.* 14, 713–726.
- Rohatgi, R., and Snell, W.J. (2010). The ciliary membrane. *Curr. Opin. Cell Biol.* 22, 541–546.
- Ronquillo, C.C., Bernstein, P.S., and Baehr, W. (2012). Senior-Løken syndrome: A syndromic form of retinal dystrophy associated with nephronophthisis. *Vision Res.* 75, 88–97.
- Rosenbaum, J.L., and Witman, G.B. (2002). Intraflagellar transport. *Nat. Rev. Mol. Cell Biol.* 3, 813–825.
- Rosenbluth, J., and Palay, S.L. (1961). The fine structure of nerve cell bodies and their myelin sheaths in the eighth nerve ganglion of the goldfish. *J. Cell Biol.* 9, 853–877.
- Sánchez, I., and Dynlacht, B.D. (2016). Cilium assembly and disassembly. *Nat. Cell Biol.* 18, 711–717.
- Sanderson, M.J., Dirksen, E.R., and Satir, P. (1985). The antagonistic effects of 5-hydroxytryptamine and methylxanthine on the gill cilia of *Mytilus edulis*. *Cell Motil.* 5, 293–309.
- Sang, L., Miller, J.J., Corbit, K.C., Giles, R.H., Brauer, M.J., Otto, E.A., Baye, L.M., Wen, X., Scales, S.J., Kwong, M., et al. (2011). Mapping the NPHP-JBTS-MKS protein network reveals ciliopathy disease genes and pathways. *Cell* 145, 513–528.

- Saraste, M., Sibbald, P.R., and Wittinghofer, A. (1990). The P-loop - a common motif in ATP- and GTP-binding proteins. *Trends Biochem. Sci.* *15*, 430–434.
- Sasaki, T., Kikuchi, A., Araki, S., Hata, Y., Isomura, M., Kuroda, S., and Takai, Y. (1990). Purification and characterization from bovine brain cytosol of a protein that inhibits the dissociation of GDP from and the subsequent binding of GTP to smg p25A, a ras p21-like GTP-binding protein. *J. Biol. Chem.* *265*, 2333–2337.
- Satir, P. (2005). Tour of organelles through the electron microscope: A reprinting of Keith R. Porter's classic Harvey Lecture with a new introduction. *Anat. Rec. A Discov. Mol. Cell Evol. Biol.* *287*, 1184–1204.
- Satir, P., and Christensen, S.T. (2007). Overview of structure and function of mammalian cilia. *Annu. Rev. Physiol.* *69*, 377–400.
- Satir, P., and Christensen, S.T. (2008). Structure and function of mammalian cilia. *Histochem. Cell Biol.* *129*, 687–693.
- Sayer, J.A., Otto, E.A., O'Toole, J.F., Nurnberg, G., Kennedy, M.A., Becker, C., Hennies, H.C., Helou, J., Attanasio, M., Fausett, B. V, et al. (2006). The centrosomal protein nephrocystin-6 is mutated in Joubert syndrome and activates transcription factor ATF4. *Nat. Genet.* *38*, 674–681.
- Scheffzek, K., Ahmadian, M.R., Kabsch, W., Wiesmüller, L., Lautwein, A., Schmitz, F., and Wittinghofer, A. (1997). The Ras-RasGAP complex: Structural basis for GTPase activation and its loss in oncogenic Ras mutants. *Science* *277*, 333–338.
- Schmick, M., Vartak, N., Papke, B., Kovacevic, M., Truxius, D.C., Rossmannek, L., and Bastiaens, P.I.H. (2014). KRas localizes to the plasma membrane by spatial cycles of solubilization, trapping and vesicular transport. *Cell* *157*, 459–471.
- Schmick, M., Kraemer, A., and Bastiaens, P.I.H. (2015). Ras moves to stay in place. *Trends Cell Biol.* *25*, 190–197.
- Schneider, L., Clement, C.A., Teilmann, S.C., Pazour, G.J., Hoffmann, E.K., Satir, P., and Christensen, S.T. (2005). PDGFR α signaling is regulated through the primary cilium in fibroblasts. *Curr. Biol.* *15*, 1861–1866.
- Scholey, J.M. (2003). Intraflagellar transport. *Annu. Rev. Cell Dev. Biol.* *19*, 423–443.
- Scholey, J.M. (2008). Intraflagellar transport motors in cilia: Moving along the cell's antenna. *J. Cell Biol.* *180*, 23–29.
- Scholey, J.M. (2012). Kinesin-2 motors transport IFT-particles, dyneins and tubulin subunits to the tips of *Caenorhabditis elegans* sensory cilia: Relevance to vision research? *Vision Res.* *75*, 44–52.
- Schrick, J.J., Vogel, P., Abuin, A., Hampton, B., and Rice, D.S. (2006). ADP-ribosylation factor-like 3 is involved in kidney and photoreceptor development. *Am. J. Pathol.* *168*, 1288–1298.
- Schwahn, U., Lenzner, S., Dong, J., Feil, S., Hinemann, B., van Duijnhoven, G., Kirschner, R., Hemberger, M., Bergen, A.A.B., Rosenberg, T., et al. (1998). Positional cloning of the gene for X-linked retinitis pigmentosa 2. *Nat. Genet.* *19*, 327–332.
- Schweins, T., and Wittinghofer, A. (1994). GTP-binding proteins - Structures, interactions and relationships. *Curr. Biol.* *4*, 547–550.
- Scrima, A., Thomas, C., Deaconescu, D., and Wittinghofer, A. (2008). The Rap-RapGAP complex: GTP hydrolysis without catalytic glutamine and arginine residues. *EMBO J.* *27*, 1145–1153.
- Seabra, M.C. (1998). Membrane association and targeting of prenylated Ras-like GTPases. *Cell. Signal.* *10*, 167–172.

- Seabra, M.C., Reiss, Y., Casey, P.J., Brown, M.S., and Goldstein, J.L. (1991). Protein farnesyltransferase and geranylgeranyltransferase share a common α subunit. *Cell* 65, 429–434.
- Seewald, M.J., Koerner, C., Wittinghofer, A., and Vetter, I.R. (2002). RanGAP mediates GTP hydrolysis without an arginine finger. *Nature* 415, 662–666.
- Sharer, J.D., and Kahn, R.A. (1999). The ARF-like 2 (ARL2)-binding Protein, BART. *J. Biol. Chem.* 274, 27553–27561.
- Sharer, J.D., Shern, J.F., Van Valkenburgh, H., Wallace, D.C., and Kahn, R.A. (2002). ARL2 and BART Enter Mitochondria and Bind the Adenine Nucleotide Transporter. *Mol. Biol. Cell* 13, 71–83.
- Shern, J.F., Sharer, J.D., Pallas, D.C., Bartolini, F., Cowan, N.J., Reed, M.S., Pohl, J., and Kahn, R.A. (2003). Cytosolic ARL2 is complexed with cofactor D and protein phosphatase 2A. *J. Biol. Chem.* 278, 40829–40836.
- Shiba, D., Takamatsu, T., and Yokoyama, T. (2005). Primary cilia of inv/inv mouse renal epithelial cells sense physiological fluid flow: Bending of primary cilia and Ca^{2+} influx. *Cell Struct. Funct.* 30, 93–100.
- Shiba, D., Manning, D.K., Koga, H., Beier, D.R., and Yokoyama, T. (2010). Inv acts as a molecular anchor for Nphp3 and Nek8 in the proximal segment of primary cilia. *Cytoskeleton* 67, 112–119.
- Shih, T.Y., Weeks, M.O., Young, H.A., and Scolnick, E.M. (1979). Identification of a sarcoma virus-coded phosphoprotein in nonproducer cells transformed by Kirsten or Harvey murine sarcoma virus. *Virology* 96, 64–79.
- Silverman, M.A., and Leroux, M.R. (2009). Intraflagellar transport and the generation of dynamic, structurally and functionally diverse cilia. *Trends Cell Biol.* 19, 306–316.
- Simon, M.I., Strathmann, M.P., and Gautam, N. (1991). Diversity of G proteins in signal transduction. *Science* 252, 802–808.
- Simons, M., Gloy, J., Ganner, A., Bullerkotte, A., Bashkurov, M., Krönig, C., Schermer, B., Benzing, T., Cabello, O.A., Jenny, A., et al. (2005). Inversin, the gene product mutated in nephronophthisis type II, functions as a molecular switch between Wnt signaling pathways. *Nat. Genet.* 37, 537–543.
- De Smedt, F., Boom, A., Pesesse, X., Schiffmann, S.N., and Erneux, C. (1996). Post-translational modification of human brain type I inositol 1,4,5-trisphosphate 5-phosphatase by farnesylation. *J. Biol. Chem.* 271, 10419–10424.
- Smith, J.C., Northey, J.G.B., Garg, J., Pearlman, R.E., and Siu, K.W.M. (2005). Robust method for proteome analysis by MS/MS using an entire translated genome: Demonstration on the ciliome of *Tetrahymena thermophila*. *J. Proteome Res.* 4, 909–919.
- Snow, J.J., Ou, G., Gunnarson, A.L., Walker, M.R.S., Zhou, H.M., Brust-Mascher, I., and Scholey, J.M. (2004). Two anterograde intraflagellar transport motors cooperate to build sensory cilia on *C. elegans* neurons. *Nat. Cell Biol.* 6, 1109–1113.
- Sorokin, S. (1962). Centrioles and the formation of rudimentary cilia by fibroblasts and smooth muscle cells. *Cell Biol.* 15, 363–377.
- Sorokin, S.P. (1968). Reconstructions of centriole formation and ciliogenesis in mammalian lungs. *J. Cell Sci.* 3, 207–230.
- Sprang, S.R. (1997). G protein mechanisms: Insights from structural analysis. *Annu. Rev. Biochem.* 66, 639–678.
- Su, C.-Y., Bay, S.N., Mariani, L.E., Hillman, M.J., and Caspary, T. (2012). Temporal deletion

- of Arl13b reveals that a mispatterned neural tube corrects cell fate over time. *Development* 139, 4062–4071.
- Sung, C.-H., and Leroux, M.R. (2013). The roles of evolutionarily conserved functional modules in cilia-related trafficking. *Nat. Cell Biol.* 15, 1387–1397.
- Szymanska, K., and Johnson, C.A. (2012). The transition zone: An essential functional compartment of cilia. *Cilia* 1:10, 1–8.
- Tam, B.M., Moritz, O.L., Hurd, L.B., and Papermaster, D.S. (2000). Identification of an outer segment targeting signal in the COOH terminus of rhodopsin using transgenic *Xenopus laevis*. *J. Cell Biol.* 151, 1369–1380.
- Tao, B., Bu, S., Yang, Z., Siroky, B., Kappes, J.C., Kispert, A., and Guay-Woodford, L.M. (2009). Cystin localizes to primary cilia via membrane microdomains and a targeting motif. *J. Am. Soc. Nephrol.* 20, 2570–2580.
- Taschner, M., and Lorentzen, E. (2016). The intraflagellar transport machinery. *Cold Spring Harb. Perspect. Biol.* 8, 1–19.
- Taxi, J. (1961). Sur l'existence de neurones ciliés dans les ganglions sympathiques de certains vertébrés. *C. R. Soc. Biol.* 65, 1860–1863.
- Thomas, S., Wright, K.J., Le Corre, S., Micalizzi, A., Romani, M., Abhyankar, A., Saada, J., Perrault, I., Amiel, J., Litzler, J., et al. (2014). A homozygous PDE6D mutation in Joubert syndrome impairs targeting of farnesylated INPP5E protein to the primary cilium. *Hum. Mutat.* 35, 137–146.
- Tobin, J.L., and Beales, P.L. (2009). The nonmotile ciliopathies. *Genet. Med.* 11, 386–402.
- Todaró, G.J., and Green, H. (1963). Quantitative studies of the growth of mouse embryo cells in culture and their development into established lines. *J. Cell Biol.* 17, 299–313.
- Traut, T.W. (1994). Physiological concentrations of purines and pyrimidines. *Mol. Cell. Biochem.* 140, 1–22.
- Travaglini, L., Brancati, F., Silhavy, J., Iannicelli, M., Nickerson, E., Elkhartoufi, N., Scott, E., Spencer, E., Gabriel, S., Thomas, S., et al. (2013). Phenotypic spectrum and prevalence of INPP5E mutations in Joubert syndrome and related disorders. *Eur. J. Hum. Genet.* 21, 1074–1078.
- Tsang, W.Y., Bossard, C., Khanna, H., Peränen, J., Swaroop, A., Malhotra, V., and Dynlacht, B.D. (2008). CP110 suppresses primary cilia formation through its interaction with CEP290, a protein deficient in human ciliary disease. *Dev. Cell* 15, 187–197.
- Tucker, R.W., and Pardee, A.B. (1979). Centriole ciliation is related to quiescence DNA synthesis in 3T3 cells. *Cell* 17, 527–535.
- Valente, E.M., Silhavy, J.L., Brancati, F., Barrano, G., Krishnaswami, S.R., Castori, M., Lancaster, M.A., Boltshauser, E., Boccone, L., Al-Gazali, L., et al. (2006). Mutations in CEP290, which encodes a centrosomal protein, cause pleiotropic forms of Joubert syndrome. *Nat. Genet.* 38, 623–625.
- Van Valkenburgh, H., Shern, J.F., Sharer, J.D., Zhu, X., and Kahn, R.A. (2001). ADP-ribosylation factors (ARFs) and ARF-like 1 (ARL1) have both specific and shared effectors: Characterizing ARL1-binding proteins. *J. Biol. Chem.* 276, 22826–22837.
- Veltel, S., Gasper, R., Eisenacher, E., and Wittinghofer, A. (2008a). The retinitis pigmentosa 2 gene product is a GTPase-activating protein for Arf-like 3. *Nat. Struct. Mol. Biol.* 15, 373–380.
- Veltel, S., Kravchenko, A., Ismail, S., and Wittinghofer, A. (2008b). Specificity of Arl2/Arl3 signaling is mediated by a ternary Arl3-effector-GAP complex. *FEBS Lett.* 582, 2501–2507.

- Vetter, I.R., and Wittinghofer, A. (2001). The guanine nucleotide-binding switch in three dimensions. *Science* 294, 1299–1304.
- Walker, J.E., Saraste, M., Runswick, M., and Gay, N.J. (1982). Distantly related sequences in the alpha- and beta-subunits of ATP synthase, myosin, kinases and other ATP-requiring enzymes and a common nucleotide binding fold. *EMBO J.* 1, 945–951.
- Walter, P. (1994). Signal sequence recognition and protein targeting to the membrane. *Annu. Rev. Cell Biol.* 10, 87–119.
- Ward, H.H., Brown-Glaberman, U., Wang, J., Morita, Y., Alper, S.L., Bedrick, E.J., Gattone, V.H., Deretic, D., and Wandinger-Ness, A. (2011). A conserved signal and GTPase complex are required for the ciliary transport of polycystin-1. *Mol. Biol. Cell* 22, 3289–3305.
- Waters, A.M., and Beales, P.L. (2011). Ciliopathies: An expanding disease spectrum. *Pediatr. Nephrol.* 26, 1039–1056.
- Watnick, T., and Germino, G. (2003). From cilia to cyst. *Nat. Genet.* 34, 355–356.
- Wedaman, K.P., Meyer, D.W., Rashid, D.J., Cole, D.G., and Scholey, J.M. (1996). Sequence and submolecular localization of the 115-kD accessory subunit of the heterotrimeric kinesin-II (KRP85/95) complex. *J. Cell Biol.* 132, 371–380.
- Wei, Q., Zhang, Y., Li, Y., Zhang, Q., Ling, K., and Hu, J. (2012). The BBSome controls IFT assembly and turnaround in cilia. *Nat. Cell Biol.* 14, 950–957.
- Westheimer, F.H. (1987). Why nature chose phosphates. *Science* 235, 1173–1178.
- Wheatley, D. (1995). Primary cilia in normal and pathological tissues. *Pathobiology* 63, 222–238.
- Wheatley, D.N., Wang, A.M., and Strugnell, G.E. (1996). Expression of primary cilia in mammalian cells. *Cell Biol. Int.* 20, 73–81.
- Williams, C.L., Li, C., Kida, K., Inglis, P.N., Mohan, S., Semenec, L., Bialas, N.J., Stupay, R.M., Chen, N., Blacque, O.E., et al. (2011). MKS and NPHP modules cooperate to establish basal body/transition zone membrane associations and ciliary gate function during ciliogenesis. *J. Cell Biol.* 192, 1023–1041.
- Wilson, P.T., and Bourne, H.R. (1995). Fatty acylation of $\alpha\zeta$ - Effects of palmitoylation and myristoylation on $\alpha\zeta$ signaling. *J. Biol. Chem.* 270, 9667–9675.
- Wingfield, J.L., Mengoni, I., Bomberger, H., Jiang, Y.-Y., Walsh, J.D., Brown, J.M., Picariello, T., Cochran, D.A., Zhu, B., Pan, J., et al. (2017). IFT trains in different stages of assembly queue at the ciliary base for consecutive release into the cilium. *eLife* 6:e26609, 1–27.
- Wittinghofer, A. (2016). GTP and ATP hydrolysis in biology. *Biopolymers* 105, 419–421.
- Wittinghofer, A., and Herrmann, C. (1995). Ras-effector interactions, the problem of specificity. *FEBS Lett.* 369, 52–56.
- Wittinghofer, A., and Vetter, I.R. (2011). Structure-function relationships of the G domain, a canonical switch motif. *Annu. Rev. Biochem.* 80, 943–971.
- Wittinghofer, A., Scheffzek, K., and Ahmadian, M.R. (1997). The interaction of Ras with GTPase-activating proteins. *FEBS Lett.* 410, 63–67.
- Wolf, M.T.F., and Hildebrandt, F. (2011). Nephronophthisis. *Pediatr. Nephrol.* 26, 181–194.
- Wood, C.R., and Rosenbaum, J.L. (2014). Proteins of the ciliary axoneme are found on cytoplasmic membrane vesicles during growth of cilia. *Curr. Biol.* 24, 1114–1120.
- Wright, K.J., Baye, L.M., Olivier-Mason, A., Mukhopadhyay, S., Sang, L., Kwong, M., Wang, W., Pretorius, P.R., Sheffield, V.C., Sengupta, P., et al. (2011). An ARL3-UNC119-RP2 GTPase cycle targets myristoylated NPHP3 to the primary cilium. *Genes Dev.* 25, 2347–

- 2360.
- Xu, Q., Zhang, Y., Wei, Q., Huang, Y., Hu, J., and Ling, K. (2016). Phosphatidylinositol phosphate kinase PIPKI γ and phosphatase INPP5E coordinate initiation of ciliogenesis. *Nat. Commun.* 7:10777, 1–12.
- Yang, T.T., Su, J., Wang, W.-J., Craige, B., Witman, G.B., Bryan Tsou, M.-F., and Liao, J.-C. (2015). Superresolution pattern recognition reveals the architectural map of the ciliary transition zone. *Nat. Sci. Reports* 5:14096, 1–13.
- Ye, F., Breslow, D.K., Koslover, E.F., Spakowitz, A.J., Nelson, W.J., and Nachury, M. V. (2013). Single molecule imaging reveals a major role for diffusion in the exploration of ciliary space by signaling receptors. *eLife* 2:e00654, 1–16.
- Zaghloul, N.A., and Katsanis, N. (2009). Mechanistic insights into Bardet-Biedl syndrome, a model ciliopathy. *J. Clin. Invest.* 119, 428–437.
- Zhang, H., Liu, X.H., Zhang, K., Chen, C.K., Frederick, J.M., Prestwich, G.D., and Baehr, W. (2004). Photoreceptor cGMP phosphodiesterase δ subunit (PDE δ) functions as a prenyl-binding protein. *J. Biol. Chem.* 279, 407–413.
- Zhang, H., Li, S., Doan, T., Rieke, F., Detwiler, P.B., Frederick, J.M., and Baehr, W. (2007). Deletion of PrBP/ δ impedes transport of GRK1 and PDE6 catalytic subunits to photoreceptor outer segments. *Proc. Natl. Acad. Sci. U. S. A.* 104, 8857–8862.
- Zhang, H., Constantine, R., Vorobiev, S., Chen, Y., Seetharaman, J., Huang, Y.J., Xiao, R., Montelione, G.T., Gerstner, C.D., Davis, M.W., et al. (2011). UNC119 is required for G protein trafficking in sensory neurons. *Nat. Neurosci.* 14, 874–880.
- Zhang, H., Constantine, R., Frederick, J.M., and Baehr, W. (2012). The prenyl-binding protein PrBP/ δ : A chaperone participating in intracellular trafficking. *Vision Res.* 75, 19–25.
- Zhang, T., Li, S., Zhang, Y., Zhong, C., Lai, Z., and Ding, J. (2009). Crystal structure of the ARL2-GTP-BART complex reveals a novel recognition and binding mode of small GTPase with effector. *Structure* 17, 602–610.
- Zhou, C., Cunningham, L., Marcus, A.I., Li, Y., and Kahn, R.A. (2006). Arl2 and Arl3 regulate different microtubule-dependent processes. *Mol. Biol. Cell* 17, 2476–2487.
- Zimmermann, G., Papke, B., Ismail, S., Vartak, N., Chandra, A., Hoffmann, M., Hahn, S.A., Triola, G., Wittinghofer, A., Bastiaens, P.I.H., et al. (2013). Small molecule inhibition of the KRAS-PDE δ interaction impairs oncogenic KRAS signalling. *Nature* 497, 638–642.
- Zimmermann, G., Schultz-Fademrecht, C., Kuechler, P., Murarka, S., Ismail, S., Triola, G., Nussbaumer, P., Wittinghofer, A., and Waldmann, H. (2014). Structure guided design and kinetic analysis of highly potent benzimidazole inhibitors targeting the PDE δ prenyl binding site. *J. Med. Chem.* 57, 5435–5448.
- Zizzari, Z.V., Lupetti, P., Mencarelli, C., and Dallai, R. (2008). Sperm ultrastructure and spermiogenesis of Coniopterygidae (Neuroptera, Insecta). *Arthropod Struct. Dev.* 37, 410–417.

Acknowledgements

The last years were a challenging but first of all an irreplaceable and life-enhancing time that made me develop scientifically and not least personally. I would like to thank the following persons for their contribution.

Foremost, I am deeply grateful to Prof. Dr. Fred Wittinghofer for giving me the opportunity to work and complete this thesis in his research group, for his motivating supervision and guidance as Doktorvater with so much helpful input and support, also to work independently, and for inducting me into the field of small G proteins and cilia. I really appreciate his endless and infectious passion for pure science, which spread over to me already in his first lecture I attended in Bochum in 2012, and his direct and clear nature while discussing science. I acknowledge his appreciation of my work, that he was always reachable, enabled me to attend the enriching Spetses summer school and instructive scientific conferences, proofread this thesis, and that he took care for his last two PhD students beyond the official end of his group. It was the best decision and a really great honor for me to join and be part of the excellent group of this outstanding scientist. This awesome time I will never forget!

I am very thankful to Prof. Dr. Reza Ahmadian for being my first supervisor, for his direct and kind acceptance to take this role, his scientific support, and his help in the organization and formalities regarding this thesis.

I would like to thank Prof. Dr. Lutz Schmitt for being my second supervisor, his kind acceptance to do that and for his good support in scientific and organizational issues.

I am grateful to Prof. Dr. Andrea Musacchio for his kind support during the last months of my PhD and for providing the resources of his department, especially the microscopes. Also, I am thankful to Prof. Dr. Philippe Bastiaens for providing the microscopes of his department.

I am deeply grateful to all members of Fred's group for everything I learned from them, scientifically but also for the "real life", for their expertise and limitless support, for fruitful pizza seminars, scientific and non-scientific counselling, for nice lunch and coffee breaks and for all the fun we had together, for our private meetings, and for being true friends and like a "lab family". They all showed me what real teamwork is. I will always think back to this time with a more than positive feeling and I am very happy about the existence of our group beyond the official end. My special thanks go to Dr. Mandy Lokaj for her perfect mentoring and support during so many years, and for her guidance and help from the first day on in my first practical course in 2012, following master and PhD studies. I am deeply thankful to her for teaching me all the methods in the lab from molecular biology to cell biology, for the great teamwork, her

help with the cells, for always having an open ear for any kind of trouble or just for fun, and for her friendship. I am deeply grateful to Dr. Eyad Fansa for his support and guidance, for all his input and help, the great and fruitful teamwork, the table soccer breaks, the “life-changing” time in the “boy’s office”, and his friendship. I am very thankful to Susanne Terheyden for finishing our PhD side by side as the last members of the group, for all her help and support, the nice teamwork in general things in the lab, scientific discussions and non-scientific chats, and for her friendship. I would like to particularly thank Carolin Koerner for all her help, for always knowing a solution for cloning or other problems in the lab and her explanations, for keeping the group together and the lab running, and for her friendship. I am very thankful to Jana Seidel for her support and help in the lab, for being a great team partner in the cell culture to chat and to keep it in a good condition and running under any kind of difficult situation, and for her friendship. I am grateful to Rita Schebaum for taking care, for her help in organizational questions and for keeping the group together. I would like to thank Dr. Eldar Zent for his help regarding scientific and non-scientific questions or computer problems and for being an always relaxed person, Dr. Katja Gotthardt for being a nice bench neighbor, for her scientific input and teamwork, and Dr. Mamta Jaiswal for the good teamwork. I am also very thankful for the great support and input from Dr. Bernd Gilsbach, Dr. Kim Remans, Dr. Ben Schumacher, Dr. Denise Wätzlich, Dr. Björn Klink and Dr. Shehab Ismail, also for the collaboration after he became group leader at the Beatson Intitute in Glasgow. I would like to thank Sina Schumacher, who successfully completed a practical course during her bachelor in our group, for her really good support in the cell culture, the master students Bart Bruininks, Sven Lange, Felix Kipper, Sibel Uzuncayir and Nadia Seibel, and the research assistants Lukjan Roßmannek, Simon Herrmann, Pascal Hommen and Lars Caspari for their general support in the lab.

I am deeply thankful to Dr. Stefano Maffini for the great collaboration and teamwork during the last project of this thesis, the introduction to live cell imaging and the FRAP technique, for all his input, guidance and help during the experiments and to publish the project, and for his high interest in the cilia research field additionally to his daily research.

I am very grateful to all institute members for the open and friendly atmosphere, the scientific exchange, the seminars and courses, excellent resources, great events and funny parties. I would like to thank everyone else who supported me scientifically or personally during the last years, in particular Patricia Stege and Diana Ludwig for always having an open ear, Dr. Sven Müller for introducing me to fluorescence microscopy and his expertise and help for any kind of technical problem, Petra Glitz for her support in the cell culture in my first year, Walburga Hecker for the sequencing service, Lea Kremer, Dr. Marta Mattiuzzo, Dr. Katharina Overlack,

Kathrin Estel, Annika Take, and Arne Bothe. I would like to thank Prof. Dr. Heinz Neumann, Dr. Matias Hernandez, Petra Geue, Dr. Petra-Gisela Neumann-Staubitz, Martin Spinck, Neha Jain, Sheila Mainye and Sven Brandherm for sharing the lab and offices and the nice colleagueship after Fred's group became smaller. I am also thankful to Dr. Sonja Sievers and all members of the Compound Management and Screening Center for being very good lab neighbors and for sharing equipment. I would like to acknowledge Angelika Rohde, Brigitte Rose, Antje Peukert, Claudia Birke, Sabrina Janz (TU Dortmund) and Mathilde Blum (HHU Düsseldorf) for organizational support, and especially Christa Hornemann and Dr. Lucia Sironi for their commitment in the International Max Planck Research School in Chemical and Molecular Biology to enable the participation in scientific courses and career events. In this context, my gratitude goes to Dr. Deborah Bennett and Rob Thompson for excellent and extremely enriching seminars. I am grateful to the Interdisciplinary Graduate and Research Academy Düsseldorf. I would also like to thank Sigrid Rosin-Steiner for her commitment in the work council.

I am grateful to Prof. Dr. Ronald Roepman, Jeroen van Reeuwijk and Sylvia van Beersum (Radboud University Medical Center, Nijmegen), Prof. Dr. Marius Ueffing, Dr. Karsten Boldt and Nicola Horn (University of Tübingen), and Prof. Dr. Herbert Waldmann and Dr. Tom Mejuch for good collaborations, and Dr. Katarzyna Szymanska (University of Leeds) for sharing her knowledge of immunofluorescent staining of cilia under special conditions. I would like to thank Prof. Dr. Johannes L. Bos, Cristina Arpesella and the participants for the organization of a very enriching Spetses summer school.

My deepest and warmest gratitude is devoted towards my family, especially towards my mum for always believing in me, her limitless support and backing me up at any time. I am just as deeply grateful to my grandma for her support, my partner İlhan for his encouragement and understanding, and to my friends, Miriam for her mental and scientific support, Sannah for always standing together, and Janine for taking care since our childhood. In memory of my dad, my grandpa and my grandaunt. Without their love and support all these things would not have been possible and I would not be where and how I am today. Therefore, this thesis is devoted to all of them.